The Introduction of Crack Opening Stress Modeling into Strain-Life And Small Crack Growth Fatigue Analysis

by

Maria El Zeghayar

A thesis
presented to the University of Waterloo
in fulfillment of the
thesis requirement for the degree of
Doctor of Philosophy
in
Civil Engineering

Waterloo, Ontario, Canada, 2010

Author’s Declaration

I hereby declare that I am the sole author of this thesis. This is a true copy of the thesis, including any required final revisions, as accepted by my examiners.

I understand that my thesis may be made electronically available to the public.

Abstract

The work in this thesis is concerned with the mechanics of the initiation and growth of small fatigue cracks from notches under service load histories. Fatigue life estimates for components subjected to variable amplitude service loading are usually based on the same constant amplitude strain-life data used for constant amplitude fatigue life predictions. The resulting fatigue life estimates although they are accurate for constant amplitude fatigue, are always non conservative for variable amplitude load histories. Similarly fatigue life predictions based on small crack growth calculations for cracks growing from flaws in notches are non conservative when constant amplitude crack growth data are used. These non conservative predictions have, in both cases, been shown to be due to severe reductions in fatigue crack closure arising from large (overload or underload) cycles in a typical service load history. Smaller load cycles following a large near yield stress overload or underload cycle experience a much lower crack opening stress than that experienced by the same cycles in the reference constant amplitude fatigue tests used to produce design data. This reduced crack opening stress results in the crack remaining open for a larger fraction of the stress-strain cycle and thus an increase in the effective portion of the stress-strain cycle. The effective strain range is increased and the fatigue damage for the small cycles is greater than that calculated resulting in a non conservative fatigue life prediction.

Previous work at Waterloo introduced parameters based on effective strain-life fatigue data and effective stress intensity versus crack growth rate data. Fatigue life calculations using these parameters combined with experimentally derived crack opening stress estimates give accurate fatigue life predictions for notched components subjected to variable amplitude service load histories. Information concerning steady state crack closure stresses, effective strain-life data, and effective stress intensity versus small crack growth rate data, are all obtained from relatively simple and inexpensive fatigue tests of smooth specimens in which periodic underloads are inserted into an otherwise constant amplitude load history. The data required to calibrate a variable amplitude fatigue crack closure model however, come from time consuming measurements of the return of crack closure levels for small cracks to a steady state level following an underload (large cracks for which crack closure measurements are easier to make cannot be used because at the high stress levels in notches under service loads a test specimen used would fracture).

For low and moderately high hardness levels in metals crack growth and crack opening stress measurements have been made using a 900x optical microscope for the small crack length at which a test specimen can resist the high stress levels encountered when small cracks grow from notches. For very hard metals the crack sizes may be so small that the measurements must be made using a confocal scanning laser microscope. In this case the specimen must be removed from the test machine for each measurement and the time to acquire data is only practical for an extended research project. The parameters for the crack closure model relating to steady state crack closure levels vary with material cyclic deformation resistance which in turn increases with hardness. One previous investigation [1] found that the steady state crack opening level was lower and the recovery to a steady state crack opening stress level after an underload was more rapid for a hard than for a soft metal. This observation can be explained by the dependence of the crack tip plastic zone size that determines crack tip deformation and closure level on metal hardness and yield strength. Further information regarding this hypothesis has been obtained in this thesis by testing three different steels of varying hardness levels (6 HRC, 35 HRC, and 60 HRC) including a very hard carburized steel having a hardness level (60 HRC) for which no crack opening stress data for small cracks had yet been obtained.

This thesis introduced a new test procedure for obtaining data on the return of crack opening stress to a steady state level following an underload. Smooth specimens were tested under load histories with intermittent underload cycles. The frequency of occurrence of the underloads was varied and the changes in fatigue life observed. The changes in damage per block (the block consisted of an underload cycle followed by intermittent small cycles) were used to determine the value of the closure model parameter governing the recovery of the crack opening stress to its steady state level. Concurrent tests were carried out in which the crack opening stress recovery was measured directly on crack growth specimens using optical microscope measurements. These tests on metals ranging in hardness from soft to very hard were used to assess whether the new technique would produce good data for crack opening stress changes after underloads for all hardness levels. The results were also used to correlate crack closure model parameters with mechanical properties. This together with the steady state crack opening stress, effective strain-life data and the effective intensity versus crack growth rate data obtained from smooth specimen tests devised by previous researchers provided all the data required to calibrate the two models proposed in this investigation to perform strain-life and small crack growth fatigue analysis.

Acknowledgements

It is a pleasure to thank the many people that made this thesis possible.

First and foremost I offer my deepest and sincerest gratitude to my Ph.D. supervisor, Professor Emeritus Dr. Timothy Topper. With his enthusiasm and perpetual energy and his great efforts to explain fatigue concepts simply, he helped to make Metal Fatigue fun for me. He was always accessible and willing to help. Throughout my stay at the University of Waterloo, he guided me and taught me on how to run the servo-controlled electro-hydraulic testing machines. He provided encouragement, sound advice, great teaching, great company, and lots of great ideas, one simply could not wish for a better or friendlier supervisor. I would have been lost without him.

I would also like to thank my co-supervisor, Professor Khalid Soudki, who first accepted me as a coop undergraduate student and opened the door for me to do my graduate studies in Waterloo. He has made available his support in a number of ways and I wouldn't have been here without him.

I am heartily thankful to Dr. Semyon Mikheevskiy for his great efforts to explain, teach, and help to develop my thesis model using "Python" programming language. His ingenious skills in programming have made my life easier and less stressful. He was always ready to help and was a great debater on whether crack closure existed or not, I enjoyed all his insightful arguments.

I would also like to thank Dr. John Bonnen and Dr. Al Conle for their great supervision and help during my stay at the Ford Innovation and Research Center. Their extensive discussions and interesting explorations around my work have been very helpful for this study.

My warm thanks are due to Professor Gregory Glinka, I had the honor to attend his classes. His insight to Fatigue Design is second to none. He sets an example of a world-class researcher for his passion on research.

I would like to thank Mr. John Bolt from the machine shop for his great help in machining the fatigue samples used in this work. I also acknowledge, with thanks, Mr. Doug Hirst, Mr. Richard Morrison, and Mr. Robert Sluban for their great assistance in the fatigue lab.

I am indebted to my many colleagues who supported me and provided a stimulating and fun environment. I am especially thankful for Rania Al-Hammoud, Aditcha Chattopadhyay, Oxana Skiba, and Dr. Elena Atroshchenko.

My heartiest thanks go to my mom, dad, and my little sister Lena for their everlasting love and support, and their absolute confidence in me. You have always stood by my side guarding me against all odds and showing me the correct path to follow. I love you so much, and I would not have made it this far without you. My little sister has been my best friend all my life and I love her dearly and thank her for all her support and advice especially when it came to fashion. You tend to forget what's happening outside the lab after four years of working with the machines and hydraulic oil so thank you for being my fashion expert advisor throughout this period.

One of the best outcomes from these past four years is finding my best friend, and my soul-mate, Adam. Ever since he tiptoed into my life, it's been filled with love, laughter, and lots of special times. He is the best thing that ever happened to me. There are no words to convey how much I love him. Adam has been a true and great supporter and has unconditionally loved me during my good and bad times. Thank you for helping me in my studies and for every time I said "What If" you said "I'm sure" and for every time I wondered "Can I" you affirmed "You surely will". Darling thank you for knowing me more than I do. I can't wait to spend the rest of my life with you.

Dedication

To My Mom, Dad, and Lena

And to My Love and Soul-Mate

Adam

Table of Contents

List of Figures

List of Tables

Chapter 1
Introduction: Background and Literature Review

The German Inter-City Express was considered the ultimate in train travel. But in 1998, the train derailed and slammed against a concrete bridge. Carriages accordioned, and in seconds 101 passengers were killed in the world's worst high speed rail disaster [2]. Later investigations discovered the presence of fatigue cracks on the inside of the metal wheel rims that flattened into ellipsoids. This incident together with many other accidents have increased the awareness of the dangers of fatigue failures that continue to occur in components of machines, vehicles, and structures subjected to cyclic loading. Even though fatigue has become a mature discipline, inadvertent fatigue failures have continued to occur in industries such as the aircraft, railroad, and automotive industries and in structures such as bridges.

When it is exposed to *fatigue*, a component may suffer from a sudden failure after a period of repeated loading or vibration, even where the applied stress is far below a material's ultimate static strength. Failure is the end result of a process involving the initiation and growth of a crack, usually at the site of a stress concentration, such as a notch, or a geometric discontinuity.

Aircraft and marine structures, pressure vessels, power engines and generators, automobiles, and other structures exposed to repeated loading, are all affected by fatigue, and despite its complexity, many analytical methods have been developed in efforts to design against fatigue damage. It wasn't until the introduction of servo-electro-hydraulic fatigue machines, and electron microscopes that a large amount of fatigue data could be generated under constant and variable amplitude loading. These developments and the examination of fracture surfaces resulted in a number of characteristic observations and analytical concepts especially those of the application of the elastic stress intensity factor, *K*, to fatigue crack growth by Paris et al. [3] in 1961, and the crack closure phenomena that was discovered by Elber [4] in 1970.

1.1 Fatigue Cracks

Fatigue cracks may be classified according to their size i.e. micro-structurally small (crystallographic) cracks, physically short cracks, and long cracks [5]. From experimental work it was found that under uni-axial loading in air at ambient temperature, cracks (3-6 μm long) can nucleate in slip bands on the surface or in the bulk of the material.

Ma and Laird [6] indicated that crack propagation takes place in two stages. During the first stage a crack propagates on a plane of maximum shear stress (*stage I crack*), while during the second stage propagation takes place on a plane normal to the maximum normal stress (*stage II crack*).

In constant amplitude loading cyclic slip band formation is followed by propagation of the initiated micro-crack which is referred to as a microscopically short crack into the grain, and its growth rate decreases as it approaches the grain boundary. At this stage further fatigue crack growth depends on the ability of a specific micro-crack to overcome the first micro-structural barriers. This period of growth in which the crack extends to several grains is termed as micro-structurally small crack growth. The following period of growth where the effect of microstructure of the material is averaged out and crack closure has not reached a steady state level is termed as physically short crack growth.

Finally, when a few micro-cracks grow and form a larger crack that grows with a stable crack opening stress until specimen failure, the crack is termed a long crack. In the last 35 years a considerable amount of attention has been devoted to small crack behaviour. It was found that at a given stress intensity range the growth rate of short fatigue cracks is faster than that of long cracks, therefore, for fundamental as well as practical reasons it was of great importance to understand the behaviour and growth of short cracks whose growth has been predicted non-conservatively by the application of linear elastic fracture mechanics [7].

1.1.1 Micro-Structurally Small (Crystallographic) Cracks

Cracks are considered to be small when all pertinent dimensions are small compared to some characteristic length [8]. In case of micro-structurally small cracks, their length scale is compared to metallurgical variables such as the grain size. In this regime, the crack initiation and growth period is strongly affected by the microstructure of the metal and crack growth can initially take place at stresses below the fatigue limit of a material. Forsyth [9] defined the shear crack growth that takes place during this period on a plane of maximum shear as *Stage I Growth*. Miller [10] noted that the initial *Stage I Shear Crack* will usually start at a surface stress concentration and the crack will increase in size in the largest surface grain that provides the longest slip planes that are favourably oriented with respect to the maximum applied shear stress. Once the primary barrier after the first grain boundary is crossed, the crack has to grow across several neighbouring grains whose slip system may not be suitably oriented with respect to the maximum shear stress. During this stage the crack growth slows down temporary and should the applied stress level not be sufficient to propagate the crack on the available less favourably inclined slip planes, the crack will be arrested. This retardation of crack growth at barriers is significant during the period in which the small crack grows through the first few grains. Tokaji et al. [11] noticed that the crack growth rates of small cracks decreased markedly at prior austenite grain boundaries in a low alloy steel and in a ferritic-pearlitic steel. If the crack was not arrested at these barriers at the applied stress levels, crack tip plasticity increased with increasing crack length, but crack closure had not yet built

up substantially in this regime. Topper et al. [12] noted that the first few large load cycles in variable amplitude loading will provide enough local cyclic plasticity to rapidly advance a crack through the micro-structurally short crack regime.

1.1.2 Physically Short Cracks

Physically short cracks are of such a length that the resistance to crack growth by micro-structural barriers is averaged out, but crack closure has not yet built up to a steady state level [5]. Physically short cracks grow at a higher rate than long cracks for the same value of applied stress intensity factor range, ΔK, and they can also grow at values of ΔK below that of the steady state threshold value, ΔK_{th}, of long cracks. In this regime the crack size and the driving force are large enough that the micro-structural barriers can decelerate crack growth but are unable to arrest it [7]. The physically short crack regime is bounded by the upper limit of the micro-structurally short crack regime and the lower limit of the long crack regime [13].

1.1.3 Long Cracks

Different mechanisms have been proposed in the literature to describe fatigue crack extension (long cracks). Smith et al. [14] described a model based on a plastic sliding-off mechanism at the tip of an advancing crack which is now referred to as the plastic blunting process of fatigue crack extension. During the application of a tensile loading, Figure 1(*a)*, the small double notch at the crack tip serves to concentrate a highly localized plastic deformation along the slip planes of maximum shear stress (45^o to the applied uniaxial stress) (Figure 1(*b)).* As the specimen is deformed to the maximum tensile strain, the width of the slip band increases and the crack blunts into a semicircular shape (Figure 1(*c)*). Upon the application of a compressive load the direction of slip is reversed and the distance between the crack surfaces decreases. The new crack surface created during the tensile loading is partly folded by buckling into another notch (Figure 1.1 (*d)*). At the maximum compressive stress the crack tip is sharp again and the fatigue striations are formed during the unloading.

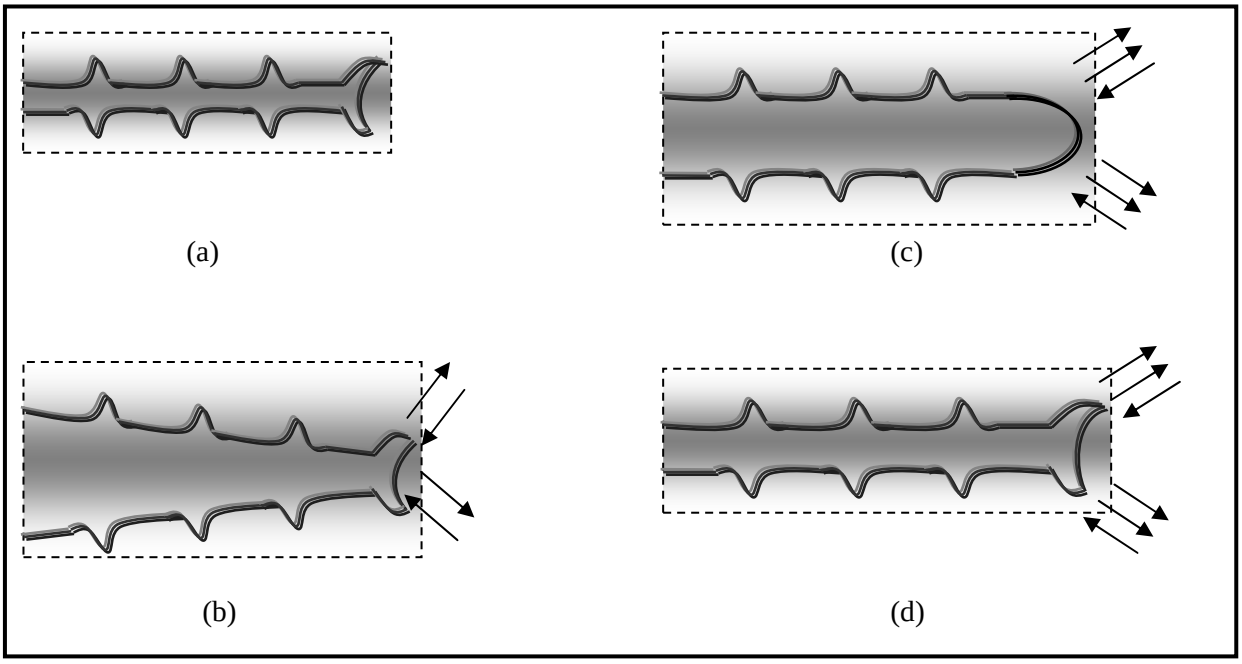

Figure 1.1 The plastic blunting process of fatigue crack extensions: (a) zero load; (b) tensile load; (c) peak tensile load; (d) reversed loading

1.2 Fatigue Crack Growth

The evolution of fatigue crack growth under cyclic loading has been the subject of intensive studies during the last century. The growing interest in fatigue crack propagation in the 1960's coincided with the rapid spread of servo-hydraulic testing systems that allowed variable amplitude testing as well as high strain constant amplitude testing. Since fatigue crack initiation and growth ultimately leads to failure of a structure or a component, researchers found that is it of great importance to study and understand the mechanisms which govern fatigue and fracture. Paris et al. [15] discovered that the stress intensity range, ΔK, was the basic driving force for fatigue crack growth. Later, a significant amount of research was allocated to understanding the discrete nature of crack initiation and propagation. Lindstedt et al. [16] studied the nucleation and the propagation of small surface cracks during non-impact low cycle fatigue in a stainless steel. They found that small cracks predominately nucleate at the surface of the specimen when it is cyclically strained. Crack nucleation was detected at roughly 10% of the fatigue life and preceded until about half of the fatigue life. Hunter et al. [17] found that near the material's fatigue limit most of the fatigue life is spent in the initiation of the crack, while in low cycle fatigue the initiation period is short compared to the propagation period which consumes most of the fatigue life.

1.2.1 Fatigue Crack Growth: Short Cracks

The anomalous growth of short fatigue cracks was first reported by Pearson [18] who tested commercial aluminum alloys in the form of plates and extruded bars under bending and concluded that linear elastic fracture mechanics could not be used to correlate the growth rate of short cracks to that of long cracks. Since then numerous investigators have reported that the growth rates of short cracks are significantly faster than those of long cracks under the same nominal stress intensity factor range (ΔK) [19]. Short crack propagation is dominated by a relatively large cyclic crack tip plasticity that alters the stress field ahead of a fatigue crack [7]. This behaviour of a short crack is seriously underestimated by classical linear fracture mechanics. However and contrary to this understanding, Sadananda et al. [20] proposed that short cracks grow under a total force consisting of both internal stresses generated at the crack tip field, and the external applied stresses. In their model they explained that the plasticity originating from the crack tip does not contribute to its closure and concluded that closure either doesn't exist or is insignificant. Instead they proposed two parameters as being the driving forces for advancing a fatigue crack, the stress intensity range, ΔK, and the maximum stress intensity, K_{max}.

In the proposed model, crack growth rates, [*da/dN*], where *a* is the crack length and *N* is the number of cycles, can be predicted by developing a [*da/dN*] relation with ΔK and K_{max} in terms of a power law in the form of:

$$\left[da/dN \right] = A(\Delta K - \Delta K_{th}^{*})^{n} (\Delta K_{\max} - \Delta K_{\max}^{*})^{m} \qquad \text{(Eq. 1.1)}$$

where ΔK_{th}^{*} and $\Delta K_{\max}^{*}$ are the two critical thresholds, ΔK_{max} is the maximum stress intensity range, and *A*, *n*, and *m* are material dependent constants.

Navarro et al. [21] promoted a micromechanical model known as the Navarro-Rios (NR) model which describes micro-structural sensitive crack propagation. The model describes the decrease in growth rate for a crack approaching a grain boundary, and also the eventual crack acceleration as the plastic zone spreads into neighbouring grains. The crack tip displacement changes in value in an oscillatory manner every time the crack approaches a grain boundary. The hindrance to the transfer of plasticity between the grains is included in the model by a numerical factor which takes into account the mismatch of the slip system at the grain boundary. The crack growth equation was given by:

$$\left[da/dN \right] = f_2 \phi_1 \qquad \text{(Eq. 1.2)}$$

where a is the crack length, N is the number of cycles, the factor f_2 represents the degree of irreversibility of slip during each stress cycle and can be equated to the fraction of the dislocations which are drawn into the crack during each reversal of stress cycle, and ϕ_1 is the crack tip displacement.

Hobson [22] proposed a model based on a grain boundary effect. He used a statistical approach to accommodate the factor describing this effect and proposed equations for micro-structurally and physically short crack growth. His micro-structurally short crack equation was given in the form:

$$\left[da_s \big/ dN \right] = C_2 (d - a_s) \qquad \text{(Eq. 1.3)}$$

where N is the number of cycles, C_2 is a material constant for the short crack region, a_s is the surface crack length, and d represents the distance to the first micro-structural barrier affecting crack growth. On the other hand, crack growth behaviour at lengths greater than the length d was expressed by the following equation:

$$\left[da_s \big/ dN \right] = C_3 a_s - D_1 \qquad \text{(Eq. 1.4)}$$

Where C_3 is a material constant and is a function of the stress-strain, a_s is the surface crack length, and D_1 represents the crack growth threshold.

Abdel Raouf et al. [23] developed a model based on surface strain localization and the reduced closure stress of short cracks. Their model for strain intensity factor was given as follows:

$$\Delta K_e = FE\Delta\varepsilon Q_\varepsilon \sqrt{\pi a} \qquad \text{(Eq. 1.5)}$$

$$Q_\varepsilon = 1 - qe^{-\alpha a} \qquad \text{(Eq. 1.6)}$$

Where, ΔK_e is the strain intensity factor range, F is a geometry factor, E is the modulus of elasticity, $\Delta\varepsilon$ is the local strain in the vicinity of the crack tip, Q_ε is the strain concentration factor, a is the crack depth measured from the free surface, q is a material constant, and α is a material parameter which is an inverse function of the grain size.

El Haddad [24] proposed a modified elastic and elastic-plastic fracture mechanics solution to predict the growth of short fatigue cracks. For elastic material behaviour, the elastic stress intensity factor, ΔK, of a short crack having a length a, was given by the following expression:

$$\Delta K = F\Delta S\sqrt{\pi(a+a_o)} \quad \text{(Eq. 1.7)}$$

where ΔS is the applied nominal stress range, a_0 is a constant for a given material and material condition and F is a geometry dependent constant**.** In plastically strained smooth and notched specimens, a strain based intensity factor was used. Rewriting Eq. 1.7 in terms of strains gives:

$$\Delta K = FE\Delta\varepsilon\sqrt{\pi(a+a_o)} \quad \text{(Eq. 1.8)}$$

where $\Delta\varepsilon$ is the nominal or local applied strains.

McEvily et al. [25] proposed a constitutive equation for the crack growth rate that takes into account the elastic-plastic nature of fatigue crack growth, the endurance limit as the controlling factor for extremely short crack propagation, and finally the closure in the wake of the crack that is a function of its length. The equation proposed in their analysis was in the following form:

$$\left[{}^{da}\!/_{dN}\right] = A\,(\Delta K_{eff} - \Delta K_{efffth})^2\left(1+\frac{\Delta K}{K_c - K_{\max}}\right) \quad \text{(Eq. 1.9)}$$

where a is the fatigue crack length, N is the number of load cycles, A is a material constant, ΔK_{eff} is the effective range of the stress intensity factor given by:

$$\Delta K_{eff} = K_{\max} - K_{op} \quad for\ K_{op} > K_{\min} \quad \text{(Eq. 1.10)}$$

$$\Delta K_{eff} = K_{\max} - K_{\min} \quad for\ K_{op} < K_{\min} \quad \text{(Eq. 1.11)}$$

where K_{max}, K_{min}, and K_{op} are the stress intensity factors for the maximum, minimum and opening stresses respectively. ΔK_{efffth} is the effective range of the stress intensity factor at the threshold level, ΔK is the stress intensity range factor, and K_c is the fracture toughness.

1.2.2 Fatigue Crack Growth: Long Cracks

Long crack fatigue growth can be described by the linear elastic fracture mechanics approach which is based on the application of the theory of elasticity to bodies containing cracks or defects where small displacements and a general linearity between the stresses and strains exist.

Irwin [26] showed that the stress ahead of a crack tip could be expressed in terms of the stress intensity factor, *K*, which depends on the loading condition, crack size, crack shape, and geometric boundaries, with the general form given by:

$$K = f(g)\sigma\sqrt{\pi a} \qquad \text{(Eq. 1.12)}$$

where σ is the remote stress applied, $f(g)$ is a geometric shape factor, and *a* is the crack length.

Paris et al. [15] proposed the following equation that has been shown to apply to the intermediate ΔK range shown in Figure 1.2:

$$\left[da/dN \right] = C(\Delta K)^m \qquad \text{(Eq. 1.13)}$$

where *C* and *m* are material constants, *a* is the crack length, *N is* the number of cycles and ΔK is the stress intensity factor range which is equal to the difference between the maximum and minimum stress intensity factors ($\Delta K = K_{max} - K_{min}$).

A plot of log *[da/dN]* versus log ΔK gives a sigmoidal curve (Figure 1.2). As shown the curve is divided into three regions. In region *A*, the cracking behaviour is associated with threshold (ΔK_{th}) effects. In region *B* the curve is essentially linear. Finally in region *C*, at high ΔK values, crack growth rates are extremely high and little fatigue life is involved. Many structures operate in region *B*, and most of the linear elastic fracture mechanics approaches were developed for this region. Under constant amplitude loading the crack growth life in terms of cycles to failure can be described by:

$$N_f = \int_{a_i}^{a_f} \frac{da}{C(\Delta K)^m} \qquad \text{(Eq. 1.14)}$$

where N_f is the number of cycles to failure, a_i is the initial crack length, and a_f is the final crack length.

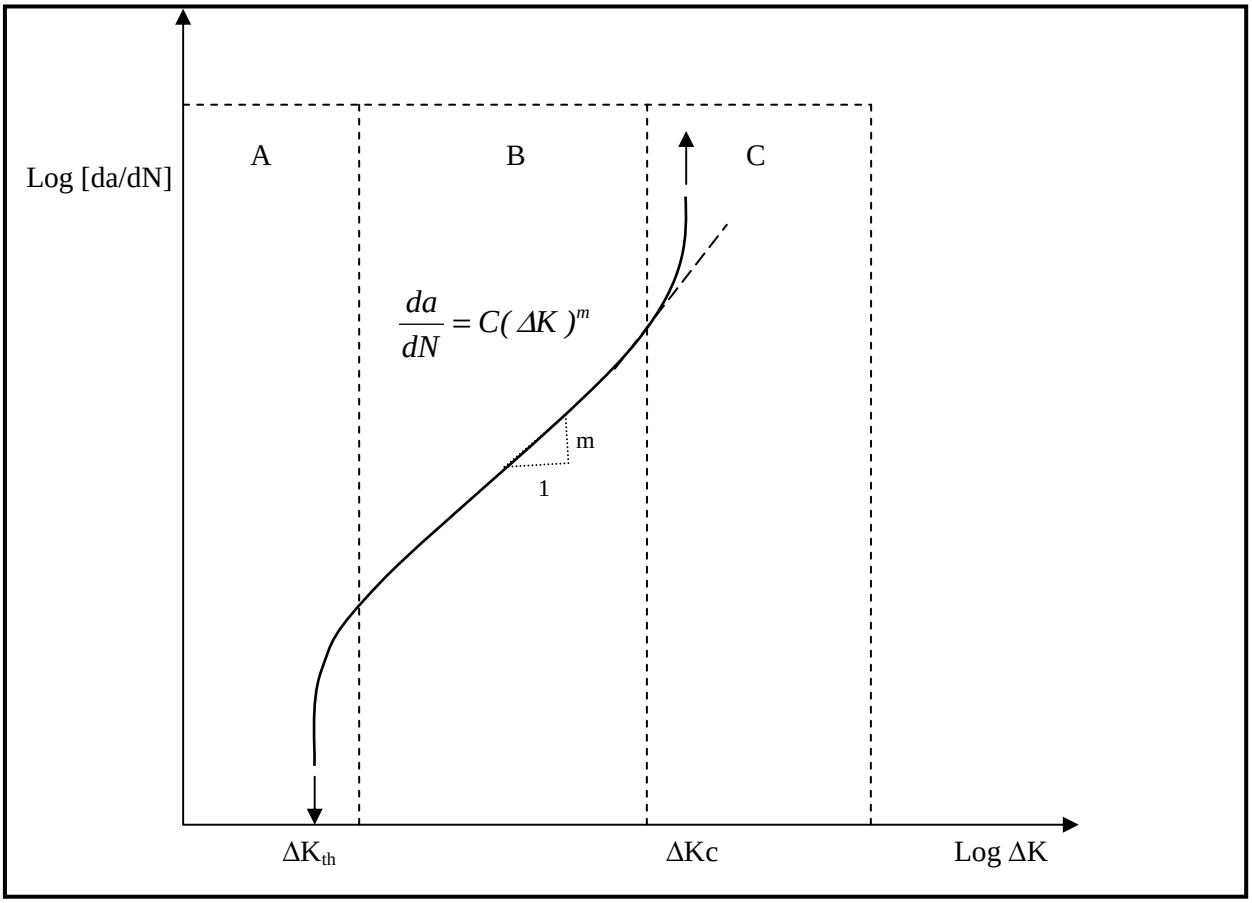

Figure 1.2 Crack growth rate [*da/dN*] versus the stress intensity range factor ΔK on a log-log scale

Mikheevskiy et al. [27] modified the "Uni-Grow" fatigue crack growth model originally proposed by Noroozi et al. [28] based on an analysis of the elastic-plastic stress-strain behaviour in the crack tip region. The fatigue crack growth expression was given in the form of:

$$\left[da/dN \right] = C\left(K_{\max,tot}^{p} \; K_{tot}^{1-p} \right)^{m} \qquad \text{(Eq. 1.13)}$$

where C is a fatigue crack growth rate constant, p is a driving force constant, $K_{max,tot}$ is the total maximum stress intensity factor, and K_{tot} is the summation of the maximum applied stress intensity factor and the residual stress intensity factor.

1.3 Fatigue Crack Closure

Since its discovery by Elber [29] in 1971, fatigue crack closure has been widely accepted as a significant mechanism affecting the crack growth behaviour of fatigue cracks, particularly in metallic materials. Fatigue crack closure involves the premature contact and consequent wedging of the crack faces during the unloading portion of a fatigue cycle at a load above the minimum load [30]. Elber [4] assumed the crack to be fully open or partially closed at positive minimum stresses because of a surplus of plastic deformation in the wake of the crack. He further introduced the concept of crack opening stress (S_{op}), the stress at which the crack becomes fully open, the effective stress range, (ΔS_{eff}), which is the difference between the maximum applied stress (S_{max}) and the crack opening stress (S_{op}) ($\Delta S_{eff} = S_{max} - S_{op}$), and the effective stress intensity range, (ΔK_{eff}) ($\Delta K_{eff} = F\Delta S_{eff}\sqrt{\pi a}$) shown in Figure 1.3. It is now generally understood that crack closure can occur under tensile loading by a variety of mechanisms discussed by Ritchie and Suresh [31]:

- Residual stress (plastic deformation) in the wake of the crack.
- Mismatch and roughness of separated crack surfaces.
- Crack surface oxidation and an asymmetric crack path.

One of the extensively studied mechanisms is plasticity induced closure. Even for this case, it has not been clearly established whether closure is caused by a band of stretched material in the wake of the growing crack, or by the compressive residual stresses ahead of the crack tip due to slip irreversibility [5]. McEvily [32] has reviewed the relative importance of several closure mechanisms and concluded that the effect of plasticity induced closure on crack growth is not as important as previously thought, except during overloads.

Figure 1.3 represents the different definitions of the stress intensity factors and ranges:

K_{max}: is the maximum stress intensity factor in a load cycle.

K_{min}: is the minimum stress intensity factor in a load cycle.

K_{th}: is the threshold stress intensity factor.

K_{op}: is the crack opening stress intensity factor.

ΔK: is the stress intensity factor range in a load cycle ($\Delta K = K_{max} - K_{min}$).

ΔK_{th}: is the threshold stress intensity factor range ($\Delta K_{th} = K_{th} - K_{min}$).

ΔK_{cl}: is the crack closure stress intensity factor range ($\Delta K_{cl} = K_{op} - K_{min}$).

ΔK_i: is the intrinsic stress intensity factor range ($\Delta K_i = \Delta K_{th} - K_{op}$).

ΔK^*: is the crack driving stress intensity factor range ($\Delta K^* = K_{max} - K_{th}$).

ΔK_{eff}: is the effective stress intensity factor range in a load cycle ($\Delta K_{eff} = K_{max} - K_{op}$), and ($\Delta K_{eff} = \Delta K_i + \Delta K^*$).

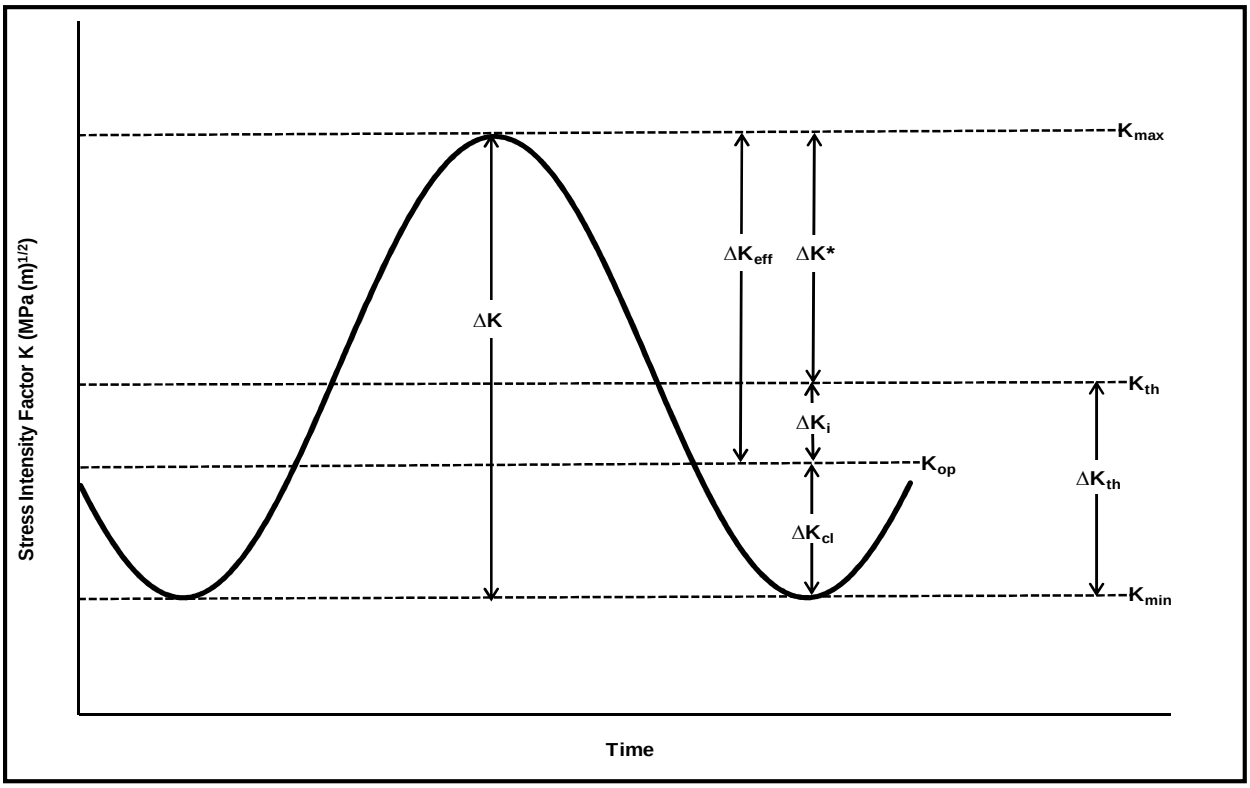

Figure 1.3 Definition of various stress intensity factors and ranges

1.4 Measuring Crack Closure

Several methods have been proposed to measure the crack opening stress (S_{op}). Since closure may involve contact of the two sides of the crack at a point beneath the observed surface plane, the only truly direct methods for observing closure are those capable of seeing beneath the crack surface and they include:

a) A confocal scanning laser microscope raster that scans a laser beam across a stationary specimen. The laser microscope produces images of specimens using reflected light, photoluminescence, and optical beam induced current.

b) Direct observations of the crack tip by using an optical microscope of high magnification. Observations on the crack tip profile can also be made with the replica technique and photogrammetry. However, these latter techniques are more time consuming than the former.

c) Compliance measurements that are essentially based on measuring the variation of the compliance with an increasing crack length. Such methods are used for automatic crack growth

measurements. As an example, a clip gauge may be mounted at the center line of a center cracked specimen, or the load line of a compact tension specimen. The clip gauge will provide readings with every crack growth increment, however care should be taken if the clip gage location is too close to the crack tip as the readings could be affected by the crack tip plasticity.

1.5 Fatigue Crack Closure in the Near-Threshold Regime

Lawson et al. [33] defined two thresholds that are currently used in fatigue. One is the fatigue crack propagation threshold which defines the stress intensity load under which cracks will not grow significantly. The second one is the fatigue limit which defines a loading criterion under which fatigue cracks that form will not propagate. Crack closure was found to play a significant role in influencing the kinetics of near-threshold crack propagation [34]. Particularly, the effects of microstructure, environment, loading condition, and crack size on the rates of near-threshold crack growth can be correlated with the development of crack closure. For many years linear elastic fracture mechanics (LEFM) has been used to describe how cracks propagate. The approach is simplest for long cracks, since in the absence of overloads, crack tip plasticity is limited in near-threshold fatigue; LEFM provided the tool of choice for describing near-threshold crack propagation. Yu et al. [35] concluded that the measured threshold stress intensity factor range, ΔK_{th}, is composed of two parts: the intrinsic stress intensity range ΔK_i and the crack opening stress intensity, K_{op}. When the stress ratio is high and the crack opening stress is below the minimum stress the measured threshold stress intensity range is ΔK_{th} equal to ΔK_i. Several factors may affect near-threshold crack propagation and they include:

- *Effect of yield strength:* Ritchie et al. [30] collected data for steels and plotted threshold stress intensity vs. yield stress. They noted that there was a negative slope; higher yield stresses led to lower thresholds. They attributed this effect to hydrogen embrittlement where the tensile stress field attracted hydrogen to the crack tip, thus weakening the metal. Other explanations for the reduction of the threshold stress intensity range in steels with increasing strength have been given based on the idea of a sharper crack tip.
- *Effect of grain size:* Topper et al. [36] concluded that microstructure has a great effect on the fatigue thresholds. Grain size effects are not entirely separable from yield stress effects due to the Hall-Petch relation which sets the yield stress as being inversely proportional to the square root of grain size [33]. Taira et al. [37] examined the growth rates of short cracks and concluded that the rate decreases significantly when the size of the plastic zone is approximately equal to the grain size. Other models [38] argued that smaller grains allow slip bands to reach the grain boundaries at lower stress intensities thus reducing the threshold and increasing the speed of propagation.

- *Effect of stress ratio:* to provide a physical explanation for stress ratio effects, crack closure is usually cited. As defined previously, crack closure is the premature closure of a crack due to the presence of an obstacle within it such as might result from plastic deformation, oxides, or metal particles. Crack closure reduces the open part of the stress intensity range as it is seen at the crack tip by limiting the range of relative motion of the two fracture surfaces of a crack [33].
- Another aspect of crack closure is the *partial crack closure phenomenon*. Bowles et al. [39] found that cracks close but not all the way to the crack tip. When a fatigue crack closes, a region near the crack tip stays open even under the minimum load. Lados et al. [40] proposed a partial closure model for ΔK_{eff} in the form of:

$$\Delta K_{eff} = K_{\max} - \frac{2}{\pi} K_{op} \qquad \text{(Eq. 1.14)}$$

where ΔK_{eff} is the effective stress intensity factor range, K_{max} is the maximum applied stress intensity factor, and K_{op} is the crack opening stress intensity factor.

1.6 Fatigue Crack Closure in Constant and Variable Amplitude Loading

For many years constant amplitude data obtained from smooth specimens has been used to evaluate the fatigue life of components. Unfortunately such data turned out to be unreliable and non-conservative for predicting variable amplitude fatigue behaviour for both smooth laboratory specimens and components in service. Due to the random nature of variable amplitude loading, modeling the crack growth in structures under such circumstances is a complex subject. Over the past three decades a number of load interaction models have been developed to correlate fatigue crack growth rates and predict crack growth under variable amplitude loading. It is now well documented in the literature that crack growth under variable amplitude loading can be partly explained through changes in fatigue crack closure and crack opening stress.

In constant amplitude fatigue loading, the crack opening stress after being reduced by an underload (compressive overload) increases to its steady state level in an approximately exponential manner. This behaviour was reported in the work of Minakawa et al. [41]. Several techniques have been employed to quantify the crack opening stress under constant amplitude loading.

DuQuesnay et al. [42] proposed an empirical model for the steady state crack opening stress, S_{opss}, under constant amplitude loading that has the form:

$$S_{opss} = \theta \sigma_{\max} \left[1 - \left(\frac{\sigma_{\max}}{\sigma_y} \right)^2 \right] + \varphi \sigma_{\min} \qquad \text{(Eq. 1.15)}$$

where σ_{max} and σ_{min} are the nominal maximum and minimum stresses in a smooth specimen, or the local maximum and minimum stresses at the notch root in a notched specimen respectively. σ_y is a material constant, θ and φ are two experimentally determined constants for each material obtained by measuring crack opening stresses.

1.6.1 Effect of Tensile Overloads

The effect of an overload to a stress level less than one half of the yield limit has often been described by examining a crack subjected to constant amplitude cyclic loading with a superimposed overload cycle [5]. Two observable facts are attributed to the application of tensile overloads. A post overload increase in crack closure level and crack growth retardation occurs when the applied overload is less than about one half the yield stress of the material. However an overload of value greater than one half the yield stress of the material will tend to decrease the closure level and accelerate crack growth.

1.6.2 Effect of Tensile Overloads Less than One Half of the Yield Strength

In the low stress region Ellyin and Wu [43] found that an overload ratio of 1.5 causes a three-fold increase in the plastic zone size ahead of the crack. Makabe et al. [44] showed that the rate of fatigue crack growth following a single tensile overload is controlled by the contraction of the material in the overload plastic zone ahead of the crack tip. Tensile overloads in constant amplitude loading increase the monotonic plastic zone size by stretching the material ahead of the crack tip. As the fatigue crack penetrates the overload plastic zone, the crack closure level increases reducing the effective stress intensity factor range, ΔK_{eff}, and results in a lower crack growth rate. Khalil et al. [45] found that an increase in crack closure level after an overload and a subsequent retardation of the crack growth occur when the applied overload is less than approximately one half of the yield stress of the material. Topper and Yu [36] studied the effect of constant amplitude loading proceeded by three repeated tensile overloads on a centre notched specimen of annealed SAE 1010 steel. The tensile overloads caused significant crack growth retardation and could even arrest crack growth.

Kim and Tai [46] showed that crack growth retardation after an overload is most effective for low stress intensity ranges and high overload ratios. Makabe et al. [44] in their study of stress ratio effects noticed that when the stress ratio was equal to zero, the usual delayed retardation of the crack growth following an overload was observed. On the other hand, when a negative stress ratio was applied, acceleration in the rate of the crack growth occurred after applying the overload. Ward-Close et al. [47] studied the effect of a single overload on crack growth rate in IMI 550 titanium alloy. They concluded that upon applying the overload, blunting of the crack tip occurs and an initial increase in the crack growth rate is observed. However, a significant retardation of the crack growth then occurs as the crack grows into the overload plastic zone in which the compressive residual stresses increase the crack closure level.

1.6.3 Effect of Tensile Overloads Greater than One Half the Yield Strength

When fatigue cracks grow from notches the local stresses at high load levels often approach or exceed the yield stress. Jurcevic et al. [48] studied the fatigue behaviour of centre notched specimens of a 2024-T351 aluminum alloy under periodic overloads of yield stress magnitude followed by smaller stress cycles. They found that the fatigue strength of the notched specimens was drastically decreased by periodic overloads and attributed this behaviour to an absence of the crack closure. Dabayeh et al. [49] showed that at the high stress levels associated with the initiation and growth of cracks from notches both tensile and compressive overloads typically cause local stresses of the order of the yield stress. These stresses cause a reduction in the crack closure level and an increase of the crack growth. Pompetzki et al. [50] investigated periodic tensile overloads of yield stress magnitude and found an acceleration of fatigue damage. They proposed a damage model based on crack closure concepts in which the crack opening stress was reduced immediately following a high stress overload.

1.6.4 Effect of Compressive Underloads

It is known now that compressive underloads applied during a constant amplitude loading test can have a marked effect on the subsequent crack propagation behaviour. Skorupa [51] attributed the crack growth acceleration after a single underload to altered residual stresses ahead of the crack tip and to a reduction of crack closure. Preloading in compression gives rise to a tensile residual stress field at a notch root thus producing a tensile stress intensity factor range, ΔK, locally within the tensile residual stress zone and thus accelerating the crack growth rate. Makabe et al. [44] reported on the effect of an underload on the crack opening stress level. They noticed that immediately following an underload the crack opening stress level was reduced to a value near zero, after an additional crack growth increment of 0.6

mm, the crack opening level had risen and was close to the level prior to the underload. Varvani and Topper [52] showed that the application of an underload in the absence of a prior overload mainly contributes to the flattening of the asperities in the crack wake that are responsible for roughness-induced crack closure. Subsequently, this increases the effective stress intensity factor and accelerates crack propagation. Dabayeh et al. [49] investigated the effect of compressive and intermittent compressive underloads on an aluminum alloy and SAE 1045 steel. They found that after a compressive underload the crack opening stress was reduced, they also noted an immediate decrease in the crack opening stress following either a near-yield stress tensile or compressive underload. Yu et al. [53] reported results on the effect of compressive overloads on fatigue crack growth. They concluded that in compression-tension tests the crack propagation rate increased and the threshold stress intensity decreased linearly with an increase in the magnitude of the compressive peak stress. Makabe et al. [44] studied the effect of applying an overload - underload sequence on the rate of fatigue crack growth. They noticed that an underload partially undid the effects of the overload by causing reverse plastic flow and that the material contraction at the crack tip during the tensile overload was replaced by bulging after the compressive overload. Dabayeh et al. [49] examined the changes in crack opening stress level after the application of a large near-yield stress level tensile-compressive overload cycle. They found that the overload lowered the crack opening stress level abruptly and that a large number of constant amplitude small cycles were needed to return the opening stress to its steady state level.

1.7 Crack Opening Stress Build-Up

Dabayeh [54] proposed an empirical formula to simulate the build-up of crack opening stress after an underload in terms of the ratio of the difference between the instantaneous crack opening stress of the small cycles (S_{op}) in the loading block history and the post overload crack opening stress level (S_{opol}), and the difference between the steady state crack opening stress of the small cycles (S_{opss}) and the post overload crack opening stress level:

$$\frac{\left(S_{op}-S_{opol}\right)}{\left(S_{opss}-S_{opol}\right)}=1-\psi\ Exp\left(-b\left(N/N_{0.8}\right)^{\alpha}\right) \qquad \text{(Eq. 1.16)}$$

where ψ, b, and a are material constants, N is the number of cycles following the overload, $N_{0.8}$ is the number of cycles following the overload at which the normalized recovered stress (S_{op}-S_{opol}) / (S_{opss}-S_{opol}) reaches 80% of its steady-state level. However, Khalil et al. [55] found that the application of Dabayeh [54] formula to complex load histories was complicated. They suggested the use of a simpler model

initially proposed by Vormwald and Seeger [56] which relates the change in the crack opening stress in a given cycle to the difference between the current crack opening stress, S_{cu}, and the steady state crack opening stress, S_{opss}, in the form of:

$$\Delta S_{op} = m(S_{opss} - S_{cu}) \qquad \text{(Eq. 1.17)}$$

where ΔS_{op} is the increase in crack opening stress during a load cycle and m is a material constant.

1.8 Purpose and Objective of the Thesis

The significance of crack closure arises from the fact that it is related to fatigue crack growth under service loads, and until now most of the proposed models in the literature do not provide satisfactorily results to predict even qualitatively the growth of fatigue cracks under variable amplitude loading. Fatigue life estimates for components subjected to variable amplitude service loading are usually based on the same constant amplitude strain-life data used for constant amplitude fatigue predictions. Although the resulting fatigue life estimates are accurate for constant amplitude fatigue, they are always non-conservative for the initiation and growth of cracks in variable amplitude load histories. Similarly fatigue life predictions based on small crack growth calculations for cracks growing from flaws in notches are non-conservative when constant amplitude crack growth data are used. These non-conservative predictions have been shown to be due to severe reductions in fatigue crack closure arising from large (overload or underload) cycles in a typical service load history. Smaller load cycles following a large near yield stress overload cycle experience a much lower crack opening stress than that experienced by the same cycles in the reference constant amplitude fatigue tests used to produce design data. This reduced crack opening stress results in the crack remaining open for a larger fraction of the stress-strain cycle and thus an increase in the effective portion of the stress-strain cycle. The effective strain range is increased and the fatigue damage for the small cycles is greater than that calculated resulting in a non-conservative fatigue life prediction.

The main thrust of this thesis is to:

1. Provide a better understanding of fatigue crack closure behaviour in small cracks at the high stress levels they experience while they are growing through notch stress fields.
2. Provide a better understanding of the underloads and the way they accelerate small crack growth and damage.
3. Develop a test procedure to obtain data for crack opening stress recovery to a steady state level after underloads (and the associated crack closure parameter) from smooth specimen tests.
4. Calibrate models to perform strain-life and small crack growth fatigue analysis.

5. Provide information concerning the way metal hardness affects the steady state crack closure level, the rate of crack opening stress recovery to a steady state level after an underload and the average crack closure level in variable amplitude fatigue.

To be accepted for use in industry a fatigue design procedure, the fatigue analysis model and the data needed for its implementation have to be shown to give accurate predictions in tests that closely model in-service conditions. In addition the analysis models should be easy to use and the fatigue data required should come from inexpensive tests. Provided that accurate data for crack opening stress recovery after an underload are successfully generated from the proposed smooth specimen underload fatigue tests, all the data needed to implement the fatigue analysis model can be obtained from smooth specimen tests at similar cost to that required to generate the currently used constant amplitude fatigue data. After making a few changes to the crack closure model to improve the manner in which it determines the cycles for which the crack opening stress should be increased (it will not increase for a cycle in which no crack growth takes place) the model parameters are calibrated using data generated from smooth specimen tests. The model is then used in strain-life and crack growth analyses to predict fatigue lives of specimens subjected to two SAE load histories that are used as standards in the automotive industry. Test samples included a smooth specimen used to examine strain-life predictions and a notched specimen with a flaw in the notch root used to examine predictions made using short crack fracture mechanics.

1.9 Outline of the Thesis

- *Chapter 2* provides a description of the two models used in this thesis to predict fatigue lives under variable amplitude loading; the effective strain-life curve model and the fatigue crack growth model.
- *Chapter 3* describes the materials used in this study, their mechanical properties, the experimental program, the apparatus used, and the test techniques.
- *Chapter 4* examines the experimental and the theoretical results for Dual Phase 590 steel. Underload fatigue data, measured steady state crack opening stresses and crack opening stress build-up under three stress ratios, the results of damage tests and the calibrated closure constant "*m*" used to predict the crack opening stress build-up, and crack growth rates are also presented in this chapter. Finally the predicted fatigue lives using the effective strain-life model and the fatigue crack growth model are compared with experimental results under two service load histories.

- *Chapter 5* examines the experimental and the theoretical results for SAE 1045 steel. Underload fatigue data, measured steady state crack opening stresses and crack opening stress build-up under three stress ratios, the results of damage tests and the calibrated closure constant "*m*" used to predict the crack opening stress build-up, and crack growth rates are also presented in this chapter. Finally the predicted fatigue lives using the effective strain-life model and the fatigue crack growth model are compared with experimental results under two service load histories.
- *Chapter 6* examines the experimental and the theoretical results for AISI 8822 steel. Underload fatigue data as well as steady state crack opening stresses are presented in this chapter. Results of the damage tests and the calibrated closure constant "*m*" used to predict the crack opening stress build-up are also provided in this chapter. Finally the predicted fatigue lives using the effective strain-life model are compared with the experimental fatigue lives for two service load histories.
- *Chapter 7* discusses the outcomes of this investigation and provides a comparison of the results for the three materials used.
- *Chapter 8* provides the general conclusions of the thesis and future recommendations.

Chapter 2
Analytical Modeling

2.1 Introduction

The main objective of this thesis is to provide a better understanding of fatigue crack closure behaviour in small cracks at the high stress levels they experience while they are growing through notch stress fields, and the way in which compressive underloads accelerate small crack growth and damage. Another aim of this work is to develop a methodology and a test procedure to obtain the constants for an effective strain-life curve, an effective stress intensity crack growth curve, an equation for crack opening stress recovery to a steady state level after underloads, and the associated steady state crack closure parameter, all this from easily performed smooth specimen fatigue underload tests rather than from time consuming direct measurements of changes in small fatigue crack closure stress. Two fatigue life prediction models are adopted in this work; the effective strain-life fatigue model and the effective fatigue crack growth model.

2.2 Effective Strain-Life Fatigue Prediction Model

The usual analysis procedure for variable amplitude fatigue calculates the fatigue damage based on constant amplitude strain-controlled fatigue tests of smooth specimens. The resulting predictions are typically non-conservative due to a load interaction effect in variable amplitude fatigue. Moreover, two investigations [57] and [58] have shown that for variable amplitude loading, experimental fatigue lives can be lower than the fatigue lives predicted using constant amplitude fatigue data by factors as great as 10. The reason for this is that the large load cycles which cause local notch stresses of the order of yield stress reduce the crack opening stress and increase the effective stress for subsequent smaller cycles thus increasing their damage [59]. Important components of this model are the crack opening stresses and strains. Once crack opening strains are available, the effective strain in a cycle can be calculated directly as the difference between the maximum strain and the crack opening strain. However, measuring crack opening stresses in order to calculate the crack opening strains at the high local stress levels and short crack lengths associated with the growth of cracks from stress raisers is time consuming and requires equipment not found in many laboratories [49]. One of the aims of this thesis is to obtain the parameters for the model with a minimum amount of testing effort by developing a new test procedure (Chapter 3, Section 3.3.3.2) for modeling changes in crack opening stress level and fatigue damage using data derived from periodic underload fatigue tests of smooth specimens.

2.2.1 Layout of the Effective Strain-Life Fatigue Model

The components used to implement this model and predict fatigue lives under variable amplitude loading are as follows:

1. Determination of the material properties (monotonic and cyclic) through a series of monotonic tension tests and fully reversed constant amplitude strain controlled tests.
2. Calculation of the local stresses and strains in a variable amplitude load history by following the stress-strain history on a reversal by reversal basis.
3. Rainflow cycle counting of the applied loading history to determine the closed stress-strain loops.
4. Calculation of the crack opening stresses (S_{op}) for each closed loop cycle in the loading history.
5. Calculation of the effective strain range ($\Delta\varepsilon_{eff}$) for each closed loop cycle in the loading history.
6. Calculation of the damage of each closed loop cycle in the loading history.
7. Fatigue failure is predicted when the damage sum reaches unity.

Figure 2.1 shows the algorithm for this model.

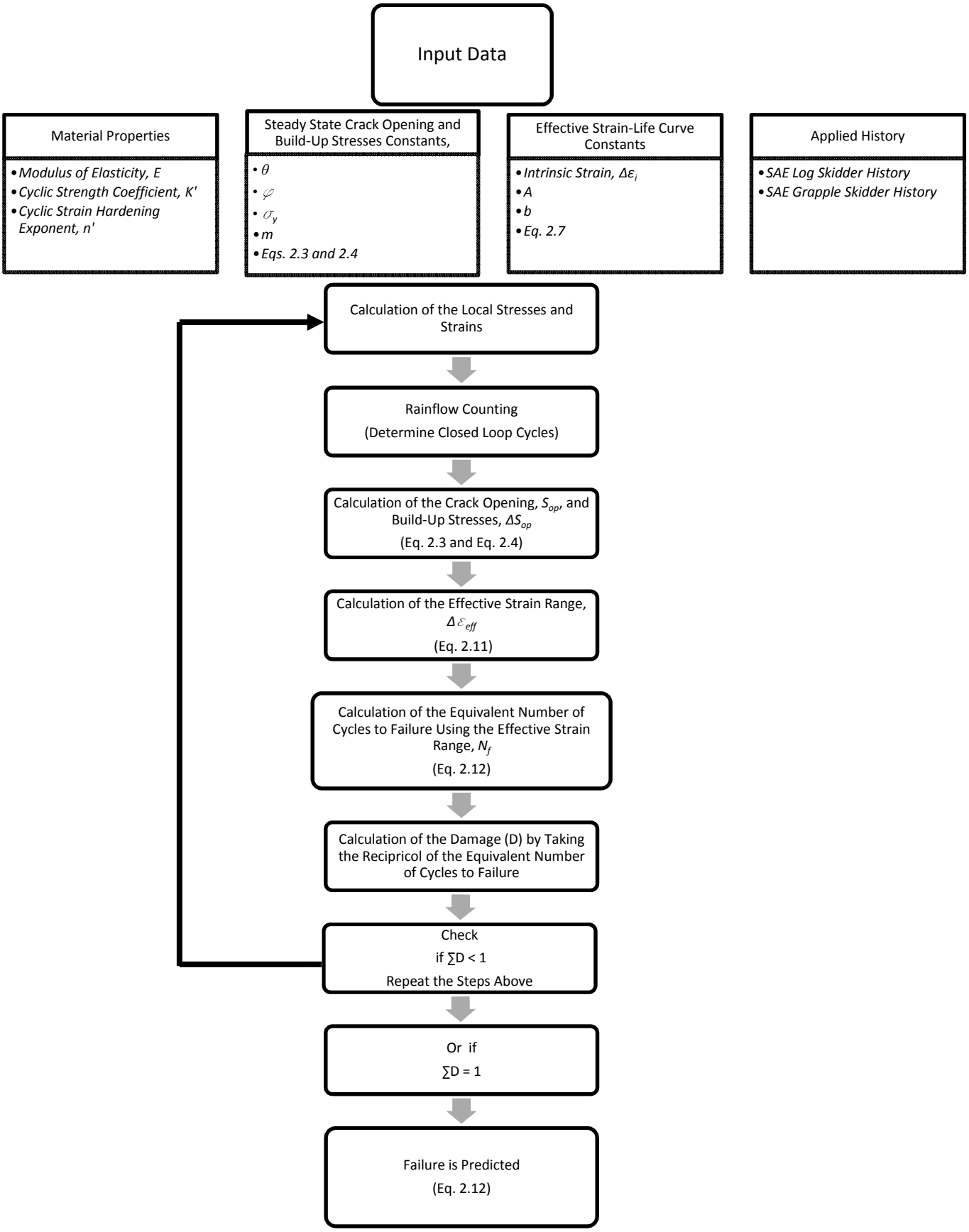

Figure 2.1 Algorithm for the effective strain-life model

2.2.2 Determination of Material Properties

Monotonic and cyclic properties of the three materials used were determined through a series of tension tests and fully reversed constant strain amplitude tests. The results are summarized in Chapter 3 Sections 3.1.1, 3.1.2, and 3.1.3.

2.2.3 Calculation of the Local Stresses and Strains

The material's cyclic stress-strain curve and a doubled stress-strain curve were employed to estimate the local stresses and strains for a given loading history for the smooth specimens.

$$\frac{\Delta\varepsilon}{2} = \frac{\Delta\sigma}{2E} + \left(\frac{\Delta\sigma}{2K'}\right)^{1/n'} \qquad \text{(Eq. 2.1)}$$

$$\Delta\varepsilon = \frac{\Delta\sigma}{E} + 2\left(\frac{\Delta\sigma}{2K'}\right)^{1/n'} \qquad \textit{Double Stress-Strain Curve} \qquad \text{(Eq. 2.2)}$$

where K' is the cyclic strength coefficient, n' is the cyclic strain hardening exponent, and E is the modulus of elasticity. The three constants mentioned above were obtained through a series of fatigue tests under constant amplitude loading as explained in Chapter 3 section 3.3.2.

2.2.4 Rainflow Cycle Counting

The Rainflow Cycle Counting method described in ASTM Standard No. E1049 [60] was used to reduce the complex applied variable amplitude histories to closed hysteresis loops with defined maximum and minimum stresses and strains.

2.2.5 Calculation of the Crack Opening Stresses

2.2.5.1 Crack Opening Stresses under Constant Amplitude Loading

Under constant amplitude loading, the crack opening stress increases to a level and then remains constant at this level which is referred to as the steady state crack opening stress. Figure 2.2 describes the increase in crack opening stresses (in an exponential manner [41]) with crack length under constant amplitude loading. After a short build up distance (in this case the crack opening stress starts below the steady state opening stress due to the application of a compressive underload), the level of the crack opening stress remains constant with further cycling.

Several techniques have been employed to quantify the steady state crack opening stress under constant amplitude loading. In this thesis two methods were used to obtain the steady state crack opening stresses:

1. Direct measurements of the steady state crack opening stress (for 3 stress ratios*) through a series of experimental tests described in Chapter 3 Section 3.3.4.
2. Derivation of the steady state crack opening stresses using the constant amplitude and the effective strain-life curves as explained in Section 2.8.2 and in Appendix A.

The data obtained from the two previous methods were used to obtain the material constants in the equation proposed by DuQuesnay et al. [42] (Eq. 2.3) for calculating the steady state crack opening stress (S_{opss}) under constant amplitude loading:

$$S_{opss} = \theta \sigma_{\max} \left[1 - \left(\frac{\sigma_{\max}}{\sigma_y} \right)^2 \right] + \varphi \sigma_{\min} \qquad \text{(Eq. 2.3)}$$

where σ_{max} and σ_{min} are the nominal maximum and minimum stresses in a stress-strain cycle in a smooth specimen, or the local maximum and minimum stresses at the notch root in a notched specimen respectively. σ_y is a material constant, θ and φ are two experimentally determined constants for each material obtained by fitting Eq. 2.3 to either calculated (from the constant amplitude and the effective strain-life curves) or measured crack opening stress data.

* The stress ratio is defined as the minimum stress in a cycle divided by the maximum stress $\left(R = \sigma_{\min} / \sigma_{\max} \right)$

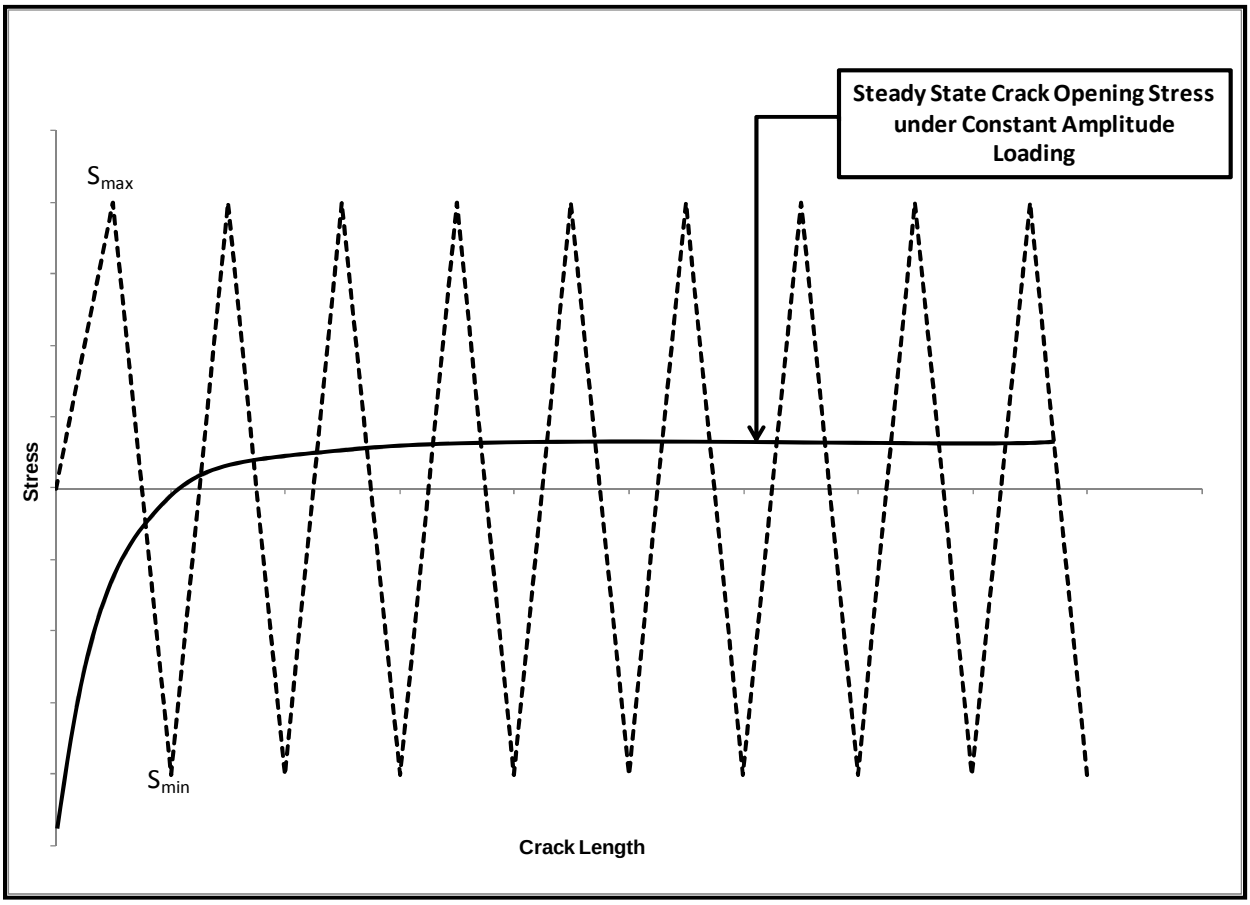

Figure 2.2 Steady state crack opening stress under constant amplitude loading

2.2.5.2 Crack Opening Stress Build-Up

For variable amplitude fatigue loading it is very important to take into account the load interaction effect. There are abrupt crack closure decreases during large near yield stress cycles in a variable amplitude loading history. These large cycles result in a greater effective stress range (see Figure 2.3) and therefore a greater damage for the following smaller cycles than there would be for cycles in the constant amplitude reference tests used to produce the conventional strain-life fatigue data. In order to model the crack opening stress changes during a loading history, a crack opening stress build-up equation [56] and [1] was used:

$$\Delta S_{op} = m(S_{opss} - S_{cu}) \qquad \text{(Eq. 2.4)}$$

where ΔS_{op} is the change in crack opening stress, S_{opss} is the steady state crack opening stress, S_{cu} is the current crack opening stress, and m is a material constant obtained through a series of experimental tests described in Chapter 3 Section 3.3.3.2. This equation describes the recovery of the crack opening stress after the application of an underload to its steady state condition.

2.2.6 The Effective Strain-Life Curve

The effective strain-life curve was generated through a series of underload fatigue tests described in Chapter 3 Section 3.3.3.1. The effective strain-life curve served several purposes including:

1. Fitting fatigue lives under a variable amplitude loading history (underload tests).
2. Calibrating the constants in Eq. 2.3.
3. Calculating the steady state crack opening stresses of closed loop cycles in a load history.
4. Calculating the fatigue damage of each closed loop cycle in a load history.
5. Predicting the fatigue lives under variable amplitude loading.

2.2.6.1 Constructing the Effective Strain-Life Curve

In order to construct the effective strain-life curve a series of underload fatigue tests were performed (Chapter 3, Section 3.3.3.1). The aim of these tests was to keep the crack opening stress under the minimum stress of the small cycles (see Figure 2.3 - Left) through the frequent application of a compressive near yield limit underload so that we would have fully effective small cycles free from crack closure. The effective strain range (see Figure 2.4) is the range of a strain for which a fatigue crack is open during a cycle, and it is given as the difference between the maximum strain and the greater of the crack opening strain or the minimum strain in a cycle. Previous work at Waterloo [61] introduced a damage parameter given by:

$$E\Delta\varepsilon^{*} = E\Delta\varepsilon_{eff} - E\Delta\varepsilon_{i} \qquad \text{(Eq. 2.5)}$$

Where E is the elastic modulus of elasticity and $\Delta\varepsilon_i$ is a material's intrinsic fatigue limit strain range below which a fully open crack will not cause fatigue damage. The strain range $\Delta\varepsilon^*$ is the part of the strain range which causes fatigue crack growth and damage. This parameter was found to be related to the fatigue life by a power law [62]:

$$E\Delta\varepsilon^{*} = A(N_f)^{b} \qquad \text{(Eq. 2.6)}$$

where A and b are material constants determined from underload fatigue tests.

The $E\,\Delta\varepsilon^*$ *vs.* N_f and the $E\Delta\varepsilon_i$ vs. N_f curves were obtained by choosing a value of $E\Delta\varepsilon_i$ which made the curve of $E\,\Delta\varepsilon^*$ values (calculated from Eq. 2.5) *vs.* N_f linear on logarithmic scale. In this process $\Delta\varepsilon_{eff}$ was the strain range of the small cycles in an underload test. For curve fitting purposes, an additional data

point was added to the underload curve (based on prior experimental observations) by calculating the effective strain range at a 2% total strain range assuming that the crack in the 2% strain range constant amplitude test opens at one half the minimum stress [49]. After obtaining the $E\,\Delta\varepsilon^*$ range and the values of A and b in Eq. 2.6, the effective strain-life curve was constructed using Eq. 2.7:

$$\Delta\varepsilon_{eff} = \frac{A}{E}(N_f)^b + \Delta\varepsilon_i \qquad \text{(Eq. 2.7)}$$

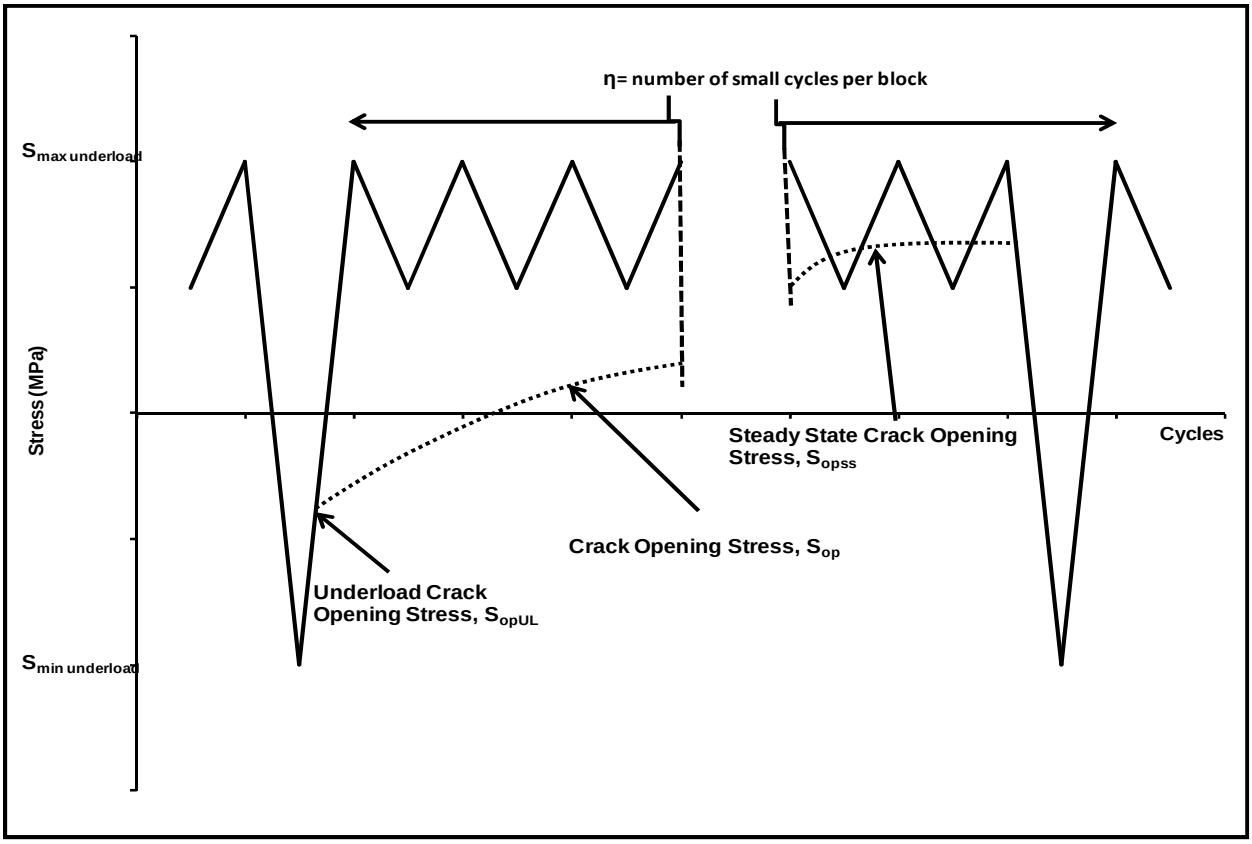

Figure 2.3 Crack opening stress build-up after underload cycles in variable amplitude history

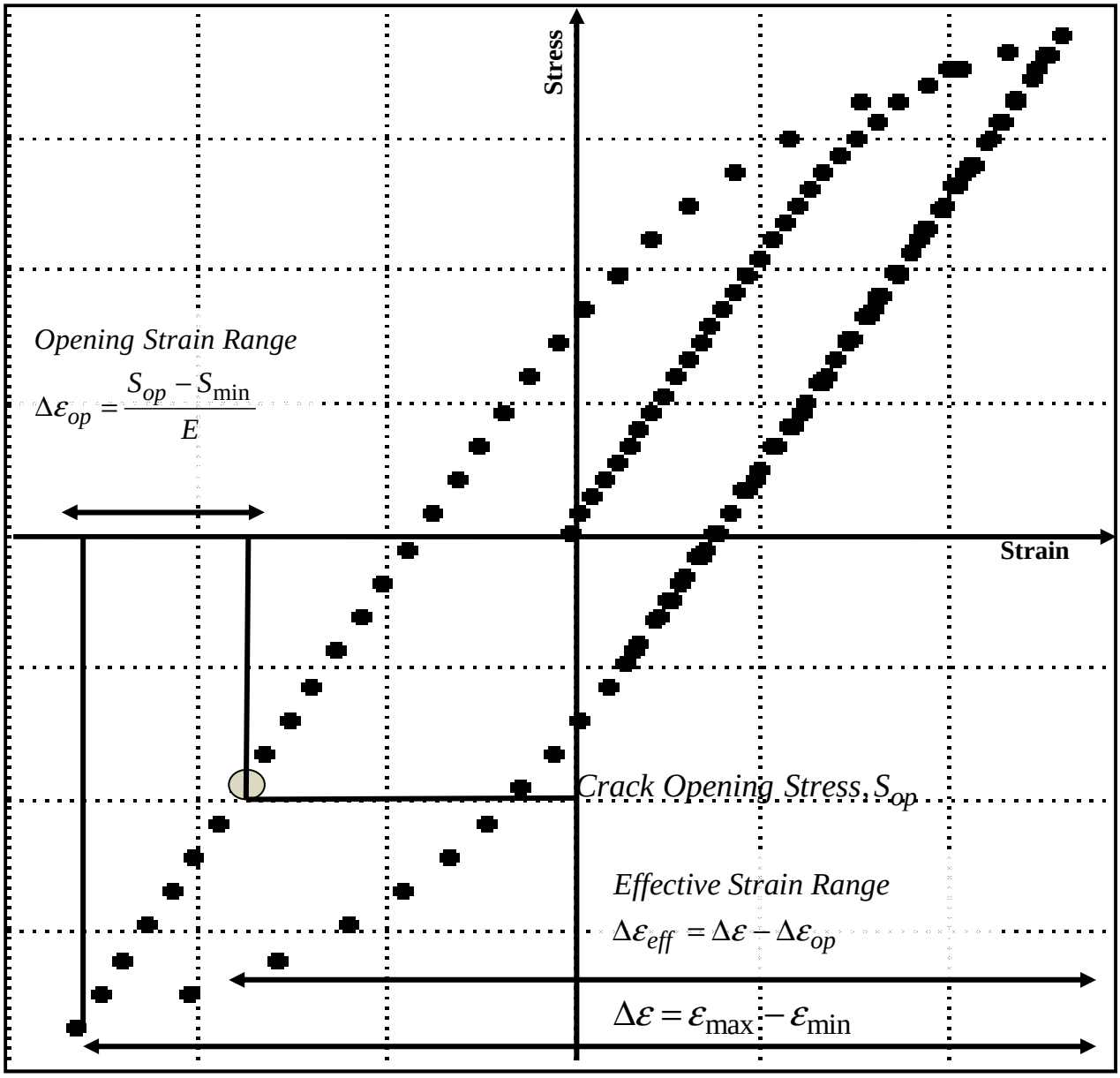

Figure 2.4 Definition of the effective and crack opening strain ranges in a stress-strain loop cycle

2.2.6.2 Using the Effective Strain-Life Curve to Calculate the Steady State Crack Opening Stresses

The constant amplitude and effective strain-life curves were used to calculate the steady state crack opening stresses. The data obtained was then used to obtain the constants in DuQuesnay's equation (Eq. 2.3). The difference between the strain range at a given fatigue life in a fully reversed constant amplitude fatigue life curve, $\Delta\varepsilon_{CA}$, and that in the effective strain-life curve at a given fatigue life, $\Delta\varepsilon_{eff}$, given in Eq. 2.8 is equal to the difference between the constant amplitude test minimum strain, ε_{min}, and the estimated crack opening strain, ε_{op}, in the constant amplitude stress-strain loop (see Figure 2.4).

$$\Delta\varepsilon_{CA} - \Delta\varepsilon_{eff} = \varepsilon_{op} - \varepsilon_{\min} = \frac{S_{opss} - S_{\min}}{E} \qquad \text{(Eq. 2.8)}$$

Therefore the estimated constant amplitude steady state crack opening stress (S_{opss}) can be written as follows:

$$S_{opss} = S_{\min} + E(\Delta\varepsilon_{CA} - \Delta\varepsilon_{eff}) \qquad \text{(Eq. 2.9)}$$

The values of S_{opss} were then used to obtain the constants in the equation for the steady state crack opening stress under constant amplitude loading proposed by DuQuesnay et al. [42] by fitting Eq. 2.3 to the data obtained from Eq. 2.9.

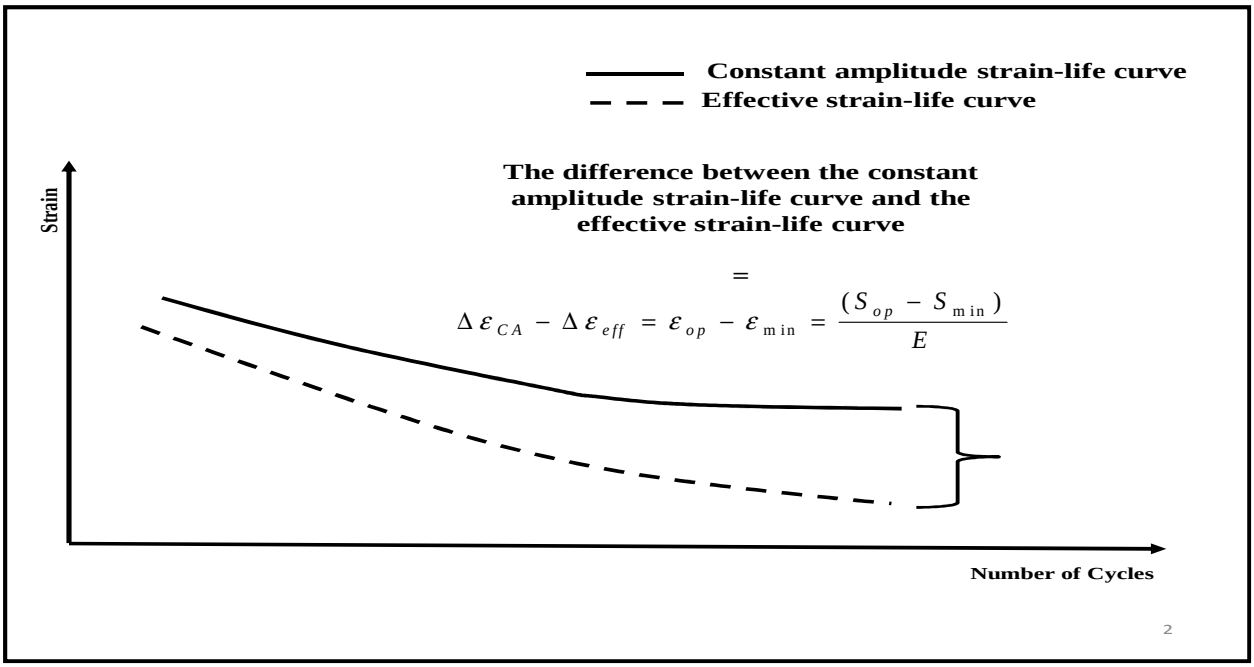

Figure 2.5 The difference between the constant amplitude and the effective strain range

2.2.7 Fatigue Damage Calculation

DuQuesnay [63] proposed a model to calculate the damage done by small cycles following an underload based on the effective strain range. In his model several assumptions were made:

- Crack growth and damage occur during the portion of a cycle during which the effective strain range is above an intrinsic threshold value.
- Large "underload" cycles immediately decrease the effective stress range and thereby increase the damage done by subsequent smaller cycles.
- Small cycles have a negligible effect on the damage done by underload cycles and the small cycles large enough to do fatigue damage cause the effective stress range to decrease towards the steady state level.

DuQuesnay [63] applied Miner's damage summation to a periodic underload history consisting of blocks of one underload followed by varying numbers of smaller constant amplitude smaller cycles to obtain:

$$1 = \sum D_{OL} + \sum D_{SS} \quad \text{(At failure)} \qquad \text{(Eq. 2.10)}$$

Where D_{OL} is the damage due to the underloads, and D_{ss} is the damage due to the small cycles. In this investigation DuQuesnay's damage model and the effective strain-life curve were used instead of the traditional constant amplitude strain-life curve to make fatigue life predictions. The damage for a cycle was obtained by entering the effective strain into the effective strain-life curve and setting the damage equal to the reciprocal of the number of cycles to failure. Failure was predicted when the value of damage reached unity.

2.2.8 Fatigue Life Predictions for Service Load Histories

Two types of loading history were used to investigate the fatigue lives under variable amplitude loading; the SAE Grapple Skidder History, and the SAE Log Skidder History. Each applied history was scaled to give different maximum stress ranges and was then applied to smooth specimens under stress control.

In performing the fatigue life calculations the following steps were used:

1. The local stresses and strains in a specimen were calculated for the applied load history.
2. Rainflow counting was used to obtain the closed loop stress-strain cycles for the load history.
3. For the first closed loop cycle, the value of the steady state crack opening stress (S_{opss}) was calculated using Eq. 2.3.
4. For other closed loop cycle that followed, the crack opening stress (S_{op}) was calculated based on the following assumptions:
    - Using Eq. 2.3, the crack opening stress levels were modeled assuming that the crack opening stress for a given cycle instantaneously decreased to the constant amplitude steady state level for that cycle if this steady state crack opening stress (S_{opss}) was lower than the current opening stress (S_{cu}).
    - If the steady state crack opening stress (S_{opss}) was greater than the current opening stress (S_{cu}), the crack opening stress of that cycle followed the exponential build up formula of Eq. 2.4 unless the range of stress in that cycle was below the intrinsic stress range, or the maximum stress in that cycle was below zero in which case it didn't change because the crack would not advance to change the crack opening stress (these cycles for which there was no crack growth were not used in calculating the crack opening stress build up).
    - If the above condition did not apply, the crack opening stress increment calculated using Eq. 2.4 was added to the current level to give the opening stress at the end of the cycle.
    - This procedure was repeated for each cycle in the load history.
    - In summary, Eq. 2.3 together with Eq. 2.4 were used to calculate the crack opening stress levels for a cycle. If the stress level obtained from Eq. 2.3 was below the current stress level, the crack opening stress was lowered to the calculated level. If the level was higher, the crack opening stress was increased by the amount given by Eq. 2.4
5. After obtaining the crack opening stress of a cycle, the effective strain range was calculated using the following equation:

$$\Delta\varepsilon_{eff} = \Delta\varepsilon_{CA} - \Delta\varepsilon_{op}$$

$$\Rightarrow \qquad \text{(Eq. 2.11)}$$

$$\Delta\varepsilon_{eff} = \Delta\varepsilon_{CA} - \left(\frac{S_{op} - S_{\min}}{E} \right)$$

6. The effective strain range obtained from the previous step was then used to calculate the damage of the cycle using the effective strain-life curve:
    - First, the equivalent number of cycles were obtained by rearranging Eq. 2.7 into:

$$N_f = \left(\frac{E(\Delta\varepsilon_{eff} - \Delta\varepsilon_i)}{A} \right)^{1/b} \qquad \text{(Eq. 2.12)}$$

    - The damage of the cycle was calculated by taking the reciprocal of the equivalent number of cycles obtained using Eq. 2.12.
7. Steps 1 through 6 were applied to each closed loop cycle in the load history and the damage was summed. Failure was predicted when the summation of the damage reached unity.

2.3 Fatigue Crack Growth Model

The prediction of fatigue life using a strain based fracture mechanics approach together with models of crack closure was shown to yield accurate results for elastic and inelastic propagation of both short and long cracks under variable amplitude loading [64]. The two fundamental pieces of material data required for this type of analysis when applied to notched components are the closure-free crack growth rates (See Chapter 3, Section 3.3.5 for closure-free crack growth rate tests) vs. stress intensity factor range data, and crack opening stress vs. maximum and minimum stress data obtained from DuQuesnay's equation (Eq. 2.3) calibrated using directly measured crack opening stress data or data obtained from the constant amplitude and the effective strain-life curves (Section 2.2.6.2).

2.4 Layout of the Fatigue Crack Growth Model

The components used to implement the fatigue crack growth model and predict fatigue lives under variable amplitude loading were as follows:

1. Determination of the material properties (monotonic and cyclic) through a series of monotonic tension tests and fully reversed constant amplitude tests.
2. Calculation of the local stresses and strains by following the stress-strain history due to the applied load history on a reversal by reversal basis.
3. Rainflow cycle counting of the applied loading history to determine the closed stress-strain loops.
4. Calculation of the crack opening stresses for each closed loop cycle in the loading history.
5. Calculation of the effective strain range for each closed loop cycle in the loading history.
6. Calculation of the effective strain intensity factor.
7. Calculation of the crack increments and the total crack length.
8. Fatigue failure was predicted when the maximum stress intensity exceeded the fracture toughness or if the crack length exceeded half the specimen width.

Figure 2.6 shows the algorithm for this model.

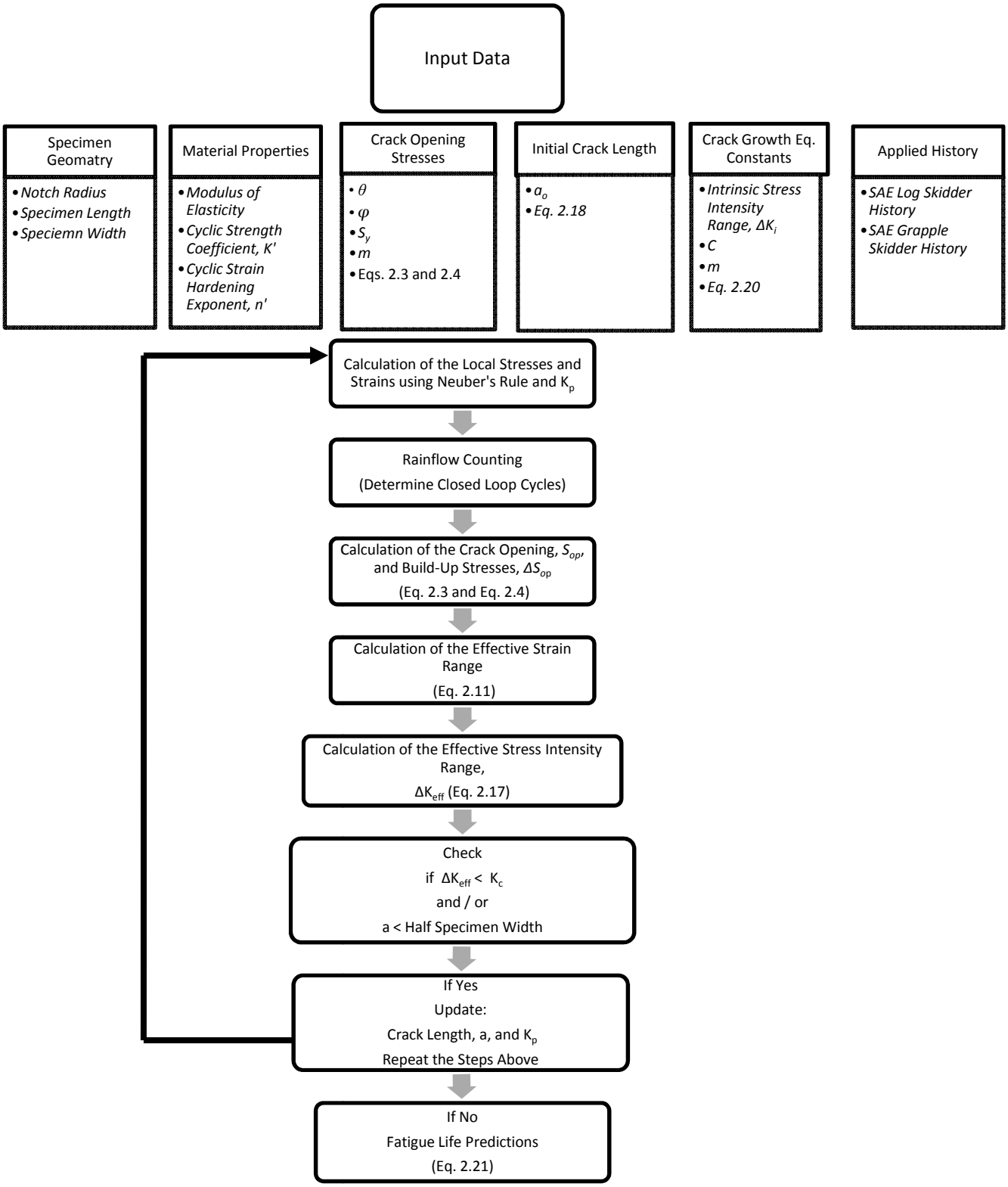

Figure 2.6 Algorithm for the crack growth model

2.4.1 Determination of Material Properties

Monotonic and cyclic properties of the three materials used were determined through a series of tension tests and fully reversed constant amplitude strain controlled tests. The results are summarized in Chapter 3 Sections 3.1.1, 3.1.2, and 3.1.3.

2.4.2 Calculation of the Local Stresses and Strains

Neuber's rule and the material's cyclic stress-strain curve were employed to estimate the local stresses and strains at the notch root for a given load history. Neuber's rule states that the geometric mean of the stress and strain concentration factors is equal to the elastic stress concentration factor k_t (Eq. 2.13) during plastic deformation.

$$k_t = \sqrt{k_\sigma k_\varepsilon} \qquad \text{(Eq. 2.13)}$$

El Haddad and Topper [24] suggested the use of a stress concentration factor k_p (Eq. 2.14) for a short crack emanating from a notch root to calculate stress intensity factors during the initial growth of a crack in a notch.

$$k_p = \sqrt{\frac{c}{2(\rho/2+a)}}\left(1+\frac{\rho}{2(\rho/2+a)}\right)(1+1/2\sqrt{\rho/c}) \qquad \text{(Eq. 2.14)}$$

where c is the notch radius, ρ is the radius of curvature and a is the crack length measured from the edge of the notch. For a circular notch, the term $\left(1+\frac{1}{2}\sqrt{\frac{\rho}{c}}\right)$ is constant and is equal to $k_t/2$, and ρ is equal to c. Then Eq. 2.14 takes the form:

$$k_p = \frac{k_t}{2}\sqrt{\frac{c}{2(c/2+a)}}\left(1+\frac{c/2}{(c/2+a)}\right) \qquad \text{(Eq. 2.15)}$$

For long cracks, it was assumed that the total crack length is equal to the crack length a plus the notch radius c and the value of k_p was taken as follows:

$$k_p = \sqrt{\frac{a+c}{a}} \qquad \text{(Eq. 2.16)}$$

The value of k_p was then used together with the Ramberg-Osgood cyclic stress-strain curve (Eq. 2.2) and Neuber's rule to obtain the local stresses and strains in the region around the crack tip for both elastic and inelastic conditions.

2.4.3 Calculation of the Effective Strain Based Intensity Factor

Elber [29] introduced the concept of an effective part of a stress cycle during which a crack was open as the portion of the cycle contributing to crack growth. El Haddad et al. [24] developed a strain based intensify factor that accounted for the increased strains experienced by small cracks growing through the first few grains of a metal to describe the growth of short fatigue cracks in terms of an effective strain range. Their expression is given by Eq. 2.17 and was adopted in this model:

$$\Delta K_{eff} = FE\Delta\varepsilon_{eff}\sqrt{\pi(a_o + a)} \qquad \text{(Eq. 2.17)}$$

Where F is a geometric factor, E is the modulus of elasticity, $\Delta\varepsilon_{eff}$ is the effective strain range obtained by subtracting the crack opening strain of a cycle from the total strain range (See Eq. 2.11), and a_o is a fictitious initial crack length given by Eq. 2.18. El Haddad et al. [24] also showed that the threshold stress intensity factor and a_o were dependent on grain size. They introduced an effective initial crack length a_o into their descriptions of stress intensity factor for short cracks. As the crack length decreased, the length a_o constituted an increasing fraction of the effective length until at zero length it represented the crack length at which the fatigue limit stress intensity was equal to the threshold stress intensity and fracture mechanics would predict that a crack would propagate into the interior of the specimen. The value of a_o was obtained by assuming that the threshold stress intensity range at a very short crack length would approach the threshold stress intensity of the material (ΔK_{th}) at a strain equal to the intrinsic fatigue limit ($\Delta\varepsilon_i$) so that a_o took the following form:

$$a_o = \left(\frac{\Delta K_{th}}{FE\Delta\varepsilon_i}\right)^2 \frac{1}{\pi} \qquad \text{(Eq. 2.18)}$$

2.4.4 Effective Fatigue Crack Growth Curve and Fatigue Life Predictions

As mentioned earlier Paris et al. [15] proposed the fatigue crack propagation law:

$$\frac{da}{dN} = C(\Delta K)^m \qquad \text{(Eq. 2.19)}$$

where *da/dN* is the change in crack length per cycle, and *C* and *m* are material constants. In this investigation the effective crack growth rate curve was used to predict fatigue lives:

$$\frac{da}{dN} = C(\Delta K_{eff} - \Delta K_i)^m \qquad \text{(Eq. 2.20)}$$

where ΔK_i is the intrinsic stress intensity range, *C* and *m* are two material constants. Fatigue life predictions were carried out by a numerical integration along the closure free crack growth curve between the initial and final crack lengths a_o and a_f as follows:

$$N_f = \int_{a_o}^{a_f} da / C(\Delta K_{eff} - \Delta K_i)^m \qquad \text{(Eq. 2.21)}$$

2.4.5 Deriving the Closure Free Crack Growth Curve

Elber [29] proposed that when the crack growth rate was plotted against the effective stress intensity factor, the crack growth rate for all stress ratios could be represented by a single curve. The derivation of the closure free crack growth curve (Eq. 2.20) from the effective strain-life curve was treated as an inverse problem by choosing a crack growth curve that predicted the observed fatigue lives which were taken as the number of cycles required to grow the crack using Eq. 2.17. From a large body of experimental threshold measurements completed by Miller [65] and data from others [66] the values of ΔK_i were observed to be grouped tightly in the range between 2.5 to 3.0 MPa $m^{1/2}$ for a variety of steels and at about 1 MPa $m^{1/2}$ for a variety of aluminum alloys.

Referring to Figure 2.7, the following steps were used to construct the closure free crack growth curve:

- An initial value of the slope *m* in Eq. 2.20 was set to 2 as suggested by [67].
- The log-log linear portion of McEvily's representation of the crack growth rate curve [25], *da/dN vs.* ΔK^* (Eq. 2.23), was derived from the log-log linear portion of the effective strain-life curve, $E\Delta\varepsilon^*$ *vs.* N_F.
- For the first trial in calculating the fatigue life at a low strain level $E\Delta\varepsilon^*_1$, the crack growth rate in Eq. 2.20 for the first cycle was the crack growth rate corresponding to the value of ΔK^*_1 when the initial crack length, a_o, in Eq. 2.18 was set to zero.

- Taking the value of the slope m as 2, and the ΔK_i as 2.5 MPa $m^{1/2}$, the constant C was obtained from Eq. 2.20 .
- Repeated trials were used to calculate the fatigue life for the strain $E\Delta\varepsilon^*_1$.
- If the calculated life was greater than N_{F1}, then the crack growth rate da/dN_1 estimated in the previous step was too low, and so was increased by increasing the constant C in Eq. 2.20.
- If the calculated fatigue life was less than N_{F1}, the constant C was decreased. This step was repeated until the calculated fatigue life matched N_{F1}.
- The estimate of the slope m in Eq. 2.20 was then refined by calculating the fatigue life at a high strain level, $E\Delta\varepsilon^*_2$ in Figure 2.7.
- If the calculated life was greater than N_{F2}, the slope m was increased above the assumed value of 2 to increase the crack growth rate.
- If the calculated fatigue life was less than N_{F2}, the slope m was decreased. This step was repeated until the calculated fatigue life matched $N_{F2.}$

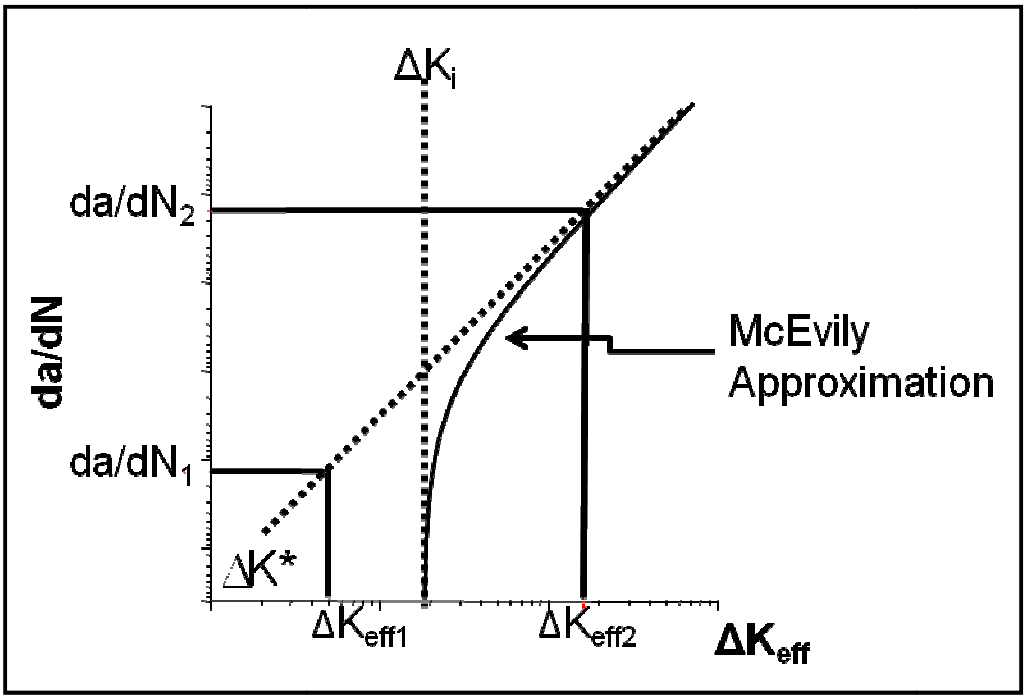

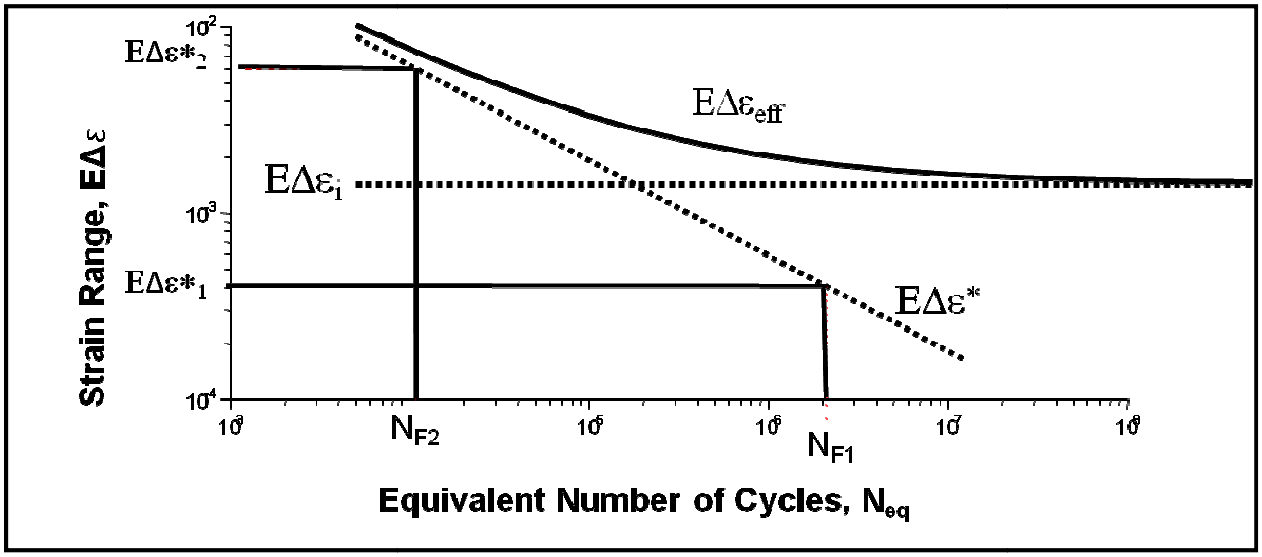

Figure 2.7 Deriving the ΔK* vs. da/dN curve from EΔε* vs. N_f curve

Chapter 3
Materials and Experimental Methods

3.1 Materials

The materials used in this investigation are dual phase DP 590 steel, SAE 1045 medium carbon steel, and AISI 8822 carburized case steel. DP 590 steel belongs to the family of advanced high strength steels (AHSS) that has been introduced and gradually adopted in vehicle structures as lightweight materials. In general AHSS exhibit higher ultimate strength than the previously used low carbon steels and therefore thinner sections can be used in vehicle construction to result in same or better quality of the final part while reducing the weight. SAE 1045 steel is used extensively by all industry sectors for applications requiring more strength and wear resistance than the low carbon mild steels can provide with typical applications including: axles, bolts, connecting rods, hydraulic clamps and rams, shafts, and spindles. AISI 8822 is a nickel-chromium-molybdenum carburizing steel of fairly high hardenability. In components it has a high core strength and a durable carburized case steel making it suitable for many heavy duty applications such as shafts and gears.

3.1.1 DP 590 Steel

DP 590 steel in the as-received condition is one of the materials used in this study. Specimens were fabricated from DP 590 flat steel sheets 2 mm in thickness. The test specimen geometry and dimensions shown in Figure 3.1 were chosen so that they were adequate to resist buckling in addition the radius of the sample was continuously varied decreasing from infinity in a shape determined by finite element calculations to give a stress concentration of less than one percent. For high strain amplitudes (up to the 1% strain level), and to increase buckling resistance two specimens were laminated together using M-Bond AE-10 adhesive epoxy and left for 24 hours for the epoxy to cure before testing. The chemical composition of the material is shown in Table 3.1. The mechanical properties (monotonic and cyclic curves) as determined in this study are shown in Figure 3.2 and are tabulated in Table 3.2.

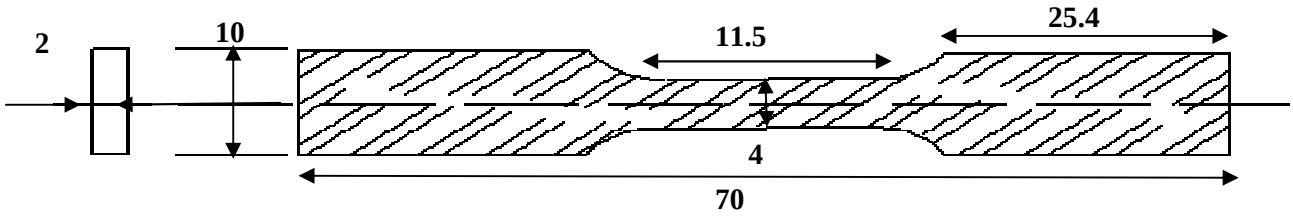

Figure 3.1 DP 590 specimen geometry (all dimensions are in mm)

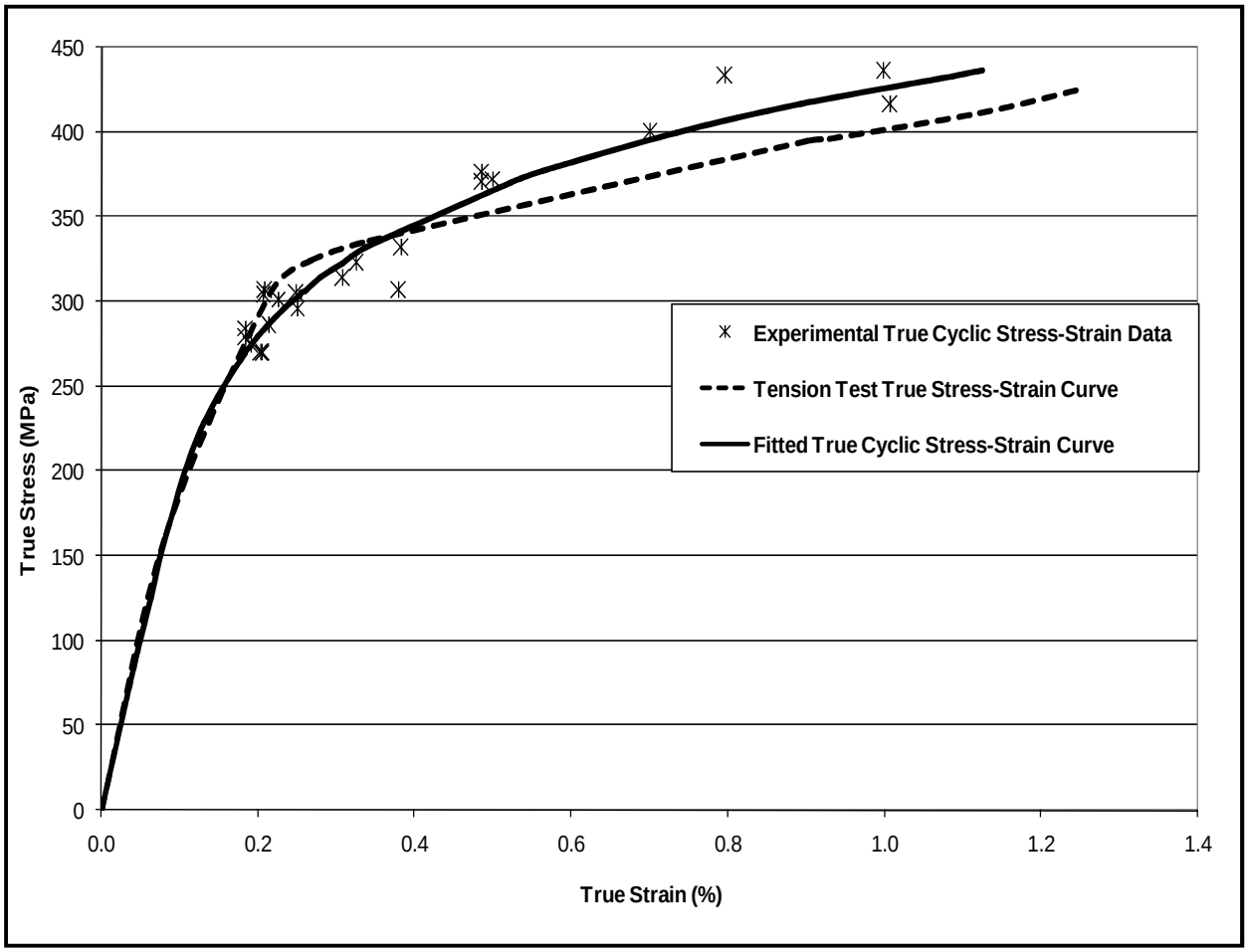

Figure 3.2 Monotonic and cyclic stress-strain curves of DP 590 steel

Table 3.1 Chemical composition of DP 590 steel (percentage by weight)

Alloy	C	Mn	P	S	Si	Cu	Ni	Mo	Cr	Cb	V	Al	Sn	N
DP 590	0.09	1.01	0.01	0.01	0.28	<0.02	<0.02	<0.02	0.02	<0.008	<0.008	0.04	0.01	0.01

Table 3.2 Mechanical (monotonic and cyclic) properties of DP 590 steel

Mechanical Properties	Units	Magnitude
Elastic Modulus, E	MPa	209,000
Yield Strength, S_y	MPa	349
Ultimate Tensile Strength, S_u	MPa	523
True Fracture Stress, σ_f	MPa	643
True Fracture Strain	%	76
% Elongation	%	34
% Reduction of Area	%	53
Monotonic Tensile Strength Coefficient, *K*	MPa	730
Monotonic Tensile Strain Hardening Exponent, *n*		0.12
Cyclic Yield Strength, (0.2% offset) = *K'(0.002) n'*	MPa	338
Cyclic Strength Coefficient, *K'*	MPa	949
Cyclic Strain Hardening Exponent, *n'*		0.166
Fatigue Strength Coefficient, σ'_f	MPa	806
Fatigue Strength Exponent, *b*	-	-0.083
Fatigue Ductility Coefficient, ε'_f	-	0.351
Fatigue Ductility Exponent, *c*	-	-0.5
Hardness, Rockwell C	HRC	6

3.1.2 SAE 1045 Steel

Smooth, cylindrical gauge length specimens with the geometry and dimensions shown in Figure 3.3 were prepared in accordance with ASTM standard E606 - 04 from 19.05 mm diameter hot rolled bars of SAE 1045 steel with the loading axis of each specimen parallel to the direction of rolling. The material was tested in a quenched and tempered condition; it was heated to 845^{o}C, quenched in oil, and then tempered for 150 minutes at 315 ^{o}C. The chemical composition of the SAE 1045 steel is shown in Table 3.3. The specimen surface preparation was performed in a manner that resulted in a minimum influence on the variability in fatigue lives and that introduced little surface metal deformation especially in the gauge length. The gauge sections of the fatigue specimens were mechanically polished in the loading direction using successively no. 240, no. 400, no. 500, and no. 600 grades of emery paper. After polishing, a thin band of M-coat D acrylic coating was applied under the clip gage location in the central gauge section to prevent scratching of the smooth surface by the knife edges of the clip gauge strain extensometer, thus reducing the incidence of knife edge failures. The monotonic and cyclic curves as determined in this study are shown in Figure 3.5 and tabulated in Table 3.4.

In addition, threaded specimens were fabricated from SAE 1045 steel bars. The geometry and dimensions of round threaded notched specimens with a flat gauge length profile are shown in Figure 3.5. These specimens were used for crack growth rate and crack opening stress measurements. The flat test section contained a single edge notch of R = 0.3 mm radius. The gauge length of the specimen was roughed out on a lathe then finished by progressively shallower cuts. The threads were then cut while the specimen remained in the lathe to ensure concentricity along the loading axis. The ASTM Standard E606-04 recommended hand polishing of the specimen in the loading direction using progressively finer grades of emery paper which vary from no. 240 to no. 600. A final polish using diamond powder was applied to the gauge length with a very fine cloth to enhance crack closure observations.

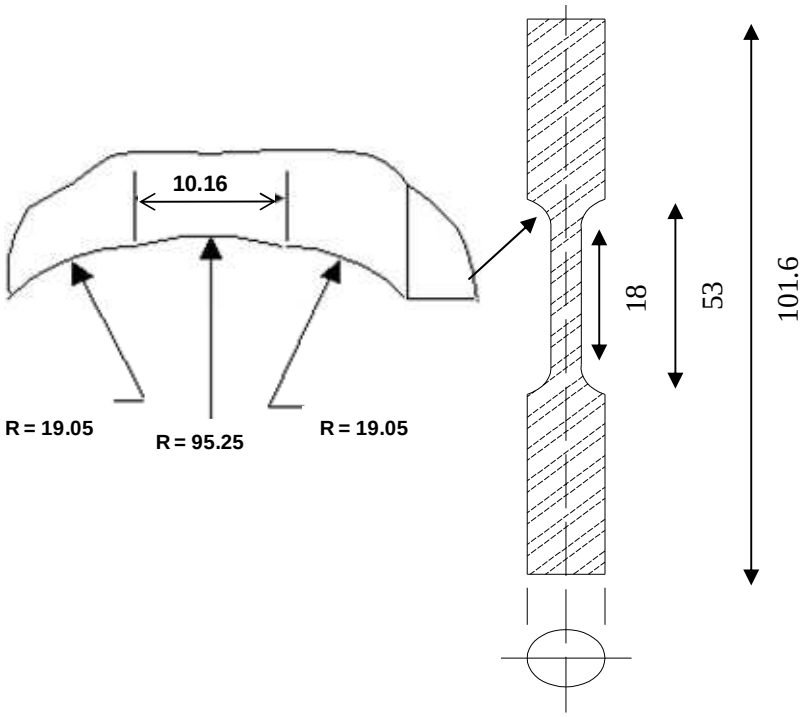

Figure 3.3 Smooth specimen geometry of SAE 1045 steel (all dimensions are in mm)

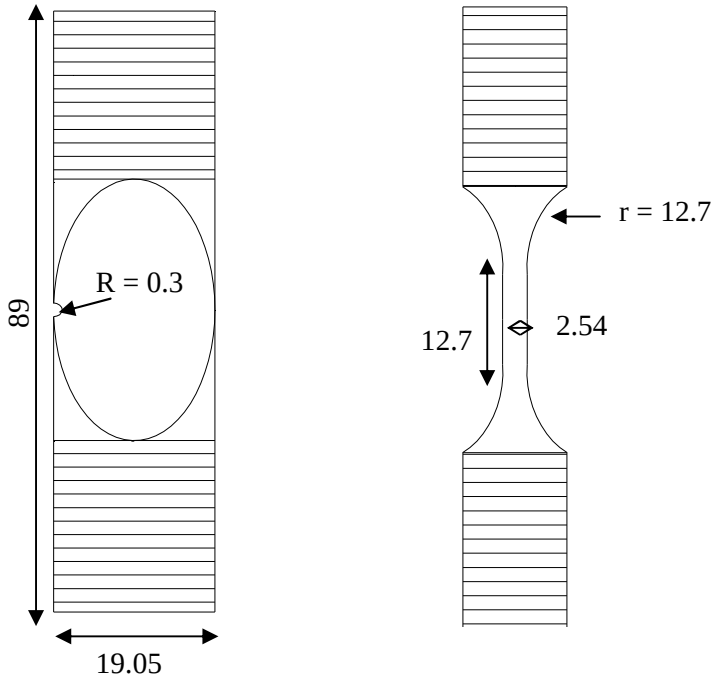

Figure 3.4 Threaded specimen geometry of SAE 1045 steel (all dimensions are in mm)

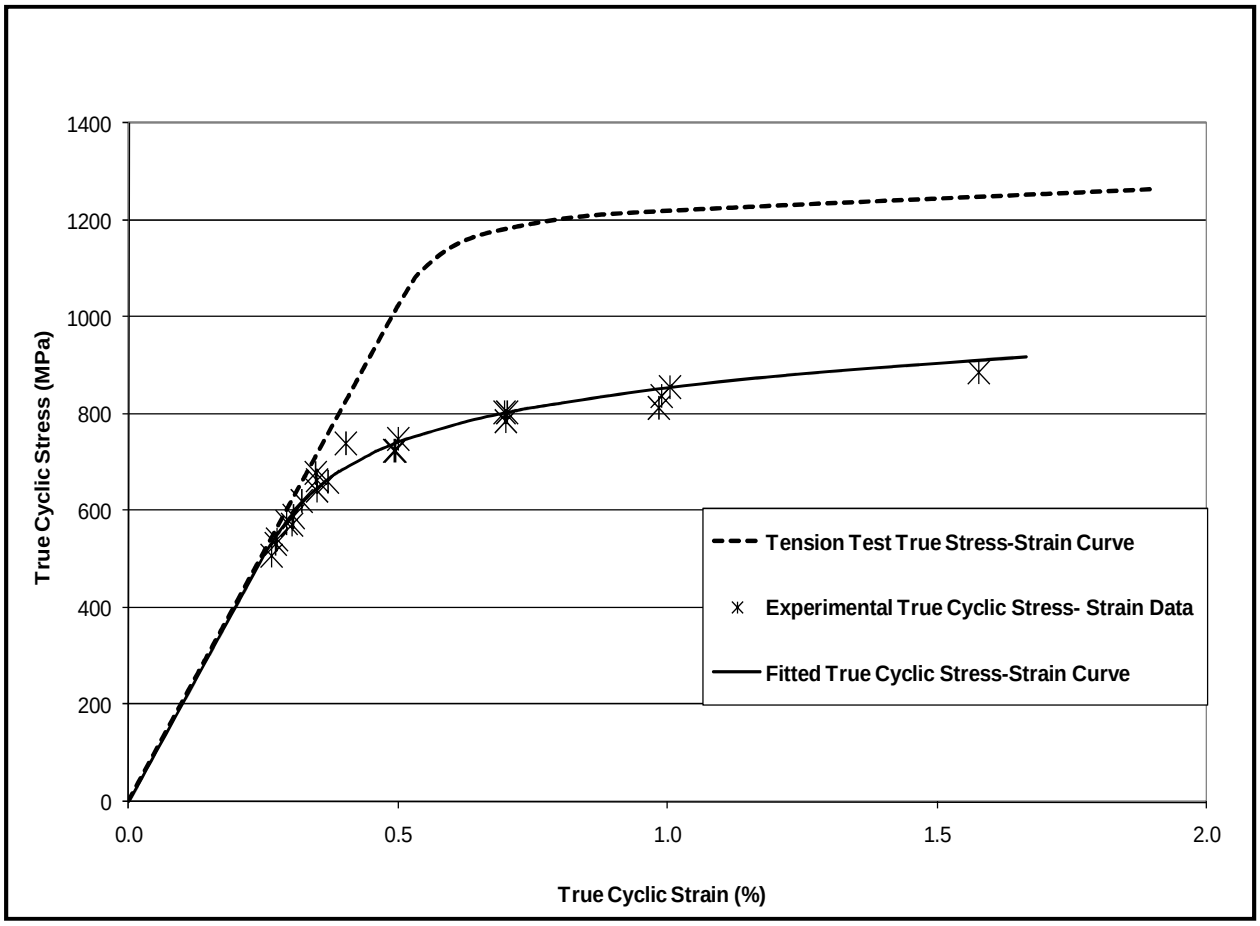

Figure 3.5 Monotonic and cyclic stress-strain curves of SAE 1045 steel

Table 3.3 Chemical composition of SAE 1045 steel (percentage by weight)

Alloy	C	Mn	P	S	Si	Cu	Ni	Mo	Cr	Cb	V	Al	Sn	N
SAE 1045	0.46	0.81	0.027	0.023	0.17	0.27	-	-	0.15	-	-	-	-	-

Table 3.4 Mechanical (monotonic and cyclic) properties of SAE 1045 steel

Mechanical Properties	Units	Magnitude
Elastic Modulus, E	MPa	205,000
Yield Strength, S_y	MPa	1200
Ultimate Tensile Strength, S_u	MPa	1271
True Fracture Stress, σ_f	MPa	1879
True Fracture Strain	%	56
% Elongation	%	14
% Reduction of Area	%	43
Monotonic Tensile Strength Coefficient, *K*	MPa	1470
Monotonic Tensile Strain Hardening Exponent, *n*		0.033
Cyclic Yield Strength, (0.2% offset) = *K'(0.002) n'*	MPa	767
Cyclic Strength Coefficient, *K'*	MPa	1410
Cyclic Strain Hardening Exponent, *n'*		0.098
Fatigue Strength Coefficient, σ'_f	MPa	1813
Fatigue Strength Exponent, *b*	-	-0.094
Fatigue Ductility Coefficient, ε'_f	-	0.577
Fatigue Ductility Exponent, *c*	-	-0.6
Hardness, Rockwell C	HRC	35

3.1.3 AISI 8822 Steel

Smooth, cylindrical gauge length specimens with the geometry and dimensions shown in Figure 3.6 were prepared in accordance with ASTM standard E606 - 04 from 20 mm diameter bars of AISI 8822 steel with the loading axis of each specimen parallel to the direction of rolling. The material was tested in a quenched and tempered condition. The samples were through-carburized by austenitizing at 927 ^{o}C in an atmosphere with a 0.9% carbon potential. The samples were then quenched in 66 ^{o}C degree oil, and then tempered at 218 ^{o}C. The chemical composition of the AISI 8822 steel is shown in Table 3.5. The specimen surface preparation was performed in a manner that resulted in a minimum influence upon the variability in fatigue lives and that introduced little surface metal deformation especially in the gauge length. The gauge sections of the fatigue specimens were mechanically polished in the loading direction using successively no. 240, no. 400, no. 500, and no. 600 grades of emery paper. After polishing, a thin band of M-coat D acrylic coating was applied under the clip gage location in the central gauge section to prevent scratching of the smooth surface by the knife edges of the clip gauge strain extensometer, thus reducing the incidence of knife edge failures. The monotonic and cyclic curves are shown in Figure 3.7 and tabulated in Table 3.6.

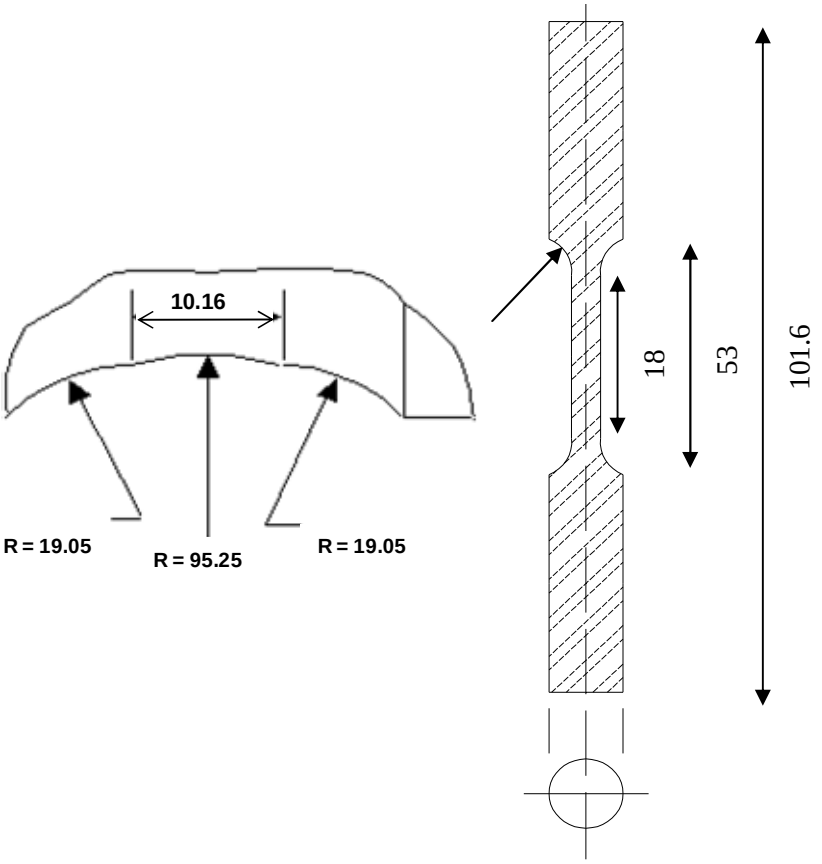

Figure 3.6 Smooth specimen geometry of AISI 8822 steel (all dimensions are in mm)

Table 3.5 Chemical composition of AISI 8822 steel (percentage by weight)

Alloy	C	Mn	P	S	Si	Cu	Ni	Mo	Cr	Cb	V	Al	Sn	N
AISI 8822	0.22	0.86	0.013	0.025	0.17	-	0.43	0.39	0.54	0.24	0.004	0.028	0.01	-

Table 3.6 Mechanical (monotonic and cyclic) properties of AISI 8822 steel

Mechanical Properties	Units	Magnitude
Elastic Modulus, E	MPa	209,000
Yield Strength, S_y	MPa	-
Ultimate Tensile Strength, S_u	MPa	1480
True Fracture Stress, σ_f	MPa	1480
True Fracture Strain	%	0.87
% Elongation	%	0.87
% Reduction of Area	%	-
Monotonic Tensile Strength Coefficient, *K*	MPa	-
Monotonic Tensile Strain Hardening Exponent, *n*		-
Cyclic Yield Strength, (0.2% offset) = *K'(0.002) n'*	MPa	-
Cyclic Strength Coefficient, *K'*	MPa	-
Cyclic Strain Hardening Exponent, *n'*		-
Fatigue Strength Coefficient, σ'_f	MPa	2234
Fatigue Strength Exponent, *b*	-	-0.109
Fatigue Ductility Coefficient, ε'_f	-	-
Fatigue Ductility Exponent, *c*	-	-
Hardness, Rockwell C (HRC)	-	60

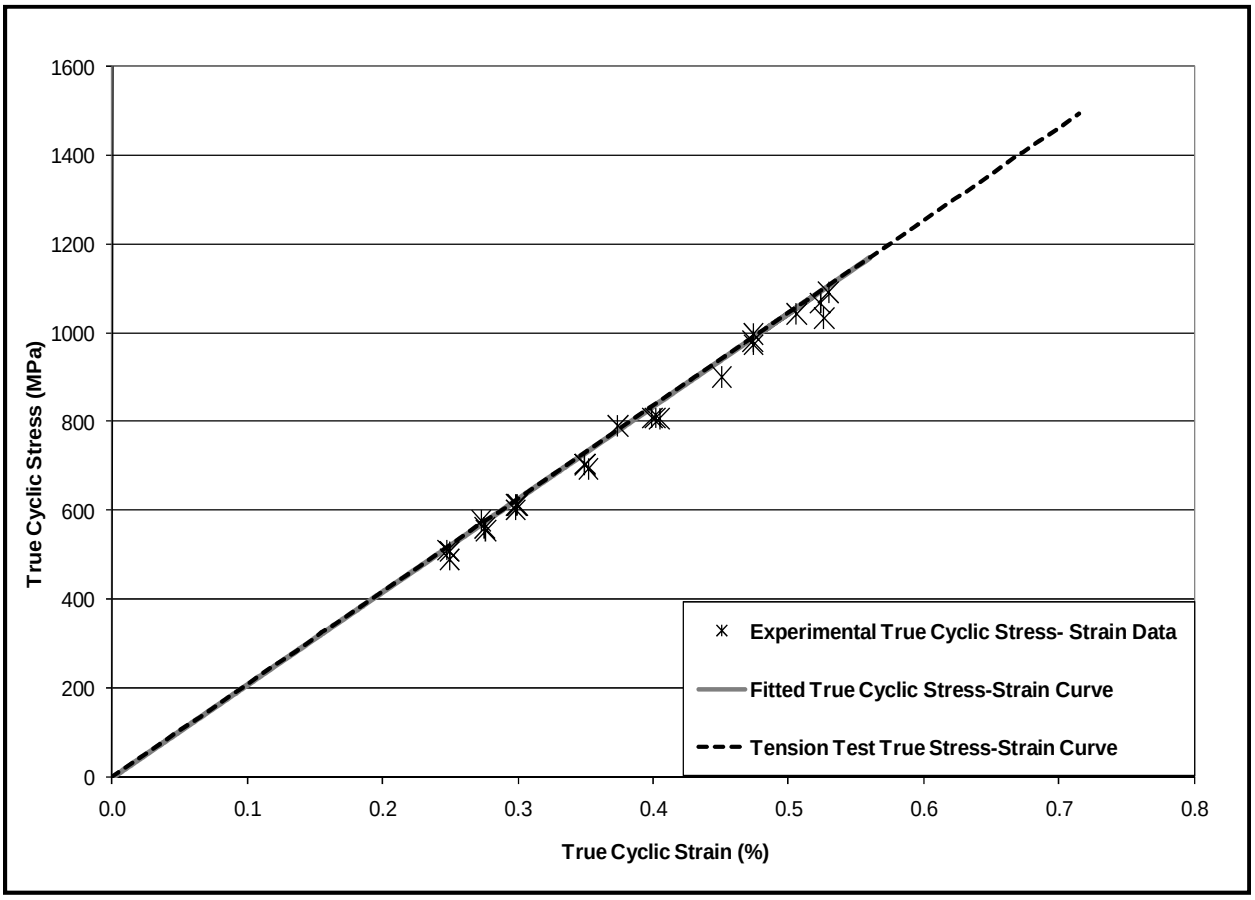

Figure 3.7 Monotonic and cyclic stress-strain curves of AISI 8822 steel

3.2 Specimen Gripping and Alignment

All fatigue tests were carried out using an MTS servo-controlled closed-loop electro-hydraulic testing machine. A process control computer controlled by FLEX [68] software was used to output constant strain amplitudes for constant strain amplitude tests and constant amplitude stresses for the underload history tests. The typical gripping assembly for a smooth cylindrical specimen is shown in Figure 3.8 (a). Prior to testing, the load train alignment (load cells, grips, specimen, and actuator) was checked. Then the smooth specimen was inserted and secured into the lower grip, and the hydraulic actuator was raised until the second end of the specimen was inserted and secured into the upper grip. The gripping assembly for flat sheet specimens is shown in Figure 3.8 (b). The specimen was inserted into the lower grip and secured by tightening a screw that moves the clamping wedges and clamps the specimen with enough force to prevent slipping during the fatigue tests.

The other end was then inserted into the upper grip and secured by tightening the wedge grips with another screw. For strain controlled tests, an axial extensometer was mounted on the specimen gauge section and held in place by means of wire springs. For the threaded specimens, the gripping assembly is shown in Figure 3.8 (c). The specimen was threaded into the lower grip and secured by tightening a machined lock-nut which ensured that the axis of the specimen was parallel to the axis of the grip. The second end of the specimen was threaded into the other grip and secured with a second machined lock-nut. The hydraulic actuator was raised until the lower grip was immersed in the attached pot containing liquid wood's metal, which was then frozen. This procedure ensured that the axis of the specimen was coincident with the loading axis of the testing frame, and that the gauge section of the specimen was not subjected to residual stresses induced during the assembly process. Figure 3.8 (d) shows an overview of the position of the optical microscope used in this investigation.

a)

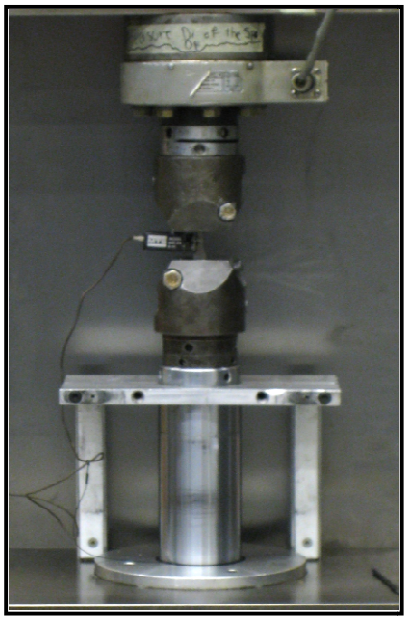

b)

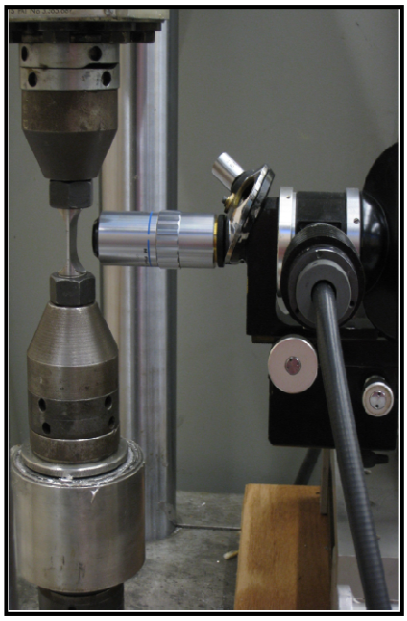

c)

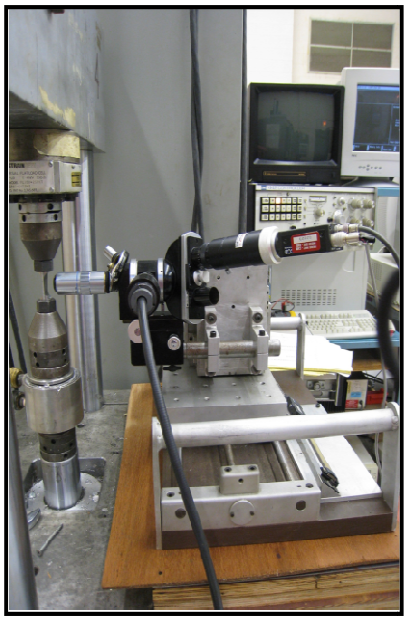

d)

Figure 3.8 Test set-up for a) smooth specimens, b) flat sheet specimens, c) threaded specimens d) the 900x short focal length optical microscope

3.3 Experimental Program

The following sections describe the experiments performed on the materials used in this investigation. A summary of all the tests is provided in Table 3.7.

3.3.1 Monotonic Tensile Tests

Tension tests were carried out on dual phase DP 590 steel, SAE 1045 medium carbon steel, and AISI 8822 carburized case steel. These tests provided information on the strength and ductility of the material under uniaxial tensile stresses as well as the engineering monotonic tensile stress-strain curves.

3.3.2 Fully Reversed Constant Amplitude Tests

These tests were used in the determination of the fatigue properties (cyclic properties) of the steels studied in this investigation and to generate the cyclic stress-strain and the total strain-life curves. Fatigue tests were carried out using an MTS servo-controlled closed-loop electro-hydraulic testing machine with a process control computer controlled by FLEX software to output constant strain and stress amplitudes in the form of sinusoidal waves. Axial, constant strain amplitude, fully reversed (R = -1) strain-controlled fatigue tests were performed on SAE 1045, and AISI 8822 steel smooth specimens, as well as on DP 590 flat sheet steel specimens. The stress-strain limits of each specimen were recorded at logarithmic intervals throughout the test via a peak reading voltmeter. Specimen failure was defined as a 50% drop in the tensile peak load from the peak tensile load observed at one half of the expected specimen life. The loading frequency of the tests varied from 0.05 Hz to 3 Hz. For fatigue lives greater than 100,000 cycles (once the stress-strain loops had stabilized) the specimens were tested in load control. For load controlled tests, failure was defined as the separation of the smooth specimen into two pieces. The test frequencies used in this case were between 50 and 100 Hz.

3.3.3 Underload Fatigue Tests

3.3.3.1 Underload Fatigue Tests used in Constructing the Effective Strain-Life Curve

The effective strain-life curve was derived from periodic underload tests performed under stress control consisting of a repeated load cycle block (Figure 3.9). The block consisted of a single underload cycle followed by a number of smaller load cycles that had the same maximum stress as the underload cycle. The minimum stress of the small cycles was changed from test to test and was set at different percentage of the fatigue limit (Figure 3.10). This block was then repeated until the specimen failed. The aim was to have the large cycle (underload cycle) occur frequently enough that the crack opening stress remained below the minimum stress of the smaller load cycles so that subsequent crack growth during

small cycle application was crack closure free. The underload cycle in this work was set equal to the fully reversed constant amplitude stress level that will give a fatigue life of 10,000 cycles [42]. The reason for this choice is to achieve a large reduction in crack opening stress without expending an undue fraction of the total damage in the large cycles. The number of small cycles in the second block was chosen so that they were responsible for 80 to 90% of the damage to the specimen and that they were free from crack closure. The equivalent fatigue life for the small cycles in the underload test was obtained by calculating the damage done by the underload cycles and subtracting it from unity to obtain the fraction of the total damage done by the small cycles. Then the number of small cycles was divided by the fraction of the damage done by them to obtain their equivalent fatigue life. As mentioned previously theses tests were used to construct the effective strain-life curve (Eq. 2.7) by finding the values of the constants *A* and *b* and the intrinsic strain range $\Delta\varepsilon_i$.

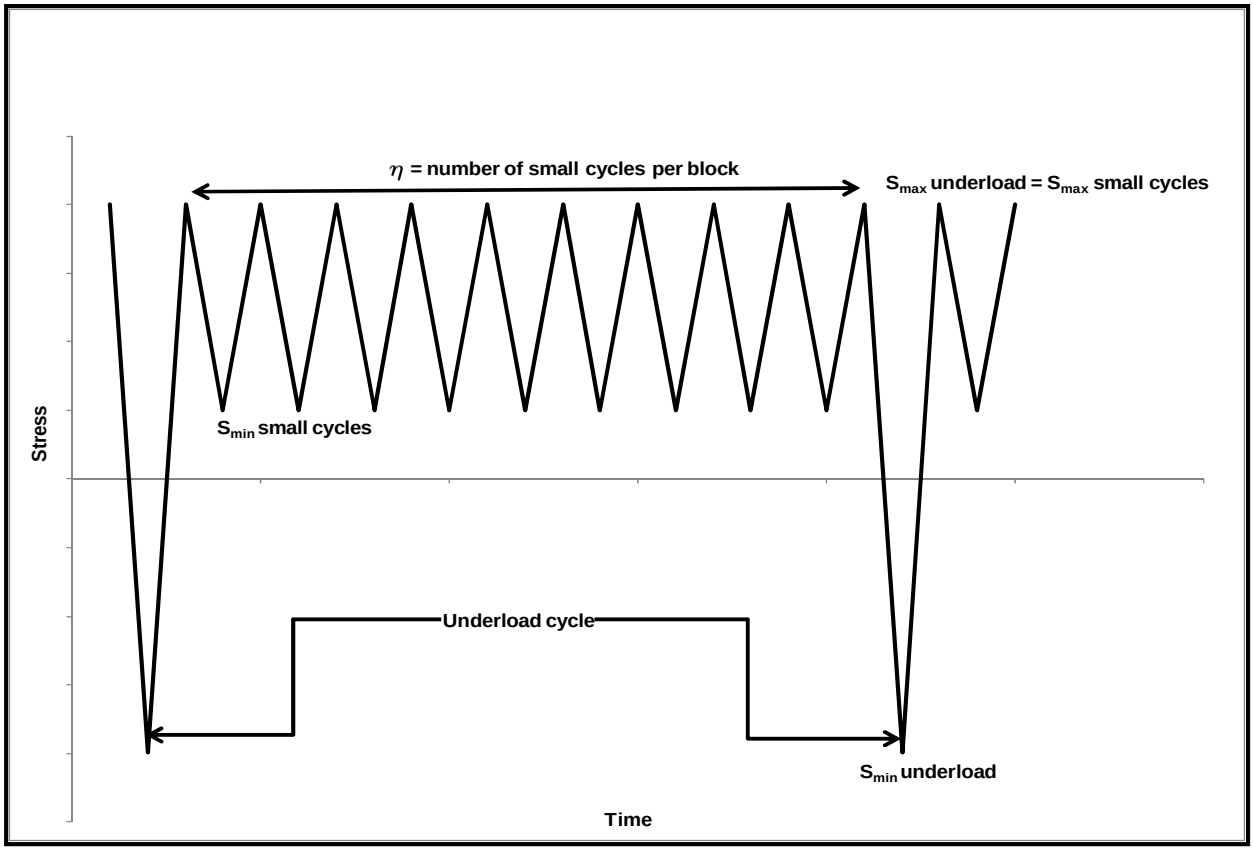

Figure 3.9 Underload fatigue test configuration

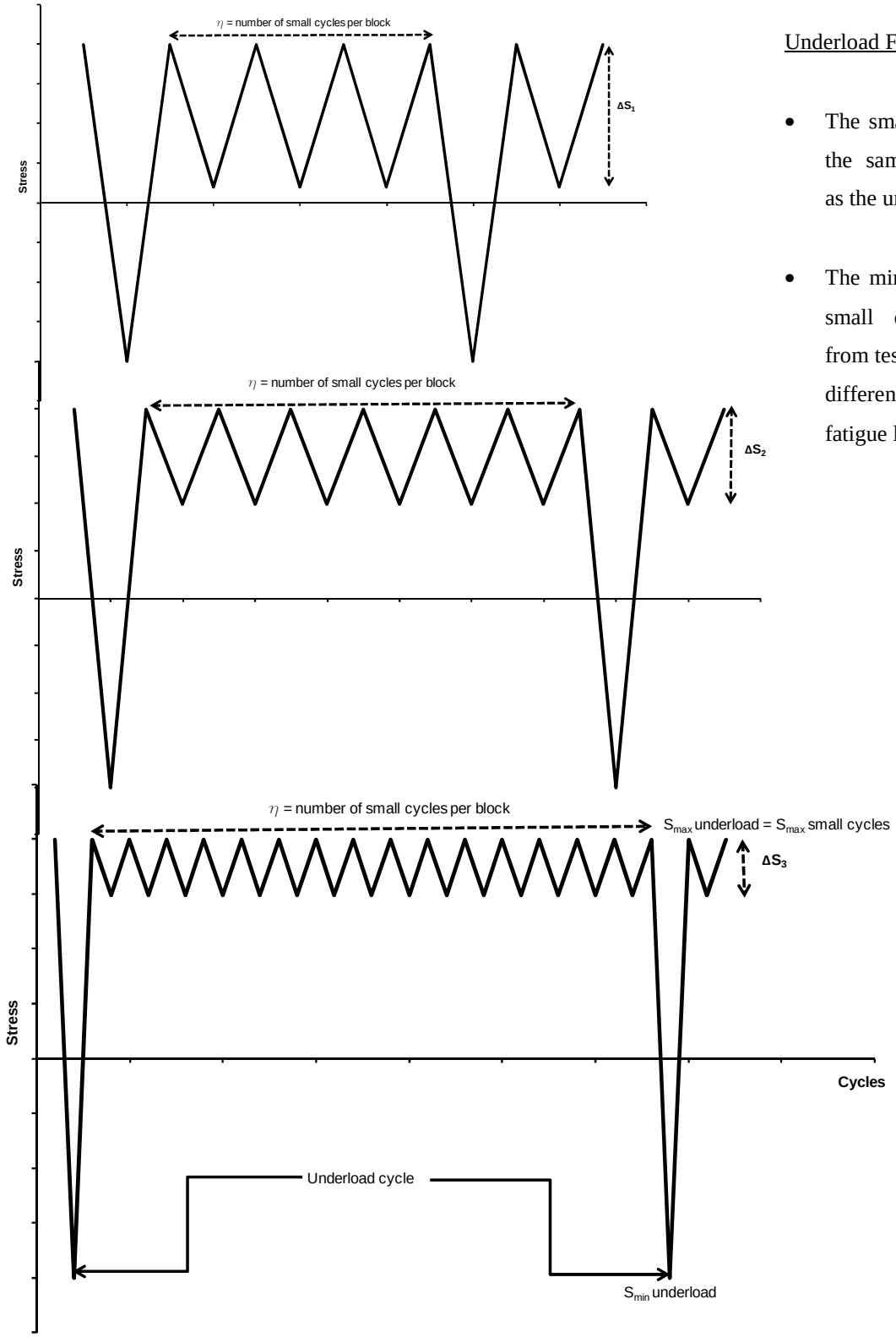

Underload Fatigue Tests

- The small load cycles have the same maximum stress as the underload cycle.
- The minimum stress of the small cycles is changed from test to test and is set at different percentage of the fatigue limit.

Figure 3.10 Underload fatigue tests used in constructing the effective strain-life curve

3.3.3.2 Underload Fatigue Tests used in Deriving the Crack Closure Damage Parameter *"m"*- Damage Tests

In this section a new test procedure for obtaining data on the return of the crack opening stress to a steady state level following an underload is introduced. Smooth specimens were tested under load histories with intermittent underload values. The frequency of occurrence of the underloads was varied from test to test and the changes in the fatigue lives were observed. The changes in damage per block were then used to determine the value of the closure model parameter "*m*" in Eq. 2.4 that described the recovery of the crack opening stress to its steady state level. The experimental work in this section consisted of a series of underload fatigue tests, where the underload cycle was set equal to the fully reversed constant amplitude stress level that gave a fatigue life of 10,000 cycles [42] and a block of small cycles having the same maximum stress as the underload cycle. During these tests only the number of small cycles per block was varied and the stress range of the small cycles was constant in all of the tests. The procedure for obtaining the closure parameter *"m"* is described in Appendix B.

3.3.4 Crack Opening Stress Measurements

These tests were used to measure the steady state crack opening stresses (Eq. 2.3) and the crack opening stress build-up (Eq. 2.4). The tests were conducted on DP 590 steel and the SAE 1045 steel. Crack opening stress measurements were made by a 900x power short focal length optical microscope at given cycles after an underload was applied. The load history consisted of repeated blocks of a large underload followed by constant amplitude small cycles until a steady state crack opening stress was reached. The procedure followed in measuring the crack opening stress was to stop the test at the maximum stress of the chosen cycle and then decrease the load manually until the two crack surfaces touched each other at 0.2 mm behind the crack tip. Two sets of readings were recorded and averaged for each crack opening stress and crack closure stress measurements at cycle numbers 1, 2, 5, 10, 20, 50, 100, 200, 500, 1000, 2000, 5000, and 10000 after each application of an underload.

3.3.5 Closure Free Crack Growth Tests

Crack growth in terms of the effective stress intensity was measured under a load history consisting of high stress underloads followed by constant amplitude load cycles where the frequency of the underload cycles was chosen to give fully open stress cycles. Cracks were started in single edge notch (0.3 mm radius) specimens using zero to compression cycling [69]. The procedure for obtaining closure free load cycles followed the methodology proposed by Dabayeh and Topper [49], where a high, near yield underload was applied followed by constant amplitude cycles that had the same maximum stress as

the underload cycle. The number of small cycles was chosen such that the damage due to underloads did not exceed 20% and that the crack opening stress as it built-up after the underloads did not reach the minimum stress of the small cycles before the next underload was applied.

3.3.6 Mean Stress Tests

In AISI 8822 steel the steady state crack opening stress levels derived from underload and fully reversed constant amplitude fatigue tests indicated that crack opening stress levels were so low that stress cycles with minimum stresses above zero would be fully open. This suggested using constant amplitude tests with positive minimum stresses to generate additional fully effective strain-life data. These mean stress tests were conducted in several series on AISI 8822 steel. In each series the maximum stress had a constant value and the stress range was lowered for each specimen until the fatigue limit was reached. These tests were used to extend the effective strain-life curve of AISI 8822 steel to high strain range levels. The minimum stress was varied from 4 MPa to a tensile value which was approximately 40% of the true fracture stress of the material. The tests had cycles that were fully effective where the crack opening stress was less than the minimum stress of the cycle.

3.3.7 Service Load History Tests

Crack opening stress levels under service load spectra were measured for two automotive service spectra with different mean stresses. The results were compared to the estimates made using the calibrated crack opening stress models. The two spectra were the torsion channel of the Society of Automotive Engineers SAE Grapple Skidder History (GSH) with a positive mean stress (Figure 3.11) and the Cable Channel of the SAE Log Skidder History (LSH) with zero mean stress (Figure 3.12). The SAE GSH was supplied in the form of normalized sequential peak and valley points with a maximum value of 318 and a minimum value of -238 and containing 41,112 reversals. The SAE LSH was supplied in the form of normalized sequential peak and valley points with maximum value of 7.3 and a minimum value of -7.7 and contains 13,344 reversals. The two spectra were scaled to various maximum and minimum stress ranges. The maximum upper limit to the maximum stress range in the scaled histories was chosen so that a fatigue crack would grow out of the notch and avoid large scale plasticity in the specimen.

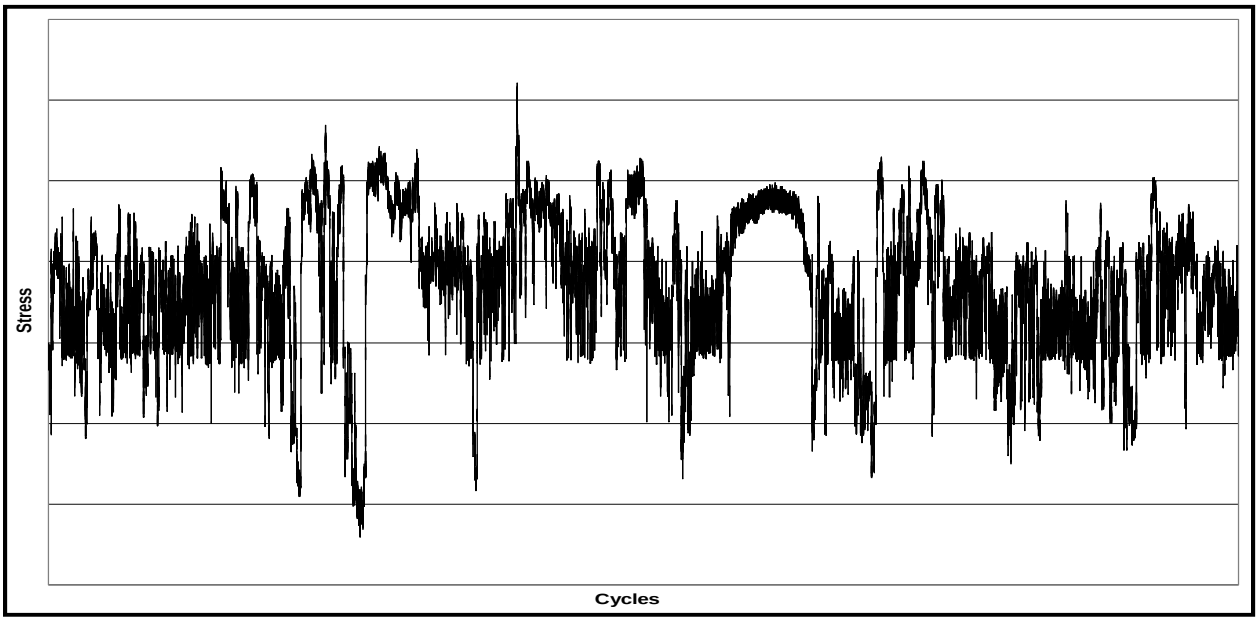

Figure 3.11 SAE Grapple Skidder History

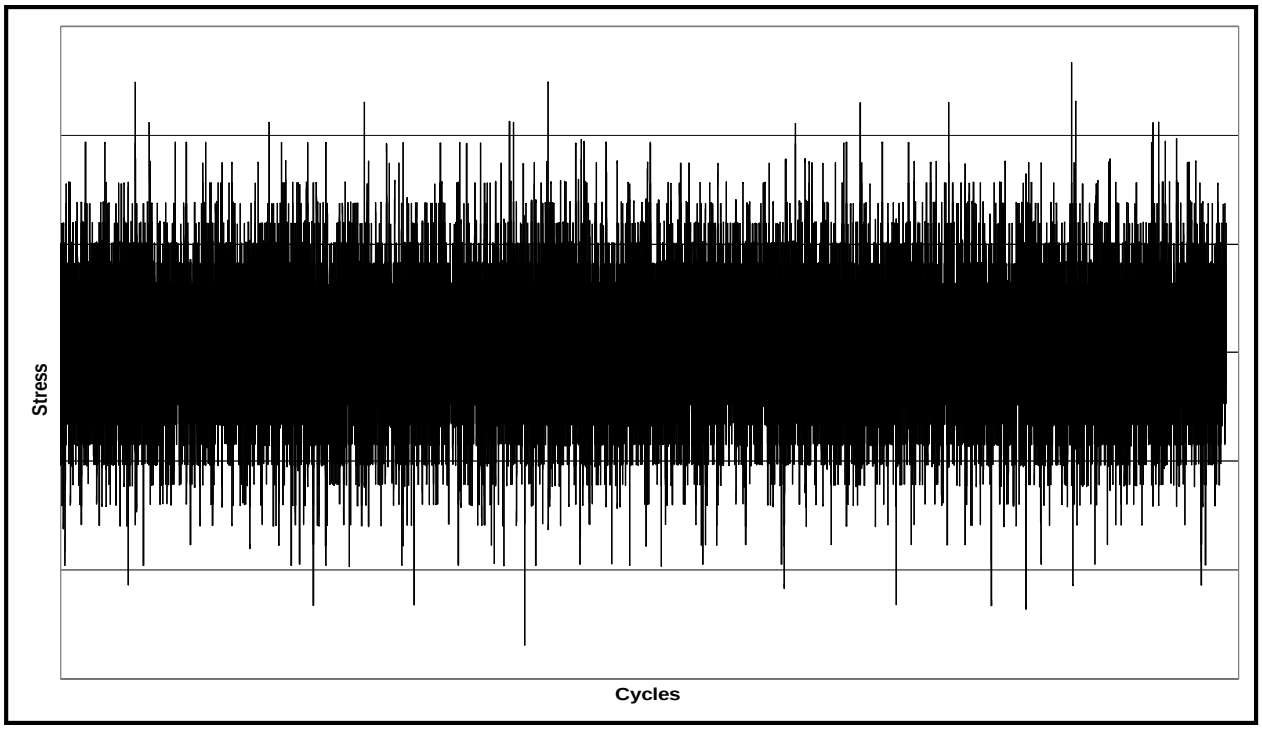

Figure 3.12 SAE Log Skidder History

Table 3.7 Summary of the experimental tests performed on the three steels

Type of Tests	Used To :	Material Constants / Properties Obtained:	Notes
Monotonic tests	• Determine material's monotonic properties • Construct the monotonic stress-strain curve	• Elastic modulus of elasticity, E • Yield strength, S_y • Ultimate tensile strength, S_u • True fracture stress, σ_f • True fracture strain • % Elongation • % Reduction in area • Monotonic tensile strength coefficient, K • Monotonic tensile hardening exponent, n	
Fully reversed constant amplitude tests	• Determine material's cyclic properties • Construct the cyclic stress-strain curve • Construct the strain-life curve	• Cyclic yield strength • Cyclic strength coefficient, K' • Cyclic strain hardening exponent, n' • Fatigue strength coefficient, σ'_f • Fatigue strength exponent, b • Fatigue ductility coefficient, ε'_f • Fatigue ductility exponent, c	
Underload fatigue tests	• Construct the effective strain-life curve • Determine the constants for the effective strain-life curve • Derive the steady state crack opening stresses from the effective strain-life curve • Determine the constants for the steady state crack opening stress equation • Derive the closure free crack growth curve and its constants	• Intrinsic fatigue limit strain range, $\Delta\varepsilon_i$ • Constants in the effective strain-life curve: A and b • Constants in the steady state crack opening stress, Eq. 2.3: θ and φ • Closure free crack growth curve constants, Eq. 2.20: C and m	• The constants for the effective strain-life curve are in Eq. 2.7 • The steady state crack opening stresses were derived from the effective strain-life curve using Eq. 2.9 • Eq.2.3 is the steady state crack opening stress equation • The constants for the closure free crack growth curve are presented in Eq. 2.20
Damage tests	• Determine the crack closure damage parameter in the stress build-up Eq. (Eq. 2.4)	• Crack closure damage parameter, m	• Eq. 2.4 is the stress build-up equation
Crack opening stress measurements	• Compare the measured steady state crack opening stresses with the derived ones from the effective strain-life curve and the calculated ones using Eq. 2.3 • Compare the measured crack opening stress build-up with the calculated ones from Eq. 2.4 • Compare the measured crack opening stresses under the service load histories with the calculated crack opening stresses using the Effective Strain-Life Model and the Effective Crack Growth Model		• Steady state crack opening stress measurements were performed under three stress ratios (-1, 0, and 0.8) • Crack opening stress build-up measurements were performed under three stress ratios (-1, 0, and 0.8)
Closure free crack growth tests	• Compare the measured crack growth rates with the derived ones from the effective strain-life curve	• Calibrate the constants in the closure free crack growth curve: C and m	• The derivation of the closure free crack growth rates are presented in Chapter 2, Section 2.4.5
Mean stress tests	• Obtain data points used in the effective strain-life curve at high strain ranges • Provide better fitting of the effective strain-life curve at high strain ranges		• Performed on AISI 8822 steel only
Service load histories	• Obtain experimental fatigue lives under variable amplitude loading		• The two histories were scaled to different maximums and minimums

Chapter 4
Experimental Results for Dual Phase (DP) 590 Steel

4.1 Introduction

The experimental results for DP 590 steel are presented in this chapter. The monotonic and cyclic stress-strain curves as well as mechanical properties for this material are presented in Chapter 3 Section 3.1.1. The results in this chapter include all the tests performed to develop the effective strain-life model as well as the fatigue crack growth model.

4.2 Effective Strain-Life Curve

4.2.1 Strain-Life Curve

The strain-life curve was constructed from 25 axial, constant amplitude, fully reversed (R = -1) strain-controlled fatigue tests (Table 4.1) using a servo-controlled closed-loop electro-hydraulic testing machine with a process control computer controlled by a software [68] to output constant strain or load amplitudes in the form of sinusoidal waves. It can be seen in Figure 4.1 that the DP 590 steel exhibited a significant amount of plastic strain even at long lives (10^7 cycles). The plot of the plastic strain amplitude versus fatigue life (Figure 4.1) reflected a departure from the usual linearity of the Coffin-Manson relationship. Similar non-linear behaviour was reported in [70] for 2024-T4 and 7075-T6 aluminum alloys. Due to the significant plastic strains observed, the maximum usable frequency in strain controlled tests without causing specimen overheating was 20 Hz.

Table 4.1 Constant amplitude strain-life data for DP 590 steel

Test #	True strain amplitude (%)	True stress amplitude (MPa)	True plastic strain amplitude (%)	True elastic strain amplitude (%)	Fatigue life (reversals to failure)
1	0.998	436	0.784	0.209	2,000
2	1.007	416	0.802	0.199	2,340
3	0.797	433	0.586	0.207	4,000
4	0.700	400	0.506	0.191	7,600
5	0.499	373	0.320	0.178	15,200
6	0.486	377	0.305	0.180	16,000
7	0.486	370	0.307	0.177	19,600
8	0.383	332	0.223	0.159	80,000
9	0.379	306	0.232	0.147	89,000
10	0.325	323	0.170	0.154	47,600
11	0.309	314	0.158	0.150	78,600
12	0.250	296	0.108	0.142	173,200
13	0.249	305	0.103	0.146	180,000
14	0.225	302	0.080	0.144	333,840
15	0.213	286	0.076	0.137	884,528
16	0.209	307	0.062	0.147	146,526
17	0.203	270	0.074	0.129	4,778,600
18	0.204	270	0.075	0.129	2,047,542
19	0.204	270	0.075	0.129	2,423,826
20	0.206	304	0.060	0.145	396,000
21	0.192	274	0.060	0.131	5,915,266
22	0.184	285	0.048	0.136	1,380,000
23	0.182	279	0.048	0.133	*10,100,418

*3 Run-Out Tests

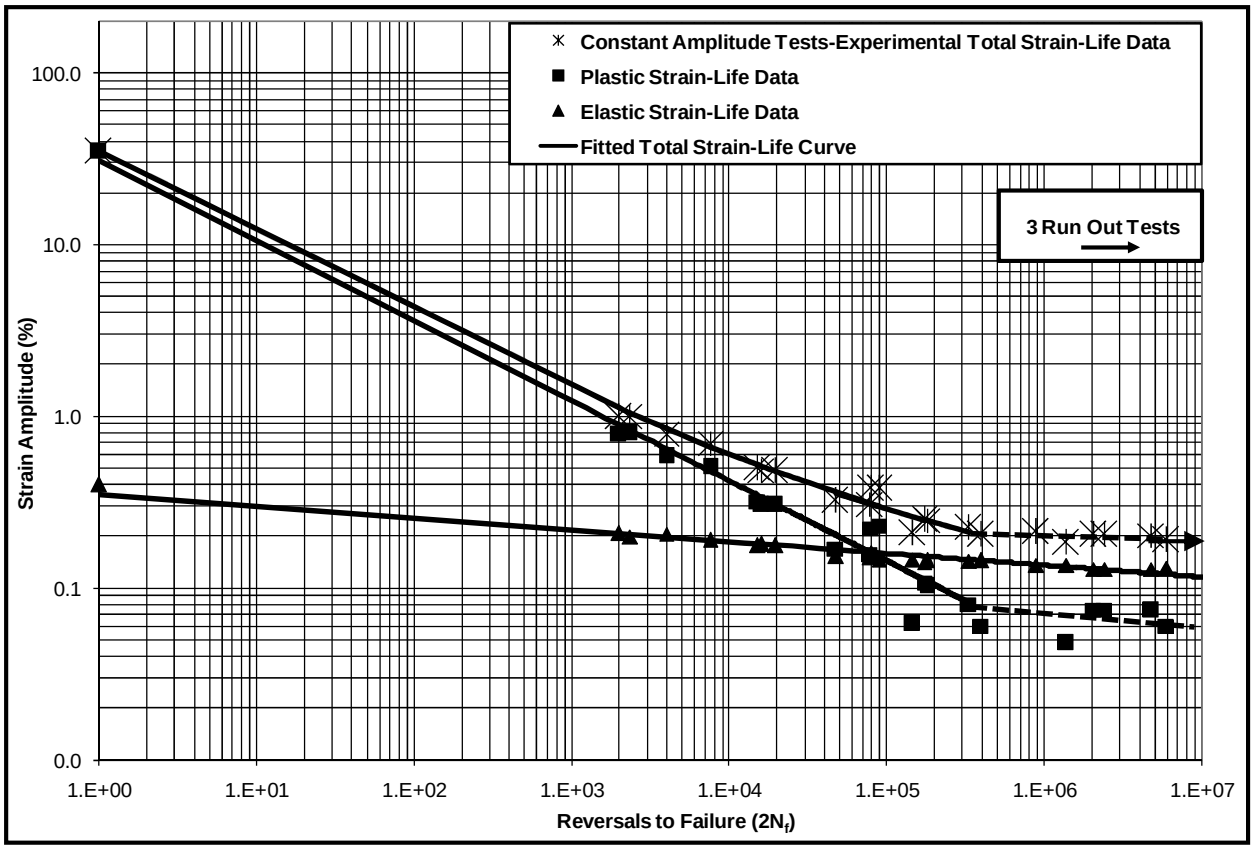

Figure 4.1 Fitted strain-life curve for DP 590 steel

4.2.2 Underload Fatigue Data and the Effective Strain-Life Curve

The effective strain-life curve was derived from 20 periodic underload fatigue tests performed under stress control consisting of a repeated load cycle block. The block consisted of a single underload cycle followed by a number of smaller load cycles that had the same maximum stress as the underload cycle. This block was then repeated until the specimen failed. The aim of this test was to have the large cycle (underload cycle) occur frequently enough that the crack opening stress remained below the minimum stress of the smaller load cycles so that subsequent crack growth during small cycle application was crack closure free. The underload cycle in this work was set equal to the fully reversed constant amplitude stress level that gave a fatigue life of 10,000 cycles (339 MPa). The reason for this choice was to achieve a large reduction in crack opening stress without expending an undue fraction of the total damage in the large cycles. The number of small cycles in the second block was chosen so that they were responsible for 80 to 90% of the damage to the specimen and that they were free from crack closure. Table 4.2 shows the underload fatigue tests configuration. The periodic underload fatigue data for the DP 590 steel specimens are shown in Figure 4.2 together with the constant amplitude strain-life curve. The derived effective strain-life curve is shown in Figure 4.3, the constants A and b in the effective strain-life curve equation (Eq. 2.11) were found to be 87.0 and -0.50 respectively. The intrinsic strain range, $\Delta\varepsilon_i$, was found to be 0.085%.

Table 4.2 Underload fatigue tests for DP 590 steel

Underload cycle 339 MPa in tension -339 MPa in compression						
Small cycles						
Test #	Stress amplitude (MPa)	Strain amplitude (%)	Number of small cycles in the block	Failure life	Number of underload cycles	Equivalent cycles to failure
1	279	0.13	200	50,053	249	51,076
2	251	0.12	100	77,252	765	82,823
3	237	0.11	100	107,084	1060	118,595
4	237	0.11	100	143,000	1416	164,939
5	223	0.11	100	155,400	1539	181,847
6	209	0.10	100	219,616	2174	277,846
7	195	0.09	120	163,800	1354	187,886
8	181	0.09	200	287,893	1432	334,338
9	167	0.08	200	418,648	2083	526,165
10	153	0.07	230	960,000	4156	1,635,599
11	145	0.07	250	550,000	2191	701,510
12	140	0.07	1,000	1,334,177	1333	1,537,838
13	126	0.06	2,800	2,800,050	1000	3,110,056
14	117	0.06	3,000	3,000,000	1000	3,332,222
15	112	0.05	4,500	8,031,952	1784	9,773,817
16	106	0.05	10,000	9,668,529	967	10,702,493
17	98	0.05	10,000	7,163,823	716	7,715,540
18	92	0.04	10,000	*10,000,000	1000	*11,110,000

*3 Run-Out Tests

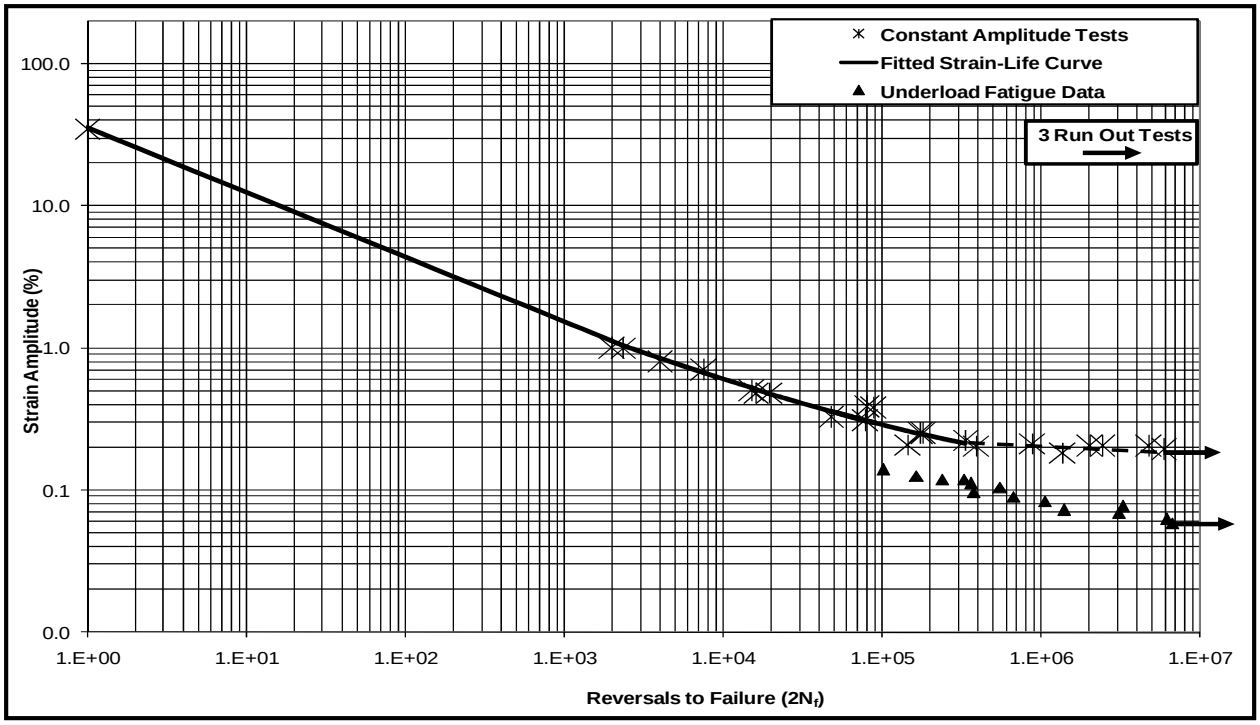

Figure 4.2 Underload fatigue data for DP 590 steel

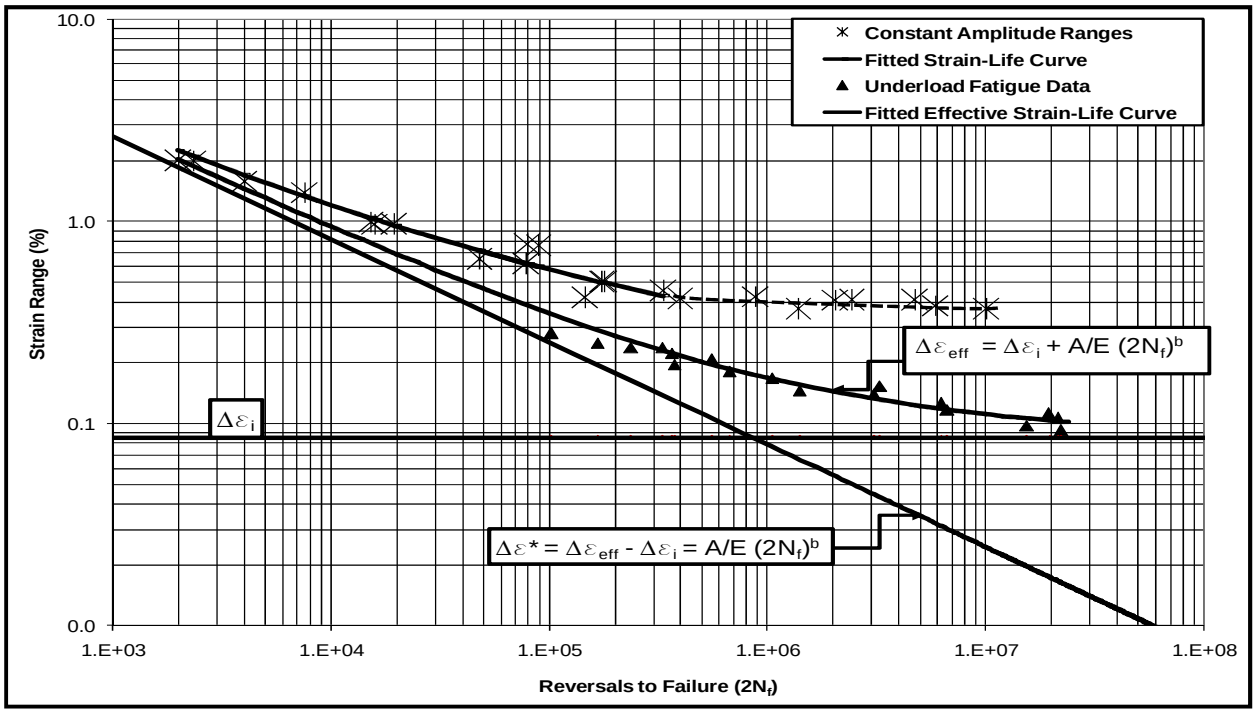

Figure 4.3 Fitted effective strain-life curve for DP 590 steel

4.2.3 Steady State Crack Opening Stresses

Steady state crack opening stresses were modeled using DuQuesnay's equation (Eq. 2.3). A series of crack opening stress measurements (Chapter 3, Section 3.3.4) were performed on DP 590 steel under 3 stress ratios (-1, 0, and 0.8) to calibrate the constants in the equation. A loading sequence of a typical test consisted of an underload of yield stress magnitude (339 MPa in these tests) followed by fully reversed constant amplitude cycles until a steady state crack opening stress was reached. The procedure for measuring the crack opening stress was to stop the test at the maximum stress of the chosen cycle and then decrease the load manually until the two crack surfaces touched each other at 0.2 mm behind the crack tip. Two sets of readings were recorded using a 900x power short focal length optical video microscope and averaged for each crack opening stress at cycles 1, 10, 50, 100, 200, 500, 1000, 2000, 3000 and 5000 after each application of an underload. The steady state crack opening stress (Figures 4.4, 4.5, and 4.6) initially increased linearly with the maximum stress in a cycle, it then levelled off at about one half of the material yield stress and then decreased until it fell below zero when the plastic zone at the crack tip expanded rapidly as the metal yield stress was approached. Figure 4.7 shows a comparison of the steady state crack opening stresses for the 3 stress ratios (-1, 0, and 0.8).

As mentioned previously in Chapter 2, Section 2.2.6.2, the steady state crack opening stresses were also obtained from the constant amplitude and effective strain-life curves, Figure 4.8 shows the crack opening stresses derived from the constant amplitude and effective strain-life curves together with crack opening stresses obtained from DuQuesnay's equation (Eq. 2.3) and measured stresses for a stress ratio R = -1. The two constants θ and φ in Eq. 2.3 were found to be 0.9 and 0.05 respectively.

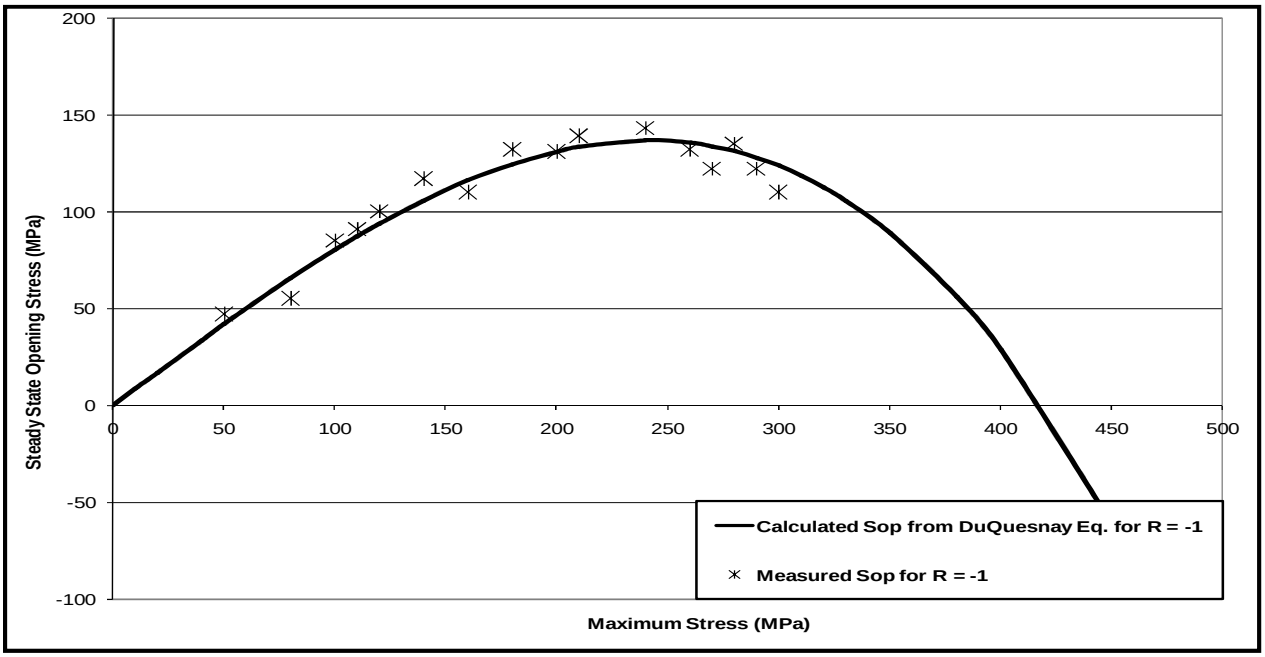

Figure 4.4 Steady state crack opening stress measurements for R = -1 for DP 590 steel

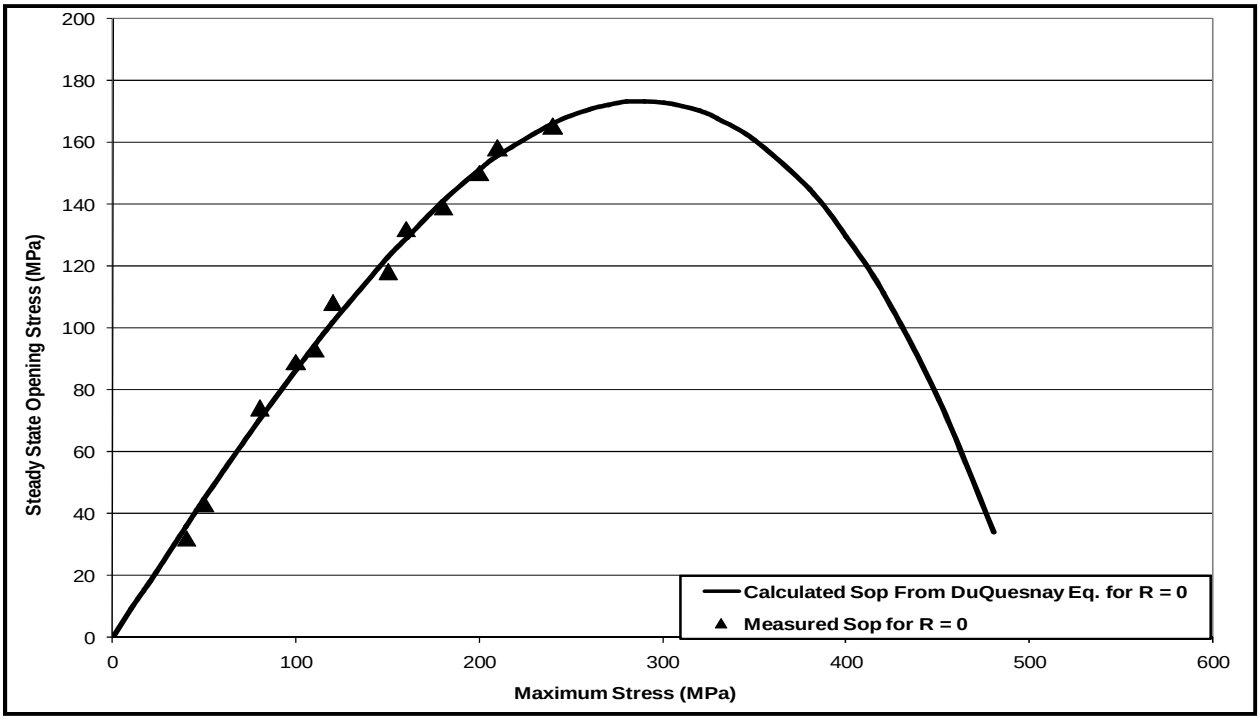

Figure 4.5 Steady state crack opening stress measurements for R = 0 for DP 590 steel

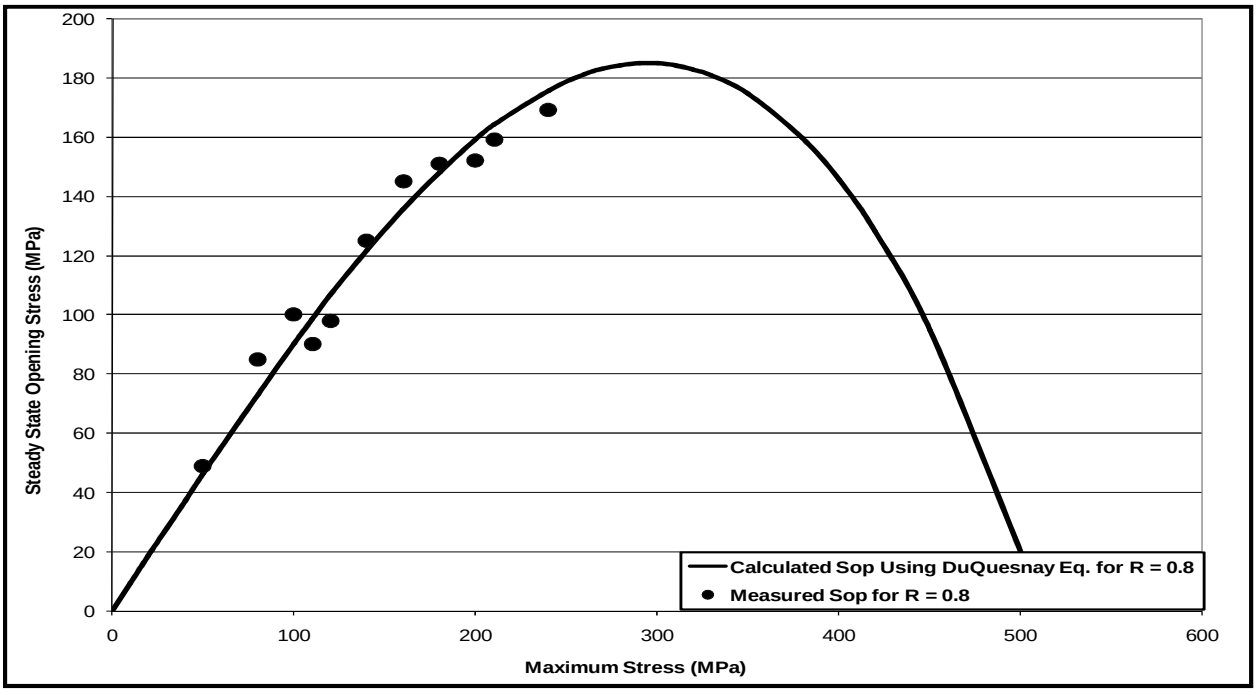

Figure 4.6 Steady state crack opening stress measurements for R = 0.8 for DP 590 steel

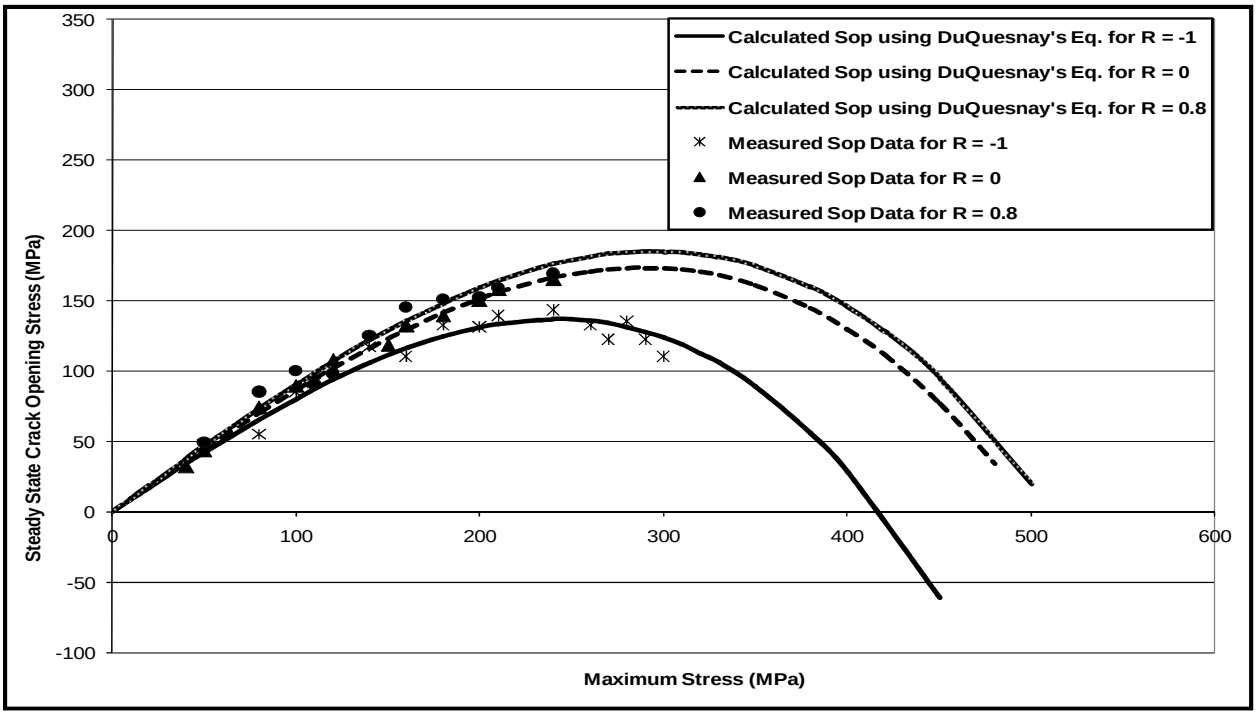

Figure 4.7 Comparison of the steady state crack opening stresses for 3 stress ratios

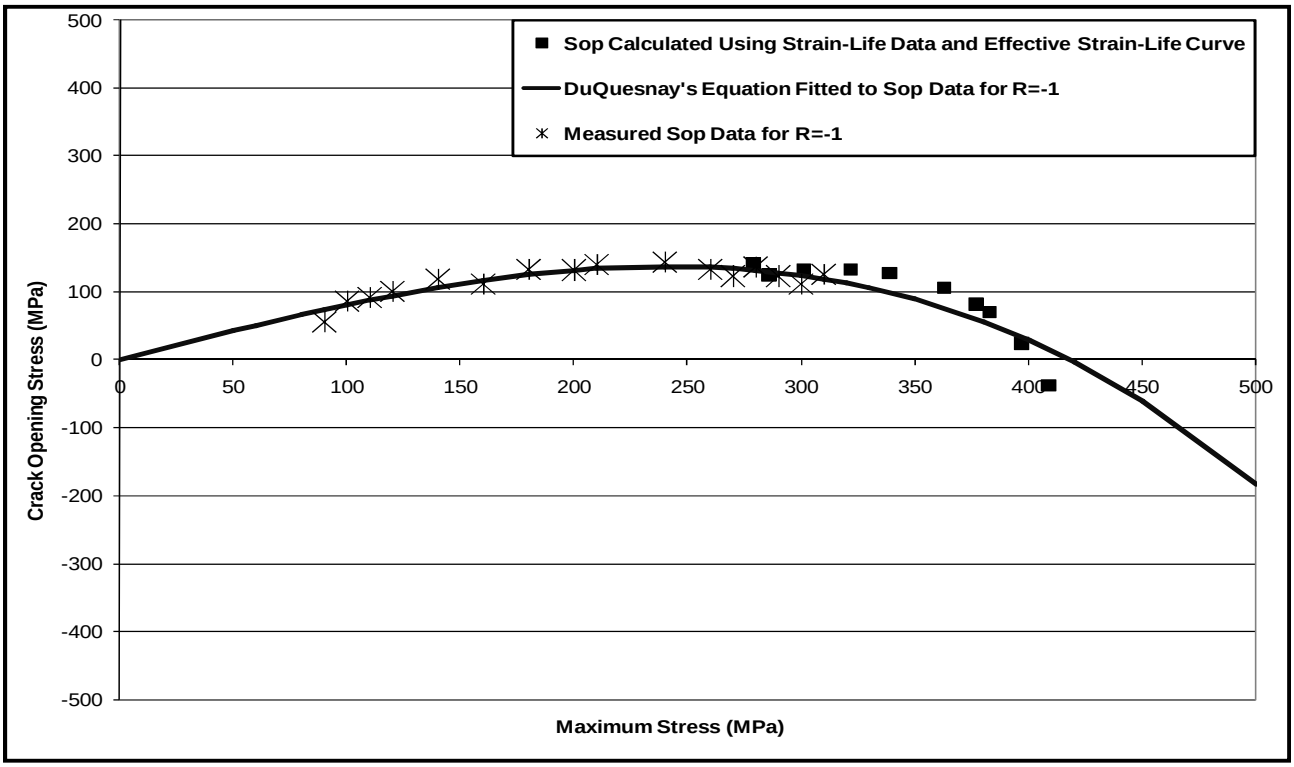

Figure 4.8 Steady state crack opening stress estimates derived from smooth specimen data fitted to DuQuesnay's equation for DP 590 steel

4.2.4 Determining the Crack Closure Parameter *"m"*

In this section a new test procedure for obtaining data on the return of the crack opening stress to a steady state level following an underload is introduced. Smooth specimens were tested under load histories with intermittent underloads and a fixed level of strain in the intervening constant amplitude cycles. The frequency of occurrence of the underloads was varied from test to test and the changes in fatigue life were observed. Table 4.3 gives the tests results. The changes in damage per block were then used to determine the value of the closure model parameter "*m*" in Eq. 2.4 that described the recovery of the crack opening stress to its steady state level. The experimental work in this section consisted of 14 underload fatigue tests where the underload cycle was set equal to the fully reversed constant amplitude stress level that gave a fatigue life of 10,000 cycles (339 MPa), and the amplitude of the small cycles was set to 200 MPa. During these tests only the number of small cycles per block was varied and their corresponding damage was calculated by subtracting the damage due to the underloads from unity. After calculating the equivalent damage done by the small cycles, the damage per cycle was plotted against the number of small cycles per block (Figure 4.9). These data were then fitted by iteratively assuming "*m*" values and calculating the crack opening stress for each small cycle in the loading block using Eq. 2.4.

Then the value of (S_{op} - S_{min} / E) (where S_{op} is the crack opening stress, S_{min} is the minimum stress of the small cycles in the loading block, and E is the modulus of elasticity) was subtracted from $\Delta\varepsilon$ (the total strain range) for each cycle to obtain the effective strain range ($\Delta\varepsilon_{eff}$). The damage was then calculated by entering $\Delta\varepsilon_{eff}$ in the effective strain-life curve shown in Figure 4.3. The damage per cycle was then summed up and divided by the number of small cycles per block to obtain the average damage per cycle. The value of "*m*" was iteratively varied to obtain a good fit of the calculated curves to the measured average damage per block. Appendix B explains the complete procedure for calculating the damage done by small cycles and fitting "*m*" to the calculated damage.

In Figure 4.9, we see three zones. The application of a large underload cycle decreased the crack opening stress from its steady state level to a value less than the minimum stress of the small cycles. As long as the crack opening stress was less than the minimum stress, the damage per cycle was constant and this is shown in the first zone (zone A-B). However as cycling progressed, the crack opening stress increased and as soon as it exceeded the minimum stress, the effective strain range of the small cycles and the damage per cycle decreased as shown in the second zone (zone B-C). In the third zone (zone C) the crack opening stress reached the steady state level for the small cycles resulting in a constant damage per cycle. A value of m = 0.023 gave a good fit to the measured damage per cycle versus the number of small cycles per block. This value of "*m*" was then used in Eq. 2.4 to calculate the changes in the crack opening stress of the small cycles after the application of an underload.

Table 4.3 Damage tests configuration for DP 590 steel

Underload cycle 339 MPa in tension -339 MPa in compression									
Small cycles									
Test #	Stress amplitude (MPa)	Strain amplitude (%)	Number of small cycles in the block	Failure life	Number of underload cycles	Damage done by small cycles	Equivalent cycles to failure	Number of blocks	Damage done by each cycle
1	230	0.11	200	194,171	966	0.90	221,338	966	4.5E-06
2	230	0.11	50	68,646	1,346	0.87	81,784	1,346	1.2E-05
3	230	0.11	300	132,459	440	0.96	140,132	440	7.1E-06
4	230	0.11	100	107,084	1,060	0.89	123,208	1,060	8.1E-06
5	230	0.11	100	143,000	1,416	0.86	174,004	1,416	5.7E-06
6	230	0.11	600	237,435	395	0.96	250,035	395	4.0E-06
7	230	0.11	1,000	360,915	361	0.96	378,534	361	2.6E-06
8	230	0.11	5,000	608,186	122	0.99	617,984	122	1.6E-06
9	230	0.11	10,000	621,037	62	0.99	626,083	62	1.6E-06
10	230	0.11	70	147,183	2,073	0.79	199,536	2,073	5.0E-06
11	230	0.11	2,000	436,448	218	0.98	449,112	218	2.2E-06
12	230	0.11	20	71,925	3,425	0.66	124,695	3,425	8.0E-06
13	230	0.11	40	62,894	1,534	0.85	76,877	1,534	1.3E-05
14	230	0.11	400	281,251	701	0.93	309,056	701	3.2E-06

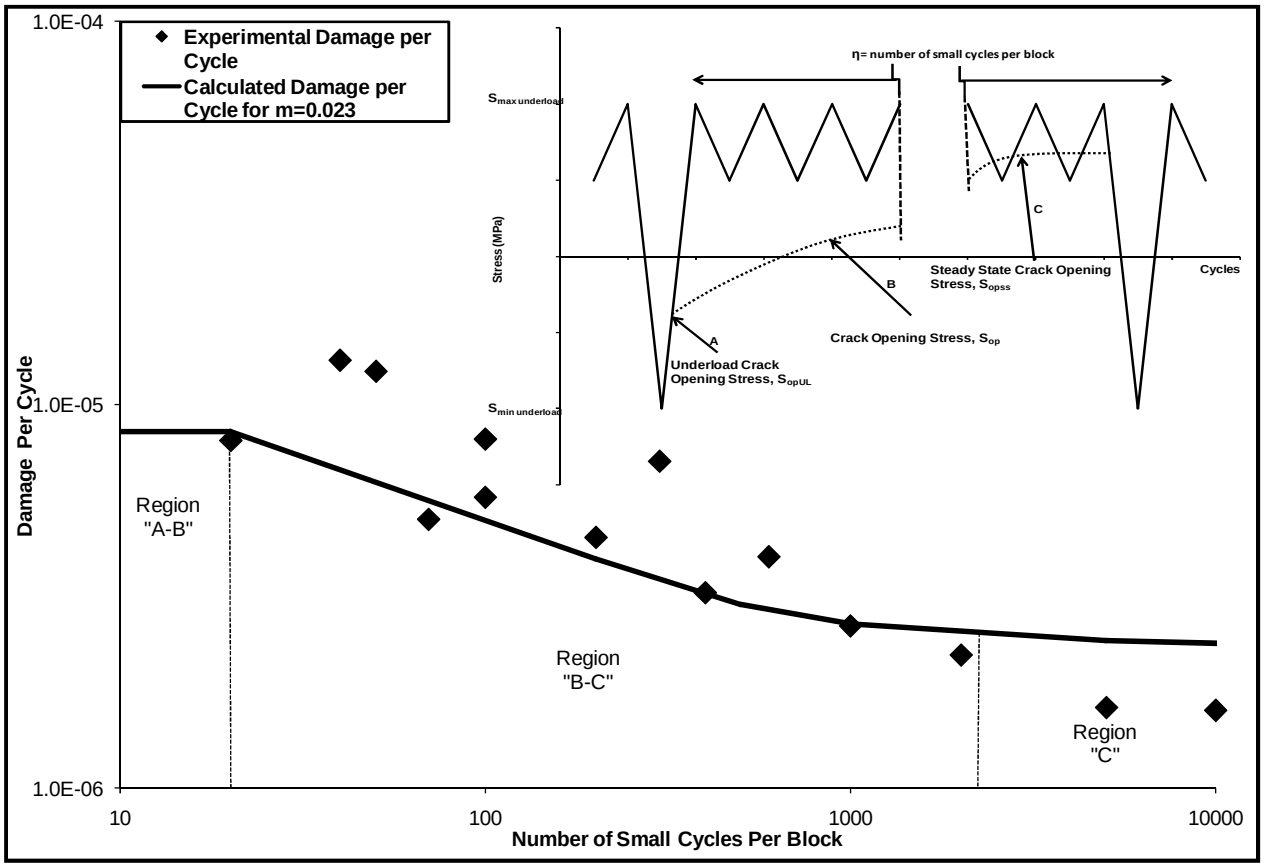

Figure 4.9 Fitted "*m*" to damage calculations for DP 590 steel

4.2.5 Crack Opening Stress Build-Up Measurements

After obtaining the crack closure parameter "*m*", the crack opening stress build-up equation (Eq. 2.4) was used to model the changes in the crack opening stress during a loading history and derive crack opening stress values that were then compared to measured values. Crack opening stress measurements (Figures 4.10, 4.11, and 4.12) were made for 3 stress levels using the previously described underload block load history under stress control. In the first test, an underload cycle with peak of -330 MPa compression and 200 MPa in tension was followed by 1000 constant amplitude small cycles at a stress ratio R = 0.8 with a maximum stress of 200 MPa and minimum stress of 160 MPa. The surface crack length at the time of measurement was 1.04 mm. In the second test the underload cycle had a stress of -330 MPa in compression and 200 MPa in tension, followed by 1000 constant amplitude small cycles with a stress ratio R = 0. The crack length at the time of the measurement was 0.98 mm and the maximum and the minimum stress peaks of the small cycles were 200 MPa and zero MPa, respectively. In the third test, the underload cycle peaks were -330 MPa in compression and 200 MPa in tension, followed by 1000 constant amplitude small cycles with a stress ratio R = -1. The maximum and the minimum stresses of the

small cycles were 200 MPa and -200 MPa, respectively. Again, the procedure for measuring the crack opening stress was to stop the test at the maximum stress of the chosen cycle and then decrease the load manually until the two crack surfaces touched each other at 0.2 mm behind the crack tip. Two sets of readings were recorded and averaged for each crack opening stress at cycles 1, 10, 50, 100, 200, 500, and 1000 after each application of an underload. Figures 4.9, 4.10, and 4.11 show the crack opening stress build-up measurements and predicted curves derived from Eq. 2.4 fitted to m = 0.023 for stress ratios.

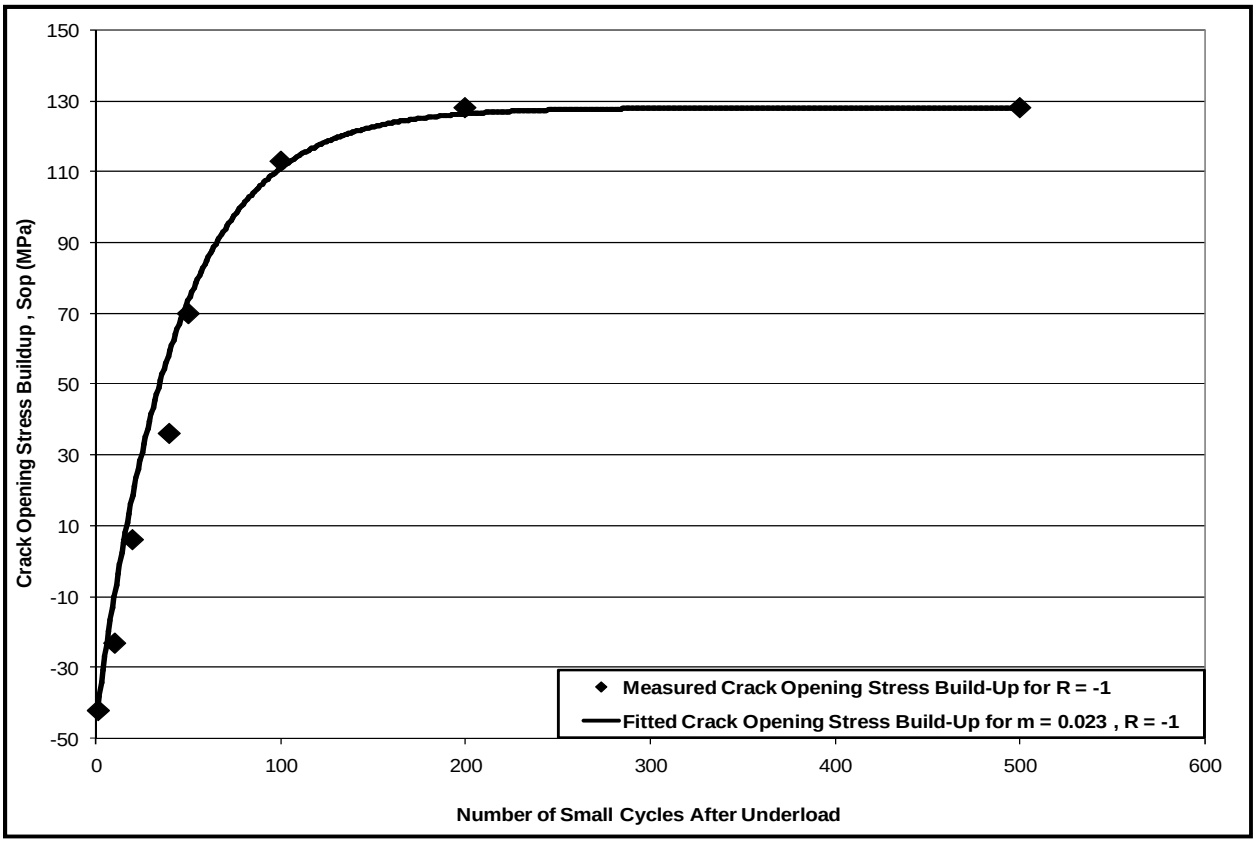

Figure 4.10 A comparison of a crack opening stress build-up curve fitted to m = 0.023 with measured data for R = -1 for DP 590 steel

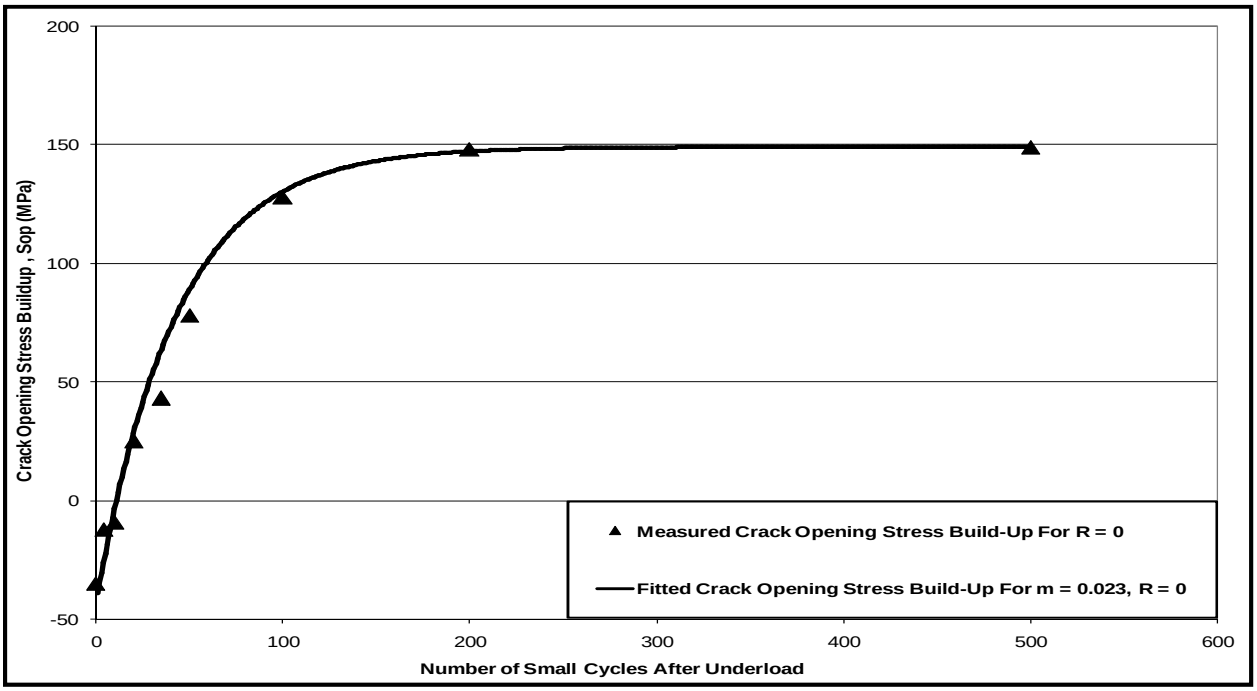

Figure 4.11 A comparison of a crack opening stress build-up curve fitted to *m* = 0.023 with measured data for R = 0 for DP 590 steel

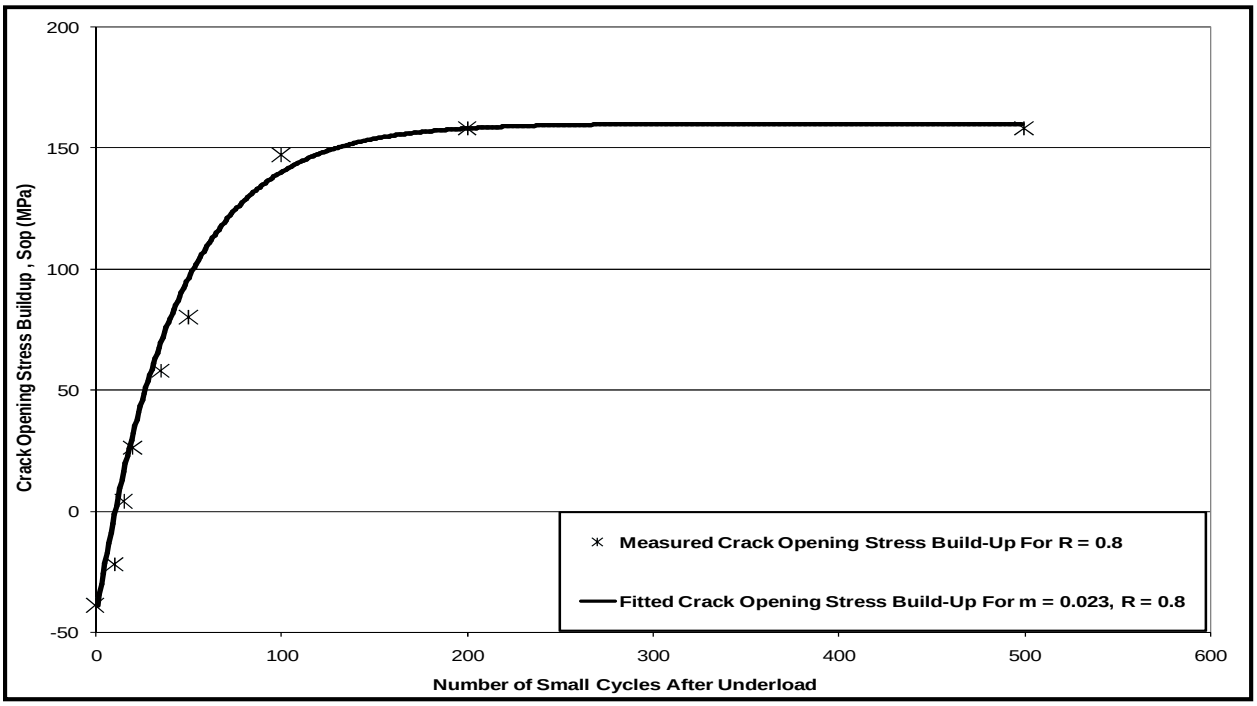

Figure 4.12 A comparison of a crack opening stress build-up curve fitted to *m* = 0.023 with measured data for R = 0.8 for DP 590 steel

4.2.6 Fatigue Life Predictions for Service Load Histories using the Effective Strain-Life Model

In this section a model that used the effective strain-life curve and the $\Delta\varepsilon^*$ damage parameter was used to predict fatigue lives for tests under two service load histories (the Log Skidder History and the Grapple Skidder History). Each history was scaled to give various maximum stress ranges and applied to a smooth specimen under stress control.

4.2.6.1 Results for the Log Skidder History

11 Fatigue tests were performed on smooth specimens under different scaled values of the Log Skidder history. As mentioned previously the history consisted of 13,344 reversals and for each test, the history was scaled to different maximum stress amplitudes. Figure 4.13 shows the predicted fatigue lives using the effective strain-life model together with experimental fatigue lives for the Log Skidder history.

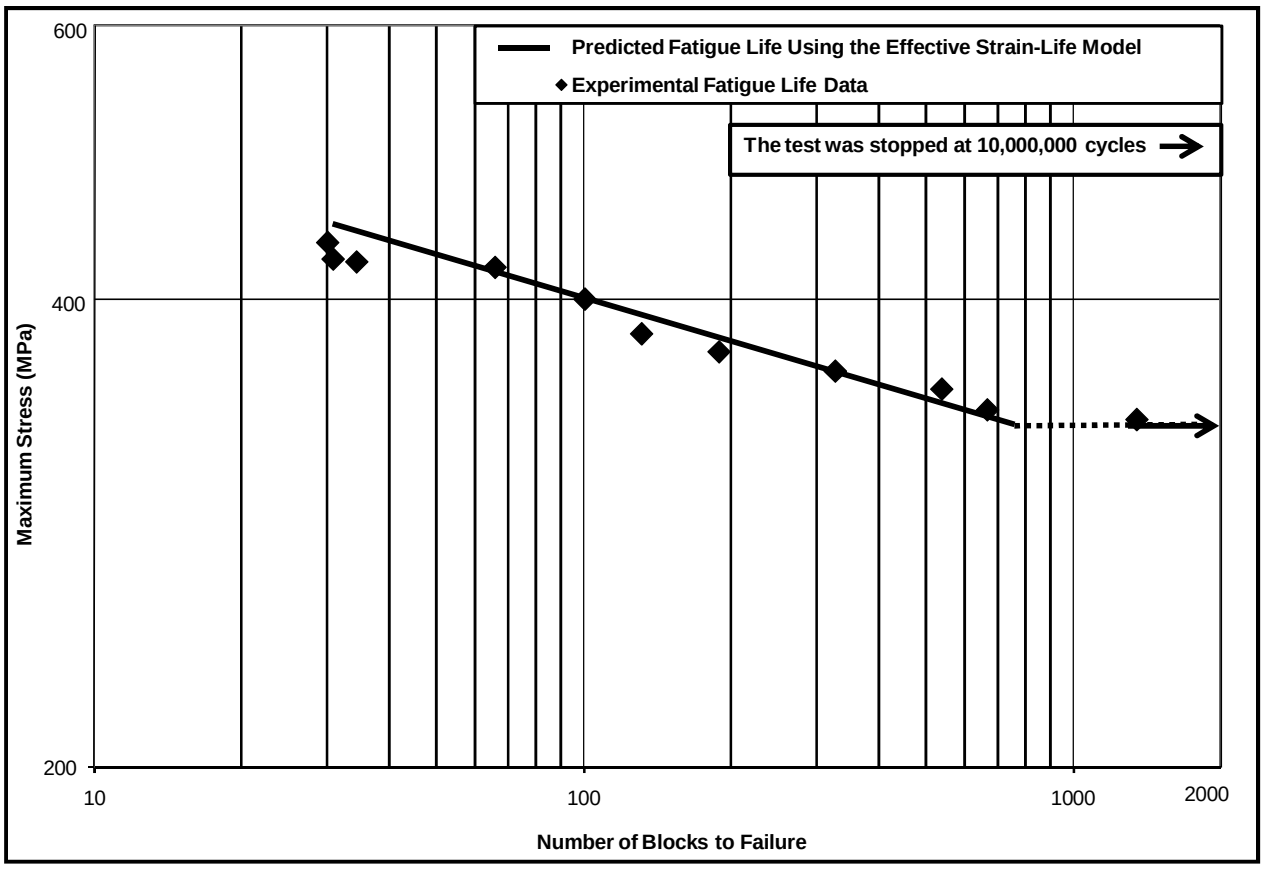

Figure 4.13 Experimental and predicted fatigue lives versus maximum stress for DP 590 steel subjected to the Log Skidder History

4.2.6.2 Results for the Grapple Skidder History

In this part 13 fatigue tests were performed on DP 590 smooth specimens under different scaled Grapple Skidder Histories. The history consisted of 41,112 reversals and in each test different scaled maximum stress amplitudes were applied. Figure 4.14 shows the predicted fatigue lives using the effective strain-life model together with experimental fatigue lives for the Grapple Skidder History.

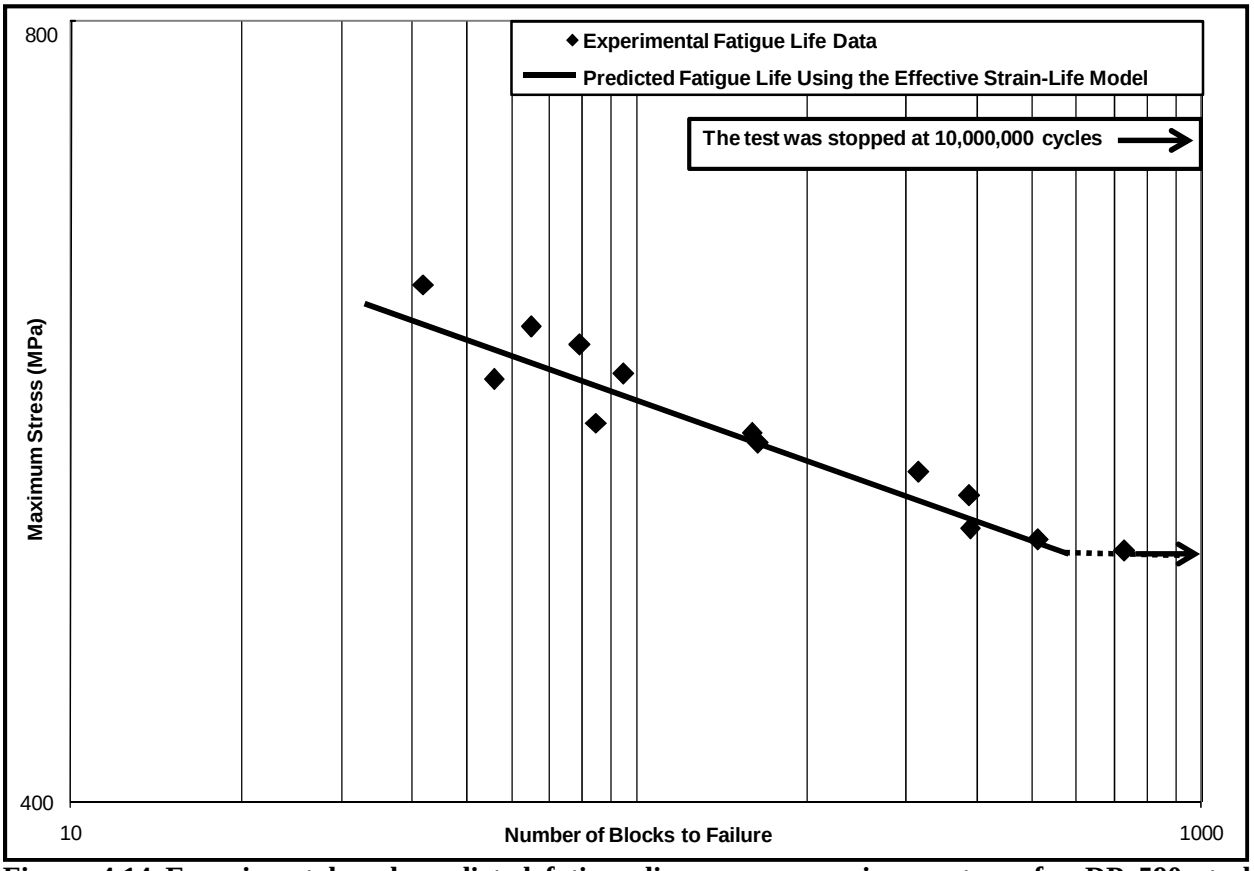

Figure 4.14 Experimental and predicted fatigue lives versus maximum stress for DP 590 steel subjected to the Grapple Skidder History

4.3 Effective Fatigue Crack Growth Model

The work in this part included the derivation of the closure free crack growth curve (Chapter 2, Section 2.4.5) from the effective strain-life curve and comparing it with experimental measurements performed on notched samples (0.3 mm radius) under the two service load histories. Crack opening stresses were also calculated using the crack growth model and compared to measured values. Finally predicted fatigue lives under different scaled load histories were compared with experimental fatigue lives.

4.3.1 Derivation of the Closure Free Crack Growth Curve and Closure Free Crack Growth Measurements

The derivation of the closure free crack growth curve from the effective strain-life curve was presented in Chapter 2, Section 2.4.5. Closure free crack growth measurements were obtained for DP 590 steel specimens with a 0.3 mm radius notch. As a first step, the specimen was pre-cracked by applying constant amplitude cycles going from zero to -330 MPa in compression. This allowed the crack to grow out of the notch and naturally develop into a non-propagating crack, as the closure levels reached the threshold conditions under nominal cyclic compression [69] (the notch root stress peaks were tensile). After the crack was developed, crack opening stresses were measured under a variable amplitude load history by the methodology given by Dabayeh et al. [49]. A travelling optical microscope of a magnification of 900x was mounted on the machine facing the specimen. A vernier with an accuracy of 0.0001 mm was attached to the microscope to measure changes in crack length. The technique reported was to apply a block of loading history consisting of an underload followed by small cycles which have the same maximum stress as the underload cycle. The minimum stress of the small cycles was varied from test to test to produce a succession of different ΔK_{eff} values. The underload cycle was chosen as the constant amplitude stress level that would give a fatigue life of 10,000 cycles (-339 MPa). The number of the small cycles was chosen so that damage due to the underload cycle did not exceed 10% and that the small cycles between the underloads were free of closure by making sure that the crack opening stress as it builds-up after the underloads did not reach the minimum stress of the small cycles before the application of the next underload that would reduce the crack opening stress. Figure 4.15 shows the experimental closure free crack growth measurements together with the effective stress intensity crack growth curve derived from smooth specimen fatigue data.

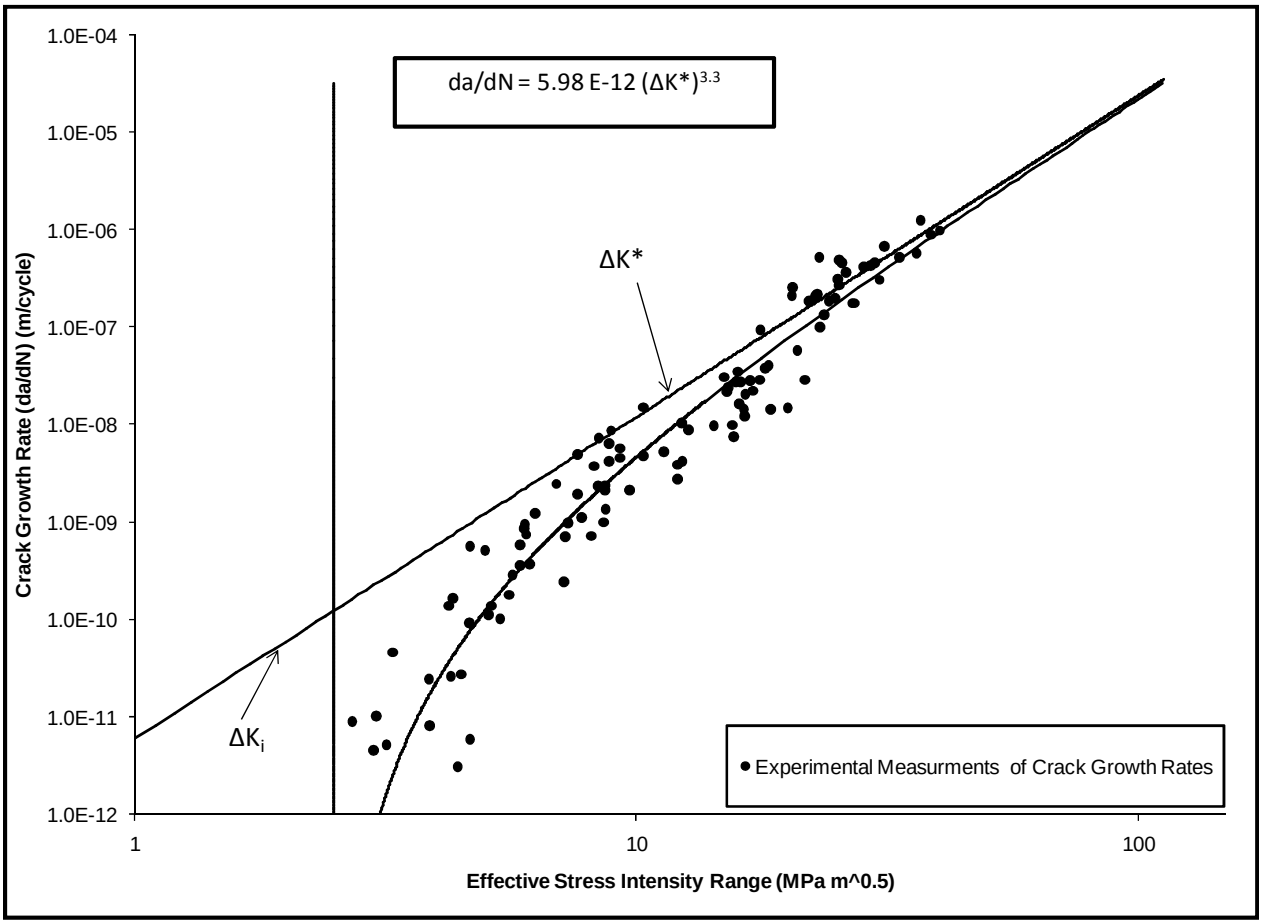

Figure 4.15 Derived effective stress intensity crack growth curve and experimental measurements of crack growth rate vs. effective stress intensity data for DP 590 steel

4.3.2 Crack Opening Stress Levels under Service Loading Histories

The crack opening stresses for DP 590 steel were measured under the SAE Grapple Skidder History and the SAE Log Skidder History. The measured values were then compared with the calculated crack opening stresses obtained from the crack growth model.

4.3.2.1 Crack Opening Stresses of DP 590 Steel under the SAE Log Skidder History

In this section, the crack opening stresses were measured for DP 590 steel under the SAE Log Skidder History. The loading spectrum was scaled to a maximum stress of 410 MPa and a minimum stress of -412 MPa. The crack opening stresses were measured using a 900x short focal length optical video microscope for different cycles and at convenient crack lengths. The procedure for measuring the crack opening stresses was to stop the test at the desired cycle number and reduce the load manually until the two surfaces of the crack touched each other at 0.2 mm behind the crack tip. Figure 4.16 shows the

nominal applied stress history together with the calculated crack opening stresses using the crack growth model and the measured crack opening stresses.

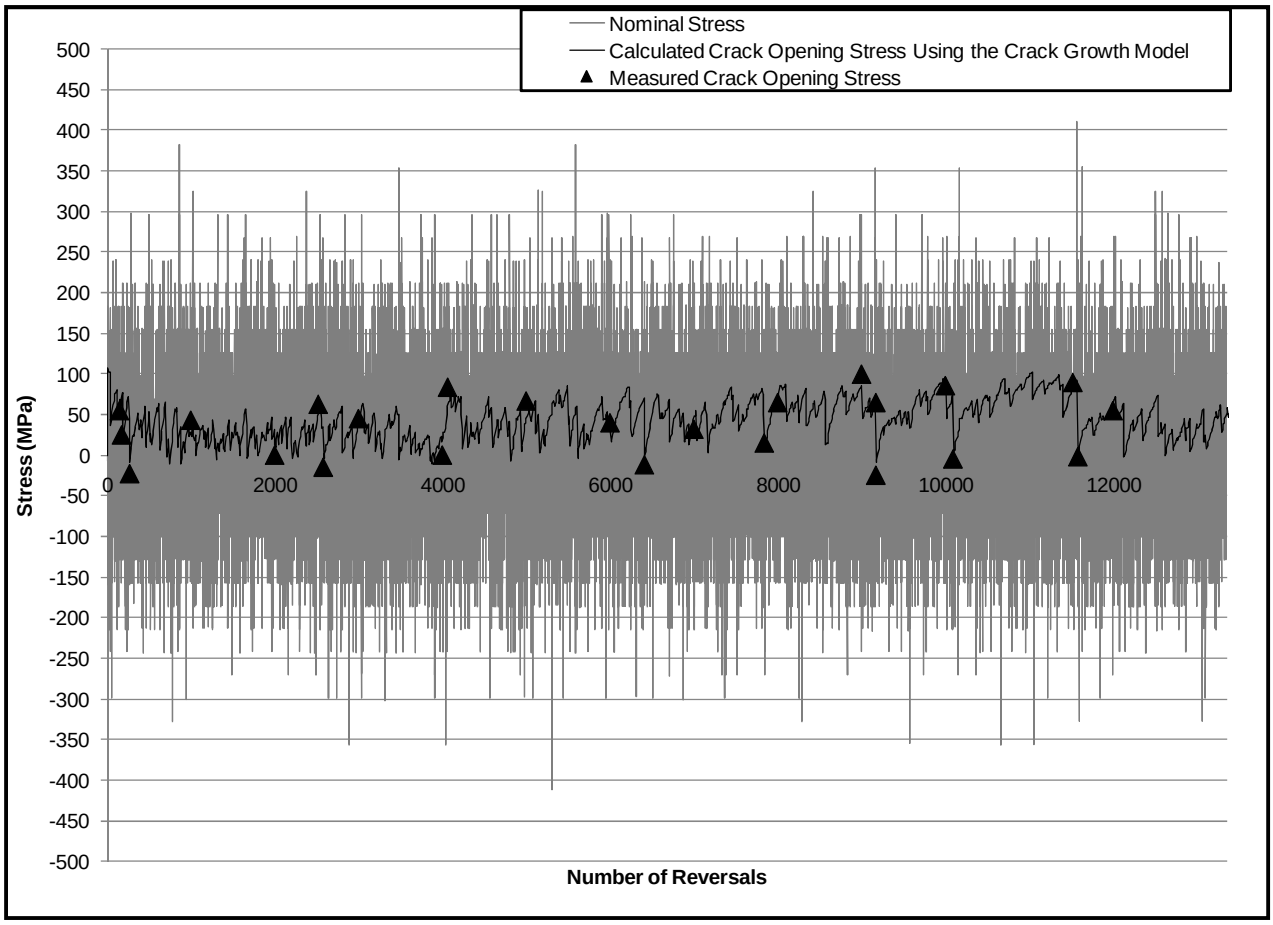

Figure 4.16 Calculated crack opening stresses and measured crack opening stresses for DP 590 steel under the SAE Log Skidder History scaled to a maximum stress of 410 MPa

4.3.2.2 Crack Opening Stresses of DP 590 Steel under the SAE Grapple Skidder History

The crack opening stresses were measured for DP 590 steel under the SAE Grapple Skidder History scaled to a maximum stress of 470 MPa and a minimum stress of -352 MPa. Again the crack opening stresses were measured using a 900x short focal length optical video microscope for different cycles and at convenient crack lengths. The procedure for measuring the crack opening stresses was to stop the test at the desired cycle number and reduce the load manually until the two surfaces of the crack touched each other at 0.2 mm behind the crack tip. Figure 4.17 shows the nominal applied stress history together with the calculated crack opening stresses using the crack growth model and the measured crack opening stresses. For all the combination of load histories (Log Skidder History and Grapple Skidder History), the crack opening stress decreased when the specimen was subjected to a large underload cycle and then it built-up again during subsequent smaller cycles.

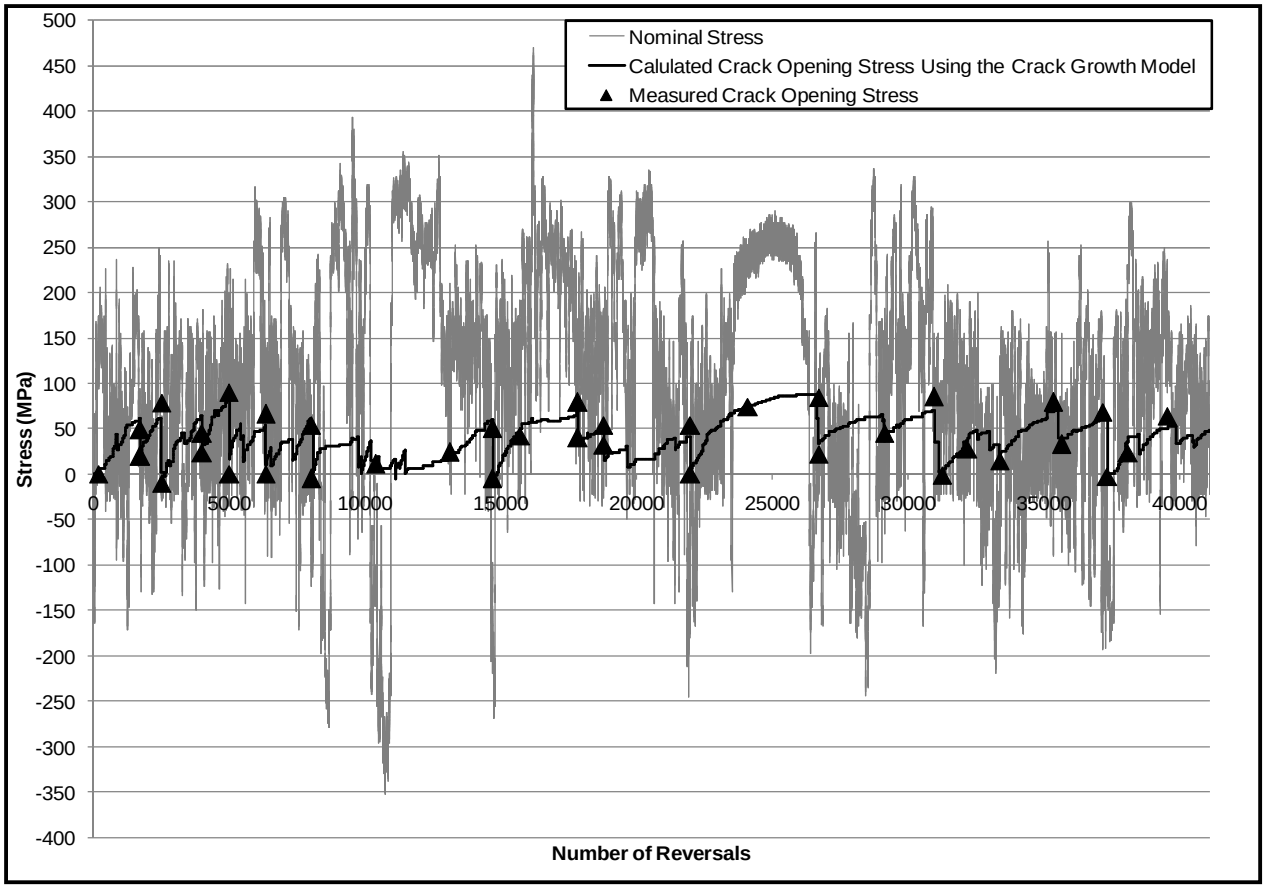

Figure 4.17 Calculated crack opening stresses and measured crack opening stresses for DP 590 steel under the SAE Grapple Skidder History scaled to a maximum stress of 470 MPa

4.3.3 Fatigue Life Predictions for Service Load Histories Using the Crack Growth Model

Fatigue life predictions based on the crack growth model are presented in this section under the two service load histories (the Log Skidder History and the Grapple Skidder History). Each history was scaled to give various maximum stress ranges and applied to a notched specimen (0.3 mm radius) under stress control. The predicted lives were then compared to the experimental values.

4.3.3.1 Results for the Log Skidder History

In this part, 11 fatigue tests were performed on notched specimens under different scaled values of the Log Skidder history. As mentioned previously the history consisted of 13,344 reversals and for each test, the history was scaled to different maximum stress amplitudes. Figure 4.19 shows the predicted fatigue lives using the crack growth model together with the experimental fatigue lives for the Log Skidder history.

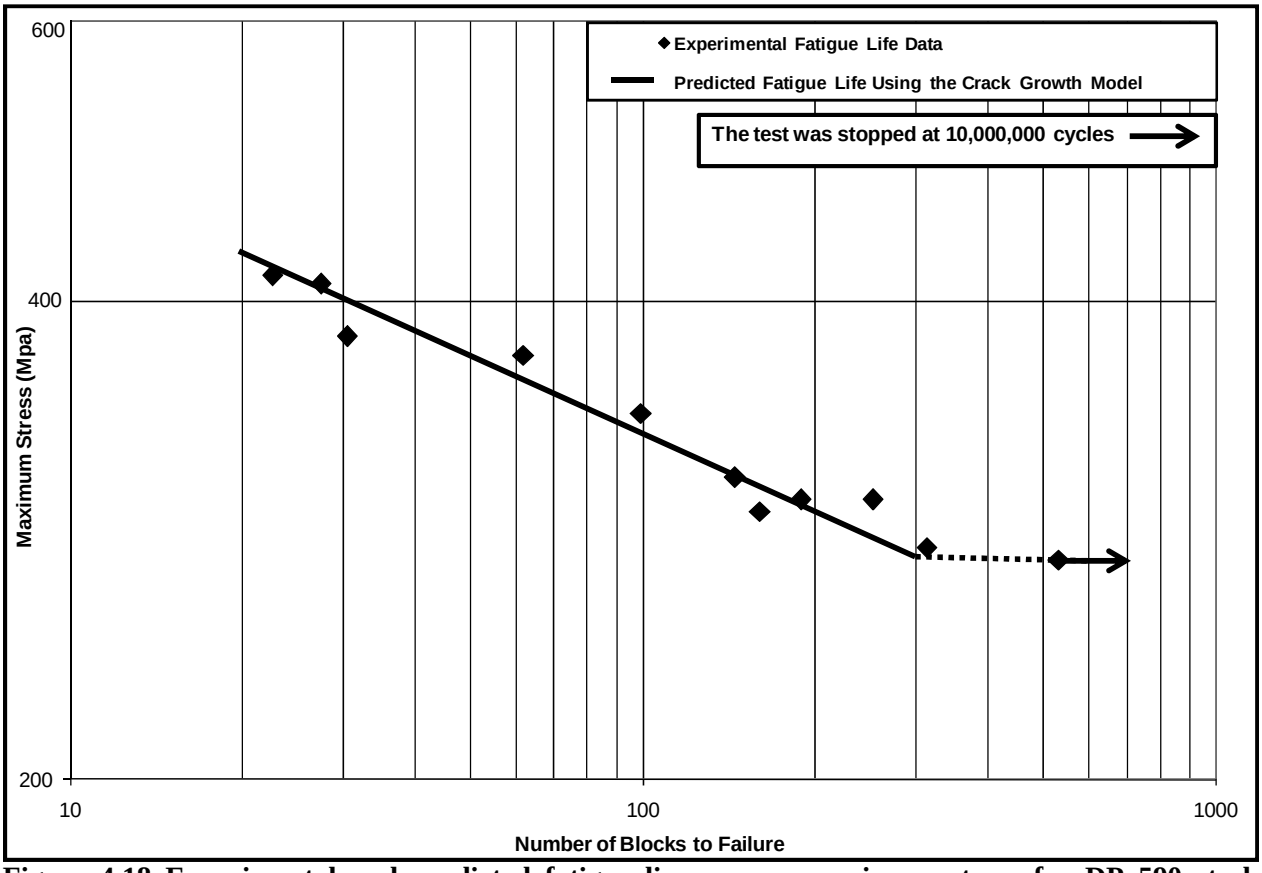

Figure 4.18 Experimental and predicted fatigue lives versus maximum stress for DP 590 steel subjected to the Log Skidder History

4.3.3.2 Results for the Grapple Skidder History

14 Fatigue tests were performed on notched specimens under different scaled values of the Grapple Skidder history. The history consisted of 41,112 reversals and for each test the history was scaled to different maximum and minimum stress amplitudes. Figure 4.19 shows the predicted fatigue lives using the crack growth model together with the experimental fatigue lives for the Log Skidder history.

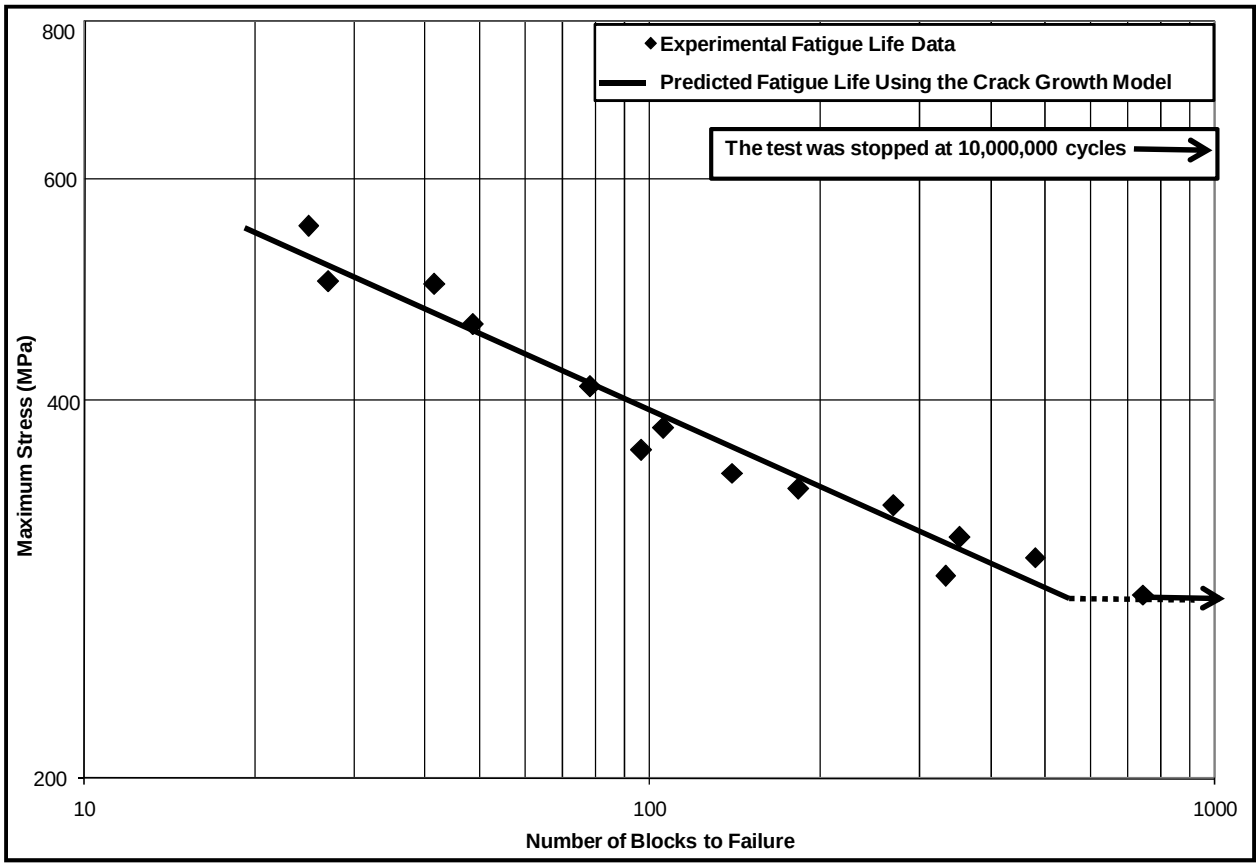

Figure 4.19 Experimental and predicted fatigue lives versus maximum stress for DP 590 steel subjected to the Grapple Skidder History

Chapter 5
Experimental Results for SAE 1045 Steel

5.1 Introduction

The experimental results for SAE 1045 steel are presented in this chapter. The monotonic and cyclic stress-strain curves as well as the mechanical properties for this material are presented in Chapter 3 Section 3.1.2. The results in this chapter include all the tests performed to develop the effective strain-life model as well as the fatigue crack growth model.

5.2 Effective Strain-Life Curve

5.2.1 Strain-Life Curve

The strain-life curve was constructed from axial, constant amplitude, fully reversed (R = -1) strain controlled fatigue tests (Table 5.1) using a servo-controlled closed-loop electro-hydraulic testing machine with a process control computer controlled by a software [68] to output constant strain or load amplitudes in the form of sinusoidal waves. Specimen failure was defined as a 50% drop in the tensile peak load from the peak tensile load observed at one half of the expected specimen life. In strain controlled tests, the loading frequency varied from 0.05 Hz to 3 Hz. For fatigue lives greater than 100,000 reversals (once the stress-strain loops had stabilized) the specimens were tested in load control. For the load controlled tests, failure was defined as the separation of the specimen into two pieces. The test frequency used in this case was 70 Hz. Figure 5.1 shows the experimental fatigue data and the fitted total strain-life curve.

Table 5.1 Constant amplitude strain-life data for SAE 1045 steel

Test #	True strain amplitude (%)	True stress amplitude (MPa)	True plastic strain amplitude (%)	True elastic strain amplitude (%)	Fatigue life (reversals to failure)
1	1.577	885	1.146	0.432	450
2	0.988	835	0.581	0.408	1,600
3	1.005	853	0.589	0.416	2,900
4	0.984	813	0.587	0.396	3,060
5	0.697	804	0.305	0.392	6,200
6	0.703	804	0.310	0.392	4,000
7	0.700	785	0.317	0.383	6,000
8	0.501	749	0.136	0.365	11,200
9	0.495	724	0.142	0.353	22,000
10	0.494	723	0.141	0.353	19,700
11	0.403	740	0.042	0.361	56,816
12	0.371	659	0.049	0.321	92,600
13	0.348	679	0.017	0.331	209,506
14	0.349	665	0.025	0.324	119,118
15	0.349	642	0.035	0.313	245,388
16	0.322	622	0.018	0.303	72,112
17	0.303	572	0.024	0.279	*10,000,000
18	0.293	577	0.012	0.281	*10,000,000
19	0.305	589	0.018	0.287	426,156
20	0.265	509	0.017	0.248	*10,000,000
21	0.273	532	0.014	0.259	*10,000,000
22	0.276	542	0.011	0.264	*10,000,000

* Run-Out Tests

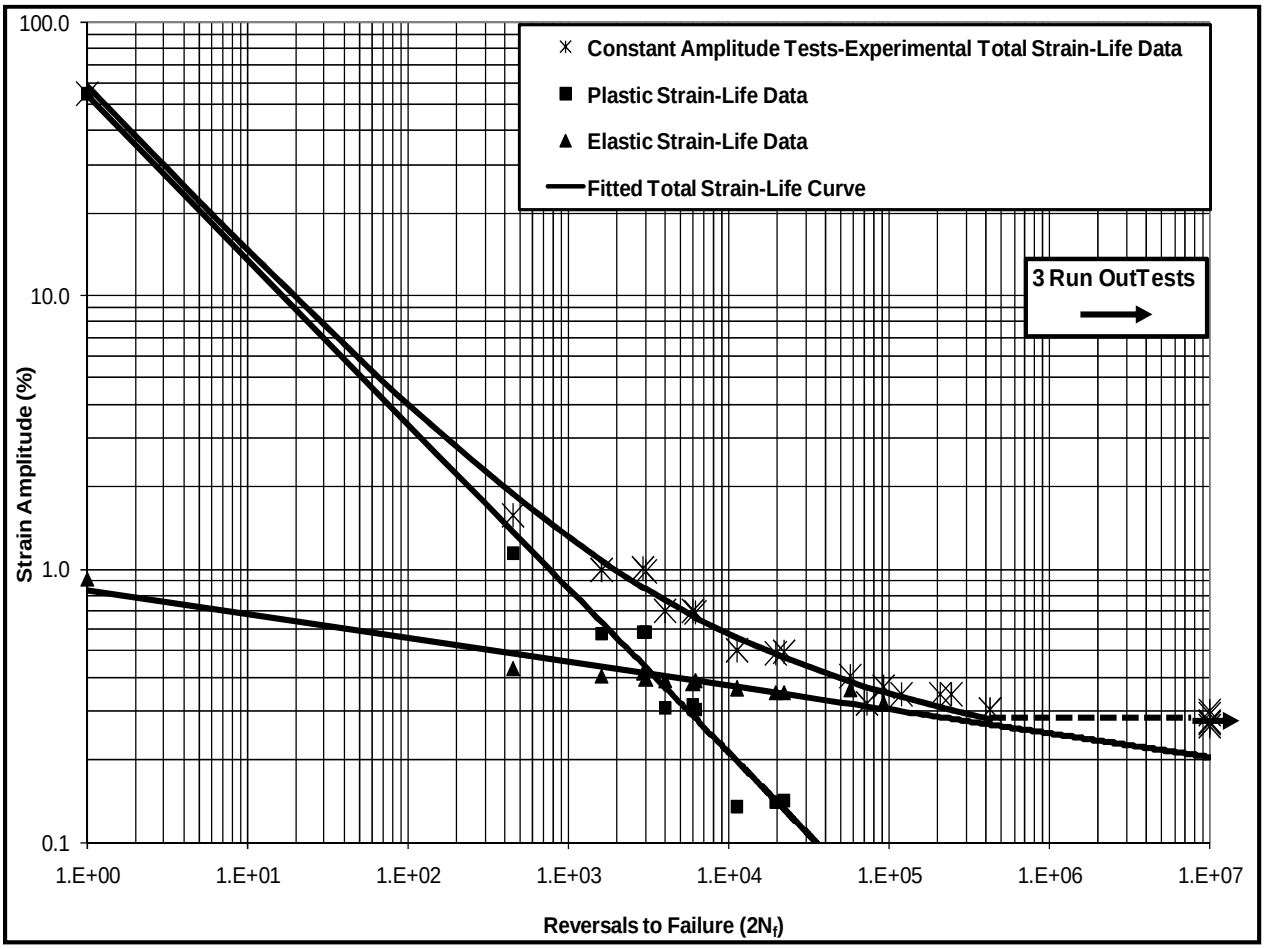

Figure 5.1 Fitted strain-life curve for SAE 1045 steel

5.2.2 Underload Fatigue Data and the Effective Strain-Life Curve

The effective strain-life curve was derived from periodic underload fatigue tests performed under stress control consisting of a repeated load cycle block. The block consisted of a single underload cycle followed by a number of smaller load cycles that had the same maximum stress as the underload cycle. This block was then repeated until the specimen failed. As mentioned previously the aim was to have the large cycle (underload cycle) occur frequently enough that the crack opening stress remained below the minimum stress of the smaller load cycles so that subsequent crack growth during small cycle application was crack closure free. The underload cycle in this work was set equal to the fully reversed constant amplitude stress level that gave a fatigue life of 10,000 cycles (725 MPa). The reason for this choice was to achieve a large reduction in crack opening stress without expending an undue fraction of the total damage in the large cycles. The number of small cycles in the second block was chosen so that they were responsible for 80 to 90% of the damage to the specimen and that they were free from crack closure.

Table 5.2 shows the tests configuration. The periodic underload fatigue data for the SAE 1045 steel specimens are shown in Figure 5.2 together with the constant amplitude strain-life curve. The derived effective strain-life curve is shown in Figure 5.3, the constants *A*, and *b* in the effective strain-life curve (Eq. 2.9) were found to be 34.2 and -0.39 respectively. The intrinsic strain range, $\Delta\varepsilon_i$, was found to be 0.27% which made the curve of $E\,\Delta\varepsilon^*$ values (calculated from Eq. 2.5) *vs.* N_f linear on logarithmic scales.

Table 5.2 Underload fatigue tests for SAE 1045 steel

Underload cycle 725 MPa in tension -725 MPa in compression						
Small cycles						
Test #	Stress amplitude (MPa)	Strain amplitude (%)	Number of small cycles in the block	Failure life	Number of underload cycles	Equivalent cycles to failure
1	553	0.27	150	18,596	125	19,299
2	526	0.26	100	81262	814	93,765
3	498	0.24	80	8860	112	8,548
4	470	0.23	50	18946	380	19,875
5	443	0.22	100	136,524	1,366	167,521
6	415	0.20	150	59,443	397	65,781
7	387	0.19	180	172,000	957	203,579
8	332	0.16	300	634,615	2,116	856,026
9	304	0.15	1,500	542,411	363	611,168
10	277	0.13	800	377,533	473	429,287
11	243	0.12	1,000	428,776	430	485,825
12	205	0.10	1,000	875,072	876	1,036,942
13	173	0.08	1,000	4,304,501	4,306	7,769,157
14	156	0.08	5,000	*5,001,500	1,001	*6,012,152

*3 Run-Out Tests

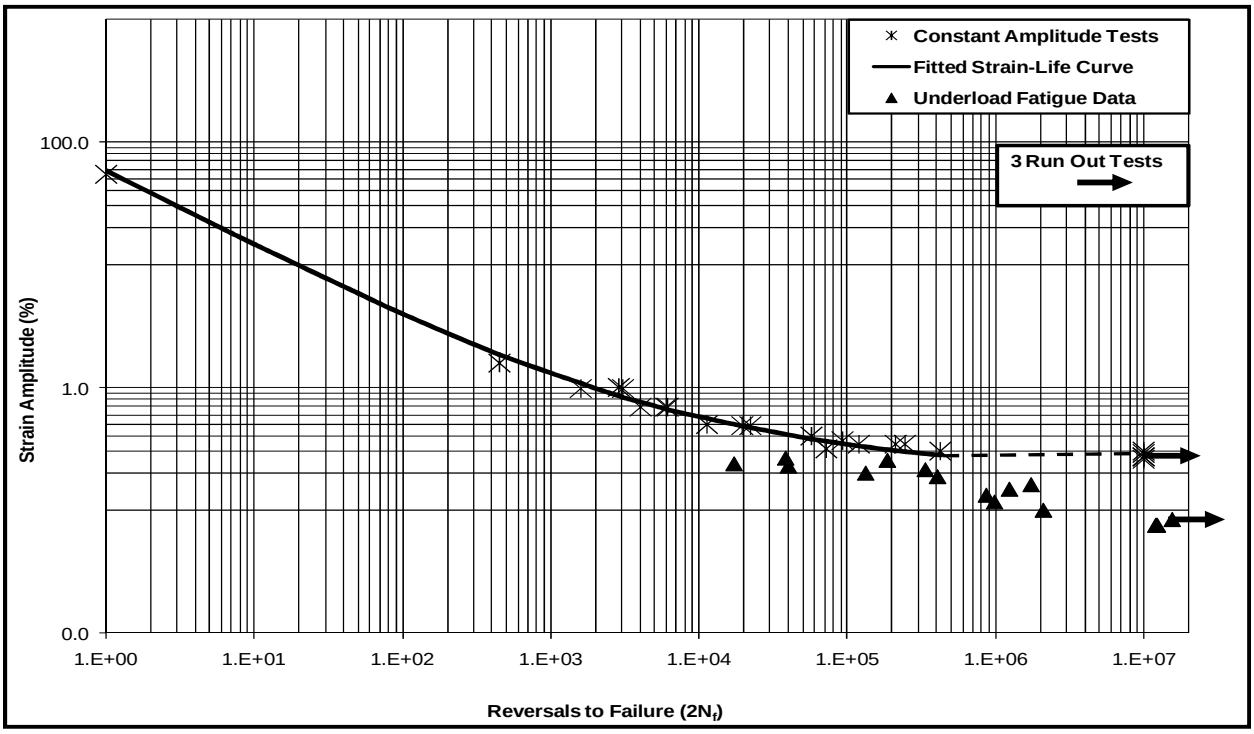

Figure 5.2 Underload fatigue data for SAE 1045 steel

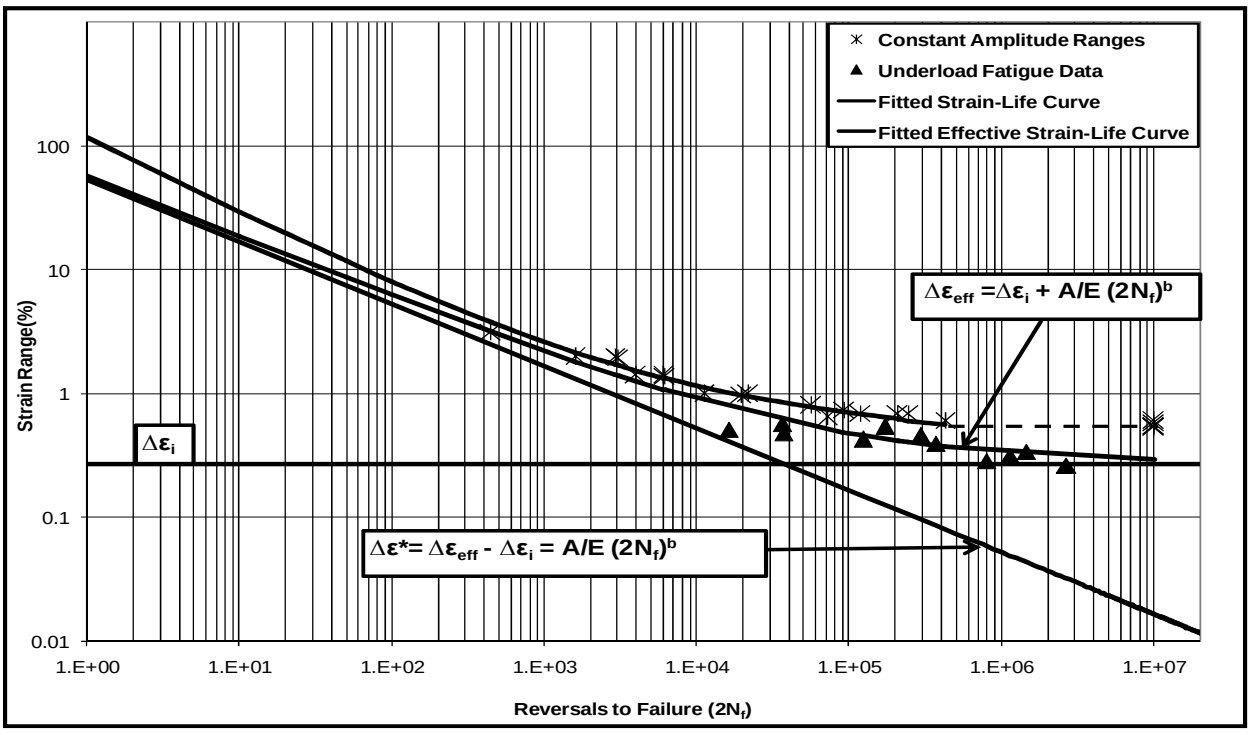

Figure 5.3 Fitted effective strain-life curve for SAE 1045 steel

5.2.3 Steady State Crack Opening Stresses

Steady state crack opening stresses were modeled using DuQuesnay's equation (Eq. 2.3). A series of crack opening stress measurements (Chapter 3, Section 3.3.4) were performed on SAE 1045 steel under three stress ratios (-1, 0, and 0.8) to calibrate the constants in the equation. A loading sequence of a typical test consisted of an underload of yield stress magnitude (729 MPa in these tests) followed by fully reversed constant amplitude cycles until a steady state crack opening stress was reached. The procedure for measuring the crack opening stress was to stop the test at the maximum stress of the chosen cycle and then decrease the load manually until the two crack surfaces touched each other at 0.1 mm behind the crack tip. Two sets of readings were recorded using a 900x power short focal length optical video microscope and averaged for each crack opening stress at cycles 1, 10, 50, 100, 200, 500, 1000, 2000, 3000, 5000, and 10, 000 after each application of an underload. The steady state crack opening stress (Figures 5.4, 5.5, and 5.6) initially increased linearly with the maximum stress in a cycle, it then levelled off at about one half of the material yield stress and then decreased until it fell below zero when the plastic zone at the crack tip expanded rapidly as the metal yield stress was approached. Figure 5.7 shows a comparison of the measured and calculated steady state crack opening stresses under 3 stress ratios (-1, 0, and 0.8). The steady state crack opening stresses were also obtained from the effective and constant amplitude strain-life curves. Figure 5.8 shows the crack opening stresses derived from the constant amplitude and effective strain-life curves together with crack opening stresses obtained from DuQuesnay's equation (Eq. 2.3) and measured stresses for a stress ratio R = -1. The two constants θ and φ in Eq. 2.3 were found to be 0.64 and 0.1 respectively.

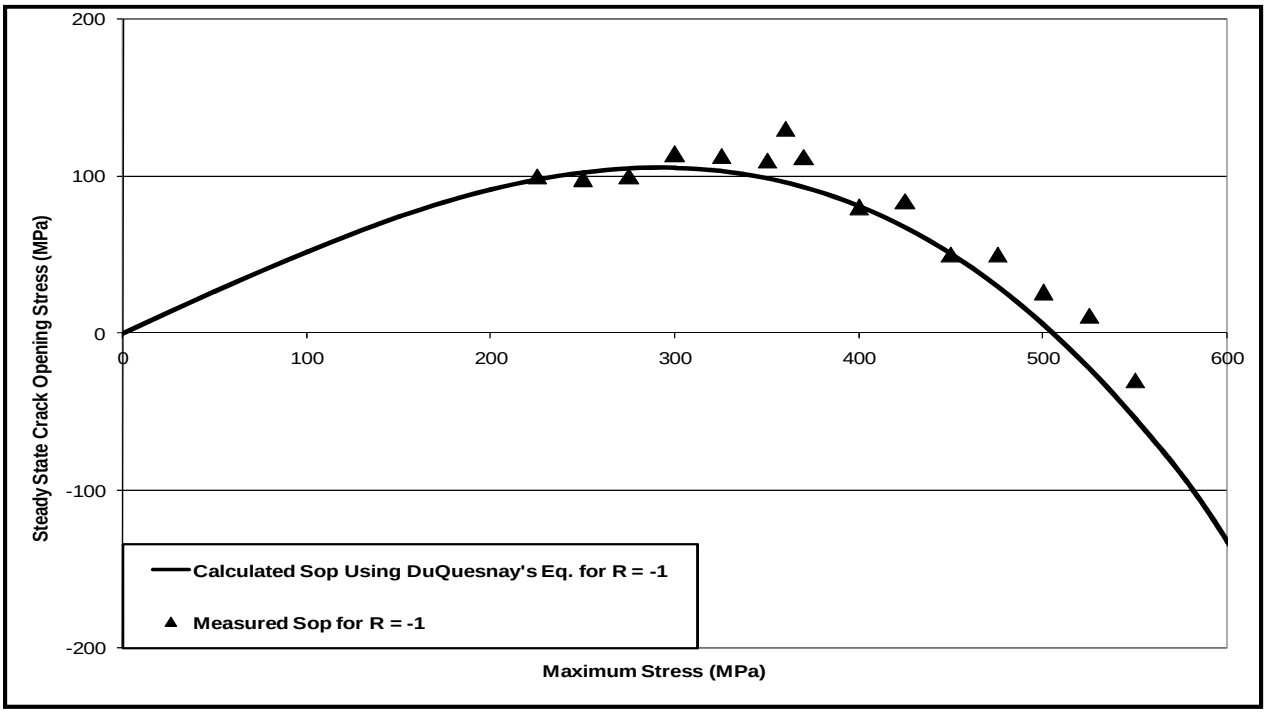

Figure 5.4 Steady state crack opening stress measurements for R = -1 for SAE 1045 steel

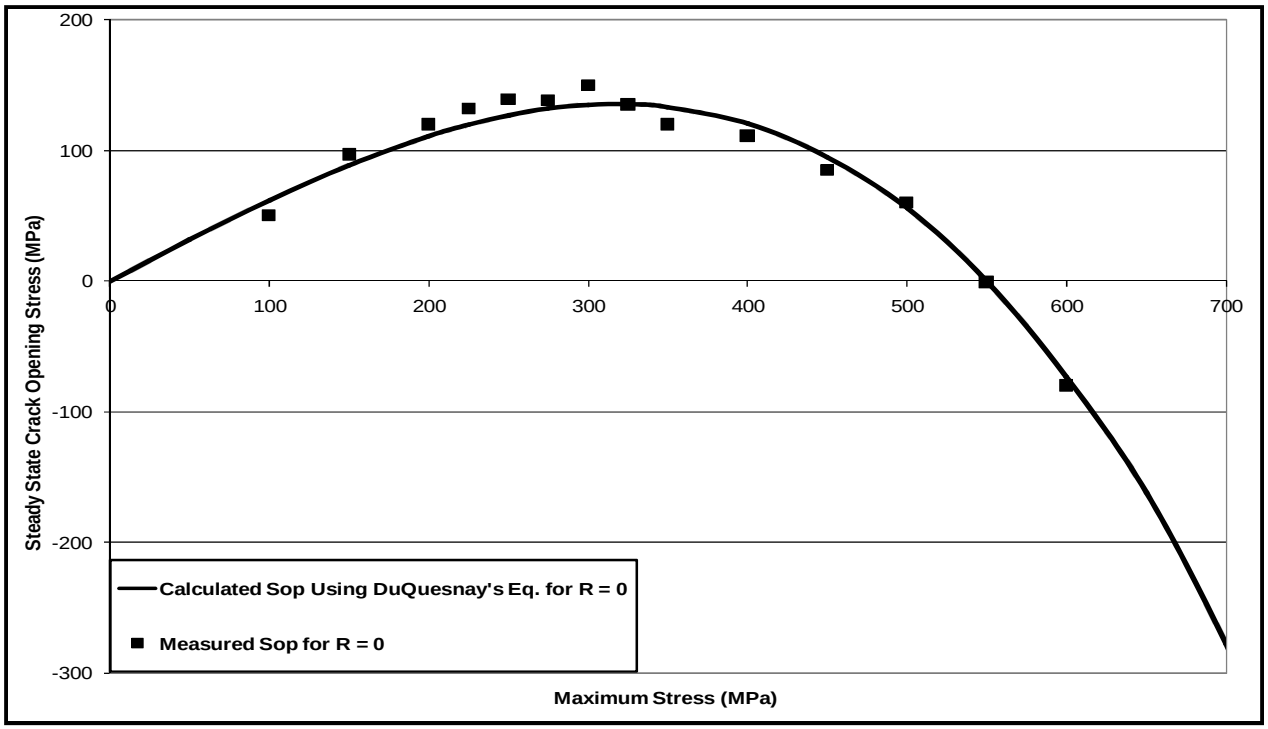

Figure 5.5 Steady state crack opening stress measurements for R = 0 for SAE 1045 steel

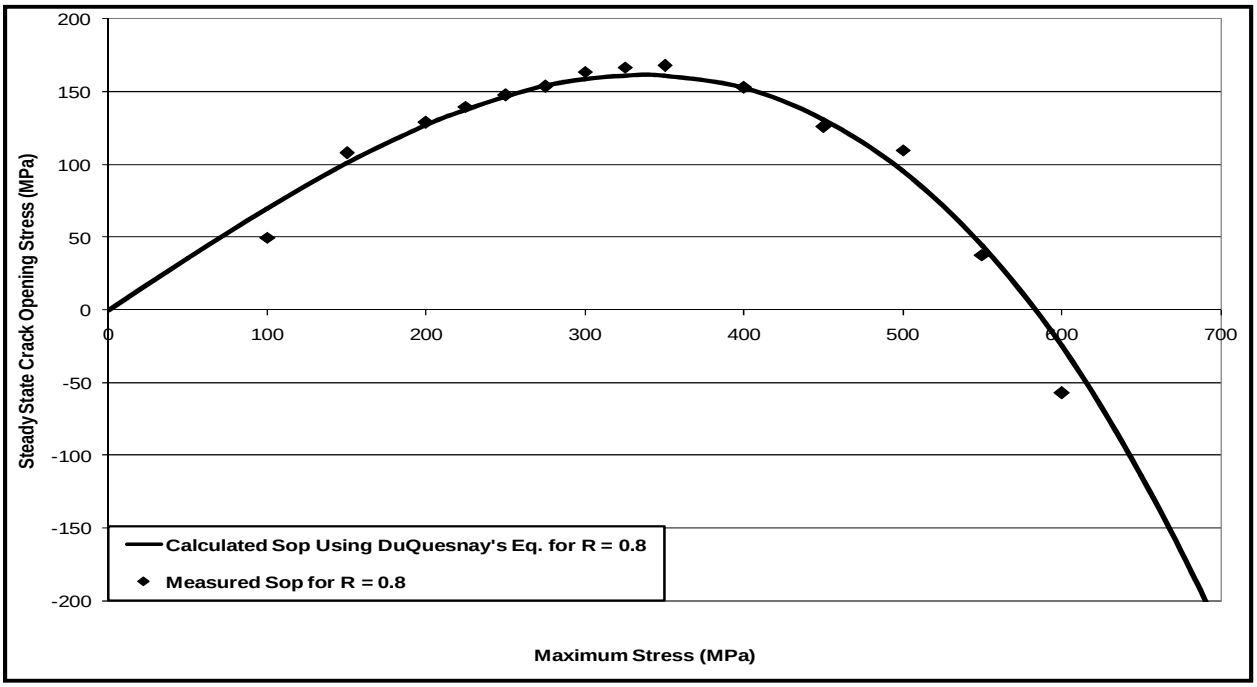

Figure 5.6 Steady state crack opening stress measurements for R = 0.8 for SAE 1045 steel

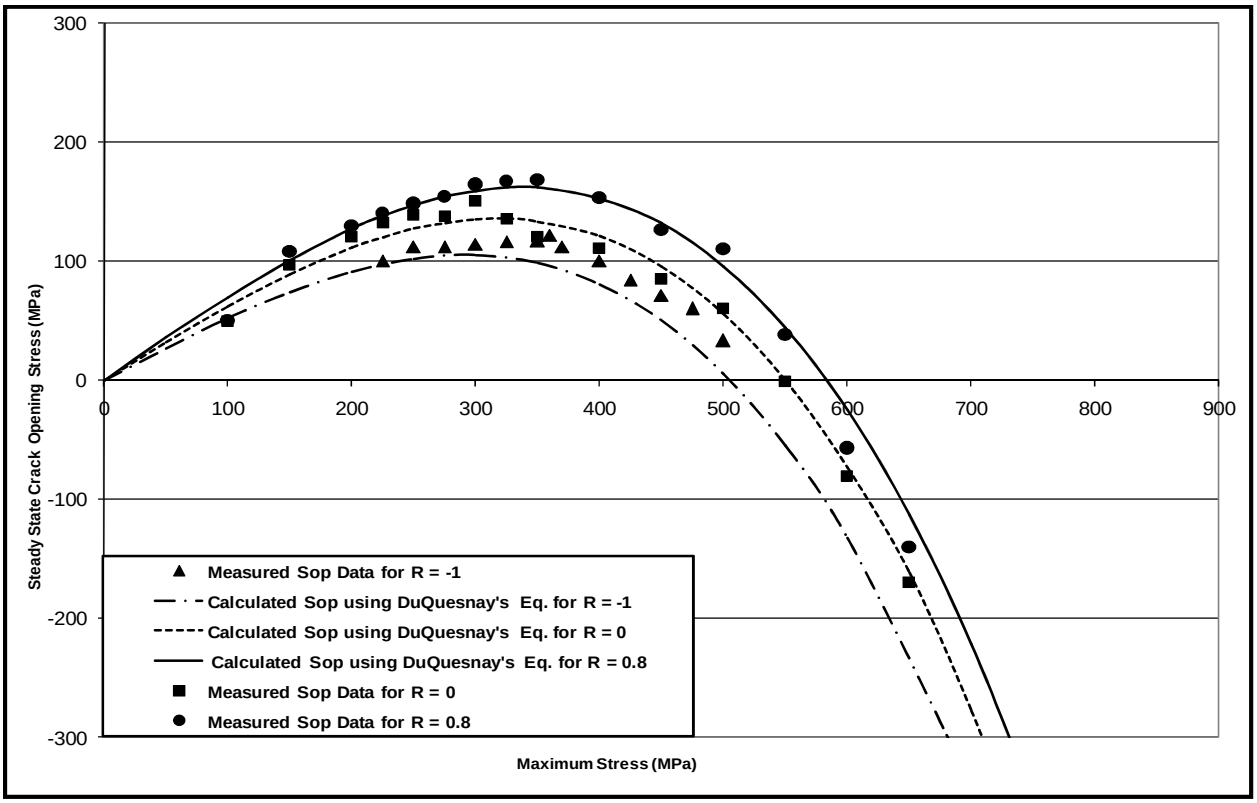

Figure 5.7 Comparison of the steady state crack opening stresses for 3 stress ratios

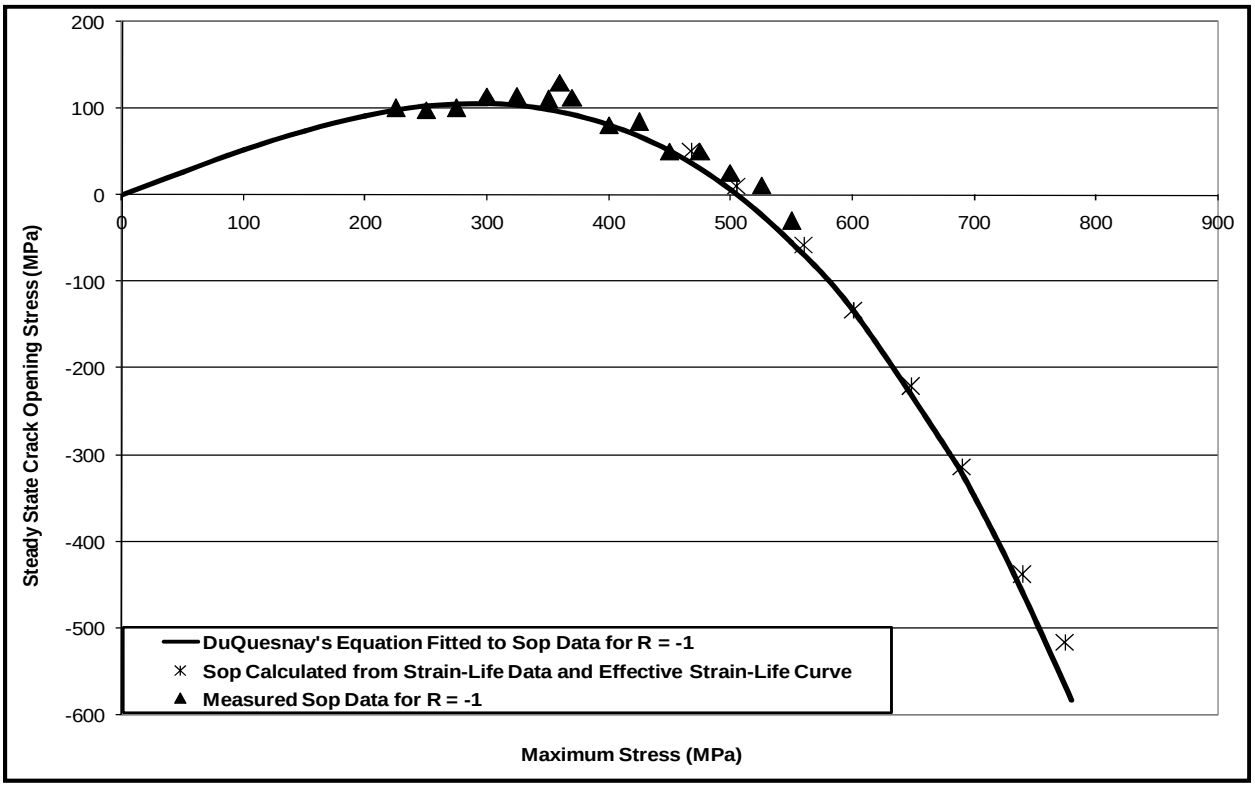

Figure 5.8 Steady state crack opening stress estimates derived from smooth specimen data fitted to DuQuesnay's equation for SAE 1045 steel

5.2.4 Determining the Crack Closure Parameter *"m"*

Smooth specimens were tested under load histories with intermittent underloads and a fixed level of strain in the intervening constant amplitude cycles. The frequency of occurrence of the underloads was varied from test to test and the changes in fatigue life were observed. Table 5.2 shows the tests results for the SAE 1045 steel. The changes in damage per block were then used to determine the value of the closure model parameter "*m*" in Eq. 2.4 that described the recovery of the crack opening stress to its steady state level. The experimental work in this section consisted of 9 underload fatigue tests where the underload cycle was set equal to the fully reversed constant amplitude stress level that gave a fatigue life of 10,000 cycles (729 MPa), and the amplitude of the small cycles was set to 200 MPa. During these tests only the number of small cycles per block was varied and their corresponding damage was calculated by subtracting the damage due to the underloads from unity. After calculating the equivalent damage done by the small cycles, the damage per cycle was plotted against the number of small cycles per block (Figure 5.9). These data were then fitted by iteratively assuming "*m*" values and calculating the crack opening stress for each small cycle in the loading block using Eq. 2.4. Then the value of (S_{op} - S_{min} / E) (where S_{op}

is the crack opening stress, S_{min} is the minimum stress of the small cycles in the loading block, and E is the modulus of elasticity) was subtracted from $\Delta\varepsilon$ (the total strain range) for each cycle to obtain the effective strain range ($\Delta\varepsilon_{eff}$). The damage was then calculated by entering $\Delta\varepsilon_{eff}$ in the effective strain-life curve shown in Figure 5.3. The damage per cycle was then summed up and divided by the number of small cycles per block to obtain the average damage per cycle. The value of *"m"* was iteratively varied to obtain a good fit of the calculated curves to the measured average damage per block. A value of m = 0.008 gave a good fit to the experimental damage per cycle.

Table 5.3 Damage tests configuration for SAE 1045 steel

Underload cycle 729 MPa in tension -729 MPa in compression									
Small cycles									
Test #	Stress amplitude (MPa)	Strain amplitude (%)	Number of small cycles in the block	Failure life	Number of underload cycles	Damage done by small cycles	Equivalent cycles to failure	Number of blocks	Damage done by each cycle
1	200	0.10	50	468,727	9,191	0.93	496,762	9,191	2.1E-06
2	200	0.10	100	475,673	4,710	0.96	489,771	4,710	2.1E-06
3	200	0.10	200	404,898	2,014	0.98	409,610	2,014	2.5E-06
4	200	0.10	1,050	590,989	562	1.00	593,145	562	1.7E-06
5	200	0.10	1,500	459,145	306	1.00	459,987	306	2.2E-06
6	200	0.10	2,000	652,778	326	1.00	654,191	326	1.5E-06
7	200	0.10	5,000	1,309,768	262	1.00	1,312,309	262	7.6E-07
8	200	0.10	6,000	1,259,014	210	1.00	1,260,963	210	7.9E-07
9	200	0.10	10,000	3,008,253	301	1.00	3,015,352	301	3.3E-07

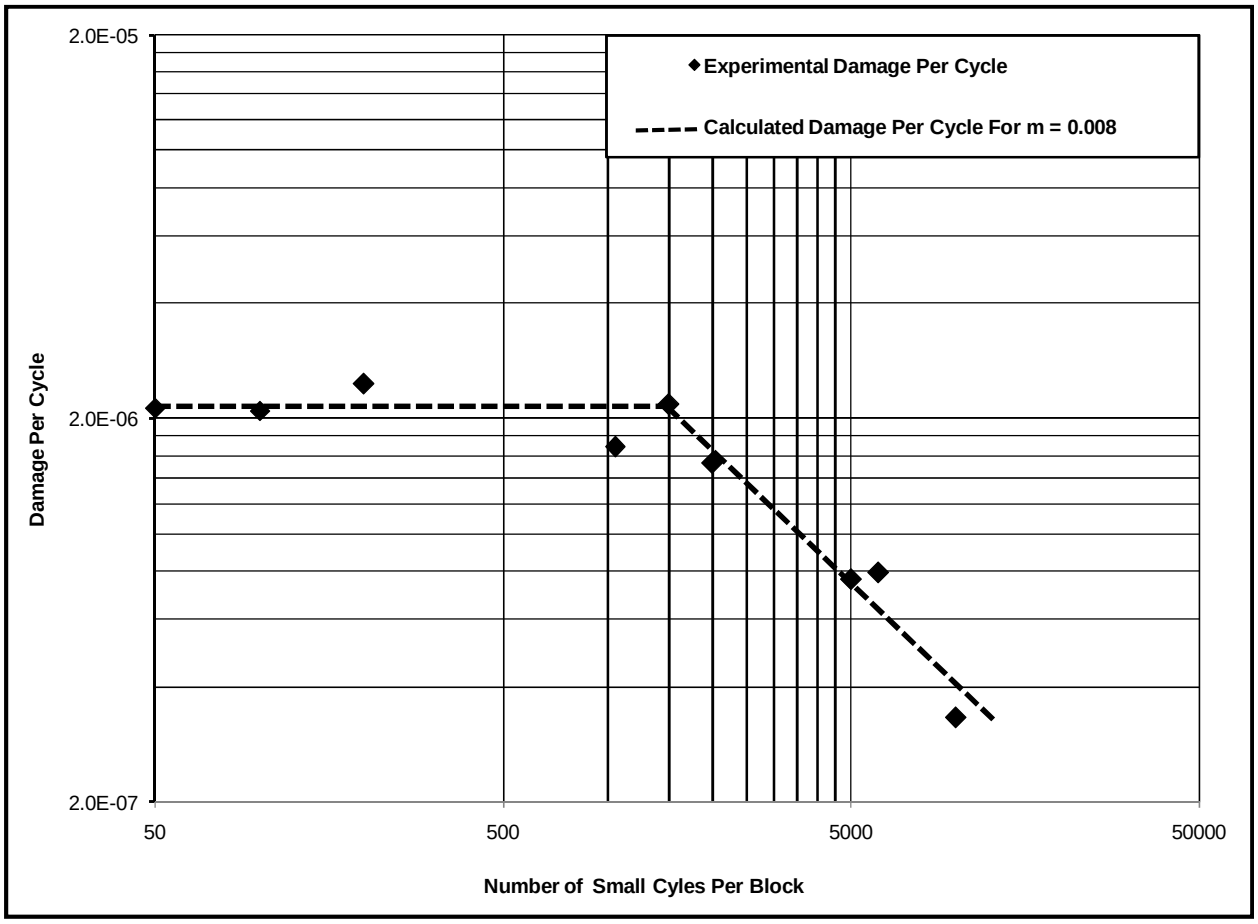

Figure 5.9 Fitted "m" to damage calculations for SAE 1045 steel

5.2.5 Crack Opening Stress Build-Up Measurements

After obtaining the crack closure parameter "*m*", the crack opening stress build-up equation (Eq. 2.4) was used to model the changes in the crack opening stress during a loading history and derive crack opening stress values that were then compared to measured values. Crack opening stress measurements (Figures 5.9, 5.10, and 5.11) were made for 3 stress levels using the previously described underload block load history under stress control. In the first test, an underload cycle with peak of -800 MPa compression and 300 MPa in tension was followed by 3000 constant amplitude small cycles at a stress ratio R = 0.8 with a maximum stress of 300 MPa and minimum stress of 240 MPa. The surface crack length at the time of measurement was 1.03 mm. In the second test the underload cycle had a stress of -800 MPa in compression and 300 MPa in tension, followed by 3000 constant amplitude small cycles with a stress ratio R = 0. The crack length at the time of the measurement was 1.08 mm and the maximum and the minimum stress peaks of the small cycles were 300 MPa and zero MPa, respectively. In the third test, the

underload cycle peaks were -800 MPa in compression and 200 MPa in tension, followed by 3000 constant amplitude small cycles with a stress ratio R = -1. The crack length at the time of the measurement was 0.95 mm and the maximum and the minimum stresses of the small cycles were 200 MPa and -200 MPa, respectively. Again, the procedure for measuring the crack opening stress was to stop the test at the maximum stress of the chosen cycle and then decrease the load manually until the two crack surfaces touched each other at 0.2 mm behind the crack tip. Two sets of readings were recorded and averaged for each crack opening stress measurement. Figures 5.10, 5.11 and 5.12 show the crack opening stress build-up measurements and predicted curves derived from Eq. 2.4 and fitted to m = 0.008 for three stress ratios.

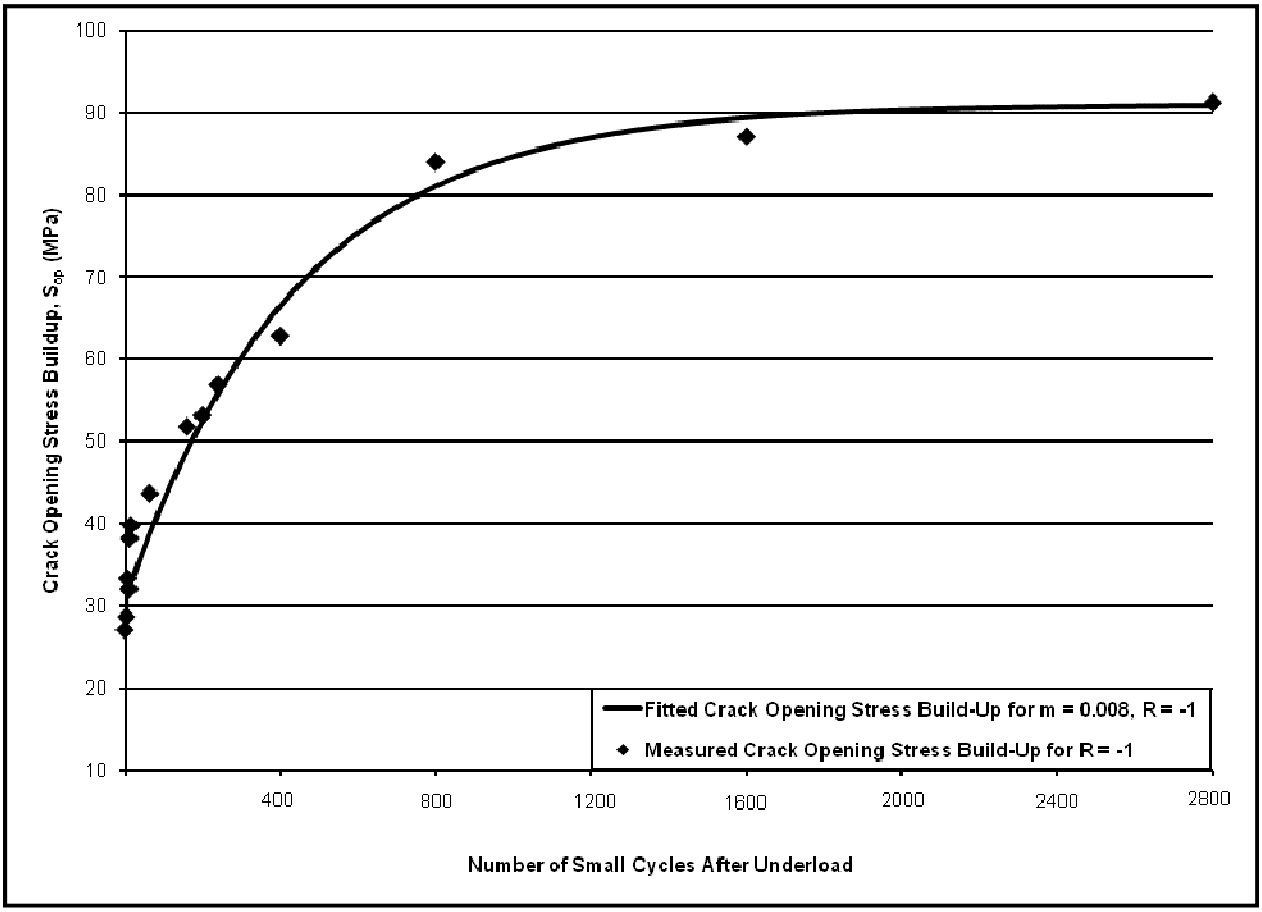

Figure 5.10 A comparison of a crack opening stress build-up curve fitted to m = 0.008 with measured data for R = -1 for SAE 1045 steel

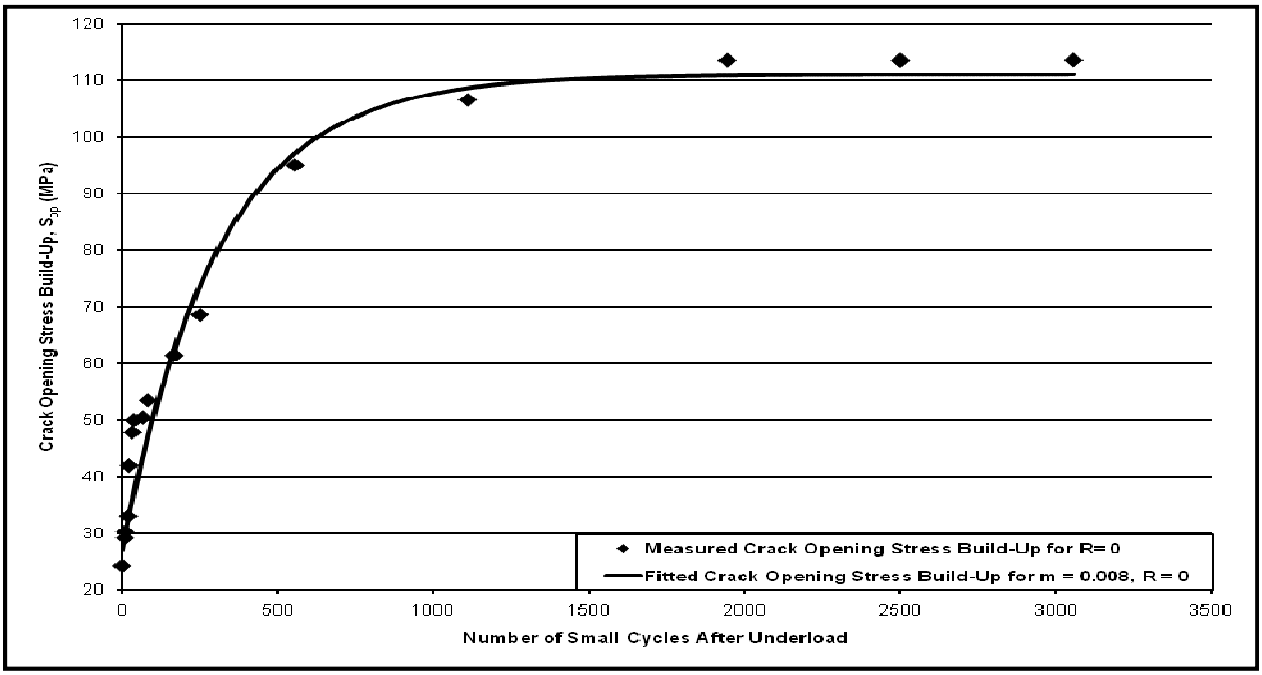

Figure 5.11 A comparison of a crack opening stress build-up curve fitted to *m* = 0.008 and with measured data for R = 0 for SAE 1045 steel

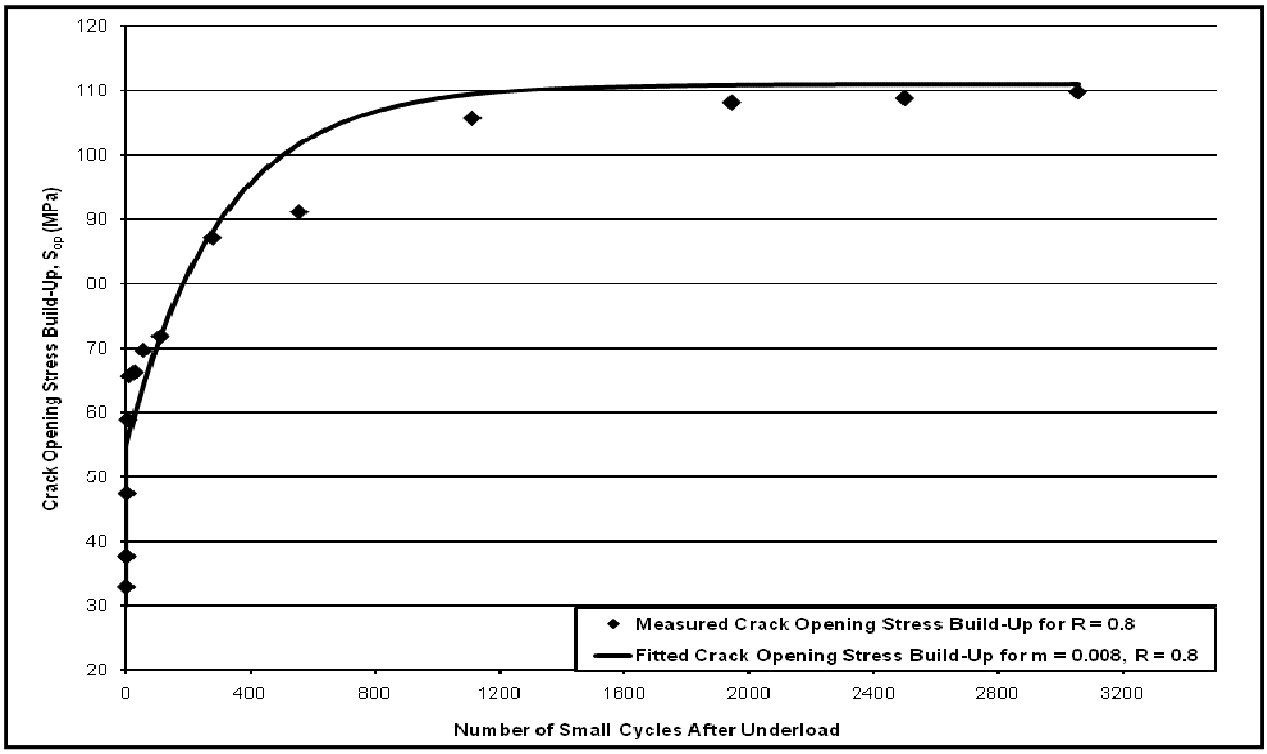

Figure 5.12 A comparison of a crack opening stress build-up curve fitted to m = 0.008 with measured data for R = 0.8 for SAE 1045 steel

5.2.6 Fatigue Life Predictions for Service Load Histories

In this section a model that used the effective strain-life curve and the $\Delta\varepsilon^*$ damage parameter was used to predict fatigue lives for tests under two service load histories. Each history was scaled to give various maximum stress ranges and applied to a smooth specimen under stress control.

5.2.6.1 Results for the Log Skidder History

In this part, 9 fatigue tests were performed on smooth specimens under different scaled values of the Log Skidder history. Figure 5.13 shows the predicted fatigue lives using the effective strain-life model fitted to the experimental fatigue lives.

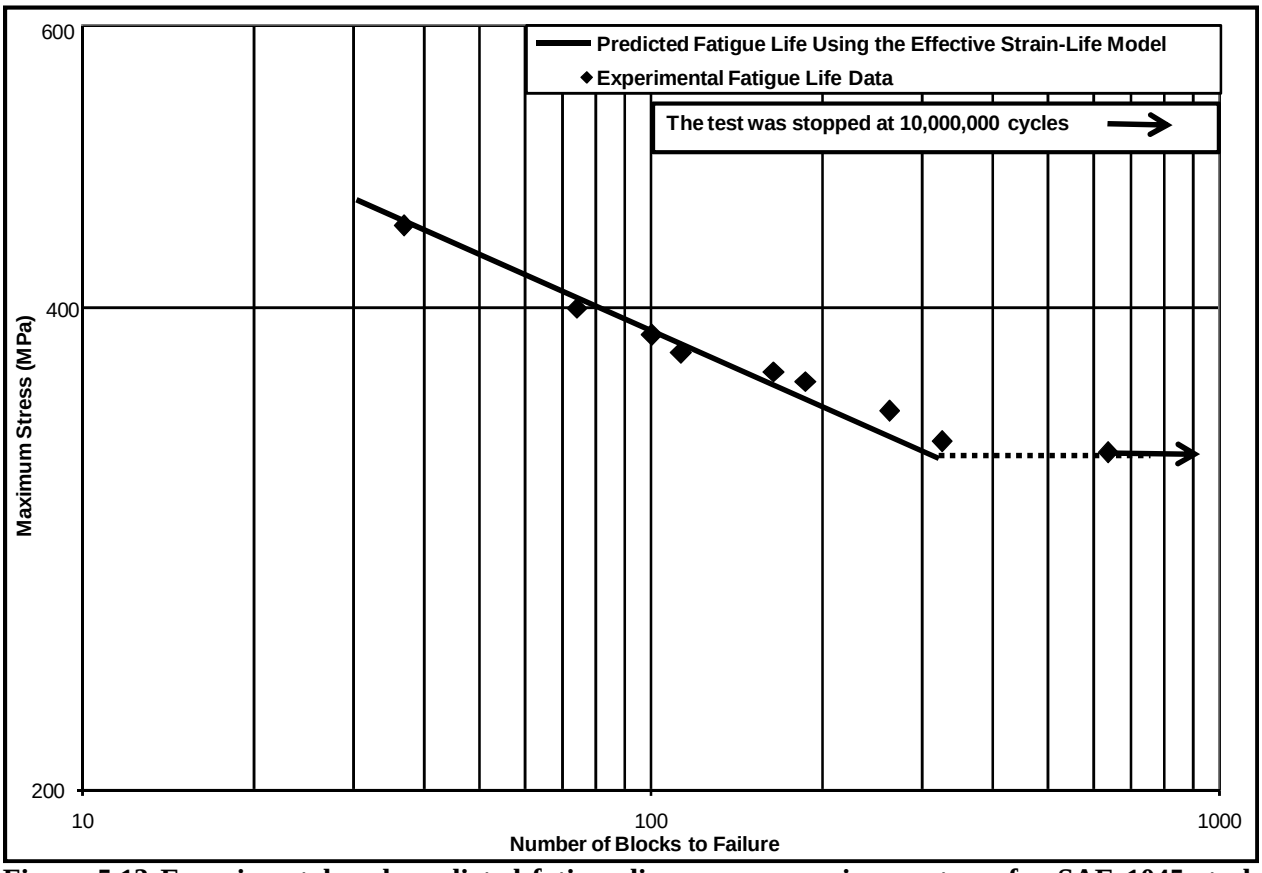

Figure 5.13 Experimental and predicted fatigue lives versus maximum stress for SAE 1045 steel subjected to the Log Skidder History

5.2.6.2 Results for the Grapple Skidder History

In this part 10 fatigue tests were performed on SAE 1045 smooth specimens under different scaled Grapple Skidder Histories. The history consisted of 41,112 reversals and in each test different scaled maximum stress amplitudes were applied. Figure 5.14 shows the predicted fatigue lives using the effective strain-life model together with the effective strain-life curve derived from experimental fatigue lives.

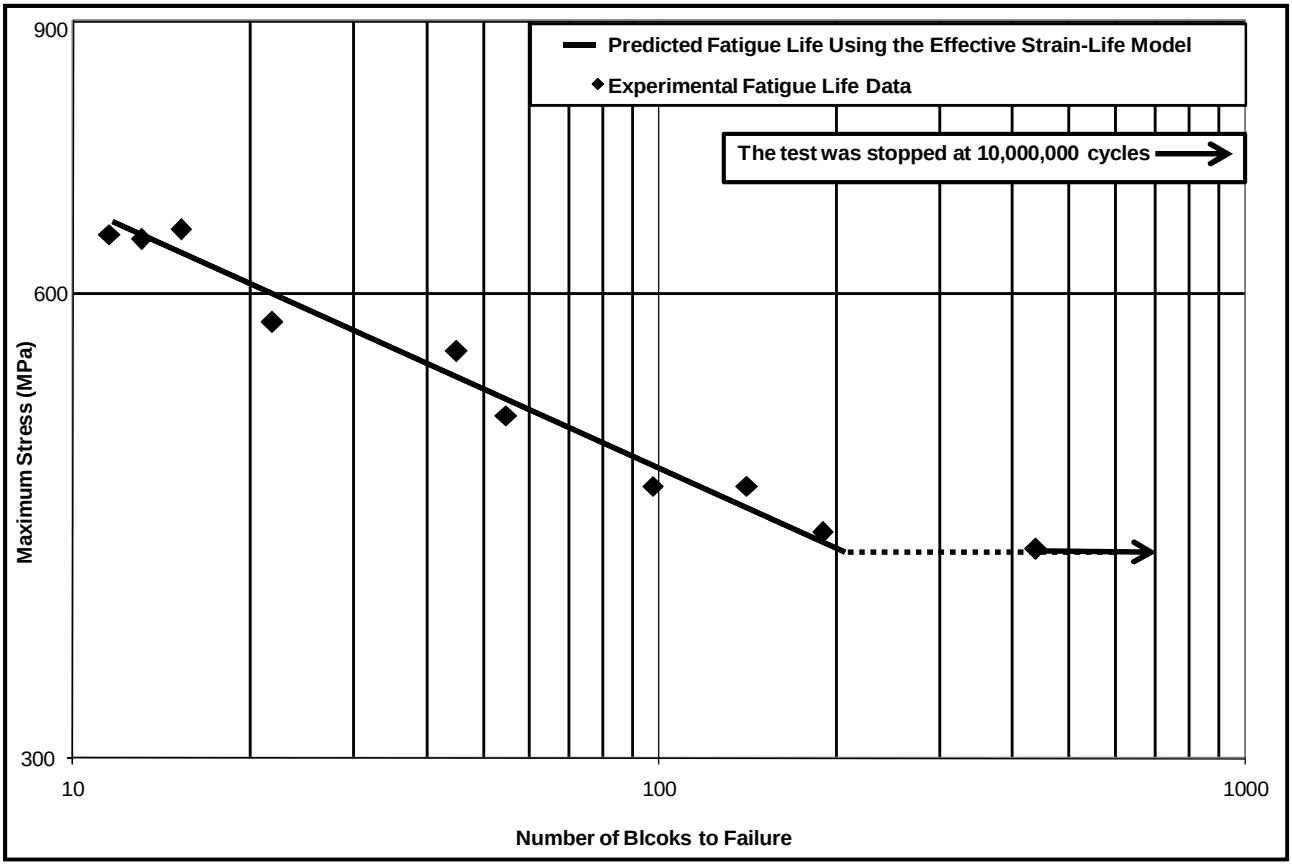

Figure 5.14 Experimental and predicted fatigue lives versus maximum stress for SAE 1045 steel subjected to the Grapple Skidder History

5.3 Fatigue Crack Growth Model

The work in this part included the derivation of the closure free crack growth curve (Chapter 2, Section 2.4.5) from the effective strain-life curve and comparing it with experimental measurements performed on notched samples (0.3 mm radius) under the two service load histories. Crack opening stresses were also calculated using the crack growth model and compared to measured values. Finally predicted fatigue lives under different scaled load histories were compared with experimental fatigue lives.

5.3.1 Derivation of the Closure Free Crack Growth Curve and Closure Free Crack Growth Measurements

The derivation of the closure free crack growth curve from the effective strain-life curve was presented in Chapter 2, Section 2.4.5. Figure 5.15 shows the derived crack growth rate curves for the SAE 1045 steel together with the experimental closure free crack growth measurements where the intrinsic stress intensity range (ΔK_i) was taken as 2.5 MPa $m^{1/2}$. Closure free crack growth measurements were obtained for SAE 1045 steel specimens with a 0.3 mm radius notch. As a first step, the specimen was pre-cracked by applying constant amplitude cycles going from zero to -653 MPa in compression. A travelling optical microscope of a magnification of 900x was mounted on the machine facing the specimen. A vernier with an accuracy of 0.0001 mm was attached to the microscope to measure changes in crack length. The technique reported was to apply a block of loading history consisting of an underload followed by small cycles which have the same maximum stress as the underload cycle. The minimum stress of the small cycles was varied from test to test to produce a succession of different ΔK_{eff} values. The underload cycle was chosen as the constant amplitude stress level that would give a fatigue life of 10,000 cycles (-729 MPa). The number of the small cycles was chosen so that damage due to the underload cycle did not exceed 10% and that the small cycles between the underloads were free of closure by making sure that the crack opening stress as it builds-up after the underloads did not reach the minimum stress of the small cycles before the application of the next underload that would reduce the crack opening stress.

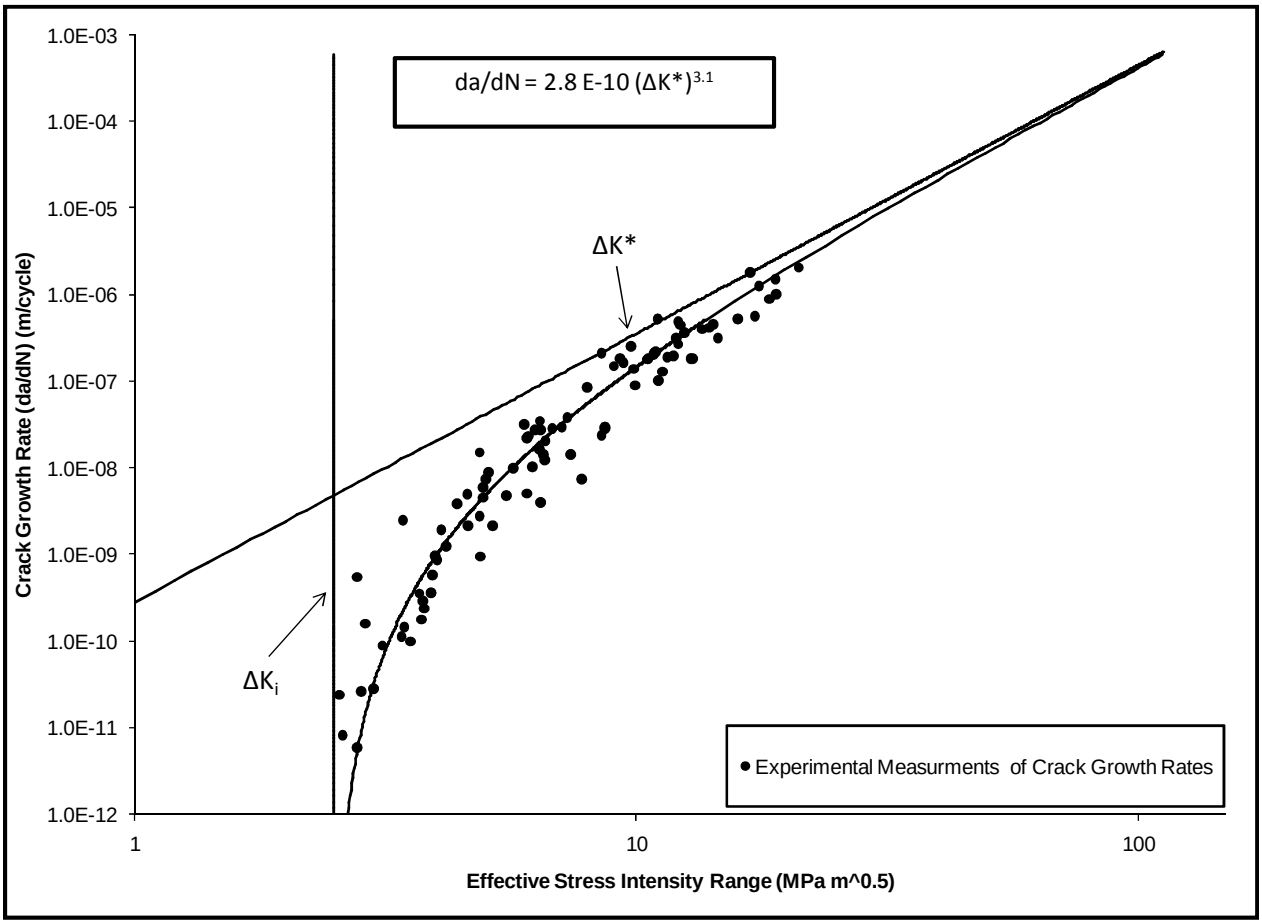

Figure 5.15 Derived effective stress intensity crack growth curve and experimental measurements of crack growth rate vs. effective stress intensity data for SAE 1045 steel

5.3.2 Crack Opening Stress Levels under Service Loading Histories

The crack opening stresses for SAE 1045 steel were measured under the SAE Grapple Skidder History and the SAE Log Skidder History. The measured values were then compared with the calculated crack opening stresses obtained from the crack growth model.

5.3.2.1 Crack Opening Stresses of SAE 1045 Steel under the SAE Log Skidder History

The crack opening stresses were measured for SAE 1045 steel under the SAE Log Skidder History. The loading spectrum was scaled to a maximum stress of 410 MPa and a minimum stress of -412 MPa. The crack opening stresses were measured using a 900x short focal length optical video microscope for different cycles and at convenient crack lengths.

Figure 5.16 shows the nominal applied stress history together with the calculated crack opening stresses using the crack growth model and the measured crack opening stresses.

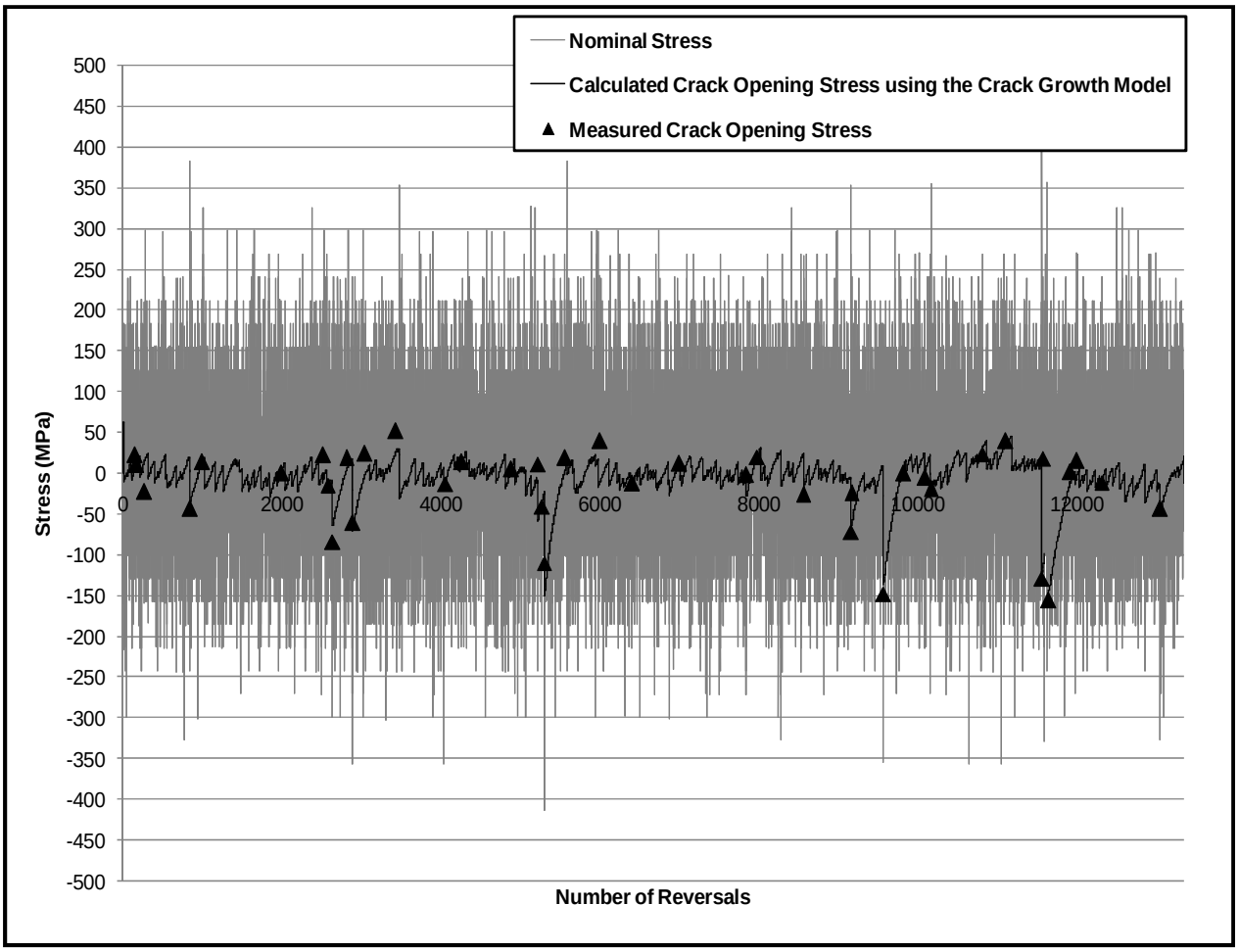

Figure 5.16 Calculated and measured crack opening stresses for SAE 1045 steel under the SAE Log Skidder History scaled to a maximum stress of 410 MPa

5.3.2.2 Crack Opening Stresses of SAE 1045 Steel under the SAE Grapple Skidder History

The crack opening stresses were measured for SAE 1045 steel under the SAE Grapple Skidder History scaled to a maximum stress of 470 MPa and a minimum stress of -352 MPa. The crack opening stresses were measured using a 900x short focal length optical video microscope for different cycles and at convenient crack lengths. Figure 5.17 shows the nominal applied stress history together with the calculated crack opening stresses using the crack growth model and the measured crack opening stresses.

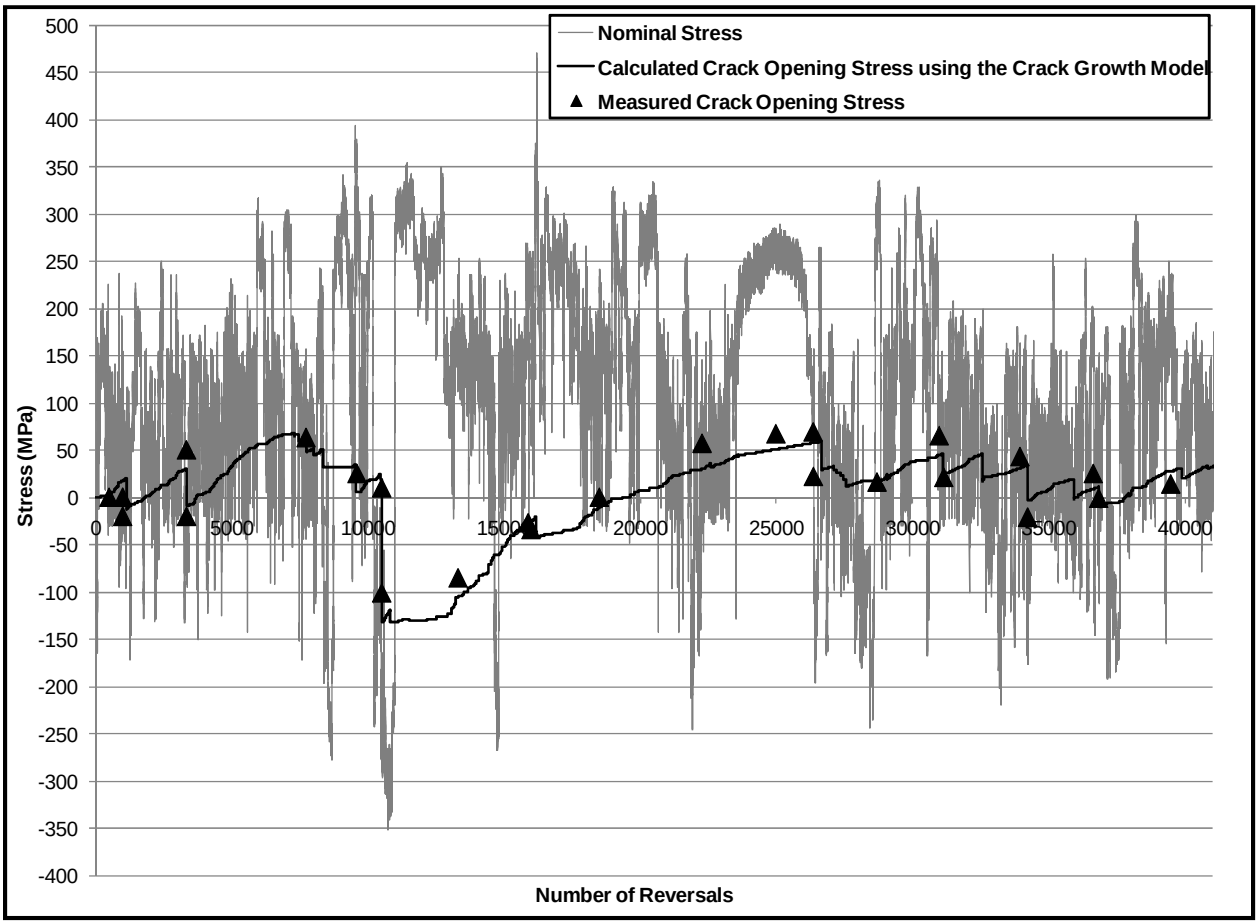

Figure 5.17 Calculated and measured crack opening stresses for SAE 1045 steel under the SAE Grapple Skidder History scaled to a maximum stress of 470 MPa

5.3.3 Fatigue Life Predictions for Service Load Histories using the Crack Growth Model

Fatigue life predictions based on the crack growth model are presented in this section under the two service load histories (the Log Skidder History and the Grapple Skidder History). Each history was scaled to give various maximum stress ranges and applied to a notched specimen (0.3 mm radius) under stress control. The predicted lives were then compared to the experimental values.

5.3.3.1 Results for the Log Skidder History

11 fatigue tests were performed on notched specimens under different scaled values of the Log Skidder history. Figure 5.18 shows the predicted fatigue lives using the crack growth model together with the experimental fatigue lives for the Log Skidder history.

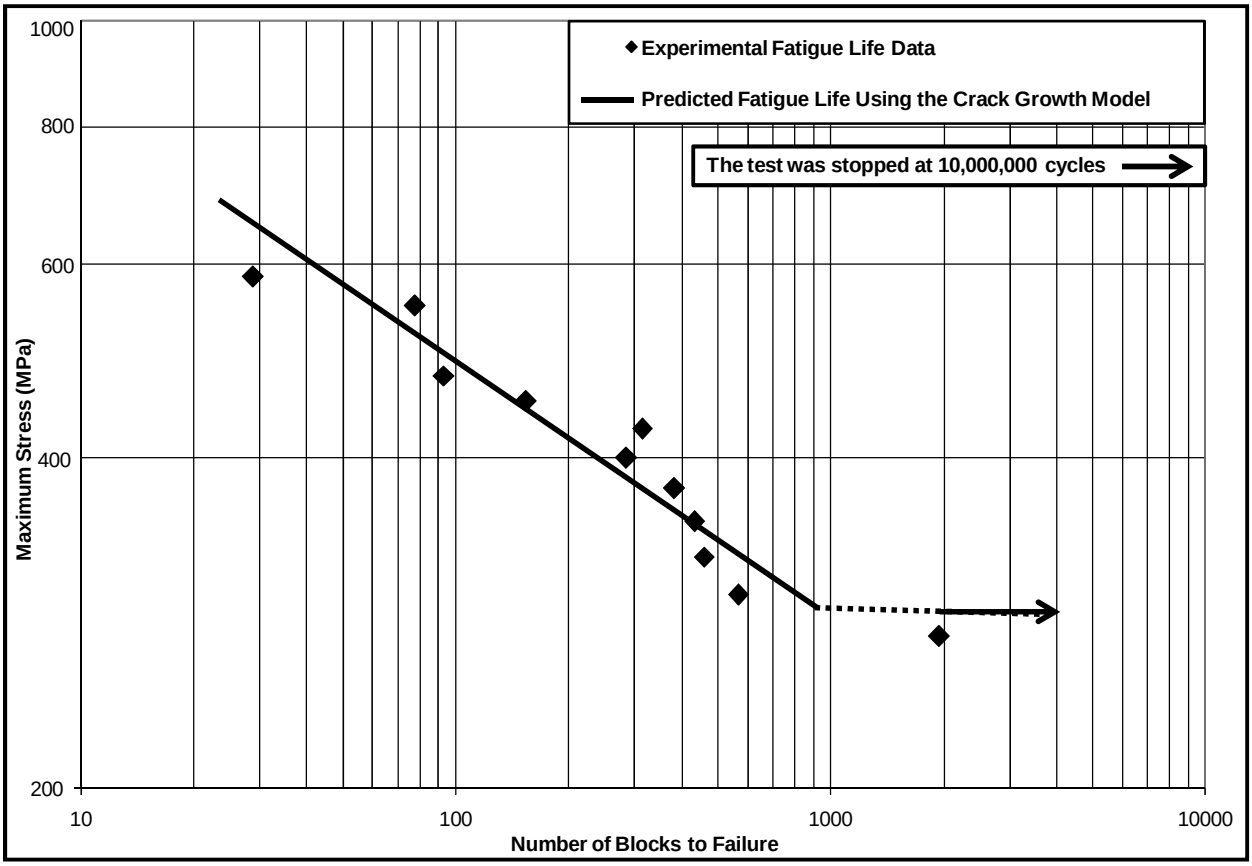

Figure 5.18 Experimental and predicted fatigue lives versus maximum stress for SAE 1045 steel subjected to the Log Skidder History

5.3.3.2 Results for the Grapple Skidder History

16 Fatigue tests were performed on notched specimens under different scaled values of the Grapple Skidder history. Figure 5.19 shows the predicted fatigue lives using the crack growth model together with the experimental fatigue lives for the Log Skidder history.

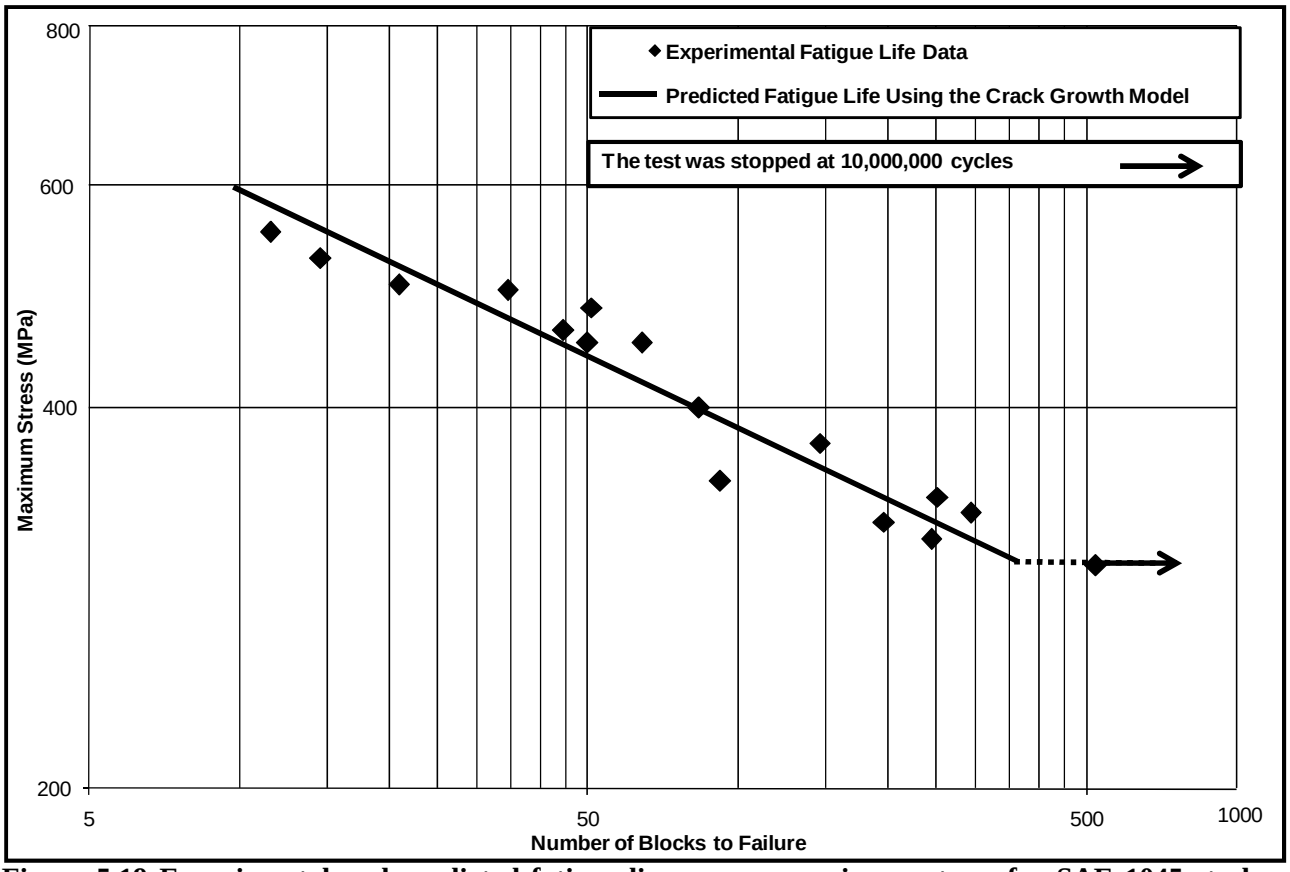

Figure 5.19 Experimental and predicted fatigue lives versus maximum stress for SAE 1045 steel subjected to the Grapple Skidder History

Chapter 6
Experimental Results for AISI 8822 Steel

6.1 Introduction

The experimental results for AISI 8822 steel are presented in this chapter. The monotonic and cyclic stress-strain curves as well as the mechanical properties for this material are presented in Chapter 3 Section 3.1.3. The results in this chapter include all the tests performed to develop the effective strain-life model. However and due to the hardness of the metal (60 HRC) crack opening stress measurements and fatigue crack growth rate measurements were not made for this material because attempts to obtain large enough cracks to permit optical measurements without fracturing the specimen were unsuccessful.

6.2 Effective Strain-Life Curve

6.2.1 Strain-Life Curve

The strain-life curve was constructed from 24 axial, constant amplitude, fully reversed (R = -1) strain-controlled fatigue tests (Table 6.1) using a servo-controlled closed-loop electro-hydraulic testing machine with a process control computer controlled by a software [68] developed at the University of Waterloo to output constant strain or load amplitudes in the form of sinusoidal waves. Specimen failure was defined as a 50% drop in the tensile peak load from the peak tensile load observed at one half of the expected specimen life. In strain controlled tests, the loading frequency varied from 0.05 Hz to 3 Hz. For fatigue lives greater than 100,000 reversals the specimens were tested in load control. For the load-controlled tests, failure was defined as the separation of the specimen into two pieces. The test frequency used in this case was 70 Hz. Figure 6.1 shows the experimental fatigue data and the fitted total strain-life curve.

Table 6.1 Constant amplitude strain-life data for AISI 8822 steel

Test #	True strain amplitude (%)	True stress amplitude (MPa)	True plastic strain amplitude (%)	True elastic strain amplitude (%)	Fatigue life (reversals to failure)
1	0.526	1035	0.000	0.526	222
2	0.529	1093	0.000	0.529	368
3	0.523	1068	0.000	0.523	1,090
4	0.506	1044	0.000	0.506	710
5	0.474	997	0.000	0.474	2,354
6	0.473	982	0.000	0.473	2,828
7	0.474	974	0.000	0.474	1,840
8	0.450	900	0.000	0.450	3,276
9	0.401	809	0.000	0.401	2,820
10	0.399	809	0.000	0.399	27,538
11	0.405	808	0.000	0.405	23,874
12	0.374	790	0.000	0.374	8,120
13	0.349	706	0.000	0.349	15,348
14	0.349	704	0.000	0.349	25,846
15	0.352	693	0.000	0.352	65,610
16	0.298	602	0.000	0.298	255,128
17	0.299	613	0.000	0.299	2,805,890
18	0.300	613	0.000	0.300	*10,000,000
19	0.273	577	0.000	0.273	168,306
20	0.276	562	0.000	0.276	*10,000,000
21	0.276	556	0.000	0.276	126,558
22	0.250	489	0.000	0.250	*10,000,000
23	0.248	511	0.000	0.248	*10,000,000
24	0.250	508	0.000	0.250	*10,000,000

*Run-Out Tests

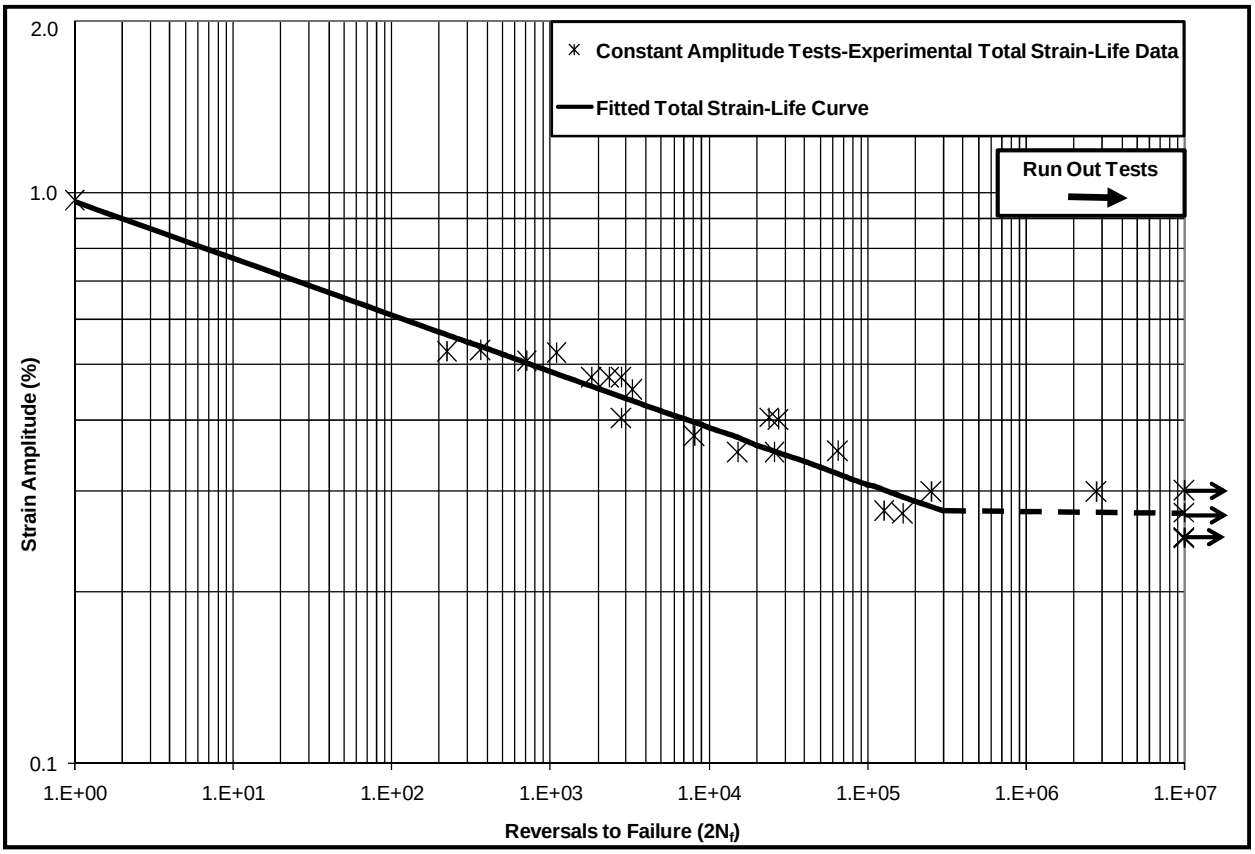

Figure 6.1 Fitted strain-life curve for AISI 8822 steel

6.2.2 Underload Fatigue Data and the Effective Strain-Life Curve

The effective strain-life curve was derived from mean stress tests and periodic underload fatigue tests performed under stress control. The periodic underload fatigue tests consisted of a repeated load cycle block of a single underload cycle followed by a number of smaller load cycles that had the same maximum stress as the underload cycle. This block was then repeated until the specimen failed. The underload cycle in this work was set equal to the fully reversed constant amplitude stress level that gave a fatigue life of 10,000 cycles (866 MPa). The number of small cycles in the loading block was chosen so that they were responsible for 80 to 90% of the damage to the specimen and that they were free from crack closure. Table 6.2 shows the underload fatigue tests configuration.

The mean stress tests were conducted in several series. In each series of tests, the maximum stress had a constant value of 1200 MPa and the stress range was lowered for each specimen by changing the minimum stress until the fatigue limit was reached. The minimum stress varied from 581 MPa to 4 MPa. Table 6.3 shows the mean stress test information for the AISI 8822 steel.

The periodic underload fatigue data and the mean stress tests for the AISI 8822 steel specimens are shown in Figure 6.2 together with the constant amplitude strain-life curve. The derived effective strain-life curve is shown in Figure 6.3, the constants *A*, and *b* in the effective strain-life curve equation (Eq. 2.11) were found to be 1.3 and -0.13 respectively. The intrinsic strain range, $\Delta\varepsilon_i$, which made the curve of $E\,\Delta\varepsilon^*$ values (calculated from Eq. 2.5) *vs.* N_f linear on logarithmic scales was found to be 0.09%.

Table 6.2 Underload fatigue tests for AISI 8822 steel

Underload cycle 866 MPa in tension -866 MPa in compression						
Small cycles						
Test #	Stress amplitude (MPa)	Strain amplitude (%)	Number of small cycles in the block	Failure life	Number of underload cycles	Equivalent cycles to failure
1	511	0.24	100	35,432	351	36,357
2	481	0.23	80	25,572	316	26,080
3	361	0.17	250	81,950	326	84,375
4	301	0.14	5,000	*5,000,000	1,000	*5,000,000
5	331	0.16	5,000	240,525	48	241,637
6	319	0.15	5,000	*5,000,000	1,000	*5,000,000
7	325	0.16	5,000	*5,000,000	1,000	*5,000,000
8	451	0.22	3,000	30,030	10	30,050
9	421	0.20	3,000	51,743	17	51,814
10	349	0.17	50	23,952	470	24,640
11	337	0.16	1,000	32,258	32	32,329

*Run-Out Tests

Table 6.3 Mean stress test results for AISI 8822 steel

Test #	Maximum stress amplitude (MPa)	Minimum stress amplitude (MPa)	Effective strain range (%)	Failure life (cycles)
1	1200	4	0.57	34,000
2	1200	113	0.52	472,560
3	1200	178	0.49	2,802
4	1200	291	0.44	5,620
5	1200	369	0.40	67,996
6	1200	496	0.34	6,526
7	1200	556	0.31	14,064
8	1200	581	0.30	1,076,266

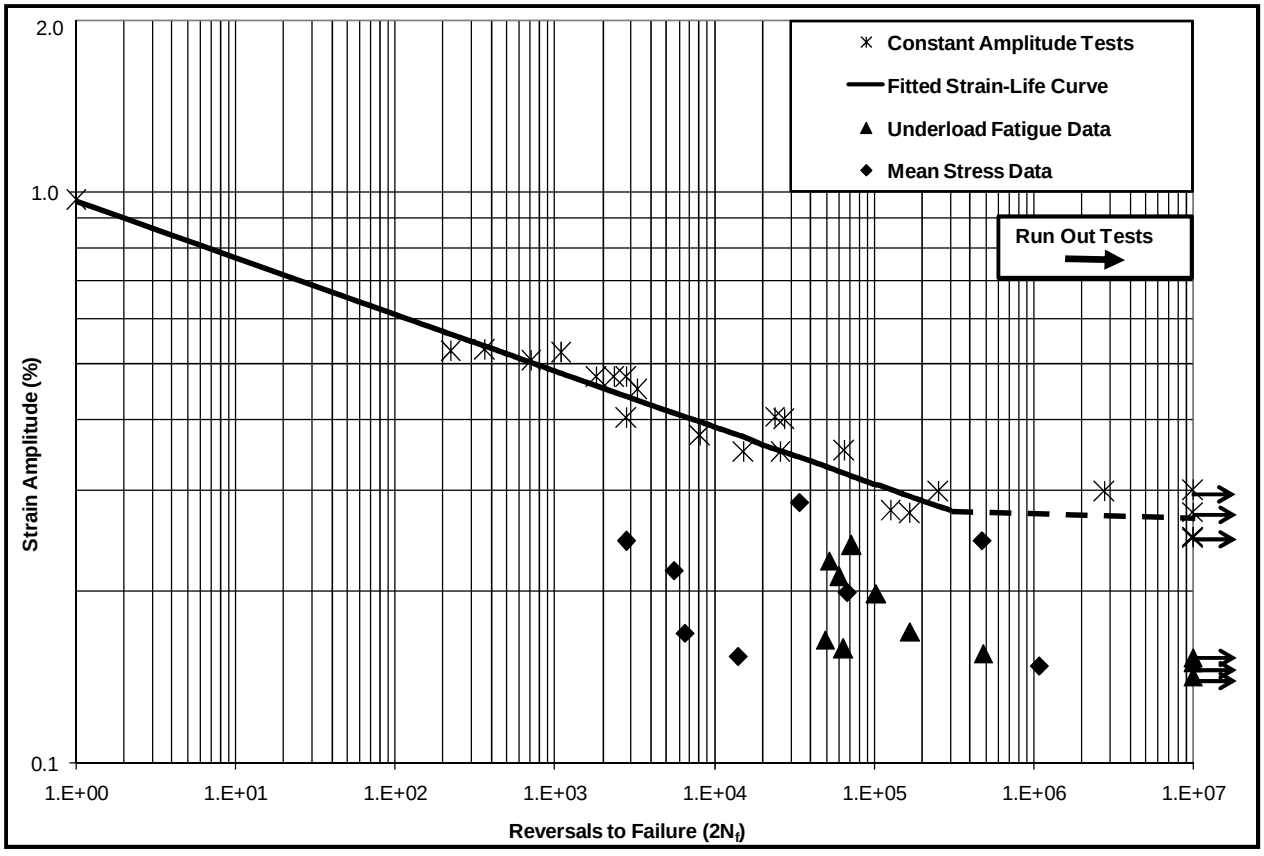

Figure 6.2 Underload fatigue and mean stress data for AISI 8822 steel

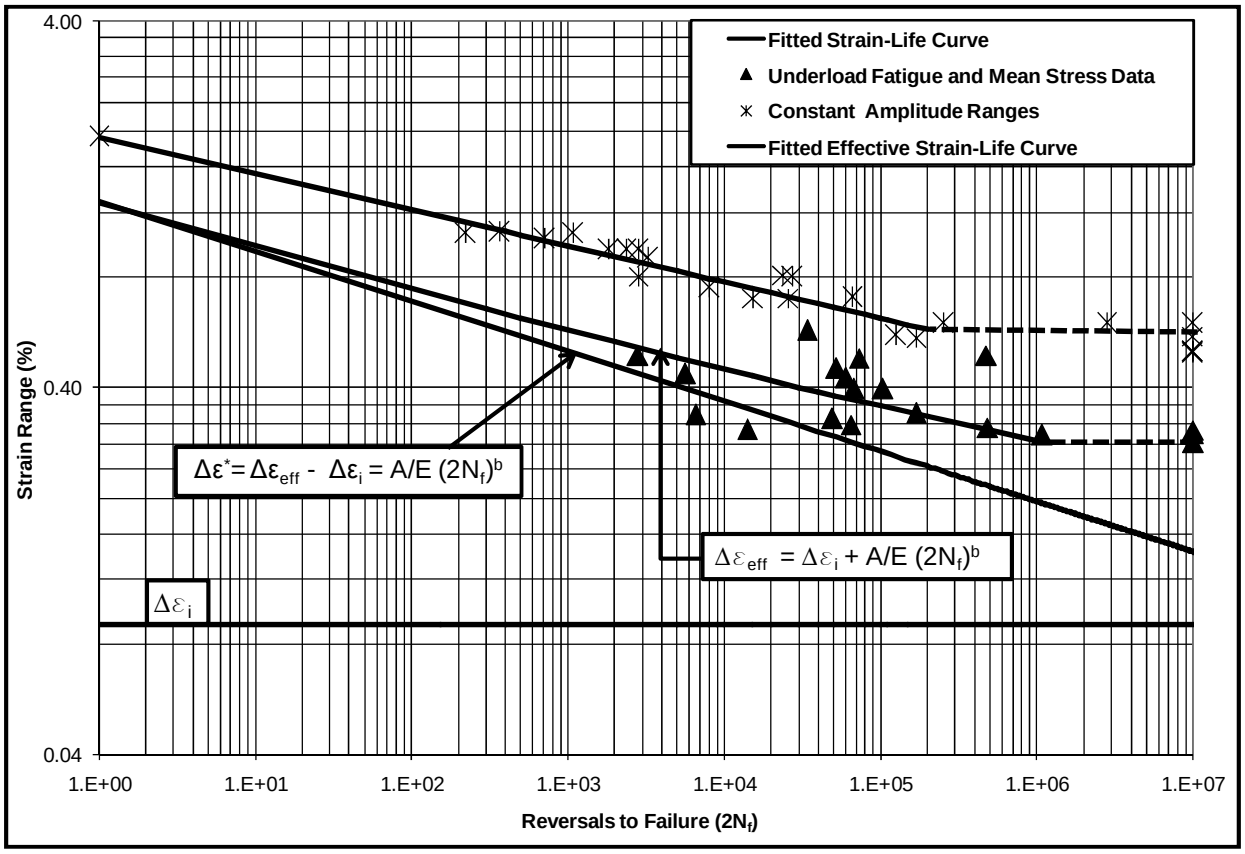

Figure 6.3 Fitted effective strain-life curve for AISI 8822 steel

6.2.3 Steady State Crack Opening Stresses

Steady state crack opening stresses were modeled using DuQuesnay's equation (Eq. 2.3). As mentioned previously crack opening stress measurements were not obtained for this material, rather the steady state crack opening stresses were obtained from the constant amplitude and the effective strain-life curve (see Chapter 2, Section 2.2.6.2 for the procedure used). Figure 6.4 shows the crack opening stresses derived from the constant amplitude and effective strain-life curves together with crack opening stresses obtained from DuQuesnay's equation (Eq. 2.3). The two constants θ and φ in Eq. 2.3 were found to be 0.05 and 0.2 respectively.

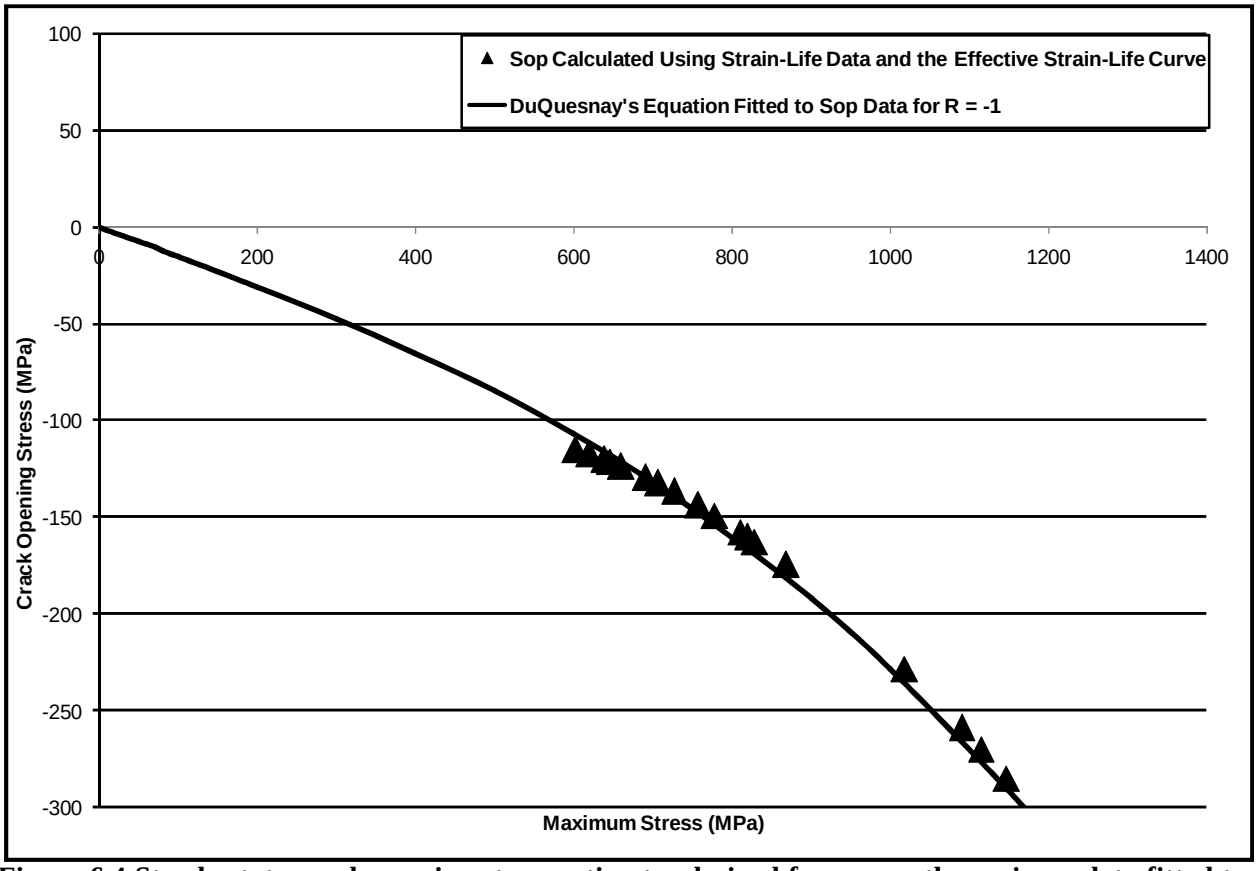

Figure 6.4 Steady state crack opening stress estimates derived from smooth specimen data fitted to DuQuesnay's equation for AISI 8822 steel

6.2.4 Determining the Crack Closure Parameter *"m"*

Smooth specimens were tested under load histories with intermittent underloads and a fixed level of strain in the intervening constant amplitude cycles. The frequency of occurrence of the underloads was varied from test to test and the changes in fatigue life were observed. Table 6.3 shows the tests results. The changes in damage per block were then used to determine the value of the closure model parameter "*m*" in Eq. 2.4 that described the recovery of the crack opening stress to its steady state level. The experimental work in this section consisted of 8 underload fatigue tests where the underload cycle was set equal to 1100 MPa in tension and -1100 MPa in compression, and the range of the small cycles was set to 600 MPa. During these tests only the number of small cycles per block was varied and their corresponding damage was calculated by subtracting the damage due to the underloads from unity. After calculating the equivalent damage done by the small cycles, the damage per cycle was plotted against the number of small cycles per block (Figure 6.5). These data were then fitted by iteratively assuming "*m*"

values and calculating the crack opening stress for each small cycle in the loading block using Eq. 2.4. Then the value of (S_{op} - S_{min} / E) (where S_{op} is the crack opening stress, S_{min} is the minimum stress of the small cycles in the loading block, and E is the modulus of elasticity) was subtracted from $\Delta\varepsilon$ (the total strain range) for each cycle to obtain the effective strain range ($\Delta\varepsilon_{eff}$). The damage was then calculated by entering $\Delta\varepsilon_{eff}$ in the effective strain-life curve shown in Figure 6.3. The damage per cycle was then summed up and divided by the number of small cycles per block to obtain the average damage per cycle. The value of "m" was iteratively varied to obtain a good fit of the calculated curves to the measured average damage per block. For this material a value of m = 0.0009 gave a good fit to the measured damage per cycle versus number of small cycles per block (see Figure 6.5).

Table 6.4 Damage tests configuration for AISI 8822 steel

Underload cycle 1100 MPa in tension -1100 MPa in compression									
Small cycles									
Test #	Stress amplitude (MPa)	Strain amplitude (%)	Number of small cycles in the block	Failure life	Number of underload cycles	Damage done by small cycles	Equivalent cycles to failure	Number of blocks	Damage done by each cycle
1	500	0.24	30	17,096	551	0.94	17,510	551	5.7E-05
2	500	0.24	50	14,728	289	0.97	14,869	289	6.7E-05
3	500	0.24	100	23,730	235	0.98	24,060	235	4.2E-05
4	500	0.24	500	15,327	31	0.98	15,344	31	6.5E-05
5	500	0.24	1,000	41,580	42	0.97	41,713	42	2.4E-05
6	500	0.24	5,000	66,976	13	0.97	67,050	13	1.5E-05
7	500	0.24	10,000	46,686	5	0.95	46,704	5	2.1E-05
8	500	0.24	100,000	132,420	1	0.98	132,432	1	7.6E-06

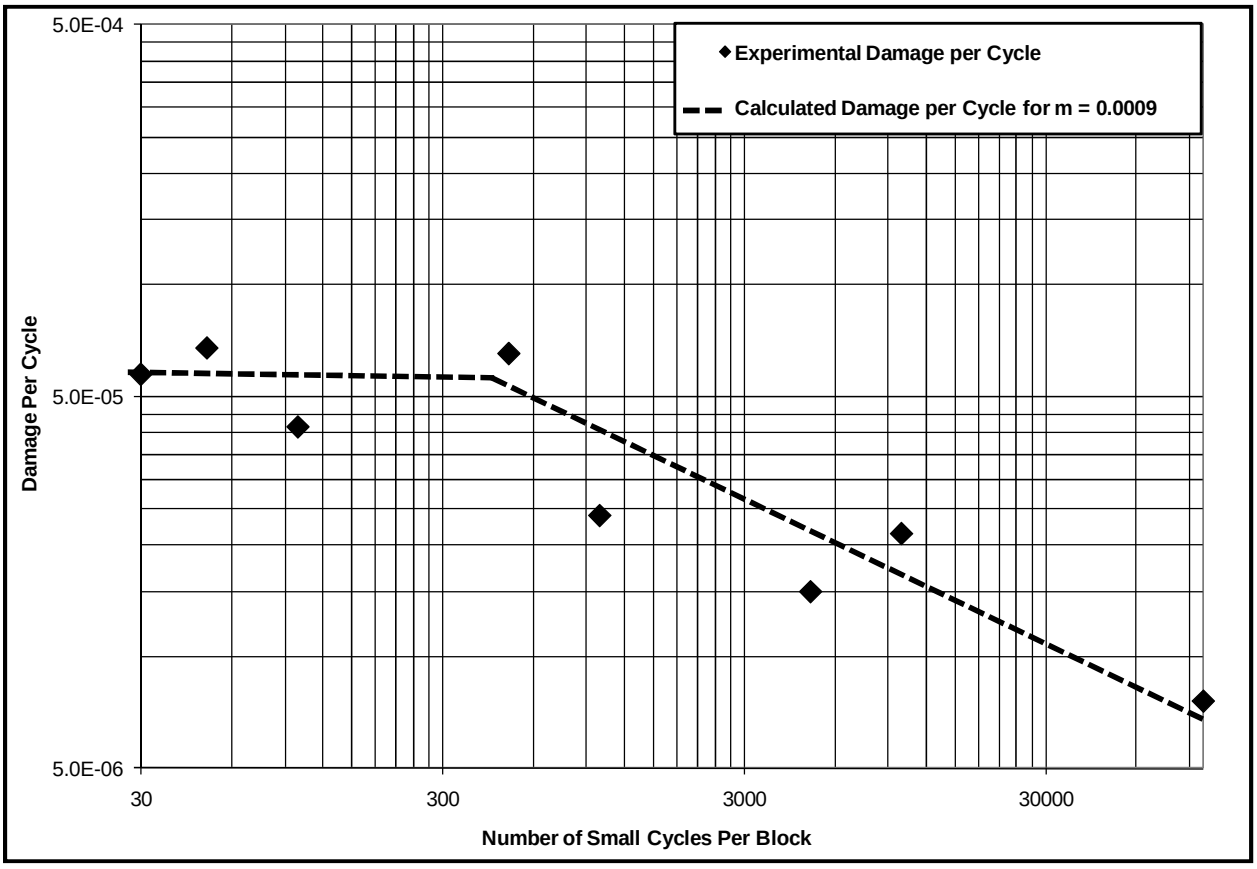

Figure 6.5 Fitted "*m*" to damage calculations for AISI 8822 steel

6.2.5 Fatigue Life Predictions for Service Load Histories

In this section a model that used the effective strain-life curve and the $\Delta\varepsilon^*$ damage parameter was used to predict fatigue lives for tests under two service load histories. Each history was scaled to give various maximum stress ranges and applied to a smooth specimen under stress control.

6.2.5.1 Results for the Log Skidder History

In this part, 11 fatigue tests were performed on smooth specimens under different scaled values of the Log Skidder history. Figure 6.6 shows the predicted fatigue lives using the effective strain-life model together with the experimental fatigue lives.

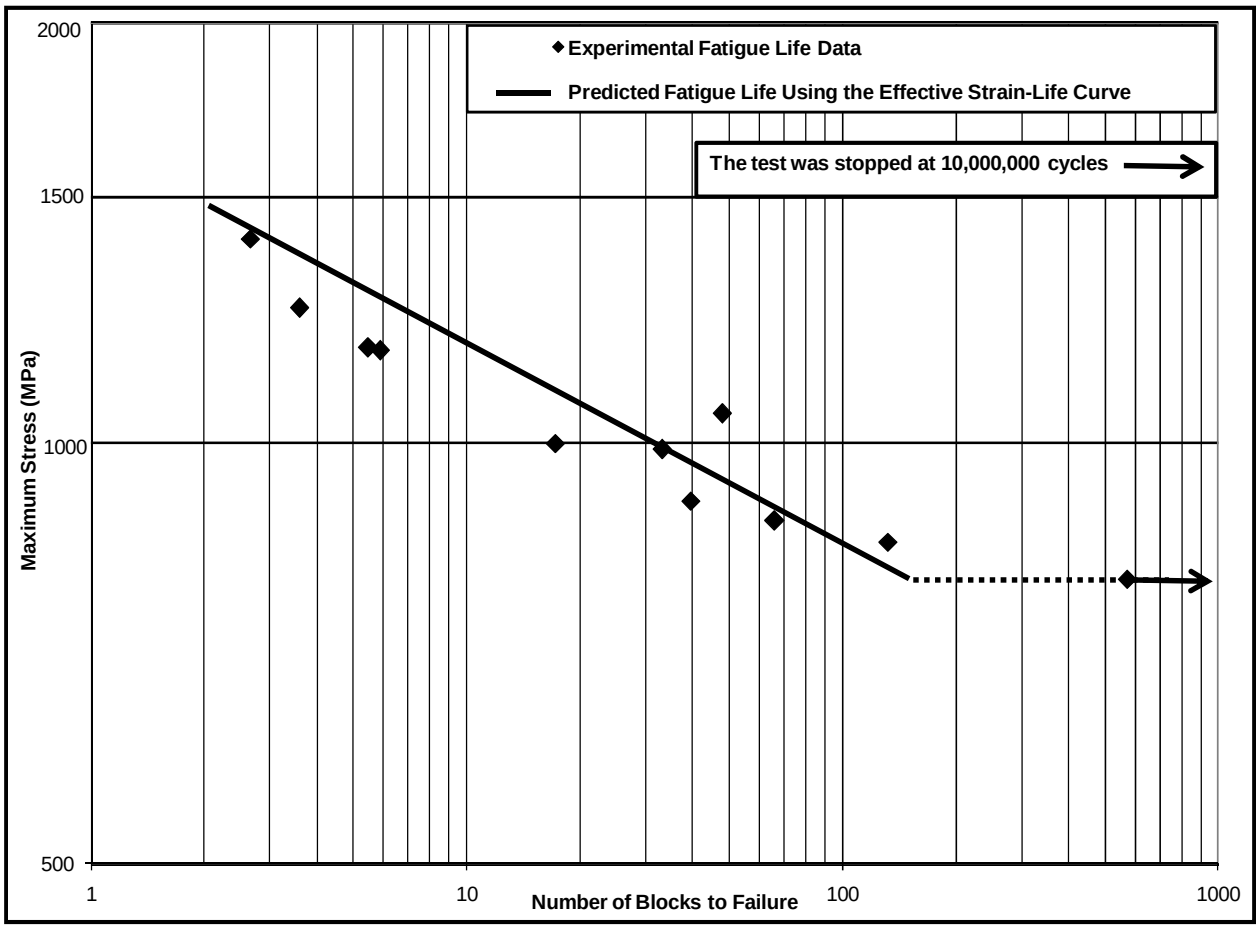

Figure 6.6 Experimental and predicted fatigue lives versus maximum stress for AISI 8822 steel subjected to the Log Skidder History

6.2.5.2 Results for the Grapple Skidder History

8 fatigue tests were performed on AISI 8822 smooth specimens under different scaled Grapple Skidder Histories. The history consisted of 41,112 reversals and in each test different scaled maximum stress amplitudes were applied. Figure 6.7 shows the predicted fatigue lives using the effective strain-life model together with the experimental fatigue lives.

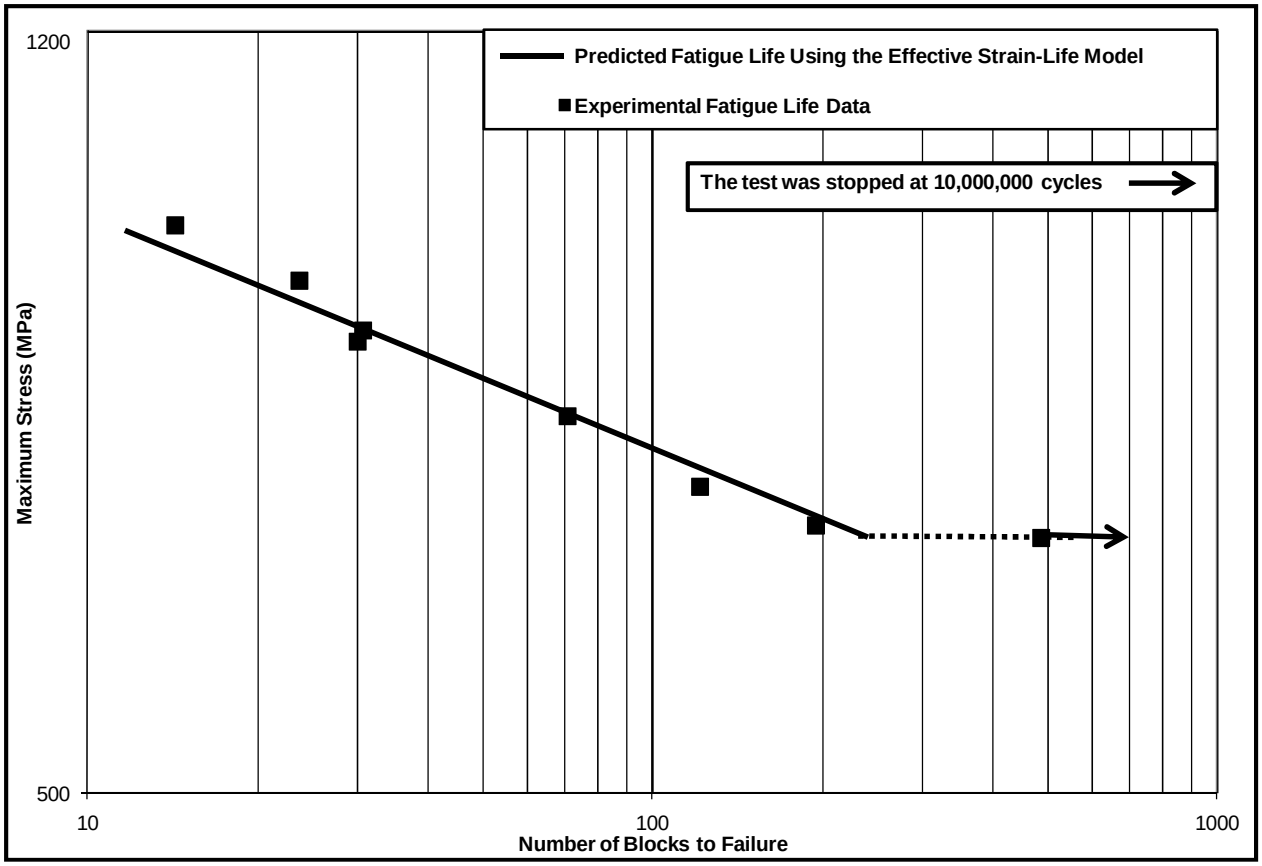

Figure 6.7 Experimental and predicted fatigue lives versus maximum stress for AISI 8822 steel subjected to the Grapple Skidder History

Chapter 7
Discussion

One of the aims of this investigation was to relate the crack closure levels experienced in metals under variable amplitude loading with the material's cyclic deformation resistance which in turn increases with metal hardness. The parameters of the crack closure models suggested in this thesis are compared for three different metals of varying hardness levels including the very hard carburized steel (AISI 8822) having a hardness level for which no crack opening stress data for small cracks has yet been obtained to the very soft DP 590 metal. Table 7.1 summarizes the mechanical (monotonic and cyclic) properties of the three metals as obtained in this investigation.

Table 7.1 Mechanical properties of the three steels used in this investigation

Mechanical Properties	**Units**	**DP 590**	**SAE 1045**	**AISI 8822**
Elastic Modulus, E	MPa	209,000	205,000	209,000
Yield Strength, S_y	MPa	349	1200	-
Ultimate Tensile Strength, S_u	MPa	623	1271	1480
True Fracture Stress, σ_f	MPa	743	1879	1480
True Fracture Strain	%	76	56	0.87
% Elongation	%	34	14	0.87
% Reduction of Area	%	53	43	-
Monotonic Tensile Strength Coefficient, *K*	MPa	730	1470	-
Monotonic Tensile Strain Hardening Exponent, *n*		0.12	0.033	-
Cyclic Yield Strength, (0.2% offset)=K'(0.002) n'	MPa	338	767	-
Cyclic Strength Coefficient, *K'*	MPa	949	1410	-
Cyclic Strain Hardening Exponent, *n'*		0.166	0.098	-
Fatigue Strength Coefficient, σ'_f	MPa	806	1813	2234
Fatigue Strength Exponent, *b*	-	-0.083	-0.094	-0.109
Fatigue Ductility Coefficient, ε'_f	-	0.351	0.577	-
Fatigue Ductility Exponent, *c*	-	-0.5	-0.6	-
Hardness, Rockwell C	HRC	6	35	60

7.1 Steady State Crack Opening Stresses

A steady state condition of crack closure is reached when the residual plastic deformations and crack closure along the crack surfaces are fully developed and stabilized under steady state loading (or constant amplitude loading) [71]. A number of researchers have provided analytical or finite element solutions for steady state crack closure at high stresses [72]. McEvily and Minakawa [73] showed that for a crack propagating under constant amplitude loading, closure builds-up to a steady state level within several hundred microns of growth, and it remains at this level for most of the fatigue life. Newman [74] developed crack opening stress equations for constant amplitude loading from crack closure model calculations for a middle-crack tension specimen. His model proposed an analytical formulation based on the Dugdale model but modified to leave plastically deformed material in the wake of the advancing crack tip. However as mentioned previously, the steady state crack opening stresses in this investigation were modeled using the DuQuesnay et al. equation [42] that relates the steady state crack opening stresses under constant amplitude loading to the maximum and minimum stresses applied:

$$S_{opss} = \theta\,\sigma_{\max}\left[1-\left(\frac{\sigma_{\max}}{\sigma_y}\right)^2\right]+\varphi\,\sigma_{\min} \qquad \text{(Eq. 7.1)}$$

Where σ_{max} and σ_{min} are the nominal maximum and minimum stresses in a smooth specimen, or the local maximum and minimum stresses at the notch root in a notched specimen respectively. σ_y is a material constant and θ and φ are two experimentally determined constants for a material. The first constant (θ) is related to the height of the stretched material (plastic zone size) in the crack wake compared to the crack opening, and the second constant (φ) is related to the reduction of the stretch by the minimum stress. Table 7.2 and Figure 7.1 show the variation of these constants with metal hardness for the three tested steels. Figure 7.2 shows the variations of the crack opening stresses calculated using Eq. 7.1 assuming the same maximum and minimum (± 100 MPa) stresses for the three steels tested.

Table 7.2 Values of DuQuesnay's constants for the three types of tested steels

Parameters	DP 590	SAE 1045	AISI 8822
Constant - θ	0.9	0.64	0.05
Constant - φ	0.05	0.1	0.2
Hardness - HRC	6	35	60

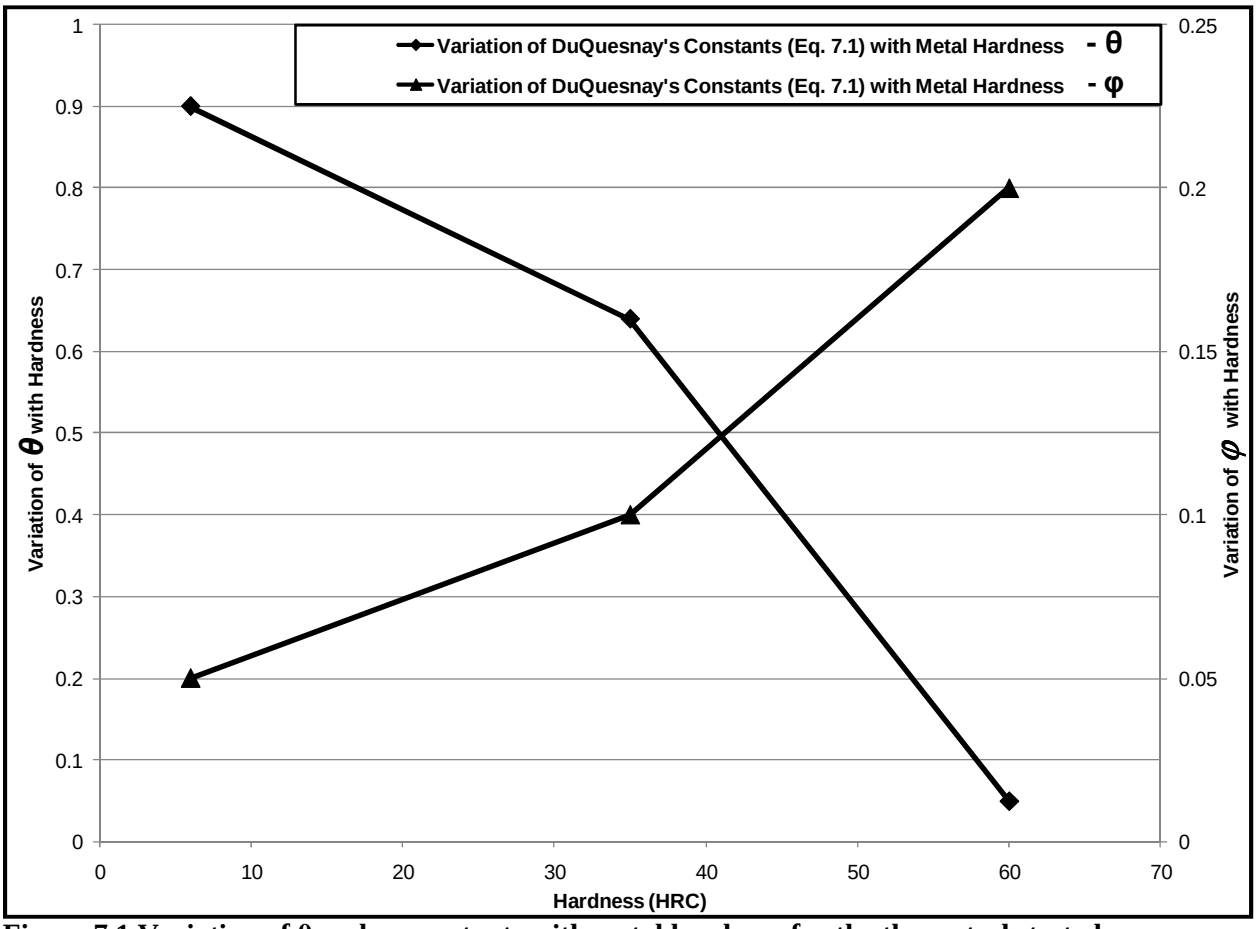

Figure 7.1 Variation of θ and φ constants with metal hardness for the three steels tested

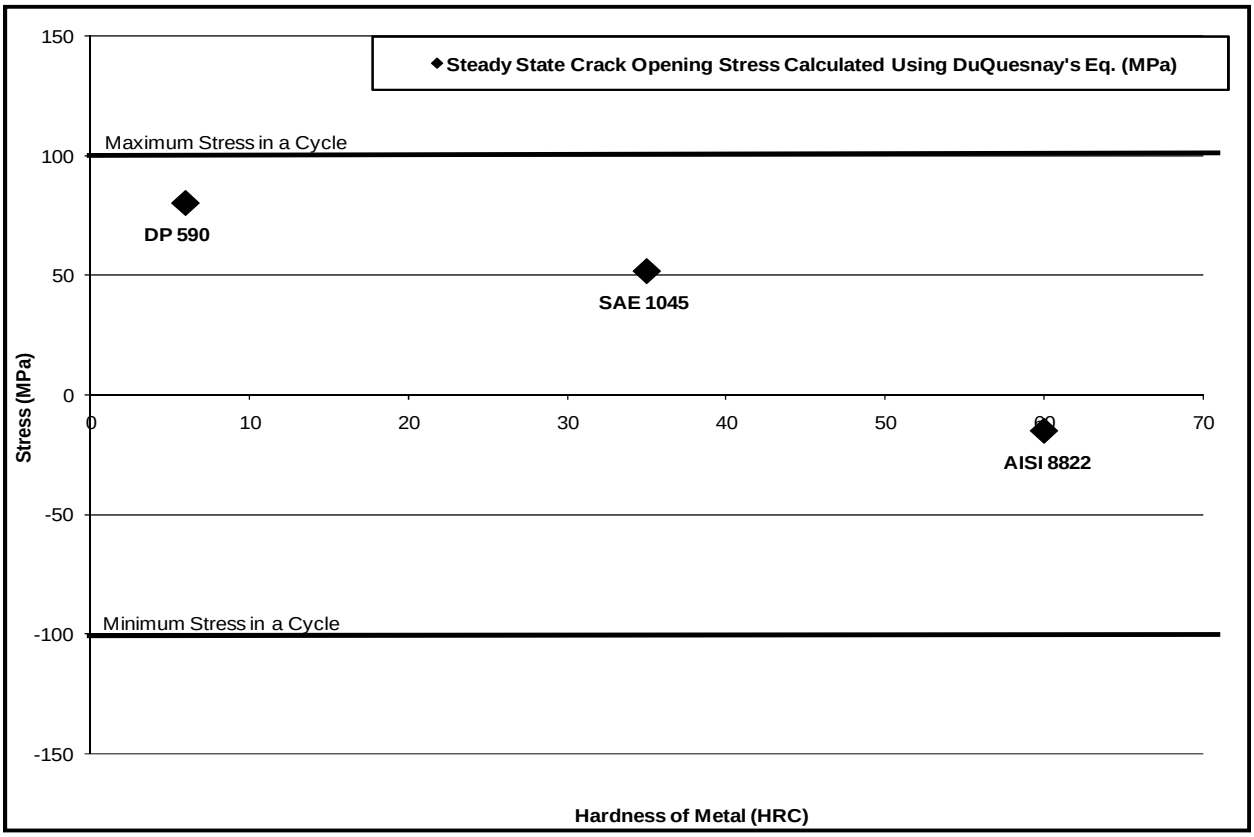

Figure 7.2 Variation of the steady state crack opening stresses for the 3 tested steels for the same maximum and minimum stress (±100 MPa)

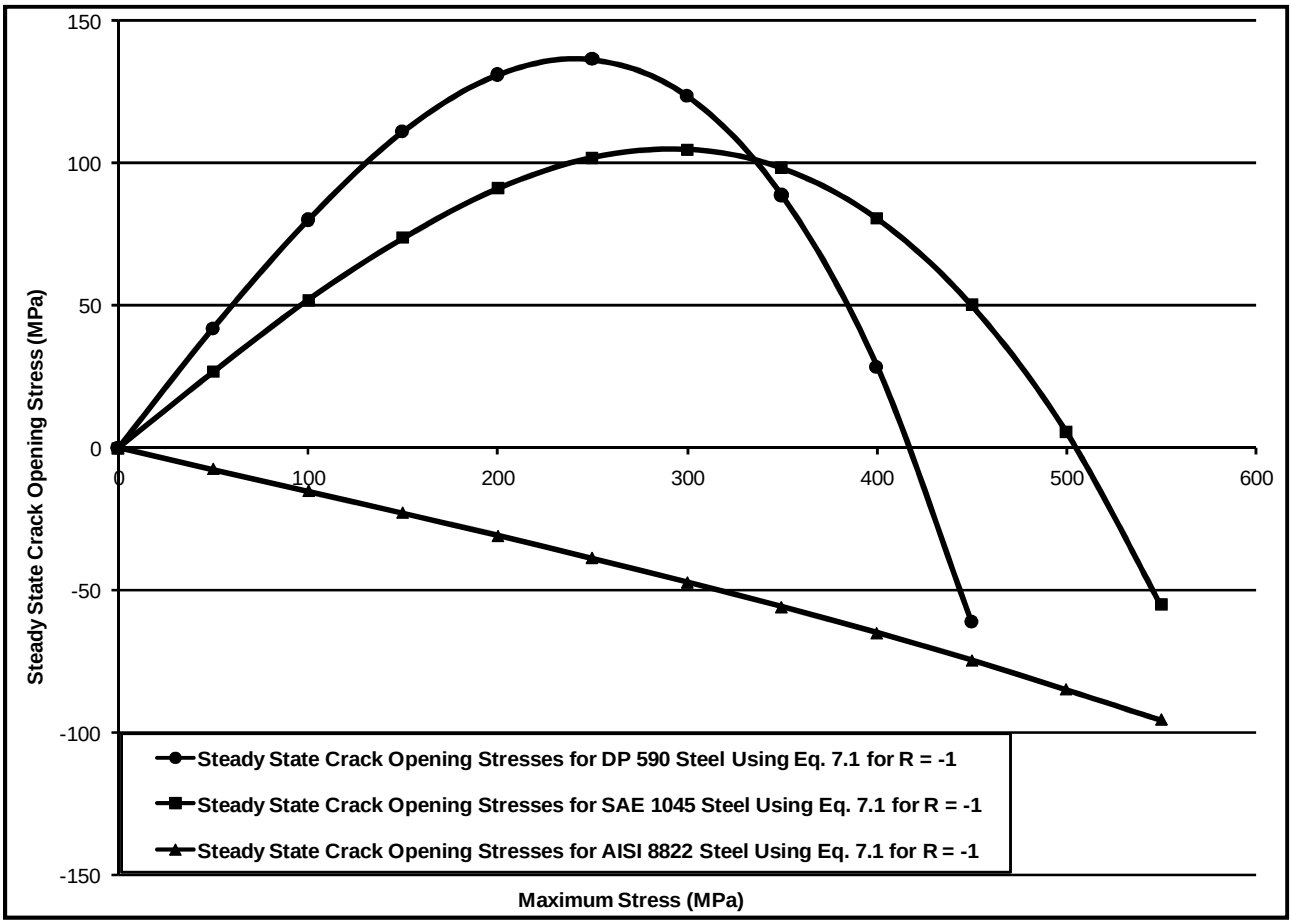

Figure 7.3 Plot of the steady state crack opening stresses for the three tested metals using DuQuesnay's equation

In Figure 7.2, the steady state crack opening stress decreases with metal hardness, it is important here to understand that when the applied maximum stress is far below the yield limit, a small scale plastic zone is formed ahead of the crack tip. This plastic zone is embedded in a surrounding elastic field which produces residual clamping stresses on the material in the crack wake. This results in a crack opening at a stress level above zero load. However as the maximum stress increases the plastic zone ahead of the crack extends and the residual elastic stresses become more remote and less effective until the yield stress is reached. In this case the whole cross section has yielded and the crack remains stretched open on unloading and a compressive stress is required to close the crack. This kind of behaviour was observed for DP 590 steel and for the SAE 1045 steel (Figure 7.3). The crack opening stress first increased with the maximum stress in a stress cycle and then levelled off at about one half of the material yield stress after which it decreased until it fell below zero when the plastic zone at the crack tip expanded rapidly as the material yield stress was approached. However for the AISI 8822 steel (the metal with the highest

hardness) the steady crack opening stresses were all negative even at low maximum stresses (Figure 7.3). This is attributed to there being almost no plastic wake to cause crack closure even at positive stress in this material and the crack opening stresses being reduced to a negative stress level by the minimum compressive stresses that caused crushing of asperities, flattening of the crack wake and bulging as they increase in magnitude. Moreover, the first constant (θ) in Eq. 7.1 tends to decrease with increasing hardness and this can be explained by the fact that the plastic zone size is inversely proportional to the material's yield limit that tends to be higher for harder metals. Therefore as the metal gets harder, its yield stress increases and consequently the size of the plastic zone and the size of the plastic wake that causes crack closure decreases.

7.2 Variation of the Crack Opening Stresses after the Application of Underloads

In the early 1960's, load interaction effects were first recognized [75] and [76]. The application of a single overload was observed to cause a decrease in the crack growth rate. This phenomenon is termed as crack retardation. As discussed previously a tensile overload in a constant amplitude fatigue test will result in an increase in the plastic zone size and the tensile stretch in front of the crack tip as compared to the baseline cyclic loading. The plastically deformed material ahead of the crack tip will tend to keep the crack open causing a decrease in the crack opening stress magnitude, S_{op}. This will then result in an increased crack growth rate. However as the crack grows into the overload plastic zone the stretched material will increase the height of the plastic wake and the crack opening stress and decrease the effective stress and effective stress intensity factor and the crack growth rate will decrease. On the other hand, compressive near yield limit underloads reduce the crack opening stress and until it recovers to its steady state level, crack growth is accelerated [35]. Varvani and Topper [52] showed that the application of a compressive near yield limit underload contributes to the flattening of the asperities in the crack wake that are responsible for roughness induced crack closure and accelerated crack growth.

In this investigation the variation in the crack opening stresses after the application of a near yield limit underload cycle was modeled using the steady state crack opening stress (Eq. 7.1) and the stress build-up equation (Eq. 7.2):

$$\Delta S_{op} = m(S_{opss} - S_{cu}) \qquad \text{(Eq. 7.2)}$$

Where ΔS_{op} is the change in crack opening stress, S_{opss} is the steady state crack opening stress, S_{cu} is the current crack opening stress, and m is a material constant obtained through a series of damage tests that will be discussed in the next section. The equation above describes the crack opening stress build-up to its

steady state condition after the application of an underload. Figures 7.4 and 7.5 show the immediate decrease in the crack opening stress from its steady state level after the application of an underload for DP 590 and SAE 1045 steels respectively. Then with further cycling the crack opening stress builds-up and returns to its steady state level assuming no more underloads are applied. It is worth mentioning here that although in the previous section it was shown that according to Eq. 7.1 (steady state crack opening stress equation), the value of the crack opening stresses for DP 590 steel were higher than for the SAE 1045 steel and examining Figures 7.4 and 7.5 we see that the stress at which the crack opened for DP 590 steel immediately after the application of an underload (-39 MPa) was lower than the stress for SAE 1045 steel (31 MPa). The reason for this is that at the high underload stress level the DP 590 steel experienced a significant amount of plasticity. Under these conditions the crack closing stress is lower than the crack opening stress. Such a difference between the crack opening stresses and the crack closure stresses is well documented in a research paper by McClung et al. [77]. They tested SAE 1026 steel under constant amplitude and block loading fatigue histories and noticed a significant difference in the crack opening stresses and crack closure stresses for high strain histories. Similar behaviour was also reported in the work of Newman [74] where he observed that the crack opening and closing levels are similar for low strain histories but may differ widely at high strains. Vorwald and Seegar [56] noted that when there was plasticity in the stress-strain loop the opening and closing strains were about the same, but since the closing strain occurred on the lower branch of the hysteresis loop it was much lower in stress than the opening strain. Equation 7.1 gives estimates of the crack opening stresses that are closer to the crack opening stresses than to the crack closing stresses in the presence of plasticity in the stress-strain loop but the actual opening after the underload cycle is at the lower crack closing stress.

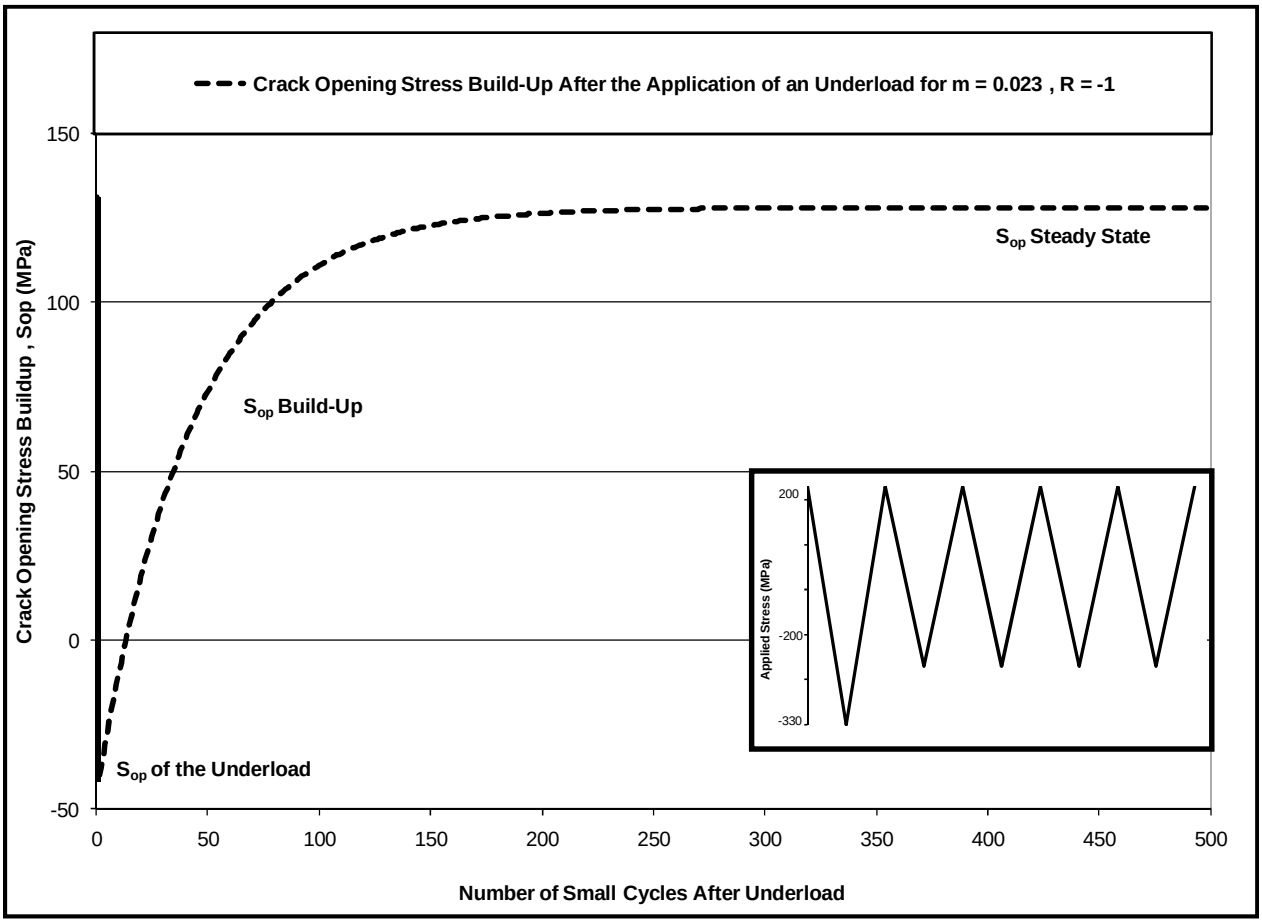

Figure 7.4 The decrease of the crack opening stress after the application of an underload and the stress build-up to a steady state level for DP 590 steel

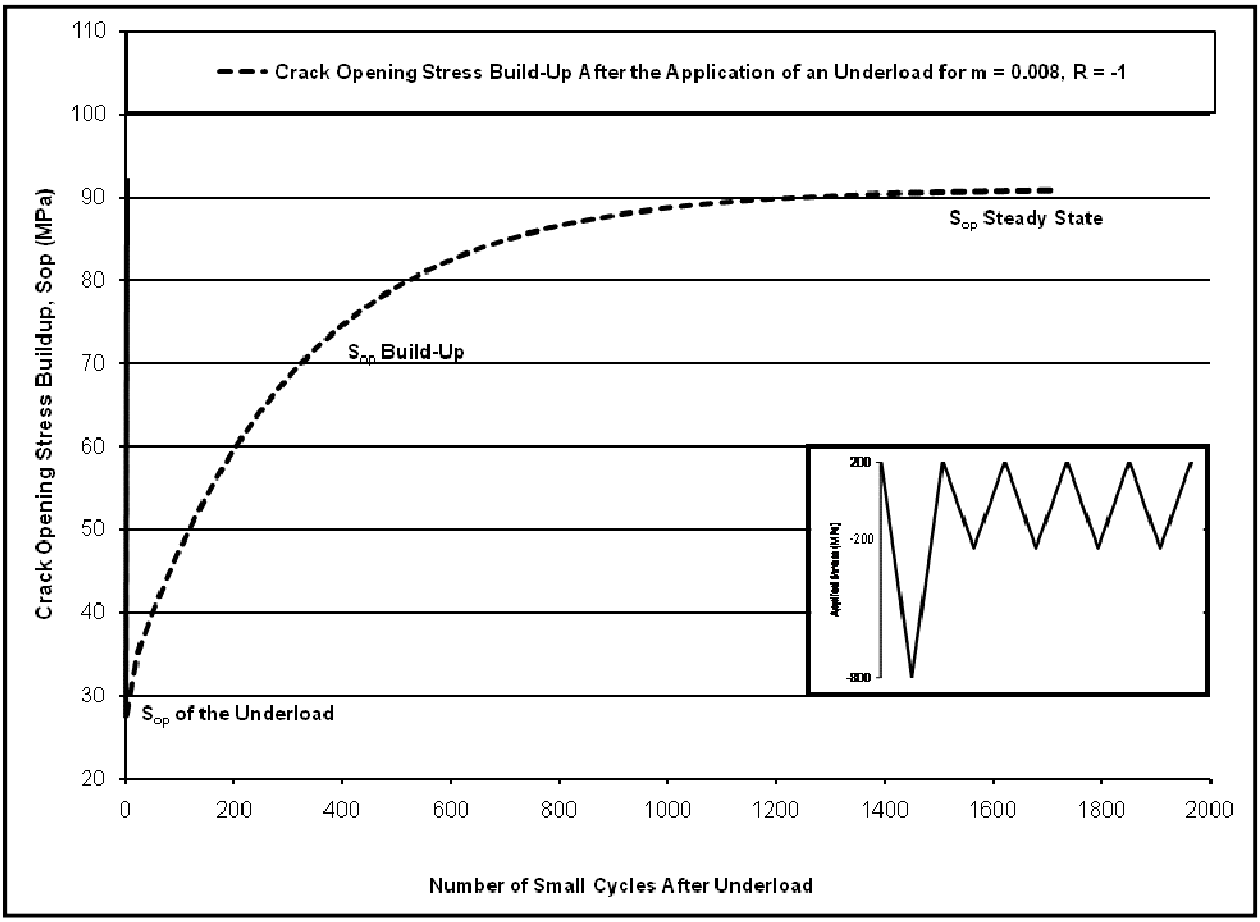

Figure 7.5 The decrease of the crack opening stress after the application of an underload and the stress build-up to a steady state level for SAE 1045 steel

7.3 Variation of the Crack Closure Parameter *"m"* in the Stress Build-Up Equation

The crack closure parameter "*m*" in Eq. 7.2 was different for the three types of steel (Table 7.3). This parameter describes the recovery of the crack opening stress to its steady state level after the application of an underload.

Table 7.3 Values of the closure parameter "*m*" for the three tested steels

Parameter	**DP 590**	**SAE 1045**	**AISI 8822**
Closure Parameter -*m*	0.023	0.008	0.0009
Hardness - HRC	6	35	60

It is obvious from the results above that the closure parameter *"m"* decreases with increasing material hardness. A similar trend was reported Khalil et al. [78] who tested SAE 1045 steel in as-received condition and in a quenched and tempered condition and found that the closure parameter decreased with increasing hardness of the metal. As expected the decrease in the crack closure parameter *"m"* (that represents the change in the difference between the steady state crack opening stress and the current crack opening stress) with increasing hardness led to a corresponding increase in the number of cycles needed for the crack opening stress to reach a steady state level after an underload. The recovery of the crack opening stresses to a steady state level for DP 590 steel, SAE 1045 steel and AISI 8822 steel are shown in Figures 7.4, 7.5, and 7.6 respectively. The DP 590 steel took about 600 small cycles (200 MPa in tension and -200 MPa in compression) to recover to its steady state level. The SAE 1045 took about 1800 small cycles (200 MPa in tension and -200 MPa in compression) to reach its steady state level and AISI 8822 steel took almost 10,000 small cycles (200 MPa in tension and -200 MPa in compression) to reach the steady state crack opening stress level.

* The crack opening stresses were not measured for AISI steel, the data shown in Figure 7.6 were obtained by calculating the crack opening and build-up stresses using Eq. 7.1 and 7.2 and the material constants obtained from experimental tests.

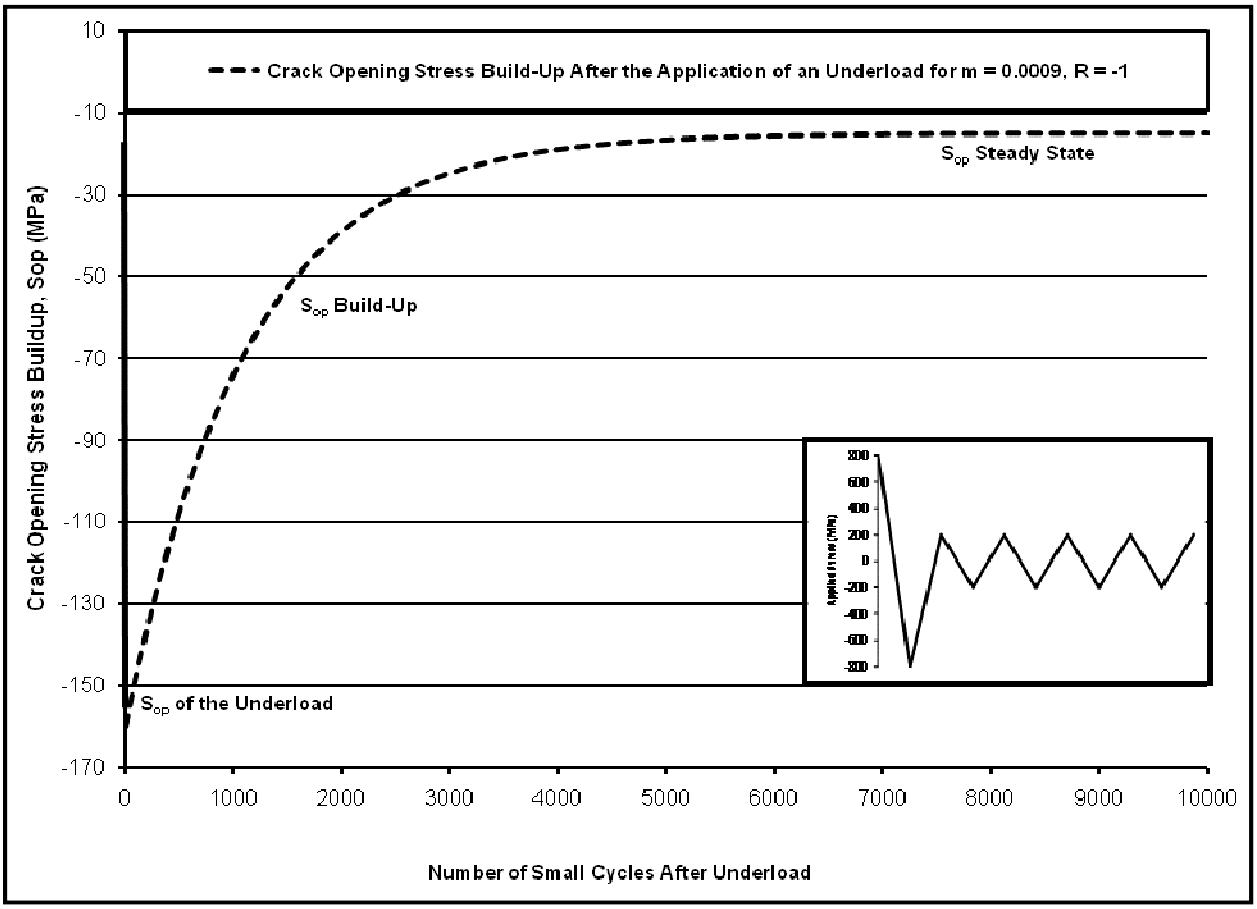

Figure 7.6 The decrease of the crack opening stress after the application of an underload and the stress build-up to a steady state level for AISI 8822 steel

7.4 Damage Tests used to Obtain the Parameter *"m"* in the Stress Build-Up Equation

One of the main goals of this thesis was to develop a new test procedure for obtaining data on the return of the crack opening stress to its steady state level following an underload. These tests were introduced in Chapter 3, Section 3.3.3.2 where smooth specimens were tested under load histories with a fixed small cycle load range and intermittent underloads. The frequency of occurrence of the underloads was varied from test to test and the changes in the fatigue lives were observed. The changes in damage per block were then used to determine the value of the closure model parameter "*m*" in Eq. 7.2 that described the recovery of the crack opening stress to its steady state level. Previous work [79] also used Eq. 7.2 to predict the changes in the crack opening stresses, however the parameter "*m*" was obtained through a series of crack opening stress measurements, where the test was stopped at a certain number of cycles and the specimen was removed from the test machine and the crack opening stress was measured

using an optical and a confocal scanning laser microscope. This procedure was extremely time consuming and was replaced in this investigation by the damage tests. The results of these tests are shown in Figures 4.8, 5.8 and 6.5 for DP 590, SAE 1045 and AISI 8822 steel respectively. The methodology is explained with reference to the damage per cycle for DP 590 steel versus the number of small cycles per block shown below in Figure 7.7. In region "A-B" the damage per cycle is constant since the crack opening stress (S_{op}) is below the minimum stress (S_{min}) of the small cycles and therefore the stress range of the small cycles is fully effective and is given by:

$$\Delta S_{eff} = S_{max} - S_{min} \qquad (S_{min} < S_{op}) \qquad \text{(Eq. 7.3)}$$

where ΔS_{eff} is the effective stress range of the small cycles, and S_{max} is the maximum stress of the small cycles. However with further cycling, the crack opening stress (S_{op}) builds-up until at the beginning of region "B-C" the crack opening stress becomes less than the minimum stress and therefore the effective stress range of the small cycles starts to decrease, and the damage done by these cycles then decreases until the crack opening stress reaches its steady state level. The effective stress range of the small cycles in this region is given by:

$$\Delta S_{eff} = S_{max} - S_{op} \qquad (S_{min} > S_{op}) \qquad \text{(Eq. 7.4)}$$

In region "C", the crack opening stress has reached its steady state level and the effective stress range of the small cycles and the damage per cycle remains constant with further cycling. The effective stress range of the small cycles in this region is given by:

$$\Delta S_{eff} = S_{max} - S_{op} \qquad (S_{min} > S_{op}) \qquad \text{(Eq. 7.5)}$$

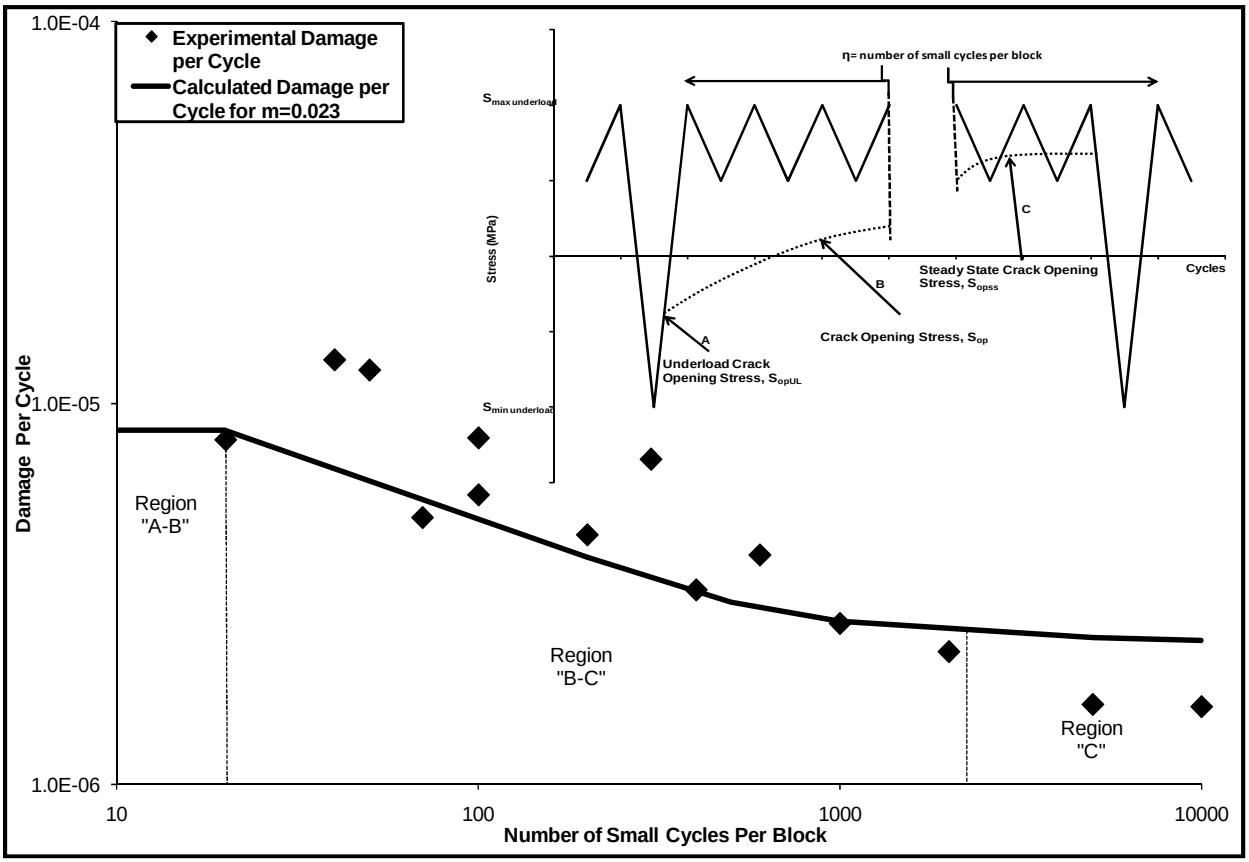

Figure 7.7 Damage per cycle versus the number of small cycles per block for DP 590 steel

7.5 Modeling the Changes in the Crack Opening Stresses under Variable Amplitude Loading

Fatigue lives under variable amplitude loading were predicted using two models in this investigation; the effective strain-life fatigue model (Chapter, Section 2.2), and the effective crack growth model (Chapter 2, Section 2.3). One of the main components common to both models is predicting the crack opening stresses for each cycle in the load history. Previous sections in this chapter (Sections 7.1 through 7.4), have discussed the variation of the crack opening stresses for each material and how large near yield limit cycles present in random histories can cause a severe decrease in the crack opening stresses and an increase in the crack growth rate or in the damage of subsequent smaller cycles. In order to predict the crack opening stresses in both of the models several conditions on how to calculate the crack opening stresses were presented in Chapter 2, Section 2.2.8 and are restated below:

1. For the first closed loop cycle, the value of the steady state crack opening stress (S_{opss}) was calculated using Eq. 7.1.
2. For other closed loop cycles that followed, the crack opening stress (S_{op}) was calculated based on the following assumptions:
    - Using Eq. 7.1, the crack opening stress levels were modeled assuming that the crack opening stress for a given cycle instantaneously decreased to the constant amplitude steady state level for that cycle if this steady state crack opening stress (S_{opss}) was lower than the current opening stress (S_{cu}).
    - If the steady state crack opening stress (S_{opss}) was higher than the current opening stress (S_{cu}), the crack opening stress in the current cycle followed the exponential build up formula of Eq. 7.2 unless the range of stress in the cycle was below the intrinsic stress range, or the maximum stress in the cycle was below zero in which case it didn't change because the crack would not advance to cause a change in the crack opening stress (these cycles for which there was no crack growth were not used in calculating the crack opening stress build up).
    - If the above condition did not apply, the crack opening stress increment calculated using Eq. 7.2 was added to the current level to give the opening stress at the end of the cycle.
    - This procedure was repeated for each cycle in the load history.
    - In summary, Eq. 7.1 together with Eq. 7.2 were used to calculate the crack opening stress levels for a cycle. If the stress level obtained from Eq. 7.1 was below the current stress level, the crack opening stress was lowered to the calculated level. If the level was higher, the crack opening stress was increased by the amount given by Eq. 7.2

In order to validate these conditions, direct measurements of the crack opening stresses were presented in Chapters 4 and 5 for DP 590 and SAE 1045 steel where they were compared with the calculated values under the Log Skidder and the Grapple Skidder Histories at different cycle numbers. In Figure 7.8 the calculated and the measured crack opening stresses are shown for a range between 3000 and 10, 000 reversals for DP 590 steel under the Log Skidder History scaled to a maximum of 410 MPa. Table 7.4 shows a comparison for the calculated crack opening stresses and all the measured values under the Log Skidder History.

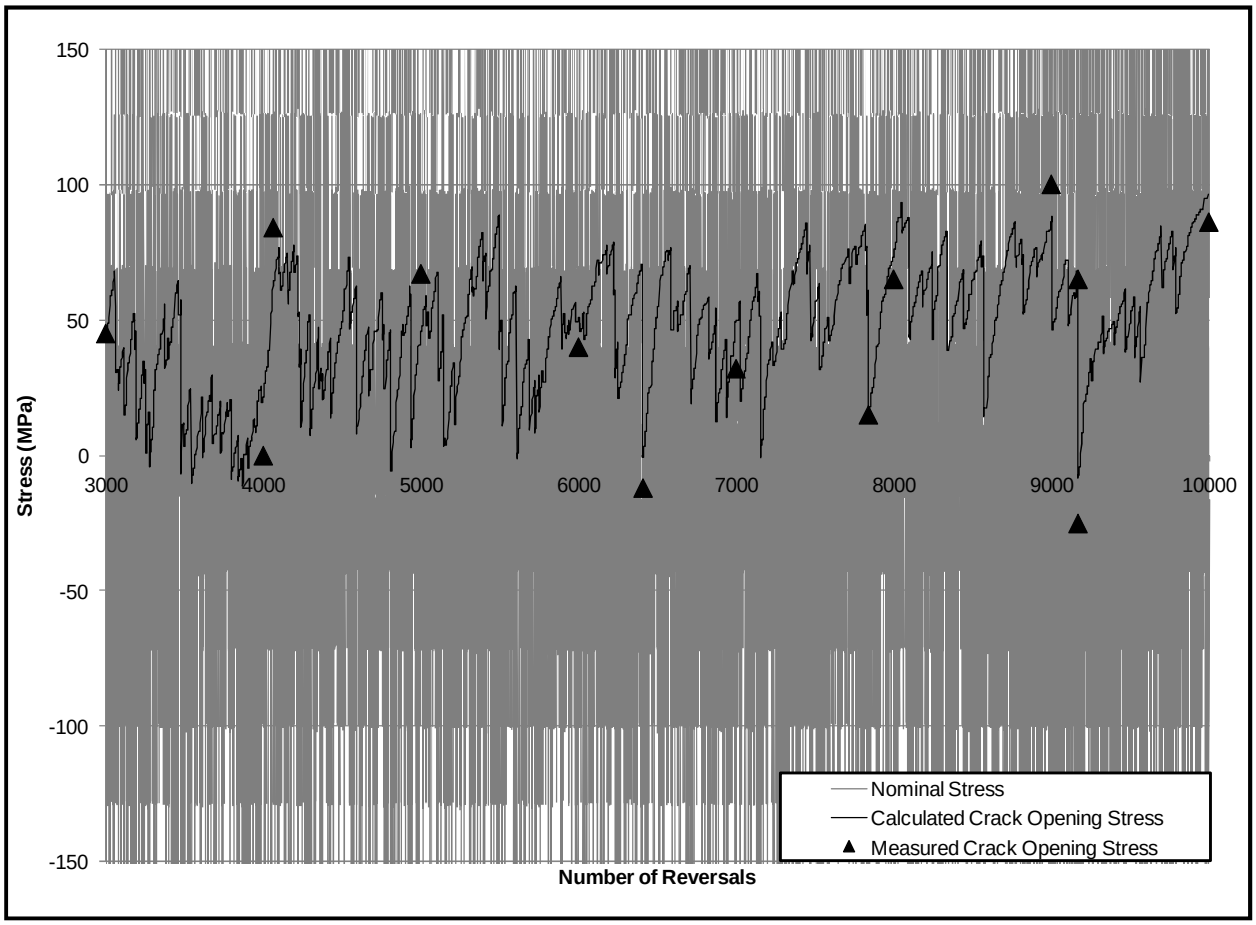

Figure 7.8 Calculated and measured crack opening stresses for DP 590 steel between 3000 and 10,000 reversals under the Log Skidder History scaled to a maximum of 410 MPa

Table 7.4 Calculated crack opening stresses and measured crack opening stresses for DP 590 steel tested under the Log Skidder History

Reversal number	Calculated S_{op} (MPa)	Measured S_{op} (MPa)
150	55	69
175	25	23
270	-23	-10
1,000	43	23
2,000	0	13
2,520	63	52
2,580	-15	-3
3,000	45	41
4,000	0	21
4,063	84	61
5,000	67	44
6,000	40	32
6,410	-12	0
7,000	32	49
7,840	15	12
8,000	65	71
9,000	100	86
9,170	-25	-9
10,000	86	95
10,090	-5	4
11,520	90	83
11,580	-2	7
12,000	55	67
14,000	30	30
16,000	10	41

Figure 7.9 shows the direct measurements for the Grapple Skidder History scaled to a maximum of 470 MPa together with the calculated values obtained for DP 590 steel between 1 and 10,000 reversals. A full comparison of the calculated crack opening stresses and measured one are presented in Table 7.5.

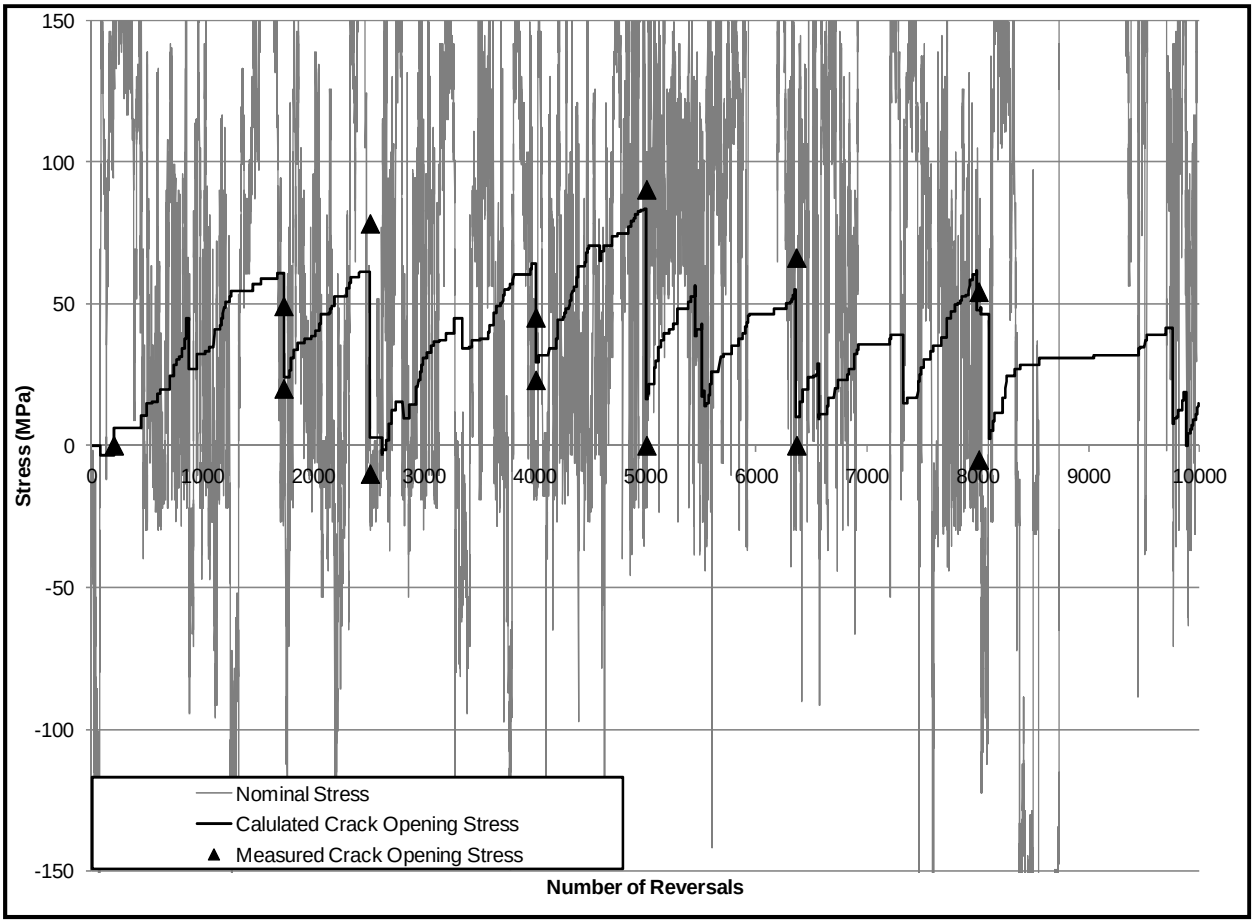

Figure 7.9 Calculated and measured crack opening stresses for DP 590 steel between 1 and 10,000 reversals under the Grapple Skidder History scaled to a maximum of 470 MPa

Table 7.5 Calculated crack opening stresses and measured crack opening stresses for DP 590 steel under the Grapple Skidder History

Reversal number	Calculated S_{op} (MPa)	Measured S_{op} (MPa)
200	0	-3
1,733	49	61
1,734	20	24
2,513	78	61
2,514	-10	3
4,009	45	64
4,010	23	64
5,009	90	84
5,010	0	16
6,363	66	55
6,364	0	10
8,009	54	48
8,010	-5	48
10,395	11	15
13,122	24	19
14,703	50	60
14,704	-5	-1
15,721	42	50
17,842	79	69
17,843	40	34
18,801	54	51
18,802	32	16
21,992	54	41
21,993	0	7
24,113	74	74
26,715	84	34
26,716	22	34
29,142	45	38
30,950	85	70
31,260	-1	3
32,193	28	39
33,387	15	18
35,370	79	69
35,662	33	40
37,189	68	64
37,346	-3	0
38,107	23	37
39,540	64	50

For the two different histories above, the crack opening stress decreased when the specimen was subjected to a large underload cycle and then built-up again during subsequent smaller cycles. The crack opening stress build-up was modeled using the exponential build-up formula (Eq. 7.2) in which the increase of the crack opening stress during each cycle in the load history was proportional to the difference between the current crack opening stress and the steady state crack opening stress of that given cycle. Similar behaviour was obtained for SAE 1045 steel, Figure 7.10 shows the calculated and the measured crack opening stresses under Log Skidder History scaled to a maximum of 410 MPa for a range between 3000 and 10,000 reversals and Figure 7.11 shows the results for the Grapple Log Skidder history scaled to a maximum of 470 MPa. Tables 7.6, 7.7, 7.8, and 7.9 show the results of the calculated and the measured values of the crack opening stresses under the Log Skidder and Grapple Skidder Histories respectively.

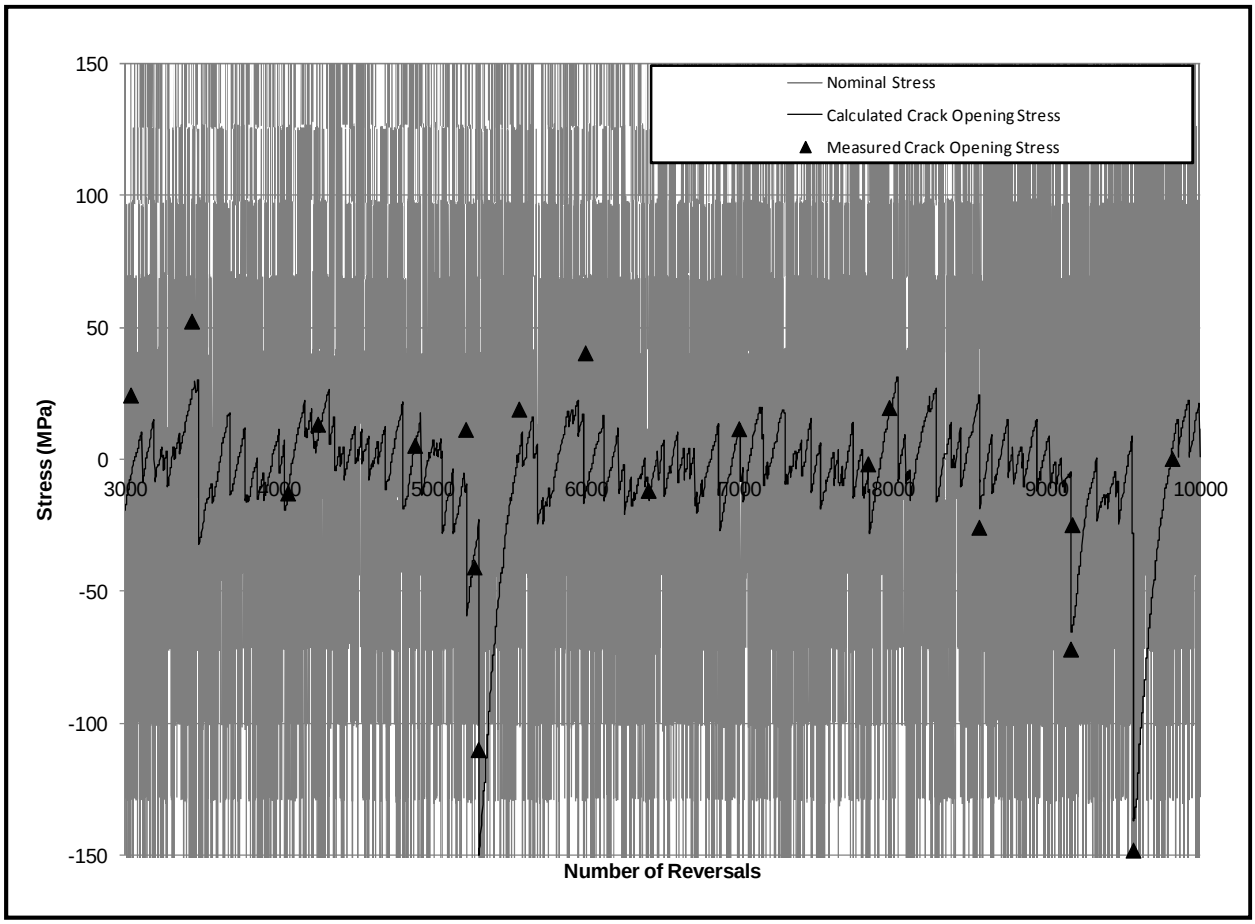

Figure 7.10 Calculated and measured crack opening stresses for SAE 1045 steel between 3000 and 10,000 reversals under the Log Skidder History scaled to a maximum of 410 MPa

Table 7.6 Calculated crack opening stresses and measured crack opening stresses for SAE 1045 steel tested under the Log Skidder History

Reversal number	Calculated S_{op} (MPa)	Measured S_{op} (MPa)
150	22	4
175	10	10
270	-23	11
850	-44	-35
2,000	0	1
2,520	22	-11
2,580	-15	-13
2,639	-84	-64
2,818	19	5
2,887	-61	-71
3,040	24	-5
4,063	-13	-11
4,258	13	10
4,890	5	6
5,221	11	3
5,277	-41	-34
5,303	-110	-150
5,568	19	3
6,410	-12	-10
7,000	11	11
7,840	-2	-12
8,563	-26	-8
9,160	-72	-65
9,170	-25	-64
9,567	-148	-137
9,821	0	5
10,090	-5	2
10,820	23	31

Table 7.7 Calculated crack opening stresses and measured crack opening stresses for SAE 1045 steel tested under the Log Skidder History – Continued

11,106	40	36
11,566	-129	-121
11,580	18	-110
11,651	-156	-148
11,920	1	-11
12,316	-12	-14
13,051	-44	-49
16,000	10	14

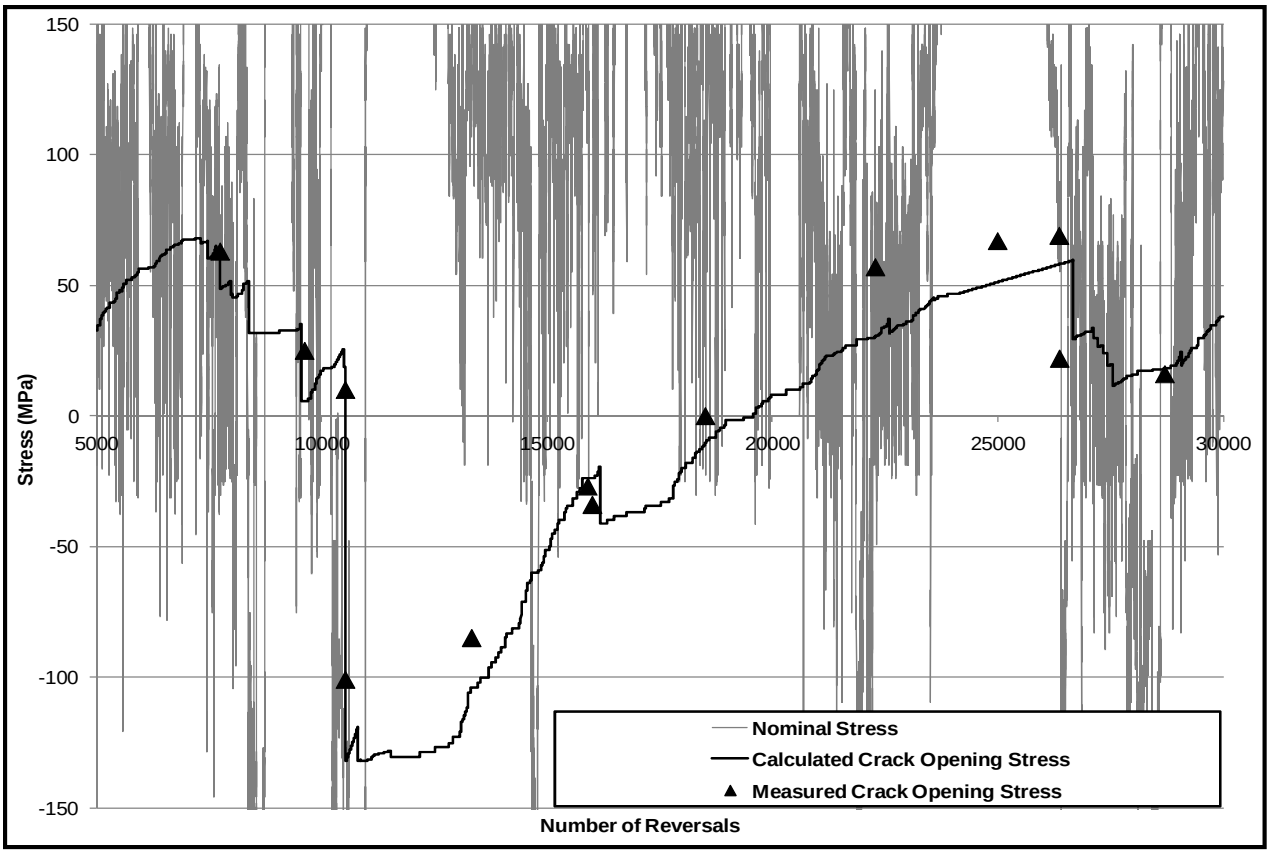

Figure 7.11 Calculated and measured crack opening stresses for SAE 1045 steel between 5000 and 30,000 reversals under the Grapple Skidder History scaled to a maximum of 470 MPa

Table 7.8 Calculated crack opening stresses and measured crack opening stresses for SAE 1045 steel under the Grapple Skidder History

Reversal number	Calculated S_{op} (MPa)	Measured S_{op} (MPa)
500	0	4
999	0	17
1,000	-20	17
3,343	50	31
3,345	-20	-8
7,736	63	49
9,610	25	6
10,517	10	19
10,518	-101	-132
13,321	-85	-104
15,899	-27	-24
16,001	-34	-24
18,512	0	-11
22,286	57	30
25,000	67	51
26,369	69	58
26,378	22	58
28,714	16	18
30,999	65	46
31,169	21	26
33,969	43	32
34,250	-21	-3
36,660	25	9
36,860	-1	-10
39,508	14	28
500	0	4
999	0	17
1,000	-20	17
3,343	50	31

Table 7.9 Calculated crack opening stresses and measured crack opening stresses for SAE 1045 steel under the Grapple Skidder History – Continued

3,345	-20	-8
7,736	63	49
9,610	25	6
10,517	10	19
10,518	-101	-132
13,321	-85	-104
15,899	-27	-24

Comparing the results for the two materials, we notice that the SAE 1045 crack opening stresses were lower than for DP 590 steel under the same scaled maximum load history (410 MPa). The effect of underloads in SAE 1045 was more severe and the recovery was slower than for the DP 590 steel.

7.6 The Effective Strain-Life Fatigue Model

7.6.1 The Effective Strain-Life Curve

The usual analysis procedure for variable amplitude fatigue calculates fatigue damage based on constant amplitude strain controlled fatigue tests of smooth specimens. The resulting predictions are typically non-conservative for cracks growing from notches due to the load interaction effect in variable amplitude loading. Large load cycles in variable amplitude loading decrease the crack opening stresses and increase the effective stress for subsequent smaller cycles. As a result the crack growth rate and damage for the smaller cycles is increased and even small cycles below the fatigue limit can cause a significant amount of damage. Previous work at Waterloo [63] introduced the effective strain-life curve for use in fatigue damage calculations under variable amplitude loading. The effective strain range, $\Delta\varepsilon_{eff}$, is the strain range for which the fatigue crack is open and is given by the difference between the maximum strain and the greater of the minimum strain or the crack opening strain. This effective strain range has been shown to be a useful parameter to account for the effects of mean stress and overloads (or underloads) on damage accumulation [61]. It has also been shown that if the effective strain range of a cycle is known, the damage and the fatigue life can be determined from the effective strain-life curve for a given material. The way the effective strain-life was derived for the materials used in this investigation was presented in Chapter 2, Section 2.2.6.1. Figures 4.3, 5.3, and 6.3 show the effective strain-life curves

for DP 590, SAE 1045, and AISI 8822 steel respectively derived from underload fatigue data. The constants for the effective strain-life curve (Eq. 7.6) for the three materials are presented in Table 7.10.

$$\Delta\varepsilon_{eff} = \frac{A}{E}(N_f)^b + \Delta\varepsilon_i \qquad \text{(Eq. 7.6)}$$

Where E is the elastic modulus of elasticity and $\Delta\varepsilon_i$ is a material's intrinsic fatigue limit strain range below which a fully open crack will not cause fatigue damage, A and b are material constants. The effective strain-life curve can be also rearranged as follows:

$$E\Delta\varepsilon^* = E\Delta\varepsilon_{eff} - E\Delta\varepsilon_i \qquad \text{(Eq. 7.7)}$$

Where;

$$E\Delta\varepsilon^* = A(N_f)^b \qquad \text{(Eq. 7.8)}$$

The strain range $\Delta\varepsilon^*$ is the part of the strain range which causes fatigue crack growth and damage. This parameter was found to be related to the fatigue life by a power law [62] shown in Eq. 7.8.

Table 7.10 The effective strain-life constants for the three materials

Parameter	**DP 590**	**SAE 1045**	**AISI 8822**
A	87.0	34.2	1.3
b	-0.5	-0.39	-0.13
$\Delta\varepsilon_i$ *(%)*	0.085	0.27	0.09
Hardness - HRC	6	35	60

It is clear from the table above that the constants A and b in the effective strain-life curve decrease with increasing material hardness.

7.6.2 Fatigue Life Predictions using the Effective Strain-Life Model

The effective strain-life curve was used to predict fatigue lives under two load histories; the Log Skidder History and the Grapple Skidder History. The fatigue life predictions made with this model presented in Chapters 4, 5 and 6 showed a good agreement with the experimental fatigues lives. The test procedure suggested gave good effective strain-life data and a reasonable estimate of the steady state crack opening stresses with a reasonable amount of testing.

The effective strain-life curve has been found to adequately account for the effects of the underloads and mean stresses present in variable histories.

7.7 Fatigue Crack Growth Model

This model as mentioned previously predicts fatigue lives using a fracture mechanics approach together with models of crack closure for short cracks emanating from notches. The two fundamental pieces of material data required for this type of analysis when applied to notched components are closure-free crack growth rates vs. stress intensity factor range data and crack opening stress vs. maximum and minimum stress data that extends to the high stress levels encountered in cracks growing from notches.

7.7.1 Derived Crack Growth Rate Curve and Measured Crack Growth Rate Data

The procedure used to derive the *da/dN vs.* ΔK_{eff} was presented in Chapter 2, Section 2.4.5 (where ΔK_{eff} is the effective stress intensity factor range) gave an adequate representation of the closure-free crack growth measurements shown in Figure 4.15 for DP 590 steel and Figure 5.14 for SAE 1045 steel. The effective crack growth curve was expressed in terms of the effective stress intensity range and was given by:

$$\frac{da}{dN} = C(\Delta K_{eff} - \Delta K_i)^m \qquad \text{(Eq. 711)}$$

Where ΔK_i is the intrinsic stress intensity range, C and m are two material constants. Table 7.11 shows the constants for the two steels, and as predicted the SAE 1045 steel has a higher crack growth rate than the DP 590 steel due to the larger crack opening stresses experienced during the service load histories.

Table 7.11 Variation of the constants in the crack growth rate curves for DP 590 and SAE 1045 steels

Parameter	DP 590	SAE 1045
C	5.98E-12	2.8E-10
m	3.3	3.1
Hardness - HRC	6	35

7.7.2 Comparison of the Predicted Fatigue Lives with Conventional Fatigue Life Analysis

Fatigue life predictions for DP 590, SAE 1045, and AISI 8822 were made using the conventional strain-life curve and the Smith-Watson-Topper (SWT) mean stress parameter. The results were compared with the predicted fatigue lives using the effective strain-life model and experimental data. Figure 7.12 shows a comparison of the predicted fatigue lives using the effective strain-life curve and the constant amplitude strain-life curve for DP 590 steel under the Log Skidder History together with the experimental results. Figures 7.13 and 14 show the predicted fatigue lives for SAE 1045 and AISI 8822 steel respectively using the effective strain-life curve and the effective strain-life curve under the Grapple Skidder History together with the experimental results. It is obvious from the results that the conventional fatigue life analysis that is based on the constant amplitude strain-life data gave seriously non-conservative fatigue life predictions while the predictions made by the method used in this thesis that takes into account crack opening stress changes due to load level interaction are much more accurate.

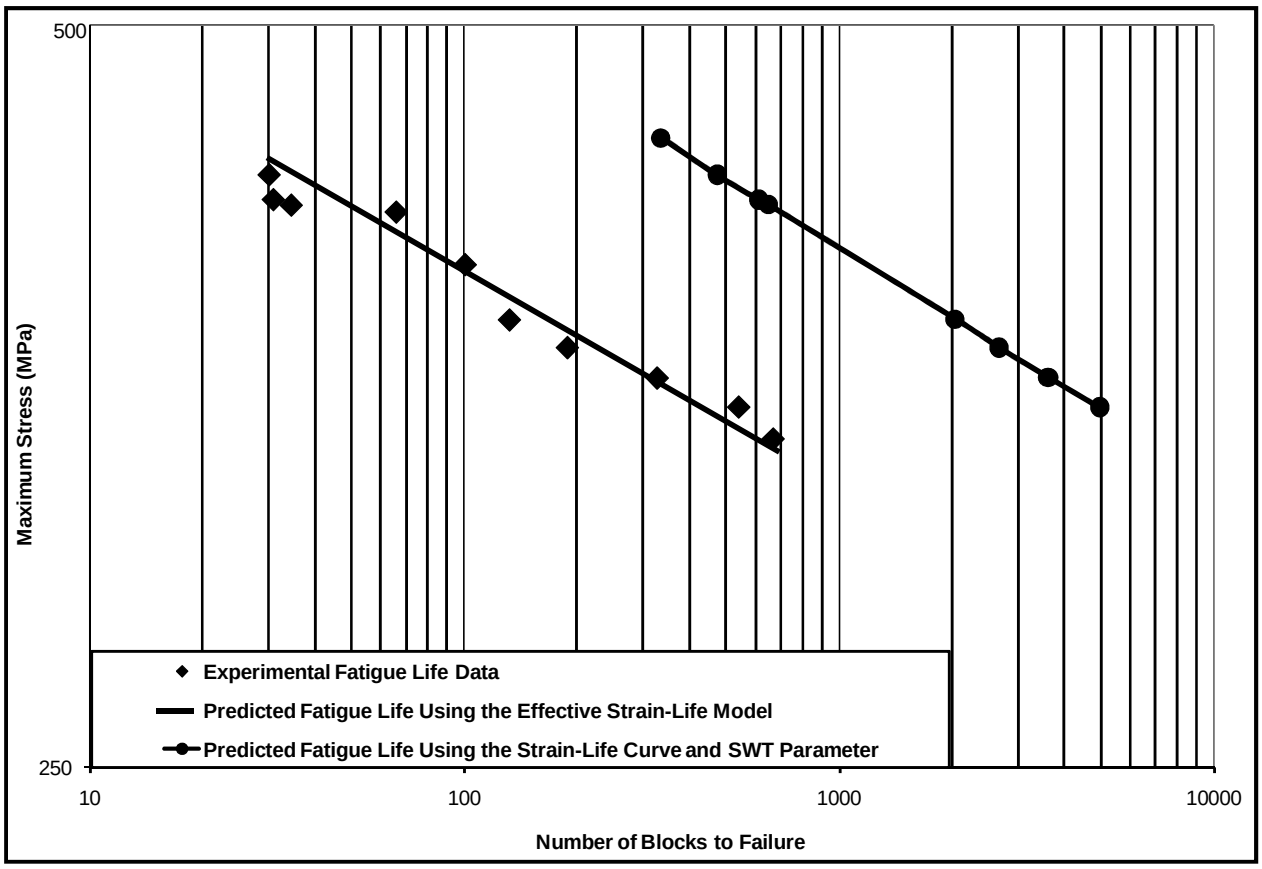

Figure 7.12 Fatigue life predictions using the effective strain-life curve and conventional strain-life techniques for DP 590 steel subjected to SAE Log Skidder History

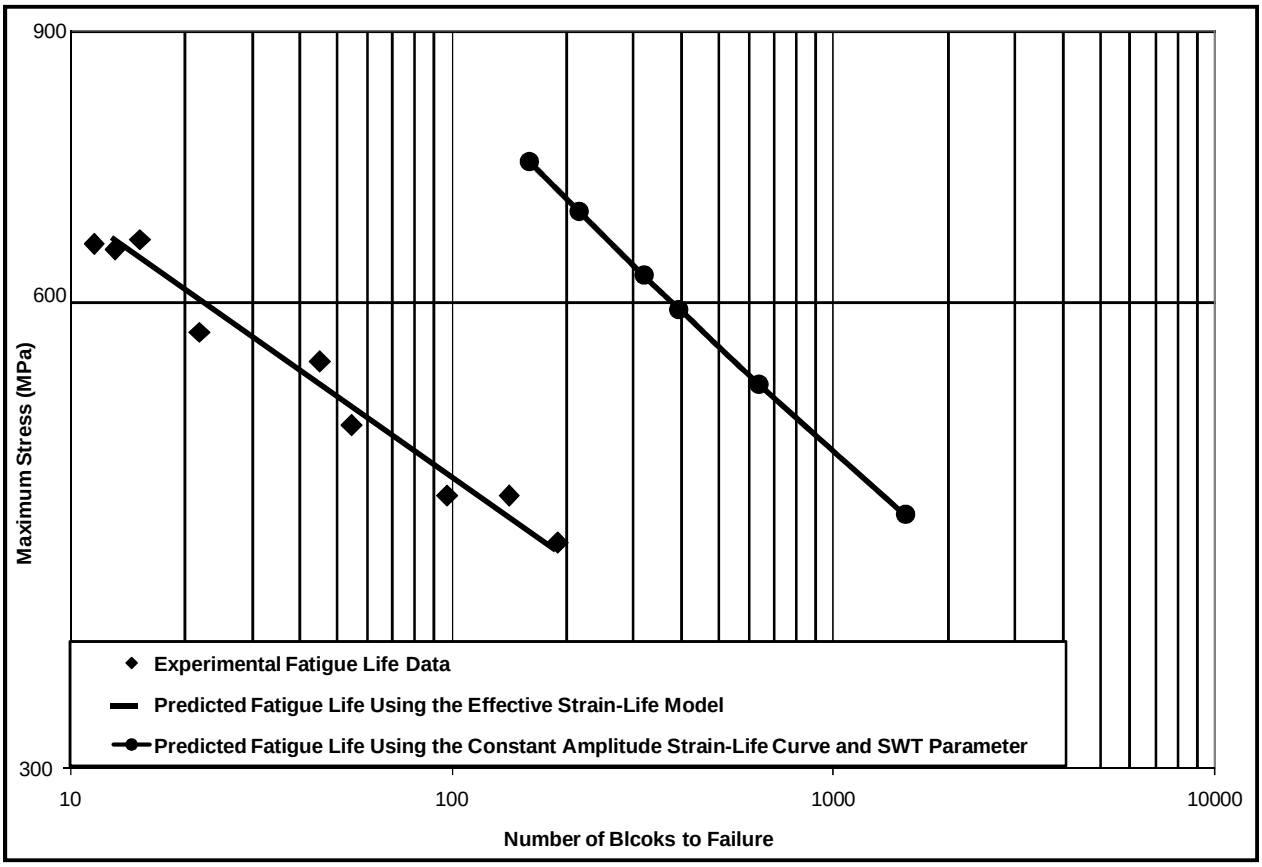

Figure 7.13 Fatigue life predictions using the effective strain-life curve and conventional strain-life techniques for SAE 1045 steel subjected to SAE Grapple Skidder History

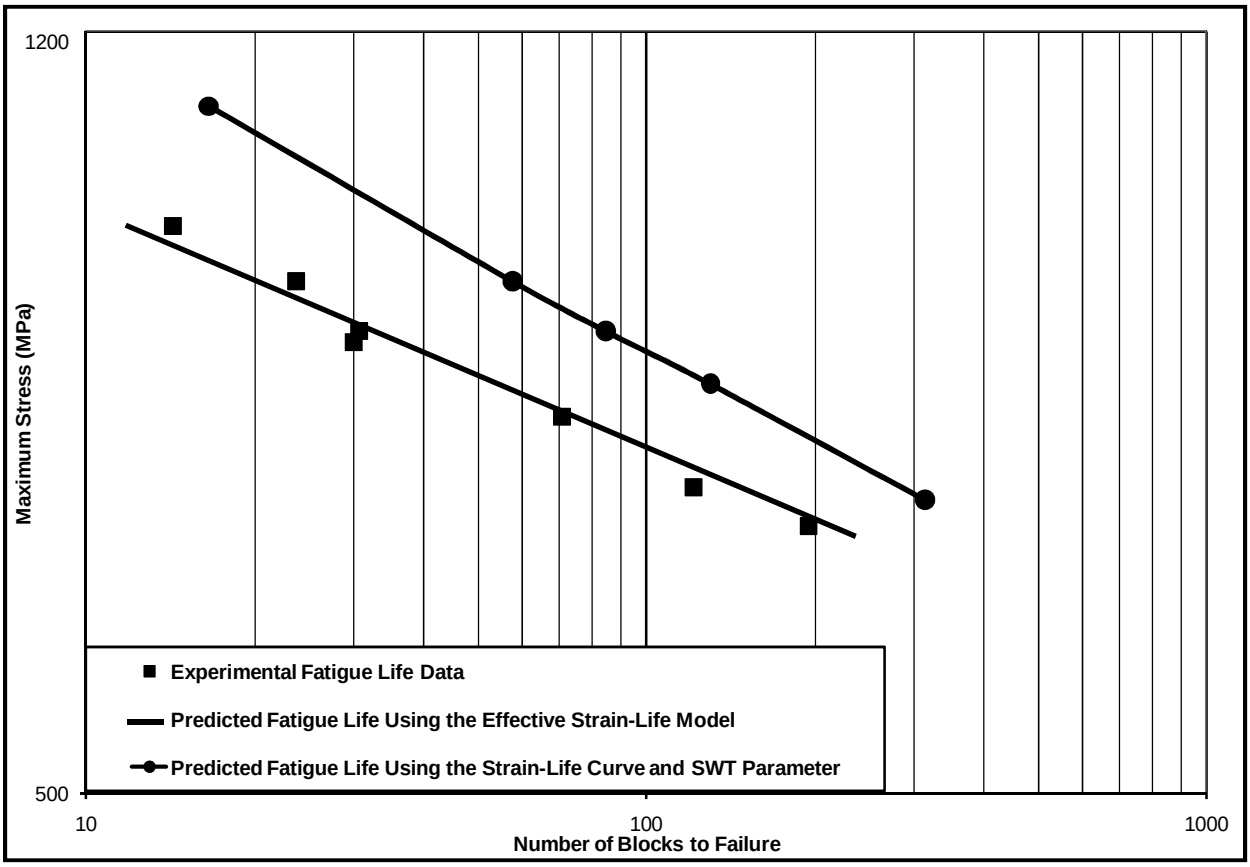

Figure 7.14 Fatigue life predictions using the effective strain-life curve and conventional strain-life techniques for AISI 8822 steel subjected to SAE Grapple Skidder History

Chapter 8
Conclusions and Future Recommendations

8.1 Conclusions

Smooth and notched samples made of three different materials of different hardnesses, namely DP 590 steel, SAE 1045 quenched and tempered steel, and AISI 8822 steel were tested to measure the crack opening stresses and fatigue lives under two SAE load histories (SAE Log Skidder History and SAE Grapple Skidder History). The work in this investigation included fully reversed constant amplitude fatigue tests, underload fatigue tests where a block that consisted of a single underload cycle followed by a number of smaller load cycles that had the same maximum stress as the underload cycle was repeated until the specimen failed, crack opening stress and crack opening stress build-up measurements made under different R-ratios, damage tests, closure free crack growth rate tests and finally service load history tests.

It was found that the crack opening stresses decreased when the specimen was subjected to large underload cycles that caused yielding of the material in the wake of the crack and a flattening of crack asperities. Then the crack opening stresses started to build-up again during subsequent smaller cycles as a new plastically stretched wake was created. The hardest metal (AISI 8822 steel) experienced very little crack closure and crack opening stress levels were low enough that stress cycles with R-ratios above 0.15 were fully open.

The rate of the recovery of the crack opening stress to its steady state level after the application of an underload was modeled by an exponential build-up formula (Eq. 7.2) in which the increase in crack opening stress during each cycle was proportional to the difference between the current crack opening stress and the steady state crack opening stress for the given cycle. It was found that the softest metal (DP 590 steel) recovered faster and took fewer cycles than the harder SAE 1045 and AISI 8822 metals to return to its steady state level after the application of an underload. The constant "m" was found to be 0.023 for the DP 590 steel, 0.008 for the SAE 1045 steel, and 0.0009 for the AISI 8822 steel. This indicates that the rate of the recovery to a steady state crack opening stress level after it has been decreased by an underload is more rapid for soft metals than for hard metals.

A new test procedure was introduced in this study to obtain data on the return of the crack opening stress to a steady state level following an underload. Smooth specimens were tested under load histories with intermittent underloads. The frequency of occurrence of the underloads was varied from test to test and the changes in the fatigue lives were observed. The changes in damage per block were then

used to determine the value of the closure model parameter "*m*" in Eq. 7.2 that described the recovery of the crack opening stress to its steady state level. The tests proved to be time efficient and can replace the current tests in which crack opening stress recovery is measured directly for crack growth specimens using an optical or confocal scanning laser microscope. The results obtained from these tests provided a good accuracy for the build-up of the crack opening stress and its recovery to the steady state level for all three steel hardness levels tested in this investigation.

Fatigue life predictions for tests performed under SAE service load histories were made by DuQuesnay et al. [59]. In their work the crack opening stresses were assumed to remain at the lowest level reached during a load history and that there was no recovery to a steady state level. Their results gave conservative fatigue life predictions under service load histories. In this investigation, the crack opening stresses were calculated for each cycle in the load history, and the crack opening stress build-up was taken into consideration. This together with the use of the effective strain-life curve that used the effective strain range of a stress-strain cycle instead of the strain range taken from the constant amplitude strain-life curve for rain-flow counted stress-strain loops gave a better fatigue life estimates than the fatigue life predictions obtained by [59] for the three types of steel under the two service load histories.

Finally the fatigue analysis models proposed in this investigation have been shown to give accurate fatigue life predictions compared to the non-conservative fatigue lives obtained through conventional fatigue life analyses (based on constant amplitude strain-life data). The analysis models were easy to use and the fatigue data required to implement them came from inexpensive tests. Data on the recovery of the crack opening stress after an underload were successfully generated from smooth specimen overload fatigue tests, and other tests required to implement the effective strain-life model and the fatigue crack growth model were obtained from smooth specimen tests at a cost not much greater than that required to generate the currently used constant amplitude fatigue data.

8.2 Recommendations for Future Work - Metal Hardness

The materials investigated in this thesis were a very soft, a medium hardness, and a very hard metal. The soft metal (DP 590 steel) experienced high levels of plastic deformation even at very long fatigue lives (10^6 cycles). The hard metal (8822 steel) didn't show any plastic strain even at a very high strain amplitude during constant amplitude fatigue tests. The results of the very soft and very hard metals should be investigated more by testing other metals with hardnesses that fall between very soft - medium, and medium -very hard. The results will provide more understanding on how the crack opening stresses after underloads recover to the steady state level.

Appendix A

Determination of Steady State Crack Opening Stress Constants

Constant amplitude fully reversed fatigue tests and underload fatigue tests were used to determine the constants in DuQuesnay's model [63] for steady state crack opening stresses (Eq. A.1).

$$S_{opss} = \theta \sigma_{\max} \left[1 - \left(\frac{\sigma_{\max}}{\sigma_y} \right)^2 \right] + \varphi \sigma_{\min} \qquad \text{(Eq. A.1)}$$

Where σ_{max} and σ_{min} are the nominal maximum and minimum stresses in a smooth specimen, or the local maximum and minimum stresses at the notch root in a notched specimen respectively. σ_y is a material constant, θ and φ are two experimentally determined constants of the material. Topper and Lam [61] proposed that the difference between the strain range at a given fatigue life on a fully reversed constant amplitude fatigue life curve, $\Delta\varepsilon_{CA}$, and that on the effective strain-life curve, $\Delta\varepsilon_{eff}$, is equal to the difference between the constant amplitude test minimum strain, ε_{min}, and the estimated crack opening strain, ε_{op}, in the constant amplitude stress-strain loop. This could be formulated as follows:

$$\Delta\varepsilon_{CA} - \Delta\varepsilon_{eff} = \varepsilon_{op} - \varepsilon_{\min} = \frac{S_{opss} - S_{\min}}{E} \qquad \text{(Eq. A.2)}$$

Therefore the estimated constant amplitude crack opening stress (S_{opss}) can be written as follows:

$$S_{opss} = S_{\min} + E(\Delta\varepsilon_{CA} - \Delta\varepsilon_{eff}) \qquad \text{(Eq. A.3)}$$

These values of S_{opss} were then calculated using the constant amplitude fully reversed and underload fatigue tests (R = -1) and plotted against DuQuesnay equation (Eq. A.1). The values of the two constants in Eq. A.1, θ and φ, were iteratively changed until a good fit of the S_{opss} *vs.* S_{max} data were obtained.

Appendix B

Obtaining the Crack Closure Damage Parameter "m" in the Stress Build-Up Equation

Previously [1], the crack closure damage parameter "*m*" in the stress build-up equation (Eq. B.1) was obtained by a series of tests where the crack opening stress build-up after the application of an underload was measured using a 900x power short focal length optical video microscope. However these tests were time consuming and required special equipments that might not be available in every fatigue laboratory. The following equation has been shown to give a good fit to the change in crack opening stress per cycle.

$$\Delta S_{op} = m(S_{opss} - S_{cu}) \qquad \text{(Eq. B.1)}$$

where ΔS_{op} is the change in crack opening stress, S_{opss} is the steady state crack opening stress, S_{cu} is the current crack opening stress, and "*m*" is a material constant.

In this work a new test procedure for obtaining the constant "*m*" was introduced (Chapter 3, Section 3.3.3.2). In these tests a block of loading history consisting of an underload of stress yield limit was applied followed by constant amplitude cycles. The stress range of the small cycles as well as the underload cycle was kept constant throughout the tests, and only the number of small cycles per block was changed. The aim of these tests was to model the damage done by the small cycles and obtain a value of "*m*" by comparing it to the damage obtained by applying the effective strain-life model.

Calculating the Damage of the Small Cycles from Experimental Tests

As mentioned previously a block of a loading history was applied to smooth samples until failure. The block consisted of an underload cycle followed by constant amplitude small cycles. For the sake of illustration, the following example is provided:

Test #	Stress amplitude of the small cycles (MPa)	Stress amplitude of the underload cycle (MPa)	Number of small cycles per block	Number of underload cycles per block	Fatigue life (cycles)
1	220	370	200	1	194,171

- The number of underload cycles in the loading history till failure was calculated as follows:

$$N_{UL} = \frac{Fatigue\ life}{Number\ of\ small\ cycles\ per\ block + 1} = \frac{194{,}171}{(200+1)} = 966\ cycles$$

- The stress amplitude of the underload cycle was chosen to be the fully reversed constant-amplitude stress level that would give a fatigue life of 10,000 cycles in a constant amplitude fatigue test,therefore the damage done by the underload cycle was :

$$D_{UL} = \frac{1}{10,000} = 0.0001$$

- Therefore the total damage due to the underload cycles was given by:

$$\frac{N_{UL}}{10,000} = \frac{966}{10,000} = 0.0966$$

- The damage done by the small cycles was obtained by subtracting the damage done by the underloads from unity:

$$D_{SC} = 1 - D_{OL} = 1 - 0.0966 = 0.9034$$

- Therefore the equivalent number of small cycles was given by:

$$Equivalent\ Number\ of\ Small\ Cycles = \frac{Fatigue\ life - Number\ of\ underloads}{Damage\ done\ by\ small\ cycles} = \frac{194{,}171 - 966}{0.9034} = 213{,}864\ cycles$$

- Number of blocks (the same as the number of underloads in the loading history)in the loading history was given by :

$$N_{UL} = \frac{Fatigue\ life}{Number\ of\ small\ cycles\ per\ block + 1} = \frac{194{,}171}{(200+1)} = 966\ cycles$$

- Therefore the damage done by a block was :

$$Damage\ per\ block = D_B = \frac{1}{Number\ of\ blocks} = \frac{1}{966} = 0.001035$$

- The damage per cycle was given as:

$$D_C = \frac{1}{Equivalent\ number\ of\ \ small\ cycles} = \frac{1}{213{,}864} = 0.000004676$$

Calculating the Damage of the Small Cycles using the "***m Block Program***"

A short program written in Python was developed to calculate the damage done by the small cycles. During this process the same block of loading history used in the experimental work was applied and the damage per cycle was obtained. Figure shows the interface of the "***m Block Program***"

Input Data

Material Properties	Underload Cycle	Small Cycles	Effective Strain-Life Curve
•Elastic modulus of elasticity, *E* •Cyclic strength coefficient, *K* •Cyclic strain hardening exponent, *n'*	•Maximum stress amplitude •Minimum stress amplitude •Steady state crack opening stress	•Maximum stress amplitude •Minimum stress amplitude •Steady state crack opening stress	•Constants : *A* and *b* •A trial value of *"m"* •Intrinsic strain Range:$\Delta\varepsilon_i$

In performing the fatigue damage calculations the following steps were performed:

1. The local stresses and strains were calculated for the applied loading block.
2. For the first cycle, the value of the steady state crack opening stress (S_{opss}) was calculated using Eq. 2.3.
3. For the other following cycles, the change in the crack opening stress (S_{op}) was calculated based on the crack opening stress build-up equation (Eq. 2.4) with an assumed value of "*m*".
4. The increment was then added to the current crack opening stress level to give the opening stress at the end of each cycle.
5. This procedure was repeated for each subsequent cycle until the calculated crack opening stress reached the given steady state stress.

6. After obtaining the crack opening stress of each cycle, the effective strain range was calculated using Eq. 2.11.
7. The effective strain range obtained from the previous step was then used to calculate the equivalent number of cycles using the effective strain-life curve and Eq. 2.12.
8. The damage per block was calculated by taking the reciprocal of the obtained equivalent number of cycles.
9. The calculated damage was then compared with the experimental damage obtained from the underload fatigue tests, and the value of "m" was iterated until the damage obtained from the program fitted the damage obtained from experiments.

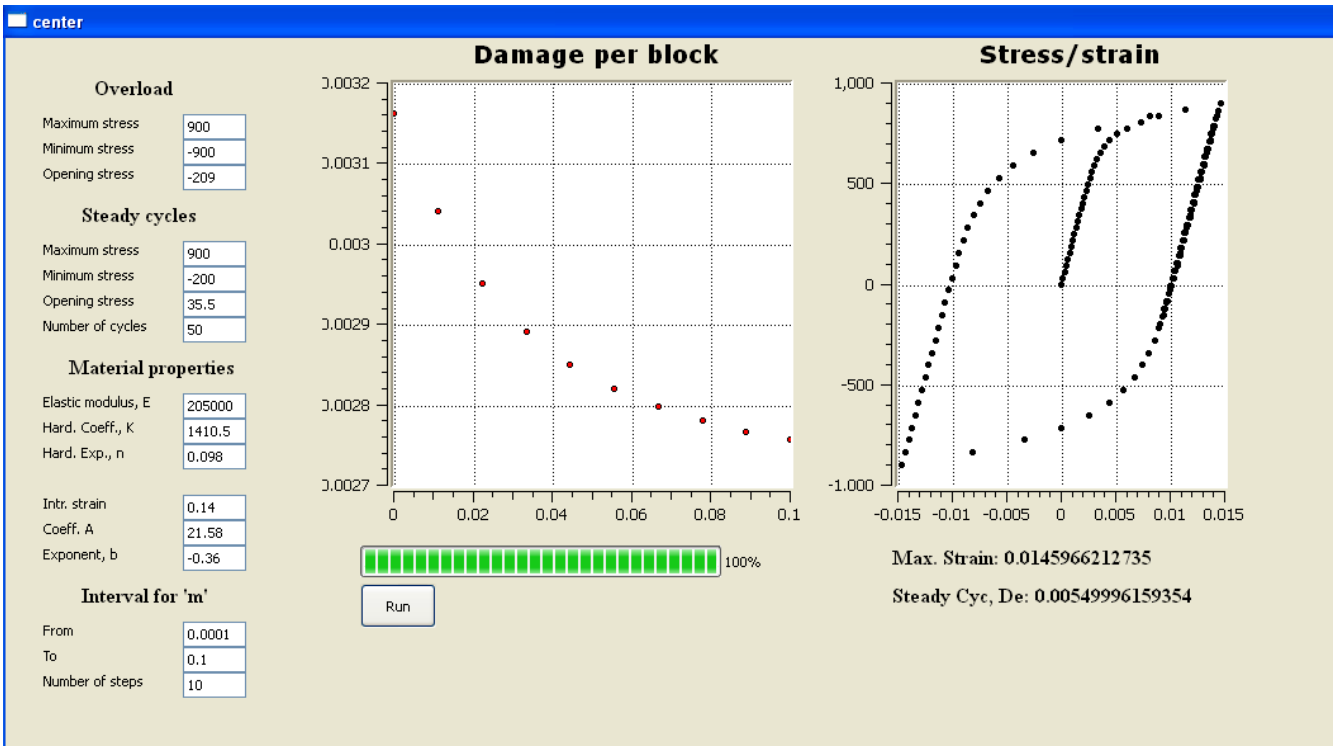

Appendix B 1 Interface of the "m Block Program"

References

[1] M. Khalil, *Effect of fatigue loading spectra on crack opening stress and crack shape development*. Waterloo, ON, Canada: Ph.D Thesis, University of Waterloo, 2002.

[2] Wikipedia. [Online]. http://en.wikipedia.org/wiki/Eschede_train_disaster

[3] P.C. Paris, M.P. Gomez, and W.E. Anderson, "A rational analytic theory of fatigue," *The Trend in Engineering* , vol. 13, no. 1, pp. 9-14, 1961.

[4] W. Elber, "Fatigue crack closure under cyclic tension," *Engineering Fracture Mechanics*, vol. 2, pp. 37-45, 1970.

[5] Fernand Ellyin, *Fatigue Damage, Crack Growth and Life Prediction*, 1st ed. London, UK: Chapman and Hall, 1997.

[6] B.T. Ma and C. Laird, "Overview of fatigue behaviour in copper single crystals. I. Surface morphology and stage I crack initiation sites for tests at constant strain amplitude," *Acta Metallurgica*, vol. 37, pp. 325-36, 1984.

[7] C.A. Rodopoulos and E.R. de los Rios, "Theoratical analysis on the behaviour of short fatigue cracks," *International Journal of Fatigue*, vol. 24, pp. 719-24, 2002.

[8] D.L. McDowell, "An engineering model for propagation of small cracks in fatigue," *Engineering Fracture Mechanics*, vol. 56, no. 3, pp. 357-77, 1997.

[9] P.E. Forsyth, *Proceedings of the Crack Propagation Symposium*, pp. I:76-94, 1961.

[10] K.J. Miller, "The bahaviour of short fatigue cracks and their initiation part II - A general summary," *Fatigue and Fracture of Engineering Materials and Structures*, vol. 10, no. 2, pp. 93-113, 1987.

[11] K. Tokaji, T. Ogawa, and S. Osako, "The growth of microstructurally small fatigue cracks in a ferritic-pearlitic steel," *Fatigue and Fracture of Engineering Materials and Structures*, vol. 11, no. 5, pp. 331-342, 1988.

[12] T.H. Topper, M.T. Yu, and D.L. DuQuesnay, "Mechanisims and mechanics of fatigue crack initiation and growth," *Proceedings of the International Symposium on Fracture Mechanics*, pp. 81-94, 1987.

[13] H. Kitagawa and S. Takahashi, "Applicability of fracture mechanics to very small cracks or the cracks in the early stage," in *Proceedings of the Second International Conference on Mechanical Behavior of Materials, ASM*, Metals Park, Ohio, 1976, p. 627.

[14] R.A. Smith and K.J. Miller, "Fatigue cracks at notches," *International Journal of Mechanical Sciences*, vol. 19, no. 1, pp. 11-22, 1977.

[15] P.C. Paris and F. Erdogan, "A critical analysis of crack propagation laws," in *J. Basic Eng. Trans. ASME 85 (D)*, 1963, pp. 528-34.

[16] U. Linstedt, B. Karlsson, and M. Nystr, "Small fatigue cracks in an austentic stainless steel," *Fatigue and Fracture of Engineering Materials and Structures*, vol. 21, no. 1, pp. 85-98, 1998.

[17] M.S. Hunter and W.G. Fricke, "Fatigue crack propagation in aluminum alloys," in *Proceedings of the American Society for Testing and Materials*, vol. 54, 1956, pp. 1038-46.

[18] S. Pearson, "Initiation of fatigue cracks in commercial aluminum alloys and subsequent propagation of very short cracks," *Engineering Fracture Mechanics*, vol. 7, pp. 235-47, 1975.

[19] C. Bjerken, "The discrete nature of the growth and arrest of microstructurally short fatigue cracks modelled by dislocation technique," *International Journal of Fatigue*, vol. 27, no. 1, pp. 21-32, 2005.

[20] K. Sadananda and A.K. Vasudevan, "Short crack growth and internal stresses," *International Journal of Fatigue*, vol. 19, no. 1, 1997.

[21] A. Navarro and E.R. de los Rios, "A microstructurally-short fatigue crack growth equation," *Fatigue and Fracture of Engineerig Materials and Structures*, vol. 11, no. 5, pp. 383-96, 1988.

[22] P.D. Hobson, "The formulation of a crack growth equation for short cracks," *Fatigue and Fracture of Engineering Materials and Structures*, vol. 5, no. 4, pp. 311-21, 1982.

[23] H. Abdel-Raouf, T.H. Topper, and A. Plumtree, "A model for the fatigue limit and short crack behaviour related to surface strain redistribution," *Fatigue and Fracture of Engineering Materials and Structures*, vol. 15, no. 9, pp. 895-909, 1992.

[24] M.H. El Haddad, K.N. Smith, and T.H. Topper, "Fatigue crack propagation of short cracks," *Journal of Engineering Materials and Technology, ASME*, vol. 20, no. 10, pp. 42-46, 1979.

[25] A.J. McEvily, S. Ishihara, H. Saki, and H. Matsunage, "On one - and two - parameter analyses of short fatigue crack growth," *International Journal of Fatigue*, vol. 29, no. 12, pp. 2237-2245, 2007.

[26] G.R. Irwin, "Analysis of stresses and strains near the end of crack traversing a plate," *Journal of Applied Mechanics*, vol. 24, pp. 361-64, 1957.

[27] S. Mikheevskiy and G. Glinka, "Elastic-plastic fatigue crack growth analysis under variable amplitude loading spectra," *International Journal of Fatigue*, vol. 31, pp. 1828-1836, 2009.

[28] A.H. Noroozi, G. Glinka, and S. Lambert, "A two parameter driving force for fatigue crack growth

analysis," *International Journal of Fatigue*, vol. 27, pp. 1277-96, 2005.

[29] W. Elber, "The significance of fatigue crack closure," in *Damage Tolerance in Aircraft Structures, ASTM STP 486*, 1971, pp. 230-42.

[30] Mc and Ritchie, "Crack closure and the fatigue-crack propagation threshold as a function of load ratio," *Fatigue and Fracture of Engineering Materials and Structures*, vol. 21, no. 7, pp. 847-55, 1998.

[31] R.O. Ritchie and S. Suresh, "Some considerations on fatigue crack closure at near-threshold stress intensities due to fracture surface morphology," *Metallurgican and Materials Transactions A*, vol. 13, no. 5, pp. 937-40, 1982.

[32] A.J. McEvily, "On crack closure in fatigue crack growth," *Mechanics of Fatigue Crack Closure, ASTM STP 982 (eds J.C. Newman, Jr. and W. Elber)*, pp. 35-43, 1988.

[33] L. Lawson, E.Y. Chen, and M. Meshil, "Near-threshold fatigue: a review," *International Journal of Fatigue*, vol. 21, pp. 15-34, 1999.

[34] P.K. Liaw, "Overview of crack closure at near-threshold fatigue crack growth levels," *Mechanics of Fatigue Crack Closure, ASTM STP 982 (eds J.C. Newman, Jr. and W. Elber)*, pp. 62-92, 1988.

[35] M.T Yu, T.H. Topper, and P. Au, "The effects of stress ratio, compressive loads and underloads on the threshold behavior of a 2024-T351 aluminum alloy," in *Proceedings of the 2nd International Conference on Fatigue and Fatigue Thresholds*, Birmingham, UK, 1984, pp. 170-190.

[36] T.H. Topper and M.T. Yu, "The effect of overloads on threshold and crack closure," *International Journal of Fatigue*, vol. 7, no. 3, pp. 159-164, 1985.

[37] S. Taira, K. Tanaka, and Y. Naki, "A model of crack tip slip band blocked by grain boundary," *Mech Res Commun* , vol. 5, pp. 375-81, 1978.

[38] M. Kikukawa, M. Jono, K. Tanaka, and M. Takatani, "Measurement of fatigue crack propagation and crack closure at low stress intensity level by unloading elastic compliance method," *Journal of the Society of Materials Science Japan*, vol. 25, pp. 899-903, 1976.

[39] C.Q. Bowles and J. Schijve, "Crack tip geomatry for fatigue cracks grown in air and vacuum," in *Fatigue Mechanisims: Advances in Qualitative Measurement of Physical Damage, ASTM STP 811 (eds J. Lankford et al.)*, Philadelphia, PA, 1983, pp. 400-26.

[40] D.A. Lados, D. Apelian, P.C. Paris, and J.K. Donald, "Closure mechanisims in AI-Si-Mg cast alloys and long-crack to small-crack corrections," *International Journal of Fatigue*, vol. 27, no. 10-12, pp. 1463-72, 2005.

[41] K. Minakawa, H. Nakamura, and A.J. McEvily, "On the development of crack closure with crack advance in a ferritic steel," *Scripta Metall.*, vol. 18, no. 12, pp. 1371-74, 1984.

[42] D.L. DuQuesnay, T.H. Topper, M.T. Yu, and M.A. Pompetzki, "The effective stress range as a mean stress parameter," *International Journal of Fatigue*, vol. 14, no. 1, pp. 45-50, 1992.

[43] F. Ellyin and J. Wu, "Elastic-plastic analysis of a stationary crack under cyclic loading and effect of overload," *International Journal of Fracture*, vol. 56, pp. 189-208, 1992.

[44] C. Makabe, A. Purnowidodo, and A.J. McEvily, "Effects of surface deformation and crack closure on fatigue crack propagation after overloading and underloading," *International Journal of Fatigue*, vol. 26, no. 12, pp. 1341-48, 2004.

[45] M. Khalil, T. Lam, and T.H. Topper, "Estimation of crack opening stresses from strain-life fatigue data," in *Fatigue and Durability Assessment of Materials, Components and Structures*, 2000, pp. 449-56.

[46] S. Kim and W. Tai, "Retardation and arrest of fatigue crack growth in A151 4140 steel by introducing rest periods and overloads," *Fatigue and Fracture of Engineering Materials and Structures*, vol. 15, pp. 519-30, 1992.

[47] C.M. Ward-Close, A.F. Blom, and R.O. Ritchie, "Mechanisms associated with transient fatigue crack growth under variable-amplitude loading:An experimental and numerical study," *Engineering Fracture Mechanics*, vol. 32, no. 4, pp. 613-38, 1989.

[48] R. Jurcevic, D.L. DuQuesnay, T.H. Topper, and M.A. Pompetzki, "Fatigue damage accumulation in 2024-T351 aluminum subjected to periodic reversed overloads," *International Journal of Fatigue*, vol. 12, no. 4, pp. 259-66, 1990.

[49] A. Dabayeh and T.H. Topper, "Changes in crack opening stress after underloads in 2024-T351 aluminum alloy," *International Journal of Fatigue*, vol. 17, pp. 261-69, 1980.

[50] M.A. Pompetzki, R.A. Saper, and T.H. Topper, "Effect of compressive underloads and tensile overloads on fatigue damage accumulation in SAE 1045 steel," *International Journal of Fatigue*, vol. 12, pp. 207-13, 1990.

[51] M. Skorupa, "Load interaction effects during fatigue crack growth under variable amplitude loading - a literature review. Part II: qualitative interpretation," *Fatigue and Fracture of Engineering Materials and Structures*, vol. 22, pp. 905-26, 1998.

[52] A. Varvani and T.H. Topper, "Closure-free biaxial fatigue crack growth rate and life prediction under various biaxiality ratios in SAE 1045 steel," *Fatigue and Fracture of Engineering Materials*

and Structures, vol. 22, no. 8, pp. 697-710, 1999.

[53] M.T. Yu, T.H. Topper, D.L. DuQuesnay, and M.S. Levin, "The effect of compressive peak stress on fatigue behavior," *International Journal of Fatigue*, vol. 8, pp. 9-15, 1986.

[54] A. Dabayeh, *Changes in crack opening stress after overloads in 2024-T351 aluminum alloys*. Waterloo, ON, Canada: M.A.Sc. Thesis, University of Waterloo, 1994.

[55] M. Khalil and T.H. Topper, "Prediction and correlation of the average crack-opening stress with service load cycles," *International Journal of Fatigue*, vol. 25, no. 7, pp. 661-70, 2003.

[56] M. Vorwald and T. Seeger, "The consequences of short crack closure on fatigue crack growth under variable amplitude loading," *Fatigue and Fracture of Engineering Materials and Structures*, vol. 14, no. 2-3, pp. 205-25, 1991.

[57] F.A. Conle and T.H. Topper, "Overstrain effects during variable amplitude service history testing," *International Journal of Fatigue*, vol. 3, pp. 130-36, 1980.

[58] N.E Dowling, "Estimation and correlation of fatigue lives for random loading," *International Journal of Fatigue*, vol. 10, no. 3, pp. 179-85, 1988.

[59] D.L. DuQuesnay, C. MacDougall, A.A. Dabayeh, and T.H. Topper, "Notch fatigue behaviour as influenced by periodic overloads," *International Journal of Fatigue*, vol. 14, no. 2,3, pp. 91-99, 1995.

[60] ASTM Standard E 1049-85 (2005), "Standard practices for cycle counting in fatigue analysis," in *Annual Book of ASTM Standards, Section Three, Metals Test Methods and Analytical Procedures*. West Conshohocken, PA: ASTM International, 2007, pp. 836-45.

[61] T.H. Topper and T.S. Lam, "Effective strain-fatigue life data for variable amplitude loading," *International Journal of Fatigue*, vol. 19, no. 1, pp. 137-43, 1997.

[62] T.H. Topper, D.L. DuQuesnay, M.A. Pompetzki, and R.A. Jurcevic, "A crack closure based model for mean stress and overload effects on fatigue damage," in *International Symposium on Fatigue Damage Measurement and Evaluation Under Complex Loadings*, Fukuoka, Japan, 1991.

[63] D.L. DuQuesnay, *Fatigue damage accumulation in metals subjected to hign mean stress and overload cycles*, Ph.D. Thesis ed. Waterloo, ON, Canada: University of Waterloo, 1991.

[64] J. Schijve, "Fatigue crack closure:observations and technical significance," in *Mechanics of Fatigue Crack Closure, ASTM STP 982*. Philadelphia, PA, USA, 1988, pp. 5-34.

[65] K.J. Miller, "Initiation and growth rates of short fatigue cracks; In Fundementals of Deformation and

Fracture Proceedings.," in *IUTAM Symposium Eshelly Memorial Conference*, Cambridge University Press, 1984, pp. 477-500.

[66] D. Taylor and J.F. Knott, "Fatigue Crack Propagation behavior of short cracks - The Effect of microstructure," *Fatigue of Engineering Materials and Structures*, vol. 4, pp. 147-55, 1981.

[67] A.J. McEvily, "Current aspects of fatigue;Fatigue crack propagation of short cracks," *Fatigue 1977 Conference*, pp. 1-9, 1977.

[68] M.A. Pompetzki, R.A. Saper, and T.H. Topper, "Software for high frequency control for variable amplitude fatigue tests," *Canadian Metallurgical Quarterly*, vol. 25, pp. 181-194, 1986.

[69] James, Jr. Newman, Judy Schneider, Aaron Daniel, and Dustin McKnight, "Compression pre-cracking to generate near threshold fatigue-crack-growth rates in two aluminum alloys," *International Journal of Fatigue*, vol. 27, no. 10-12, pp. 1432-40, 2005.

[70] T Endo and J. Morrow, "Cyclic stress-strain and fatigue behavior of representative aircraft metals," *Journal of Materials*, vol. 4, no. 1, pp. 159-75, 1969.

[71] "Proceedings of the FAA-NASA symposium on the continued airworthiness of aircraft structures," FAA Center of Excellence in Computational Modeling of Aircraft Structures, Atlanta, Georgia, 1997.

[72] F.K. Ibrahim, J.C. Thomson, and T.H. Topper, "A study of the effect of mechanical variables on fatigue crack closure and propagation," *International Journal of Fatigue*, vol. 8, no. 3, pp. 135-42, 1986.

[73] A.J. McEvily and K. Minikawa, "Fatigue crack growth threshold concepts," in *TMS AIME*, Warrendale, PA, USA, 1984, p. 517.

[74] J.C. Newman, "A crack opening stress equation for fatigue crack growth," *International Journal of Fracture*, vol. 24, pp. 131-35, 1984.

[75] J. Schijve, "Fatigue crack propagation in light alloy sheet material and structures," National Aerospace Laboratory, Amsterdam, Report MP-195 1960.

[76] C.M. Hudson and H.F. Hardrath, "Effects of changing stress amplitude on the rate of fatigue crack propagation in two aluminum alloys," NASA, TN-D-960 1961.

[77] R. Craig McClung and Huseyin Sehitoglu, "Closure behavior of small cracks under high strain faigue histories," in *Mechanics of Fatigue Crack Closure, ASTM STP 982*, J.C. Newman and Wolf Elber, Eds. Philadelphia, PA, USA: American Society for Testing and Materials, 1988, pp. 279-99.

[78] M. Khalil and T.H. Topper, "Prediction of crack opening stress levels for 1045 steel under service loading spectrum," *International Journal of Fatigue* , vol. 25, pp. 149-57, 2003.

[79] M. Khalil, *Effect of fatigue loading spectra on crack opening stress and crack shape development*, Ph.D. Thesis ed. Waterloo, ON, Canada: University of Waterloo, 2002.

[80] M.H. El Haddad, *A study of the growth of short fatigue cracks based on fracture mechanics*. Waterloo, ON, Canada: Ph.D Thesis, University of Waterloo, 1978.